Year : 2021

THE MANY WAYS OF WAKING UP FROM SLEEP - MOVING FORWARD THE ANALYSIS OF SLEEP MICROARCHITECTURE

Cardis Romain

Cardis Romain, 2021, THE MANY WAYS OF WAKING UP FROM SLEEP - MOVING FORWARD THE ANALYSIS OF SLEEP MICROARCHITECTURE

Originally published at : Thesis, University of Lausanne

Posted at the University of Lausanne Open Archive http://serval.unil.ch
Document URN : urn:nbn:ch:serval-BIB_D5841D4D0C9F0

UNIL | Université de Lausanne
Faculté de biologie et de médecine

Département des neurosciences fondamentales, UNIL
& Centre d'antalgie, Service d'anesthésiologie, CHUV

THE MANY WAYS OF WAKING UP FROM SLEEP - MOVING FORWARD THE ANALYSIS OF SLEEP MICROARCHITECTURE

Thèse de doctorat en Neurosciences

présentée à la

Faculté de Biologie et de Médecine
de l'Université de Lausanne

par

Romain Cardis

Neurobiologiste diplômée de l'Université de Lausanne, Suisse

Jury

Prof. MD. Bogdan Draganski, Président
Prof. Anita Lüthi, Directeur
Prof. Isabelle Décosterd, Co-Directeur
Prof. Paul Franken, Expert
Prof. Thomas Nevian, Expert

Thèse n° 304

Lausanne 2021

Programme doctoral interuniversitaire en Neurosciences des Universités de Lausanne et Genève

LEMANIC NEURO SCIENCE DOCTORAL SCHOOL
CHUV
UNIL | Université de Lausanne
UNIVERSITÉ DE GENÈVE

UNIL | Université de Lausanne
Faculté de biologie et de médecine

Département des neurosciences fondamentales, UNIL
& Centre d'antalgie, Service d'anesthésiologie, CHUV

THE MANY WAYS OF WAKING UP FROM SLEEP - MOVING FORWARD THE ANALYSIS OF SLEEP MICROARCHITECTURE

Thèse de doctorat en Neurosciences

présentée à la

Faculté de Biologie et de Médecine
de l'Université de Lausanne

par

Romain Cardis

Neurobiologiste diplômée de l'Université de Lausanne, Suisse

Jury

Prof. MD. Bogdan Draganski, Président
Prof. Anita Lüthi, Directeur
Prof. Isabelle Décosterd, Co-Directeur
Prof. Paul Franken, Expert
Prof. Thomas Nevian, Expert

Thèse n° 304

Lausanne 2021

Programme doctoral interuniversitaire en Neurosciences des Universités de Lausanne et Genève

LEMANIC NEURO SCIENCE DOCTORAL SCHOOL
CHUV
UNIL | Université de Lausanne
UNIVERSITÉ DE GENÈVE

UNIL | Université de Lausanne

UNIVERSITÉ DE GENÈVE

Programme doctoral interuniversitaire en Neurosciences des Universités de Lausanne et Genève

Imprimatur

Vu le rapport présenté par le jury d'examen, composé de

Président·e	Monsieur	Prof.	Bogdan	**Draganski**
Directeur·trice de thèse	Madame	Prof.	Anita	**Lüthi**
Co-Directeur·trice de thèse	Madame	Prof.	Isabelle	**Décosterd**
Expert·e·s	Monsieur	Prof.	Thomas	**Nevian**
	Monsieur	Prof.	Paul	**Franken**

le Conseil de Faculté autorise l'impression de la thèse de

Monsieur Romain Cardis

Master en biologie médicale,
Université de Lausanne, Suisse

intitulée

The Many Ways of Waking Up from Sleep -
Moving Forward the Analysis of Sleep Microarchitecture

Date de l'examen: 19 mai 2021
Date d'émission de l'Imprimatur: Lausanne, le 1 juin 2021

pour Le Doyen
de la Faculté de Biologie et de Médecine

Prof. Niko GELDNER
Directeur de l'Ecole Doctorale

THE MANY WAYS OF WAKING UP FROM SLEEP - MOVING FORWARD THE ANALYSIS OF SLEEP MICROARCHITECTURE

Thèse de doctorat en Neurosciences
Romain Cardis, 2021

Peinture de Anne Durrant Cardis

Table of content

Acknowledgements

I would like to particularly thanks Prof. Anita Lüthi, one of my thesis directors who followed me and supported me during the 5 years of my PhD. It was a great pleasure to learn all these new skills from, and alongside her. I believe that it is quite rare to find a supervisor that can adapt to each of her students the way she does, and to get the best out of each of us. I felt very free during my thesis, able to explore the scientific aspects that were motivating me the most all the while feeling greatly supported. Her scientific interest, her trust, her willingness to help us improve by transmitting her knowledge, and to learn herself from us are priceless qualities that helped and showed me the way through my thesis. I became a better scientist thanks to her example and for that I am very grateful.

My special thanks also go to Prof. Isabelle Décosterd, my other thesis director who as well supported me greatly during my thesis. She gave me the freedom to pursue my goals and her support in the pain field, in which her deep knowledge and visions greatly helped me to understand and apprehend this field. I thank her a lot for the nice discussions, the nice encouragements, and the always timely support. The translational knowledge and aspects that she brought to my thesis greatly motivated me and her appreciations made me proud of my work.

I am very grateful to Dr. Sandro Lecci who was still PhD student when I started. He greatly helped me to get started with MATLAB and introduced me to the power of DIY electronics. I thank him for the hours that we spent designing both software and hardware, and the most important thing, the choosing of the right name for these tools. His guidance shaped the direction of my thesis by helping me find the technics and tools where I could express my full potential.

I particularly thanks Dr. Laura Fernandez. She was always there to help me and to answer my constant questions about signal analysis. She helped me a lot by teaching and improving my surgery skills. She showed me how to be organized and efficient, which I am still learning by applying her advices. I thank her for her patience and her amazing lab organization, which allowed me to work in a great scientific environment where I was not missing a single tool.

Next, my good friend Alejandro Osorio-Forero, PhD student with me during my thesis. He is an amazing and so cheerful person that never failed to transmit his love of good science and engineering. I thank him very much for his contagious motivation and all our nice discussions, which were always a source of inspiration. His rigor, work ethic, and perseverance were great examples for me.

I thank Stephany Fulda, who's comments on my analysis and very active participation in the paper writing process improved my work significantly.

Finally, I would like to thank other lab members, current and previous, for their support. Dr. Paul Chu Sin Chung, who's patience, calm and great advices helped me a lot. Najma Cherrad, the star whose honesty, and energy never failed to give me smiles. Dr. Gil Vantomme, master of optimization. Guylène Kirschmann and Marie Pertin, the two amazing technicians that accomplished so much for the lab. Lila Banterle, Elena Konnova, Dr. Ludovic Gillet, Dr. Christophe Gattlen, Dr. Alexandru Deftu, Dr. Marc Suter and Manon Isler, colleagues and friends who I thank for the laughs and the great atmosphere they create in the lab.

Lastly, I would like to thank my future wife, Laura Solanelles Farré that I had the chance to meet during my PhD here at the DNF, and whose support was key to the realization of my work.

Summary

One of the defining characteristics of sleep is that it is readily reversible towards wakefulness. This is exemplified in the common daily experience of waking up in the morning. My thesis studies sleep-wake transitions that are equally common and frequent, yet often not consciously perceived and neglected as random sleep perturbations of minor significance. Using mice as an experimental species, I find that healthy non-rapid-eye-movement sleep (NREMS), also named deep restorative sleep, is a dynamic brain state showing defined, periodically recurring moments of fragility. During these, diverse types of brief arousal-like events with various combinations of physiological correlates appear, including global or local cortical activation, muscle activity, and heart rate changes. Using a mice model of chronic neuropathic pain, I find that the rules I have identified in healthy sleep serve to identify previously unrecognized sleep disruptions that could contribute to sleep complaints of chronic pain patients. The experimental and analytical methods I have developed in these studies also helped in the identification of the neuronal basis of the fragility periods of NREM sleep. Together, my studies offer novel insights and analytical tools for the study of sleep-wake transitions and their perturbance in pathological conditions linked to sensory discomfort.

More specifically, my work departed from recent findings that NREMS in mice is divided in recurring periods of sleep fragility at frequencies ~0.02 Hz, characterized by heightened arousability. Through analyzing the temporal distribution of brief arousal events termed microarousals, I hypothesized that these fragility periods could serve a time raster for the probing of spontaneous sleep perturbations. Motivated by the question of how sensory discomfort caused by pain affects sleep, I have used the spared nerve injury (SNI) model, which consists in the injury of two of the 3 branches of the sciatic nerve. I found that the role of fragility periods in timing spontaneous arousals is highly useful to identify sleep disruptions not commonly detected with standard polysomnographic measures. Thus, by scrutinizing the fragility periods of NREMS in the SNI mice, I discovered an overrepresentation of a novel form of local perturbation within the hindlimb primary somatosensory cortex (S1HL), accompanied by heart rate increases. In addition, I showed that SNI animals woke up more frequently facing external stimuli, using closed-loop methods targeting specifically the fragility or continuity periods. These findings led me to propose that chronic pain-related sleep complaints may arise primarily from a perturbed arousability. The closed-loop techniques to probe arousability could be transferred to interrogate neuronal mechanisms underlying NREMS fragility, leading to the recognition that intrusion of wake-related activity into NREMS is a previously underappreciated mechanism controlling sleep fragility and architecture.

Overall, I present my thesis to advance the view on NREMS as a dynamic heterogeneous state of which insights into its neuronal mechanisms, and its physio- and pathophysiological manifestations in animal models should be key to formulate testable hypotheses aimed to cure the suffering of sleep disorder in human.

Résumé

Une des caractéristiques qui définit le sommeil, est que l'on peut rapidement retourner à un état d'éveil. De fait, nous l'expérimentons chaque matin au réveil. Ma thèse étudie les transitions sommeil-éveil qui, bien que fréquentes, sont souvent non consciemment perçues et traitées comme des perturbations sans importance et aléatoires du sommeil. En utilisant la souris comme modèle expérimental, je montre que le sommeil sans mouvements rapides des yeux (NREMS), également appelé le sommeil profond et réparateur, est un état cérébral dynamique composé de périodes discrètes et récurrentes de fragilité face à des stimuli externe. Pendant celles-ci, plusieurs types d'évènements associés à des éveils brefs apparaissent, combinant activation corticale, activité musculaire et/ou une hausse des battements cardiaques. Je démontre que la compréhension des transitions sommeil-éveil physiologiques s'avère utile pour étudier le sommeil de souris souffrant de douleurs neuropathiques chroniques. Ces souris présentent un nouveau type de perturbations locales lors du sommeil, qui pourraient possiblement expliquer une partie des plaintes de mauvais sommeil exprimées par les patients souffrant de douleurs chroniques. Les méthodes analytiques et expérimentales que j'ai développées dans ces études ont aussi aidé à l'identification des bases neuronales de la genèse des périodes de fragilités du sommeil NREM. En somme, mes études offrent des connaissances inédites et des méthodes d'analyses pour l'étude des transitions sommeil-éveil et de leurs perturbations en conditions pathologiques.

Une étude récente du laboratoire a montré que le sommeil NREM est divisé en périodes de fragilité alternant avec des périodes de non-fragilité (continuité), environ toutes les 50 secondes ce qui donne une fréquence de 0.02 Hz. Les périodes de fragilité sont caractérisées par une hausse de « l'éveillabilité » ou propension à s'éveiller. Ma première observation est que les éveils brefs, couramment appelés micro-réveils, présentent une distribution temporelle hautement restreinte aux périodes de fragilité. Ainsi, j'ai émis l'hypothèse que ces périodes pourraient servir de moments spécialement choisis par le cerveau pour la mesure de potentielles perturbations spontanées. Motivé par la question de comment les douleurs chroniques perturbent le sommeil, je l'ai analysé chez un modèle de souris de douleurs neuropathique, le modèle de d'épargne du nerf sural (SNI). Le rôle des périodes de fragilité à restreindre les micro-réveils s'est avéré très utile pour détecter de nouvelles formes de réaction à des perturbations qui ne sont pas évidentes par des analyses classiques du sommeil. En effet, spécifiquement pendant ces périodes de fragilité, j'ai découvert une sur-représentation d'un nouveau type d'éveil local confiné au cortex somatosensoriel primaire et accompagné d'une hausse du rythme cardiaque. De plus, en utilisant de nouvelles méthodes basées sur des boucles-fermées, j'ai démontré que les souris SNI se réveillaient plus fréquemment que leurs contrôles en faisant face à des stimuli externes. Sur la base de ces découvertes, je propose que les plaintes de mauvais sommeil chez les patients souffrant de douleurs chroniques puissent prendre leur source dans une éveillabilité perturbée. Les méthodes de boucles-fermées pour analyser l'éveillabilité a aussi pu être transférée pour l'étude optogénétique des mécanismes neuronaux à la base de la fragilité

du sommeil NREM. Cela a mené à la reconnaissance que l'intrusion d'activité normalement associée à l'éveil dans le sommeil est un mécanisme de contrôle de sa fragilité et de son architecture souvent ignoré dans le domaine.

En somme, ma thèse permet une avancée de notre vision du sommeil NREM comme étant un état dynamique et hétérogène dont les mécanismes neuronaux sous-jacent, en conditions normales et pathogéniques, sont clefs pour la formulation d'hypothèses testables visant à la guérison des patients souffrant de troubles du sommeil.

Introduction

1. Waking up from sleep

Why do we sleep? This question is still to date a deep mystery. Its functions remain elusive, despite being present from a primitive quiescent state to the sleep characteristic behavior that we easily identify, in every branches of the animal world. As Alan Rechtschaffen pointed out: “If sleep doesn’t serve an absolutely vital function, it is the greatest mistake evolution ever made.”. Indeed, once asleep, an organism stops to work for finding food, water or for mating. Moreover, the reduced responsiveness increases the risk of predation. The benefits associated to sleep functions must therefore be superior to the above-mentioned pressures, and the consequences of a perturbed sleep proportionally harmful. There are many hypotheses about the functions of sleep (Krueger *et al.,* 2016), that emerged over the years that I will summarize here in a non-exhaustive manner. I will then emphasize how waking-up is an integral part of sleep and how it is relevant for my thesis specifically.

One function hypothesized is that sleep would be a state where immune functions and recuperation from infectious disease would be favorized. The immune system is indeed boosted by sleep and weakened by sleep loss (Besedovsky *et al.,* 2012; Imeri & Opp, 2009). Although this hypothesis is greatly supported by scientific evidence, it does not explain the need for disconnection from the environment. It is therefore likely that this property of sleep emerged later as an opportunistic evolution within this state of inactivity.

The inactivity of sleep is by itself serving an important function of reducing caloric use. In an environment with finite resources and day-night cycles, it is indeed an advantage to save energy while foraging is prevented or too dangerous. Reduction of caloric use could represent the original function of sleep, but again, why the disconnected state from the environment (Krueger *et al.,* 2016)? A possibility could be that this disconnected state is necessary to save energy at the brain or neuronal circuits level specifically. Studies using position emission tomography indeed demonstrated that the glucose consumption of the human brain is twice as low during slow wave sleep compared to wake (Kennedy *et al.,* 1982). In addition, it has been observed that sleep loss impaired cognitive performance (Belenky *et al.,* 2003). For example, the performance degradation in words recall and cue reaction time is proportional to previous wake-time and is subsequently restored by sleep (Rosa *et al.,* 1983). It has been proposed that the decrease of performance might be due to microsleep events in the related area of the task, itself resulting from a continuous usage of the neurons (Van Dongen *et al.,* 2011). Therefore, neurons appear to need a time off after use for metabolic replenishment, in order to maintain waking efficiency.

Interestingly, rapid-eye-movement-sleep (REMS), which transiently occurs during mammalian sleep, is a state where paradoxically, the brain metabolic rate is even higher than in wakefulness (Braun *et al.,* 1997). This suggests that metabolism replenishment is not the only function of sleep. For example, the hypothesis that sleep serves a function to maintain and improve cellular circuit connectivity has received a plethora of experimental evidences (Krueger *et al.,* 2016). Sleep is indeed accompanied by a variety of specific brain plasticity/connectivity mechanisms promoting relevant memory consolidation and adaptation to specific tasks or environment (Abel *et al.,* 2013; Inostroza & Born, 2013). In opposition, sleep loss is known to impair memory and adaptations (Rasch & Born, 2013). An explanation for the disconnection from the external world has even been associated with this hypothesis: it would be necessary to prevent new inputs "polluting" the consolidation of relevant information (Krueger *et al.,* 2016; Tononi & Cirelli, 2014).

While the entire functions of sleep are still unknown, sleep scientists strive to deepen the knowledge about this peculiar state. To study it, it is necessary to define it clearly as a behavior. To classify a behavior as sleep in a species, the following points need to be observed (i) prolonged behavioral quiescence, (ii) a species-specific posture, (iii) increased arousal threshold to respond to external stimuli (iv) rebound following sleep deprivation and (v) reversibility upon stimulation (Piéron, 1913).

This last specific aspect of sleep, its reversibility, is particularly relevant for my thesis. Sleep is indeed distinct from other inactive states such as coma or death, as responsiveness to external stimulus is only reduced and not abolished (Andrillon & Kouider, 2020). The specific neuronal circuit activity measured by electroencephalography (EEG) is as well different compared to the one observed during general anesthesia, a state in which reversibility is prevented by a pharmacological agent (Akeju & Brown, 2017). The propensity to wake-up both spontaneously or in response to an external stimulus are sleep features that can be measured and probed respectively, and that give relevant information about how specific species sleep (Keene & Duboue, 2018; Siegel, 2005). Arousability in response to an external stimulus for example can be measured and give great insights. The traditional way is to measure the arousal threshold (further developed in the next chapter), which requires an intervention. Although it is difficult to measure it in the wild (Siegel, 2005), it provides a great tool to probe sleep in laboratory or in clinical settings. In terms of spontaneous arousals, prey species have a more fragmented sleep than carnivorous species, suggesting that sleep architecture may adapt to ecological constraints (Campbell & Tobler, 1984). This arousability can however be perturbed giving rise to an abnormally elevated number of arousals, evoked or spontaneous. In chronic pain conditions for example, patients complain to suffer from ill-timed awakenings. Understanding the mechanisms behind increased arousability is therefore paramount to better understand the disturbances and potentially design new treatments.

However, full scale arousals are not the only type of perturbation observed, and most likely many other forms, or partially expressed forms are relevant for people and patients. Indeed, sleep and wake are not mutually exclusive and can sometime coexist in certain cases such as sleep-walking, or open to debate, during dreaming (Siclari *et al.,* 2017). The sleep-wake transition zone is thus not always that sharp (Andrillon & Kouider, 2020) and modified in many diseases. There is still a lot to unravel on these states and their substates, their functions, interactions and how they are perturbed by pathological conditions.

2. Diversity of awakenings

One of the defining characteristics of sleep is its rapid reversibility to wakefulness. The process of waking-up is thus an integral part of a normal sleep regulation. While waking-up is a common-day and mostly effortless experience for all of us, waking up in physiological terms involves a complex coordination between the physiology of the brain and the body. At the level of the brain, the EEG readings change from a highly synchronized slow rhythm state to a desynchronized, seemingly more active and heterogenous state. At the level of the body, the autonomic balance dominated by the parasympathetic system during sleep, is edging back toward higher metabolic activity with the activation of the sympathetic system. Among the consequences, we observe increases in heart rate, blood pressure, breathing rate and body temperature (P. Halasz *et al.,* 2004).

Clearly, the rapid and complete transition from sleep to wakefulness at the onset of the day is the most striking and physiologically best described form of awakening. However, many more events during the night can be classify as such. The American Academy of Sleep Medicine (AASM) defines the scoring rules of an awakening from NREM sleep in humans as follows: *"Score arousal during sleep stages N1, N2, N3, or R if there is an abrupt shift of EEG frequency including alpha, theta and/or frequencies greater than 16 Hz (but not spindles) that lasts at least 3 seconds, with at least 10 seconds of stable sleep preceding the change. Scoring of arousal during REM requires a concurrent increase in submental EMG lasting at least 1 second."* (Berry *et al.,* 2017). This definition surely helps the scoring of arousals but encompasses a much greater variety of how arousal can physiologically arise.

Beside the case of the most obvious awakenings consciously perceived and remembered, it has long been noted that the physiological processes underlying full wake-up may not always occur altogether (P. Halasz *et al.,* 2004). This suggests that the process of waking up may not always be complete and can involve only some and not all physiological parameters described above. For example, wake-ups can take the form of transient wake-related frequencies in the EEG without autonomic changes (P. Halasz, 1998), transient heart rate increases or limb

movements (Ferri *et al.,* 2017; Sforza *et al.,* 2000). A further diversity exists in the origins of arousals. Some of them are sensory induced, when a clear external stimulus is ascertained as their cause, and some are considered "spontaneous" when no obvious cause can be distinguished.

In addition to their intensity, composition, and origin, it has been shown that wake-related events can occur only locally in some brain areas without inducing a full awakening (Nobili *et al.,* 2011; Siclari *et al.,* 2017). This highlights the fact that the sleep state is not present to the same extent and simultaneously everywhere in the brain. Moreover, there are observations that the border zone between sleep and wake is not always that abrupt in time (Andrillon & Kouider, 2020). This suggests that there exist transitory states with characteristics that are intermediate between full-fledged awakening and sleep. Understanding the arousal diversity, their causes, and consequences therefore helps to characterize sleep as a continuous and heterogenous process, as they inform on the specific substate of the sleeper before waking up.

This chapter serves to provide an overview over these different manifestations of the transition process between sleep and wakefulness. My goal is to highlight some of the different physiological correlates that have added to the notion of this diversity. In presenting this overview, I will be in a position to situate my research results as novel contributions to further enlarge this diversity in the context of physiological and pathophysiological sleep.

2.1 Sensory stimulus-induced wake-up

Introductory remarks Although from an external point of view sleep is a state of disconnection from the environment, this disconnection is not complete. The most obvious evidence for this is that at any point during NREM or REM sleep, sensory stimuli can rapidly induce wakefulness (Andrillon & Kouider, 2020; Neckelmann & Ursin, 1993). Here I will first introduce seminal experiments/evidence/examples that link external stimulus of different modalities to waking up and how they are studied using the arousal threshold. I will give a particular focus on painful stimuli, as they are most relevant for my thesis and seem to receive a special treatment by the sleeping brain compared to other modalities (Claude *et al.,* 2015). Subsequently, I will introduce the neuronal mechanisms thought to be responsible for the loss of consciousness and representing the barrier that the stimuli must overcome to induce a sleep-wake transition (Andrillon & Kouider, 2020). Finally, I will introduce the locus coeruleus (LC) and some of its downstream targets, as they represent likely candidates for the detection of external stimuli, their integration, and the provoking of the switch from sleep to wake.

Sensory stimuli can induce wake-up. Interestingly, for the case of NREM sleep, every sensory modality except olfaction (Stuck, 2010; Stuck *et al.,* 2007) can be used to induce an

awakening. There have been many studies in human and animal models using different stimulus modalities and assessing their awakening potential. Using sound, touch (Kato *et al.,* 2004) (*Figure 1*), visual (Shang *et al.,* 2008), thermal (Lavigne *et al.,* 2000), taste stimuli (Stuck *et al.,* 2016) and as well external nociceptive stimuli (Bastuji *et al.,* 2008; Drewes *et al.,* 1997). Several general principles have emerged from these observational studies.

First, the probability of arousal depends on the intensity of the stimulus. Indeed, the intensity of the stimulus has even been used to define the arousal threshold. This useful measure is defined as the stimulus intensity required to cause an awakening and was used since a long time as an objective measure of sleep and sleep depth (M. H. Bonnet *et al.,* 1978; Rechtschaffen *et al.,* 1966). By playing sounds at specific moments, various arousal thresholds were identified depending on the sleep stage and the sleep depth (Blake & Gerard, 1937). For example, in rats, which unlike mice display multiple non-rapid-eye movement-sleep (NREMS) stages as in human, it was demonstrated that the arousal threshold is the highest in NREMS 2. As well, the threshold is higher at the beginning of the sleep phase, correlating with high delta power (Neckelmann & Ursin, 1993), a marker of sleep homeostasis as it represents sleep depth and sleep propensity that increases with time spent awake, and decreases during sleep (Borbely *et al.,* 1984).

Second, coupling two modalities like sound and touch at the same time has a higher chance to induce an awakening than sound or touch alone, suggesting a summation mechanism and a shared integration (Kato *et al.,* 2004).

Third, the saliency of the stimulus also plays a role. Using the person's own name for example, has a higher chance to induce an awakening (Portas *et al.,* 2000). Therefore, it seems that a specific weight is associated to each stimulus depending on their origin, intensity, and saliency, and that they are summated until the threshold is reached, provoking an awakening.

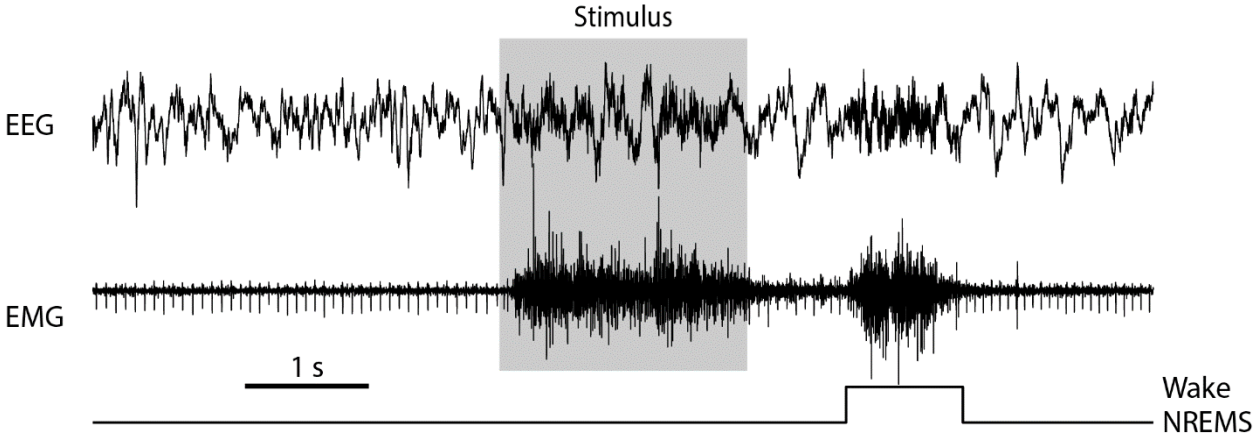

Figure 1. EEG and EMG traces in mice showing an example of an arousal induced by a stimulation taken from one of our datasets. Here the stimulation is a 2 s mild vibration from a motor attached close to the head implant of the animal.

Arousals in REMS. The case of REMS induced arousal is as paradoxical as is this form of sleep. The arousal threshold is comparable between NREMS and certain parts of REMS (Ermis *et al.,* 2010), but the neuronal activity in REMS being closer to wakefulness, raises the question of why sensory stimuli are not fully perceived. Indeed, the appearance of dreams demonstrates that conscious processing is somehow preserved. Moreover, It has been shown that auditory responses are as well are preserved in REMS, as it is the case in NREMS (Nir *et al.,* 2015). The propensity to process a stimulus is also dependent on its saliency (Perrin *et al.,* 1999). Overall, although the similitude in the responses suggest a common mechanism of dissociation from the external world as in NREMS, the profound differences in activity likely underlie the existence of two different ways of disconnection which remain to be identified (Andrillon & Kouider, 2020).

Nociceptive stimuli induced wake-up. A particular case concerns nociceptive-induced awakening. Nociception, further developed in chapter 3, is the system responsible for the detection of a potentially dangerous stimulus and its interpretation as a negative feeling. It has been demonstrated that nociceptive stimuli, unlike other modalities, have an equal chance to induce a wake-up in every sleep stage (Lavigne *et al.,* 2004) and an overall higher chance to induce an awakening than other modalities (Bastuji *et al.,* 2008; Lavigne *et al.,* 2000). Moreover, a study showed that laser-induced nociceptive stimuli during the N2 stage of NREMS have the same arousal properties if triggered inside or outside sleep spindles, which failed to depress the associated cardiovascular activation (Claude *et al.,* 2015). Sleep spindles, transient activity in the 12–15 Hz range in NREMS (L. M. J. Fernandez & Lüthi, 2020) are indeed moments when the arousal threshold is increased (Schabus *et al.,* 2012), for example when facing other challenges such as a noisy environment (Dang-Vu *et al.,* 2010). This last information illustrates the strength of nociceptive inputs to induce an awakening. It suggests that because of their highly survival purpose, their processing has an "open access" to higher centers, usually not granted to other modalities (Claude *et al.,* 2015).

Neural mechanisms of arousal from NREMS. Although sensory-induced arousals are ubiquitous and part of everyone's life, the knowledge about the brain's mechanisms to induce the switch from sleep to wake in response to a sensory stimulus is still incomplete. There are several mechanisms that have been brought forward and that most likely play complementary roles in triggering or protecting from sensory induced arousals. The first is the thalamocortical gating hypothesis, which is a mechanism proposed to be responsible for the loss of consciousness during NREMS. The thalamus is indeed the last step for sensory stimuli to pass before reaching the cortex. Because of its strategic position and functions, it has been proposed in 1994 by McCormick and Bal that the thalamus could close the gate to the cortex and thus, isolate it from the outside world during sleep (McCormick & Bal, 1994). This gating hypothesis relies in part on specific sleep rhythms, hallmarks of NREMS, generated in the thalamus and the cortex. The previously mentioned spindles, known to limit the flow of information from thalamus to cortex

(L. M. J. Fernandez & Lüthi, 2020) and the slow waves, off-periods observed in the cortex appearing on a rhythm of around once every second (Massimini *et al.,* 2003; Steriade *et al.,* 1993). While this hypothesis could account for momentary variations of the arousal threshold in NREMS, it fails to explain the complete disconnection that needs to be overcome to achieve a wake-up. Indeed, sleep spindles and slow waves are not omnipresent in NREMS and almost absent in REMS, whereas as mentioned before, the arousal threshold is comparable between NREMS and certain parts of REMS (Ermis *et al.,* 2010). Moreover, olfaction, a sensory modality that fails to induce awakening (Stuck *et al.,* 2007), is not conveyed by the thalamus and would thus not be stopped by a thalamic gating. Finally, sensory inputs where shown to still reach the cortex during NREMS and even be processed without necessarily inducing a behavioral (Andrillon & Kouider, 2020).

Another complementary explanation, the cortical gating hypothesis, proposed that the information could reach the cortex in sleep, but its propagation would be limited within it (Esser *et al.,* 2009). Perturbational studies using Transcranial Magnetic Stimulations indeed demonstrated that during NREMS, the pulses were short-lived and confined to the area where they were triggered, as opposed to long-lasting and propagating in wakefulness (Massimini *et al.,* 2005). Together these two gating hypotheses could therefore account for the loss of consciousness during sleep and the intrinsic variation of the arousal threshold within NREMS.

By which mechanism this functional connectivity could be reactivated in response to external stimulus is still not completely known. Many systems are known to play a role in the switch between sleep and wake (de Lecea *et al.,* 2012; Tyree & de Lecea, 2017). However, some neuromodulator arousal systems known to innervate the forebrain are specifically activated by sensory stimuli and thus represent prime candidates for this arousing role in response to external factors.

For example, the LC is the major noradrenergic brain area and known to be important to maintain attention during wakefulness. Not completely silent in NREMS (Aston-Jones & Bloom, 1981), neurons in the LC respond with short-latency (11.2 ± 1.9 s) action potential or group of action potentials to arousal triggering sound stimuli, and as well, start firing before spontaneous awakenings (Takahashi *et al.,* 2010). Moreover, it has been observed that its activity level is a good correlate of the momentary arousal threshold (Hayat *et al.,* 2020) and of enhanced vigilance, measured by resting state connectivity in the salience network (Zerbi *et al.,* 2019). The LC is likely just one of the areas important for arousals, but it has been best characterized in terms of its anatomical and physiological profile to contribute to the sleep-wake switch.

The forebrain targets of this ascending arousal system have so far focused on a subgroup of thalamic nuclei referred to as intralaminar and midline nuclei. The LC projects into this area as well as in autonomic premotor nuclei, and forebrain areas (Samuels & Szabadi, 2008). Key targets

of the LC able to induce a rapid state transition were identified as a subsequent point of integration of wake promoting signals, within this intralaminar and midline nuclei of the thalamus (Beas *et al.,* 2018; Van der Werf *et al.,* 2002). Specifically, it was recently demonstrated that the calretinin neurons in the dorsal medial thalamus (DMT), were sufficient to trigger a brief arousal by projecting subsequently into forebrain areas. Indeed, their activity was preceding arousal, and their activation using optogenetic could trigger short or long arousals depending on the stimulus duration (Mátyás *et al.,* 2018). The LC is therefore in a strategic position to receive external information and convey them to areas able to prepare for and provoke an awakening.

In summary, studies investigating the specific pathways taken by each modality, how they are processed by the awake or sleeping brain and testing their propensity to induce an awakening, helped to select and distinguished specific lines of investigations. Moreover, understanding how the brain disconnects from the environment and which barriers need to be overcome to achieve an awakening helped to pinpoint specific areas with the necessary functions. Finally, identifying specific nuclei responding to external stimulus, characterizing their activity and anatomical projections and subsequently testing functionally their capacity in inducing a state transition, greatly helped the understanding of this complicated and efficient detector/effector alarm system responsible for this behavior that we experience every day.

2.2 Spontaneous wake-ups without an obvious sensory stimulus

Introductory remarks. As their name implies, spontaneous arousals are wake-ups without obvious cause and occurring seemingly randomly. Like arousals caused by external factors, they are composed of electrophysiological and somatic transient changes, such as wake-related frequencies and heart rate increases. The rules to score them in human are the same as for stimulus-induced arousals, which makes their distinction from sensory-induced arousals, if necessary, somewhat complicated in a non-controlled environment (Berry *et al.,* 2017).

Here I will focus on the brief transient events with a switch back into sleep, referred to as the brief- or microarousals. They are ubiquitous in everyone's sleep, we typically don't remember experiencing them and they are considered normal sleep events (P. Halasz *et al.,* 2004). They are particularly relevant for my thesis as they are a marker of sleep fragmentation and often associated with sleep perturbation, as their amount correlates with the feeling of fatigue on the next day (Stepanski *et al.,* 1984). First, I will give an historical review of the different kind of brief arousals described in human, their characteristics, and their regulation. I will then focus on the K-complexes, grapho-elements that are the visible reaction of the sleeping brain to a perturbative event. Well described when evoked from an external input, but appearing as well spontaneously, they are particularly relevant for my thesis as they might represent the visible effect of internal perturbative cues (see Discussion). I will continue by describing the cyclic alternating pattern

(CAP) sequences, as they highlight an important cyclic property of sleep with recurrent reactions to perturbative events.

Historical review. Using polysomnography (PSG), the first description of spontaneous exit out - and followed by a quick return - into NREMS was by the French group in 1971 (Schieber *et al.,* 1971). They called it "*phase d'activation transitoire*" (PAT) with the following description: *"Increase in EEG frequencies in conjunction with decrease of amplitudes, disappearance of delta waves and spindles, transitory enhancement of muscle tone or phasic appearance of groups of muscle potentials, movements of the limbs or changes in body posture, transitory rise in heart rate.*" In summary, according to the AASM rules, these events classify as short wake intrusion events during sleep, followed by a transition back to sleep (*Figure 2*).

The microarousals in human were described later as a PAT of lesser intensity not necessarily accompanied by EMG activity but displaying an increase in heart rate (P. Halasz, 1998) (*Figure 2*). Both the PATs and the microarousals appear in different proportion across different sleep states and depending on the momentary sleep pressure. They occur preferentially in light sleep and in REMS, with a higher propensity toward the end of the resting phase when sleep pressure is low (Schieber *et al.,* 1971).

K-complexes. Another event considered a signature of arousal do not fall into the classical categories of physiological correlates of wakefulness. Indeed, the K-complexes are grapho-elements observed in human, occurring spontaneously or in response to an external stimulus and showing no signs of behavioral change (P. Halasz, 2005; Loomis *et al.,* 1937). This latter case demonstrates that sensory reactivity is preserved in NREM sleep even in the absence of an arousal. Due to their spontaneous or evoked nature, they are hard to classify as they could have their place in the previous chapter as much as this one. I mention them here because they often appear in conjunction with other types of spontaneous arousals such as the previously mentioned PAT and microarousals (P. Halasz, 2005) and that they give insights as how sleep is reacting to spontaneous or evoked events. In the EEG signal, they are defined by a negative deflection, followed by a positive component with a minimum duration of 0.5 s (Da Rosa *et al.,* 1991). They can appear isolated or in bursts of two or more (*Figure 2*), in which case they are accompanied by an increase in heart rate, although not the extent of the increases observed in PAT and microarousals (Sforza *et al.,* 2000). In terms of their appearance throughout the resting phase, they are more numerous in the descending slope of each sleep cycle and tend to decrease in the course of the night (Peter Halasz & Bódizs, 2013), a dynamic opposed to the PAT and microarousals, suggesting an antagonizing relationship.

The role of K-complexes is still not completely elucidated. As of now, the title of two-faced Janus is often used to refer to them (Ioannides *et al.,* 2019). Indeed, as they accompany spontaneous and evoked perturbations, they are considered an arousal event. However, using

micro- and macro-electrode arrays recordings in epileptic patients undergoing intervention evaluation, it was demonstrated that K-complexes, both spontaneous and evoked, are not distinguishable from the down state of the slow waves (Cash *et al.,* 2009). In that regard, they are also considered sleep deepening and protective events (Colrain, 2005; De Gennaro *et al.,* 2000; P. Halasz, 2016). Therefore, they are thought to result from the processing of a stimulus and the suppression of arousal drive to maintain the person asleep (Jahnke *et al.,* 2012); (Blume *et al.,* 2018). Their sleep promoting properties even lead to successful attempts at artificially deepening sleep using timed sound stimulations (Bellesi *et al.,* 2014).

Local aspect of K-complexes and arousal. An important aspect of K-complexes is their topographic distribution across the brain. For a time, they were thought to be non-specific diffuse events, regardless of the specific stimulus modality (P. Halasz, 2005). Later however, studies revealed the activation of specific sensory areas during the induction of K-complexes. This suggests that there is a local aspect to them, concomitant or preceding their generation and propagation in the brain. For example, a study assessed the response to three modalities (auditory, somatosensory, and visual) in NREMS in human, using source modeling of high-density EEG recordings. The negative deflection of the K-complexes was diffused, and more pronounced for auditory stimulus. The activation part of the K-complexes however seemed to have a degree of specificity for the primary sensory cortex corresponding to the modality (Riedner *et al.,* 2011). Moreover, recently their resemblance to slow-waves helped in finding that two types exist. The type I is widespread and larger, and it predominates in the early phases of sleep whereas the type II is smaller, detected more locally and arises later in sleep (Bernardi *et al.,* 2018). These results indicate that K-complexes are characterized by both a diffused answer topographically consistent for different modalities, and a local response in primary sensory area that is sensory specific.

K-complexes as reactive sleep protective event, with a local aspect specific to sensory modalities are thus a promising target of investigation for possible alteration in pathological conditions. Moreover, the fact that they can appear spontaneously suggests that either internal cues can elicit them, or that they can appear in response of naturally occurring variation in sleep depth.

Noteworthy, not only K-complexes, markers of sleep consolidation, have a local aspect. A study on data recorded from scalp and intracerebral electrodes placed in the motor cortex and the dorso-lateral prefrontal cortex demonstrated that the motor cortex showed recurrent wake-like activation in NREMS lasting from 5 to more than 60 s. Interestingly, this form of local wake was accompanied by an increase in slow wave activity within the prefrontal cortex and measured through scalp electrodes (Nobili *et al.,* 2011). This highlights that different cortical areas support the coexistence of wake-like and sleep-like electroencephalographic patterns and that a balance seems to be maintained between areas to maintain sleep.

Temporal considerations: the example of CAPs. On top of the local aspect, we observe variations in the temporal aspect for perturbative/reactive events. Arousal events, PAT, microarousals and K-complexes indeed tend to appear in phases of repeated periods with around 1-minute intervals. Called cyclic alternating pattern (CAP), these periods are described through visual observation of phasic events in human NREMS (Terzano *et al.,* 2001). They are composed of visually recognizable repeated sequences of transient EEG changes, in the form of abrupt variation in the EEG spectral properties (Terzano & Parrino, 2000). CAPs occur mostly at moments of NREMS 2 onset or termination but can appear in every sleep stage. They are divided in 3 categories depending on the type of perturbation they contain. The type A1 and A2, containing grapho-elements such as K-complexes or delta bursts (*Figure 2*) and as such, thought to be a response to an external or internal challenge to the sleep continuity. In that case and analogous to the K-complexes themselves, they are proposed to represent an active attempt to consolidate sleep. CAP of Type A3 are scored when this attempt fails, or sleep is too unstable and we observe events reminiscent of PATs and microarousals (Terzano *et al.,* 2001). It has been proposed that these recurring periods of activation during sleep would be moments when sensory inputs are facilitated and thus, increasing the detection of physiological and pathological events posing a threat to sleep continuity (Mendez *et al.,* 2016; Terzano *et al.,* 2005). To echo the concepts developed in the previous chapter, it thus seems that brief awakenings would appear at moments of lowered arousal threshold containing an internal or external perturbation.

Overall, CAP and the spontaneous arousals, by acting as a reaction to a perturbation, might allow for the measurement of yet invisible threats. Their type, cyclic occurrence and intensity give valuable information on sleep quality. Indeed, the amount and type of arousal correlate with subsequent daytime sleepiness (Stepanski *et al.,* 1984), and several diseases are associated with increased number of microarousals. In consequence, the quantification of microarousals and specifically of the CAP rate has become a classical measure of sleep perturbation. As such, the automatic detection of CAP sequences is still to date a matter of intense research (Arce-Santana *et al.,* 2020; Largo *et al.,* 2019). Such detection allows for high throughput analysis in the population and gave promising results, for example, linking CAP rate and subjectively reported sleep quality (Hartmann *et al.,* 2020). The density of such events is thus a great marker of sleep perturbation in physiological and pathological conditions, and their fine characterization gives relevant information on the type of perturbation that might elicit them.

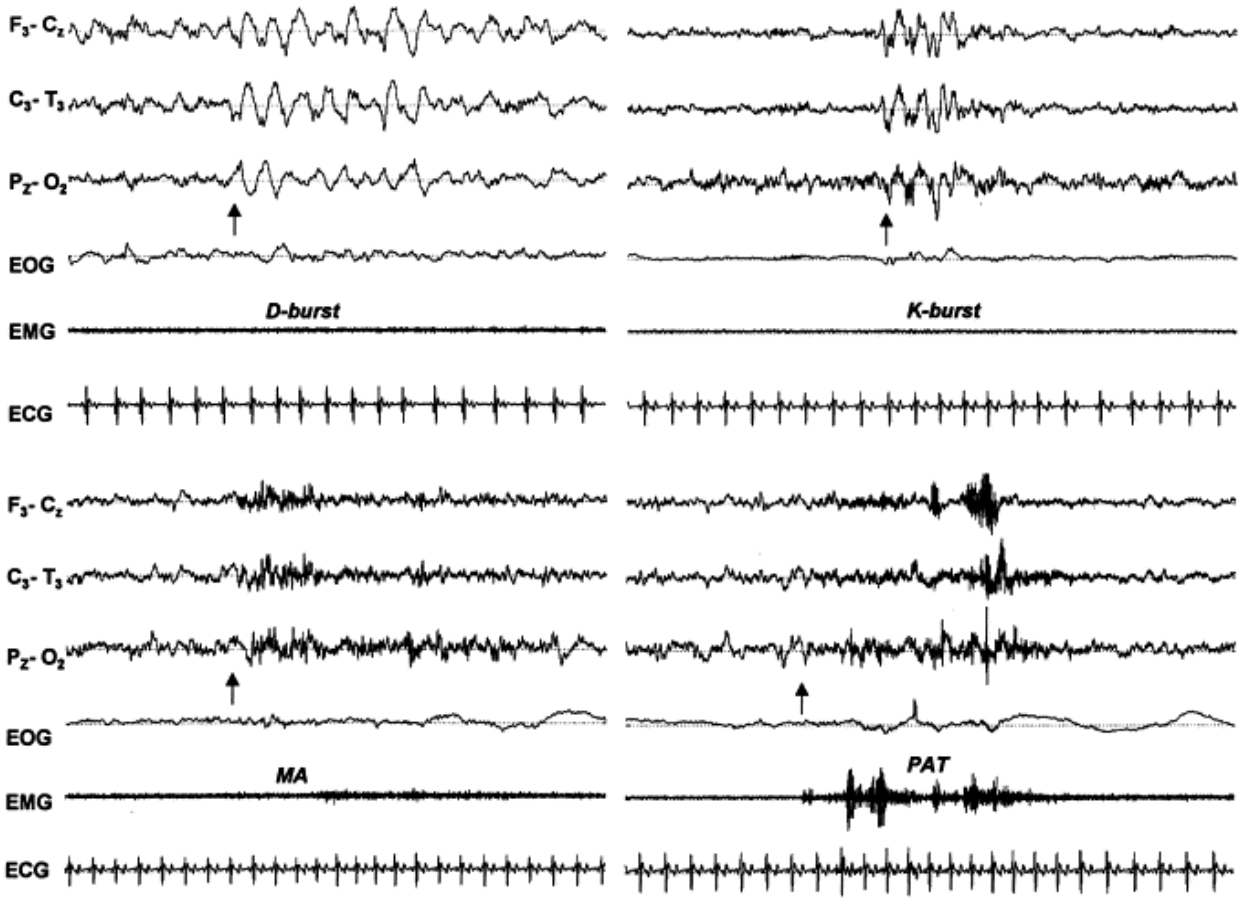

Figure 2. Obtained from Sforza et al., 2000. Example of delta burst, K-complex burst, microarousals and PAT in human from polysomnography recording.

Rodent studies for mechanisms and functions. In animals, microarousals are also observed and they are like the human events as they are defined by the following characteristics. First, they are short wake events (<16 s) displaying EEG desynchronization, transient high frequency appearance during NREMS and often accompanied by EMG activity (Franken *et al.,* 1991; Tobler *et al.,* 1996) (*Figure 3*). The upper duration limit of 16 s is a convention that has turned out to be useful for sleep architectural and regulation studies, and to characterize sleep fragmentation in mutant mice (Franken *et al.,* 1999). Second, studies in rodents show that microarousals are more frequent toward the end of the resting phase and that experimentally, sleep deprivation reduces their frequency in sleep which renders them useful to study homeostatic sleep regulation in rats (Franken *et al.,* 1991; Tobler *et al.,* 1996) and mice (Franken *et al.,* 1999). Finally, a common relationship exists in the distribution of brief wake episode durations, across at least four mammalian species; mice, rats, cats, and humans (Lo *et al.,* 2004). Therefore, animal models reproduce the events observed in human and proved to be appropriate to systematically study microarousals generation, their purpose, and the consequences of their dysregulation.

Rodent models have been useful to understand the neural origins of spontaneous arousals. They opened the possibility to understand the nature of these events and their generation by directly interrogating the neuronal circuits involved. One example involves the histaminergic system. Histaminergic neurons are located in the tuberomammillary nucleus in the posterior hypothalamus and project all over the brain (Haas & Panula, 2003). The histamine receptor 1 (H1R), mediates an arousal response when activated (Huang *et al.,* 2006). Its deletion in a KO mouse or the use of an antagonist reduced the baseline proportion of brief awakenings in the resting phase. Moreover, the increased number of brief-arousals normally induced by the histamine release using ciproxifan was prevented in the H1R KO mice et (Huang *et al.,* 2006). This suggests that H1R is involved in the state transition from sleep to wake in the context of microarousals.

Another system, the cholinergic one, was also found to be associated with microarousals. This system is known for its properties in inducing REMS through projections within the pons (Sakai *et al.,* 2001), and for its arousal properties through ascending projections in the cortex (Jones, 2003). Interestingly, mice lacking the β2 subunit of the acetylcholine receptor show a more consolidated NREMS containing fewer microarousals and longer REMS bouts than their controls (Léna *et al.,* 2004). These results show that the cholinergic system is a contributor of the organization of sleep in its capacity to interrupt NREMS and by timing REMS onset and duration.

Evidences of circuits mediating both REMS transitions and microarousals lead to hypothesize on a possible function for them. Indeed, more recently a group proposed a novel function based on their multi-site local field potential (LFP) recordings in mice. They showed a progressive increase in the coherence in the theta range between the hippocampus and cortex preceding microarousals, a process that usually lead to a REMS transition. They proposed that the microarousals would arise as a protection against an untimed transition to REMS, essentially maintaining the brain in NREMS with this quick reversal (Dos Santos Lima *et al.,* 2019).

To go further onto the protective effect of microarousal, several studies linked the appearance of microarousals with internal danger cues. As a good example, in sleep apnea the increase of carbon dioxide is perceived by the brainstem parabrachial neurons and subsequently trigger brief arousals (Kaur & Saper, 2019). This was confirmed in animal through optogenetic activation of parvalbumin neurons in the basal forebrain, the ones normally activated by the carbon dioxide sensing pathway. Interestingly, they were also activated by auditory stimuli and their optogenetic activation could reliably produce brief arousal identical to spontaneous ones (McKenna *et al.,* 2020).

Spontaneous arousals, by their appearance, generation and supposed functions are thus comparable to arousals facing external stimulus. As the knowledge of their origin and diversity unfolds, the gap between spontaneous and induced arousals is reducing. However, further

studies are still needed to understand how the sleeping brain reacts to internal cues. Furthermore, the origin and nature of some of the internal cues able to trigger spontaneous arousal are still unknown. By itself, this represents a promising novel field of investigation commensurate to the one questioning which and how external stimulus are causing awakenings. As we saw in the previous chapter, nociceptive stimulus leading to the experience of acute pain represents an external drive particularly potent at inducing an awakening. Could pain, through its maladaptive transition to chronic pain, switch from external to internal cue and perturb sleep through the mechanisms mentioned above?

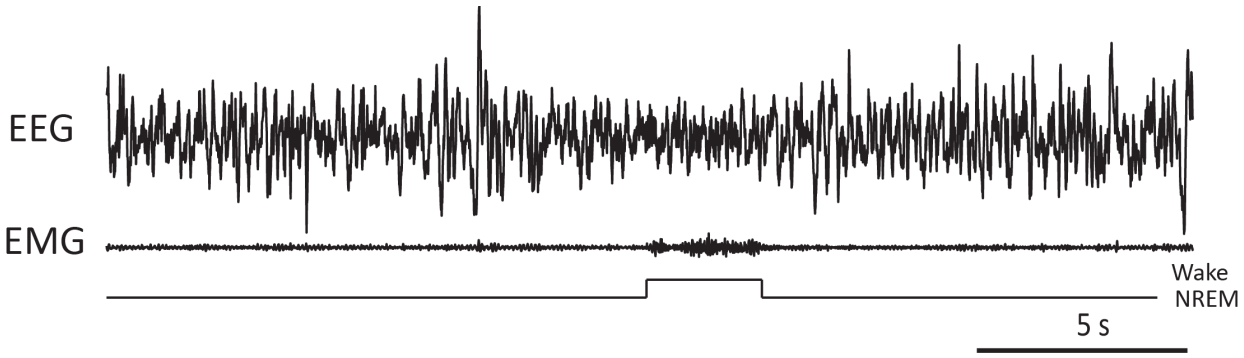

Figure 3. Example of a microarousal observed in one of our recording in mice. Note the transient high frequency EEG activity and concomitant increased EMG activity.

3. What is pain?

To better define the question concluding the previous chapter, I must introduce the nociceptive system. Unlike sleep, the reason for the existence of an acute painful experience is obvious. Evolving from a rudimentary thermal or chemical avoidance system in unicellular organisms, nociception, described by Sherrington in 1904, is an alarm system able to detect harmful stimulus and to protect from them, even before they occur (Woodworth & Sherrington, 1904). To date, pain is considered as a sensory and emotional experience protecting from actual or potential tissue damage (International association for the study of pain IASP definition). A good example of the necessity of this system is the consequence of its absence in patients suffering from congenital insensitivity to pain. Indeed, this syndrome require constant vigilance from themselves and their surroundings (Axelrod & Hilz, 2003). It is a rare genetic condition where the patient is unable to transmit peripheral nociceptive inputs along the primary sensory neuron. Similarly, but at the opposite end of the nervous system, pain asymbolia is a very rare condition where focal brain deficit (trauma, ischemia, tumor, etc.) in cortical areas involved in the emotional component of pain can lead to total impassivity to pain and can abolish reaction to intrusive stimulus (Gerrans, 2020). In both cases, other sensory modalities (touch, proprioceptive, etc.) are intact. Despite their devastating consequences, these syndromes shed the light on important mechanisms involved from the peripheral detection of harmful stimuli to the formation of the pain perception and the resulting avoidance behavior.

To understand the pain modality as a stimulus able to induce an awakening, I will introduce how they are detected and interpreted as pain by the body and the brain. Particularly relevant for the main question of my thesis, I will then describe chronic pain, a multifaceted pathological condition resulting from maladaptive pain inputs at the periphery and central level. Finally, I will mention recent advances on how pain feeling is coded in the brain and how electrophysiological rhythms helped and might help in the future to understand and measure this integrative process. This last aspect of pain and chronic pain is particularly interesting in the understanding of the potential effect of pain on sleep, as some of the rhythms overlap and therefore can help in formulating hypothesis.

3.1 From sensory terminals to the feeling of pain

Introductory remark. As the definition indicates, nociception is divided in two main steps. The detection of the stimulus at the periphery and its interpretation as painful at supra spinal central level. Normally sequential, these two processes can occur individually in some pathological conditions. In the case of a classical pain stimulus integration, the peripheral detection comes first (*Figure 4*). The path taken by a nociceptive stimulus in normal and

pathological condition is particularly relevant since it might represent the root of the sleep alterations observed in chronic pain. Thus, I will first describe how a painful stimulus is detected and conveyed to the spinal cord. Then, I will mention the main steps necessary for its interpretation in the central nervous system (CNS) and the various modulatory forces involved.

Stimulus detection. The detection of an insult, such as a pinch or a burn, is accomplished by a specific kind of peripheral neurons, the nociceptive neurons (*Figure 4*). Located in the dorsal root ganglions (DRG), or in the trigeminal ganglia, these pseudo-unipolar neurons have a peripheral ending into the innervated tissue and a central ending into the dorsal horn of the spinal cord. They are equipped with specific pain receptors, the nociceptors, able to detect mainly three different modalities: thermic, mechanic, and chemical (Dubin & Patapoutian, 2010). More recently, studies revealed that these nociceptors can even detect bacteria and other microorganisms threatening tissue integrity (Chiu *et al.,* 2016). The transduction of the input, step by which the stimulus is transformed in an electrical signal is achieved by these nociceptors in a similar way, albeit with a higher threshold, or with other sensors, as the classical sensory perception achieved by mechanoreceptors for example. This transduction occurs when a somatosensory process facilitates the opening of ion-gated channels, depolarizing the terminals (Martinac, 2012; Nilius & Honore, 2012). Voltage-gated ion channels like the ones of the NAV family then trigger an action potential and initiate the transmission of the signal toward the DRG (*Figure 4*)(McEntire *et al.,* 2016). Regarding this transmission, the classical view is that specific modalities such as mechanical and thermal were respectively conveyed by mildly, A-delta- or not myelinated, C-fibers. However, the complex distribution of nociceptors in primary sensory neurons revealed a large diversity of cell types that goes beyond the common distinction of A-delta and C categories for sensing nociceptive stimuli (Usoskin *et al.,* 2015).

Entry in the CNS and integration. The signal then reaches the first synapse in the superficial layers of the dorsal horn of the spinal cord. These synapses are surrounded by inhibitory and excitatory interneurons, as well as projections from the descending pathways (*Figure 4*) that will contribute to pain modulation (Garland, 2012). The signal is now in the CNS and will travel upward through the spinothalamic or trigeminal tract depending on its origin, body and face respectively. Once the input has reached the thalamus, specifically in the ventral posterior lateral (VPL) and the ventromedial nucleus (VPM), it is relayed to the cortex in somatosensory areas through the lateral path and to prefrontal and insular cortex areas through the medial path (Groh *et al.,* 2018), as well as subcortical areas, including the amygdala, the hypothalamus, the periaqueductal grey and the basal ganglia. The pain sensation results essentially from an integrative process and is divided in at least two main components: (i) discriminative: the location and subjective intensity of the pain, typically thought to be coded in somatosensory areas (Bushnell *et al.,* 1999), and (ii) emotional: the unpleasant and aversive feeling, thought to be mediated in limbic areas. This later sensation is likely taking place within

the insula and anterior cingulate cortex, which are consistently activated by nociceptor inputs (Tracey & Mantyh, 2007). Together, these interconnected areas are called the "pain matrix". They collectively process nociceptive information into the experience of pain and then, project back into the brainstem and the dorsal horn of the spinal cord though the descending pain modulatory system with modulatory power over nociception (De Felice & Ossipov, 2016; Legrain *et al.*, 2011; Melzack, 1999).

Pain output and modulation. This system final output is therefore a measure of the risk associated to the painful stimulus. The intensity of the stimulus itself is of course considered, but the current state and context of the individual is as well important (Leknes *et al.,* 2013). The resulting feeling of pain in response to a nociceptive stimulus, very much like the arousal response to any external one, strongly varies depending on the state of the individual. Motivation plays a critical role for example. It is common sense that athlete competing in a marathon would be powered through their pain, whereas similar pain in a non-competitive setting would alarm the runner. Expectation is as well a strong modulator of pain as placebo studies suggests (Berna *et al.,* 2011; Jensen *et al.,* 2012). The recognition and study of this effect lead to great improvement of pain management by the interactions between the patient and the physiscian (A. Fernandez *et al.,* 2019).

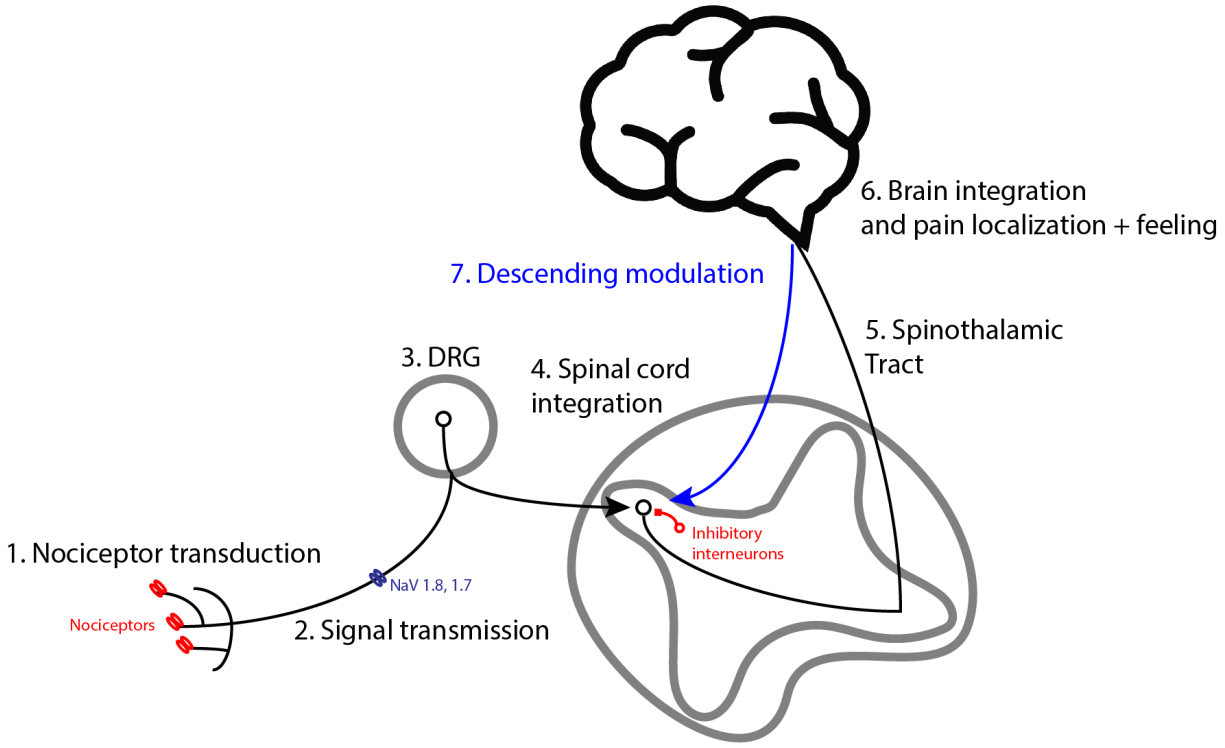

Figure 4. Summarized view of the main steps from periphery to brain, leading to the normal processing of nociceptive information.

3.2 Chronic pain: peripheral and central sensitization

Introductory remarks. The whole pain system starts as a necessary alarm for the survival of the individual. As for the arousal system, there are cases where the system increases its sensitivity in a physiological manner, and cases where we observe a pathophysiological increase in sensitivity. Framing this sensitization process is important for my thesis, as it is the basis of the transition from acute to chronic pain and could have direct effects on sleep. First, we observe a normal sensitization process occurring after repeated stimuli, very intense ones and/or tissue injury. This process is causing tonic pain associated with two major changes in sensitivity called allodynia, where a previously non-noxious stimulus become noxious and hyperalgesia, where an already noxious stimulus elicits a bigger response (Yam *et al.,* 2018). This sensitization is here to remind us to take care of a wound and to decrease movements to promote recovery. This necessary lowering of the pain threshold results from a process that involves LTP (Woolf & Salter, 2000) and returns to baseline after some time once the primary lesion is healed. Unfortunately, this system can become over-responsive, or over-active for much longer periods. When pain outlast its original cause and do not have a protective function anymore, we say that it becomes maladaptive and turns into pathological pain (Yam *et al.,* 2018). Here I will first mention how, using animal models, we can study the transition from injury to chronic pain. As I am using a model of neuropathic pain, I will introduce it with its advantages and limitations. I will then briefly mention the changes occurring through peripheral and central sensitization in the spinal cord. Finally, I will give a bigger overview on the specific changes at the level of the brain upon central sensitization, as they might be directly linked to how the brain sleeps in this pathological condition.

Chronic neuropathic pain and focus on the spared nerve injury model. The transition from acute to chronic pain is a moment of great changes both at the periphery and at the CNS level. Understanding the sequence of maladaptive events unfolding during this transition is paramount to prevent them after an accident or a surgery. Indeed, 10–50% of individuals will suffer from chronic postoperative pain, even after banal surgery (Kehlet *et al.,* 2006). This transition from normality to a hypersensitive state has been studied extensively in animals thanks to multiple models of chronic pain.

Specifically, chronic secondary neuropathic pain, where pain originate from a lesion of the nervous system (Finnerup *et al.,* 2021) and which is the most intractable form of pain, has received a particular interest. Animal models such as the spared nerve injury (SNI), or the chronic Constriction Injury (CCI) have proven to reproduce parts of the human conditions, mainly the pain hypersensitivity (Challa, 2015). The SNI model that I am using is considered severe due to its robust and long-lasting effects. It consists of the ligation and section of two branches of the sciatic nerve, classically the tibial and peroneal, leaving the sural nerve intact (Bourquin *et al.,* 2006; Decosterd & Woolf, 2000). This manipulation induces a reliable increase of sensitivity in the sural

area of the hind paw and nocifensive behavior lasting at least up to one year (Topham *et al.,* 2020). This increased sensitivity can be revealed by performing conventional tests of sensitivity such as the von-Frey for mechanical or plantar for thermal stimulations, measuring allodynia- and hyperalgesia-like behaviors in mice (Bourquin *et al.,* 2006). Even though the main aspects of the disease, the allodynia and hyperalgesia, are successfully modelled in animal, there are other aspects of chronic pain that are much harder to measure and that remain elusive despite promising advances. First, do they experience spontaneous pain as in human, or are they only more sensitive to stimulations? Studies on facial expression would certainly help to partly answer that question, as it was already proven to demonstrate pain and discomfort in animals (Dolensek *et al.,* 2020; Langford *et al.,* 2010). Second, do they reproduce the catastrophizing and the depression often found in patients? Behavioral assessment showed that SNI mice indeed tend develop anxiety and depression-like behavior after a few weeks, but results vary depending on the study indicating that this measure is subject to possible biases (Guida *et al.,* 2020).

The only way to ascertain pain in a patient and to obtain a subjective measure is to ask directly. Models of neuropathic pain are thus hard to characterize, and as often with animal models, present only correlates of the disease phenotype. However, the physiological changes associated with nerve injury, divided in two main part, peripheral- and central sensitization, are reproducible between human and mice and their characterization in animal models greatly improved our understanding of neuropathic pain and its consequences.

Changes upon peripheral sensitization. The first changes occur at the level of the nerve injury where spontaneous discharges are sent to the cell bodies of the nociceptor neurons in the DRG. Next, upon detection of the lesion and the loss of trophic support from the periphery, the DRG neurons increase or decrease the expression of different genes and signaling molecules (Berta *et al.,* 2017). This concerns not only the injured neurons; we observe similar changes in adjacent non-injured neurons that co-mingled in the DRG. This release of signaling molecules in the DRG and at the site of the injury is commonly referred to as the inflammatory soup (Yam *et al.,* 2018) which in turn, generates further spontaneous activity reaching the spinal cord. There would be much more to say about peripheral sensitization as it represents a whole field of research within the pain field. However, this would go beyond the scope of my thesis. The key points here are therefore the spontaneous ectopic activity along the peripheral and central axon branches of the DRG neurons and the increased sensitivity at the innervated area of injured and extending to non-injured neurons.

Changes upon central sensitization. There are compelling evidences that the spontaneous activity from the periphery observed in the peripheral sensitization contributes to the development of the subsequent central sensitization and chronic pain. Indeed, by inhibiting this activity at injury onset using specific pharmacological inhibitors, the long-term increase in sensitivity is prevented (Alexandrou *et al.,* 2016; Ibrahim *et al.,* 2003). The first changes result in

the facilitated response and increased firing of principal neurons within the dorsal horn of the spinal cord, which receive direct inputs from the DRG neurons. The mechanisms leading to these changes are extensively studied (Latremoliere & Woolf, 2009) and comprise for example a loss of inhibition from the neighboring interneurons. As well, it has been noted that immune cells have an important role in inducing and maintaining an inflammatory state which reduces the firing threshold of principal neurons. Indeed, studies demonstrated that T-cells infiltrate the spinal cords and microglia switch to an activated state, changes that were proven necessary to develop chronic pain (Gattlen *et al.,* 2016; Gattlen *et al.,* 2020). As for the peripheral sensitization however, the consequences on the signal conveyed to the brain is the important part for my research. Overall, central sensitization at the spinal cord level results in a gain of function of neurons and circuits along the neuraxis, measurable by the increase in membrane excitability, the reduced inhibitory drive, and the increased synaptic efficacy (Latremoliere & Woolf, 2009).

The changes occurring in the brain upon central sensitization are particularly relevant, since they may directly impact on how the brain sleeps globally, or locally in the concerned areas. For example, in the CCI animal model, it has been observed through ex-vivo patch-clamp technic that the pyramidal neurons in the anterior cingulate cortex (ACC) become more excitable due mainly to a reduced inhibitory drive from parvalbumin interneurons (Blom *et al.,* 2014). This particular aspect was again confirmed later, using in-vivo two-photon calcium imaging in awake mice. They found a bilaterally enhanced activity of pyramidal neurons in the ACC in the absence or presence of pain stimuli after SNI (Zhao *et al.,* 2018).

The primary somatosensory cortex (S1), though to code for the localization and intensity of the painful stimulus is as well subjected to profound changes with central sensitization (Bushnell *et al.,* 1999). It was first revealed through calcium imaging techniques that the pyramidal neurons in S1 were over-active spontaneously and upon nociceptive stimuli 7–8 days after injection of complete freud adjuvant (CFA) in the paw, which produces a chronic inflammatory pain (Eto *et al.,* 2011). The same observation was later observed in SNI, in which it was demonstrated that pyramidal neurons were overactive due to reduced parvalbumin and somatostatin interneurons activity. Interestingly, up-regulating somatostatin interneurons activity using a DREADD approach normalized the pyramidal cell activity and induced analgesia in these animals (Cichon *et al.,* 2017).

Chronic pain therefore is the result of a huge constellation of molecular, synaptic, morphological and circuit alterations all along the periphery and the CNS matrix coding pain. However, the causes and the mechanisms associated to these changes still require investigation (Finnerup *et al.,* 2021; Latremoliere & Woolf, 2009). In summary, the shift toward hyperexcitability is accompanied by a modified signaling and interpretation of stimulus. The facilitation of noxious and non-noxious information to travel along the pain pathway renders stimuli previously not painful, like the mere fact of standing up or say sited for too long, to

become painful. Moreover, nociceptive inputs are generated spontaneously at the periphery and or in the CNS are then falsely interpreted as pain.

3.3 Pain rhythms

Introductory remark. In clinic and in research, pain sensitivity is objectively measured by withdrawal response facing stimulus with increasing intensity. Similar to the arousal threshold, this gives a very good approximation of the individual limits, but lacks several other aspects of pain, such as ongoing spontaneous experience and the emotional part. In patients, this is in part assessed thanks to well-designed subjective scales and questionnaires, but such measures are limited and not always accessible. Therefore, there is an urgent need find a way to rate the pain intensity and spontaneous pain in population that are unable to report it clearly, such as animal models, young infants, or comatose patients. Understanding how pain is coded in the brain, or reflected in the body, from an input in the periphery or because of a disease, is thus of importance to develop such objective measure. Big steps in that direction were achieved by studying the brain rhythms associated to pain. In this part I will first justify the use of such measure in the pain field and explain why they are particularly suited for my question. I will then introduce the literature on how pain is coded and measured through oscillations in the different settings of phasic, tonic, and finally chronic pain. A particular interest on the gamma oscillation must be intertwined as this rhythm represents a promising target as pain biomarkers both in human and animals.

Why studying rhythms. Pain is the result of a dynamic interplay between areas answering the instantaneous demands and state of the individual at a timescale that could not be explained by structural changes (Kucyi & Davis, 2015). How exactly these areas are coding and modeling this information is still unknown. However, as pain result from the fast synchrony and integration between the areas of the pain matrix, it is likely that neuronal oscillations at different frequencies are responsible, or at least, correlate of the pain feeling formation. There is indeed evidence that oscillations and coherence could be the substrate of short- and long-range communication within the brain (Fries, 2015). There has been more and more interest in the study of pain rhythms, resulting in great insights in the functioning of this system (Alshelh *et al.,* 2016; Ploner *et al.,* 2017). Therefore, as they represent the correlates of a communication particularly suited for the integration of pain, variations in membrane potential revealed through electrophysiological recording are a great target of investigation for the study of pain. Moreover, as the sleep field highly rely on these measures, the correlation between pain and sleep parameters can easily be assessed by questioning the rhythms.

Coding phasic pain. Studies linking brain rhythm and pain were mostly carried on phasic pain. It is indeed easier to assess the frequency changes associated to a clear, timed defined

stimulus. From EEG and MEG data both in patients and in animal models, we know that a painful stimulus induces a pain response in three main steps. First, around 150–400 ms after the acute stimulus, there is an increase in the frequencies below 10 Hz, originating from the somatosensory, motor, and frontoparietal cortices including the insula, the secondary somatosensory, and cingulate cortices. Together, these areas form the well-known pain-related evoked potentials (Garcia-Larrea *et al.,* 2003; Lorenz & Garcia-Larrea, 2003; Ploner *et al.,* 2017). Second, around 150–350 ms, phasic pain induces an increase in gamma frequencies over somatosensory and motor areas (Gross *et al.,* 2007; Hauck *et al.,* 2007; Tan *et al.,* 2019; Yue *et al.,* 2020; Z. G. Zhang *et al.,* 2012) as well as in the insula (Liberati *et al.,* 2018). Finally, around 300–1000 ms after the stimulus, we observe a transient suppression of alpha and beta frequencies in the somatosensory and motor cortices, and occipital areas (Hu *et al.,* 2013; May *et al.,* 2012).

Gamma oscillations. Recently, the increase in gamma oscillation and the question of what it represents has received a particular interest. Localized mainly over the somatosensory cortex, it has been shown to be specific to nociceptive stimulus and to reflect the area where the stimulus is delivered (Heid *et al.,* 2020). The gamma oscillations have been found to originate from rapid firing of interneurons in the superficial layer of S1, and to facilitate the communication with the PFC (Yue *et al.,* 2020). As Gamma oscillations can appear linked to several cognitive processes such as attention, memory retrieval or learning (Benchenane *et al.,* 2011), the question whether they are functionally liked to pain or just a result of attentional shift is still debated (Ploner *et al.,* 2017). We know however that the gamma frequency increase correlates with subjective pain intensity specifically, and not with the saliency associated, as repetitive stimulus of the same intensity which reduce saliency, induce a constant gamma increase response in human (Z. G. Zhang *et al.,* 2012).

A very elegant study in mice recently dissected the functional contribution of gamma oscillation to pain and the underlying circuits involved. They showed that the gamma oscillation in S1 cortex is linked to pain intensity in mice, and that by imposing them onto the cortex using optogenetic increases pain sensitivity and produces aversive behavior. It seems that S1 mediate this effect by its crosstalk with prefrontal areas and by descending serotoninergic fibers facilitating the ascension of pain stimulus in the spinal cord (Tan *et al.,* 2019). Phasic pain subjective perception can thus be measured by and modulated by gamma oscillation in S1. Therefore, they represent a potentially useful pain biomarker usable across species and several studies are already successfully assessing its predictive power (Misra *et al.,* 2017; Sun *et al.,* 2021; Yue *et al.,* 2020).

Coding tonic pain. Longer lasting pain however is much harder to detect, as there is no way to time lock to a specific stimulus. One step toward understanding the coding of longer lasting pain was done by using longer, time-defined stimulus such as heat, to induce tonic pain.

Unlike phasic pain, tonic pain seems induce gamma oscillations in the medial prefrontal cortex more than in S1 (Schulz *et al.,* 2015). These results point toward a switch from sensory areas toward emotional- and motivational-encoding areas when pain lasts for a longer period. Further evidence even linked a gamma oscillation increase to cases of chronic low back pain, indicating that this biomarker holds true for ongoing pain without induced stimulus (May *et al.,* 2019). In animal, alpha and gamma frequency in S1 are clearly elicited for instance by tonic inflammatory pain produced by CFA injection (Tan *et al.,* 2019) (*Figure 5*). Therefore, it seems that the changes observed in phasic pain stimulus are similar, although longer lasting and processed more in emotional areas at least in human, in the case of tonic pain.

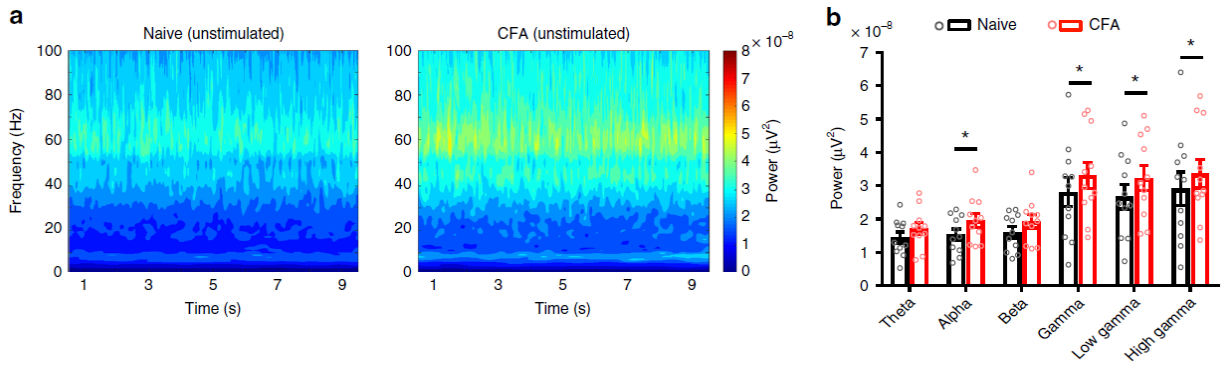

Figure 5. Adapted from Tan et al., 2019. Effect of CFA 4 days after injection in the paw, measured in contralateral S1HL. a. shows representative traces and b. mean across whole recordings.

Coding chronic pain. In the case of chronic pain, resting state network measure revealed several changes in humans. Most notably, an increase in high theta (6–9 Hz) and low beta frequency ranges (12–16 Hz) was found in patient suffering from neuropathic pain (Sarnthein *et al.,* 2006; Stern *et al.,* 2006). These changes have been proposed to cause a thalamocortical dysrhythmia. The thalamus, by shifting from alpha (10–15 Hz) toward theta, would favorized the cross-frequency coupling in beta and gamma range through the thalamocortical loop, effectively increasing these two bands in the cortex (Llinas *et al.,* 1999; Vanneste *et al.,* 2018). In animal models however, there has been reports of increased theta and beta frequencies in S1 and medial prefrontal cortex in rats injected with capsaicin, CFA, or submitted to CCI (LeBlanc, Bowary*, et al.,* 2016; LeBlanc, Lii*, et al.,* 2016; LeBlanc *et al.,* 2014). Not always in line with the findings in human, these studies raise the question of how much of the abnormal spontaneous and stimulus evoked pain experience is truly shared between species and how each band reflect specific activity in each species.

In summary, the studies indicate mostly changes in the theta and the beta range once chronic pain has set in. In humans, the changes occur mostly in prefrontal areas. One of the main consequences of chronic pain is a disturbed integration of non-nociceptive inputs as pain. A perturbed balance of oscillation within the brain would therefore represent the main culprit for these wrong associations and might play an important role in chronic pain. However, this field and specific approaches are still largely unexplored in the context of chronic pain. As was shown recently by the Kuner group (Tan *et al.,* 2019), more systematic studies directly interrogating these oscillations in animal models at different phases of chronic pain would benefit the field

4. Sleep and pain

Chronic pain patients have many complaints, among which, perturbed sleep is experienced by 45 % of them (Jank *et al.,* 2017; Treede *et al.,* 2019). These complaints take the form of difficulties to fall asleep, frequent awakenings and the feeling of fatigue during the day (Bjurstrom & Irwin, 2016; Mathias *et al.,* 2018). This relationship is bidirectional, and we observe an amplification of the symptoms if left untreated. On one hand, sleep deprivation or fragmentation increases pain sensitivity (Alexandre *et al.,* 2017; Haack *et al.,* 2020). On the other hand, pain further aggravate the sleep perturbations, resulting in a vicious circle from which it is hard to come out. This relationship is however not equilibrated. Indeed, impaired sleep seems more potent at increasing pain, than pain is at disturbing sleep (Finan *et al.,* 2013). This might represent an opportunity for treatment, by tackling the problem from the sleep side. Beyond improving quality of life, normalizing sleep in patients might relieve them from a significant fraction of their pain. However, to design proper therapy we need to understand exactly which aspect of sleep is affected in the first place. This last point represents the principal aim of my thesis and the subject of my principal research paper. In this last introductory part, I will summarize the main findings on this relationship in human, with a focus on PSG studies, to understand the phenotype that needs to be modelled in animals. Based on the observations and difficulties encountered in PSG studies, I will introduce a particular case of insomnia, the paradoxical insomnia, which could give valuable insight to disentangle the results. I will then mention some animal studies and how so far, they have helped in understanding how sleep is affected by chronic pain and which limitations were met.

4.1 Human complaints and phenotype

Introductory remark. There has been numerous studies and subsequent reviews examining what exactly is perturbed in the sleep of patients suffering from chronic pain(Kelly *et al.,* 2011; Menefee *et al.,* 2000; Moldofsky, 2001) Most studies rely on subjective sleep assessment (Morin *et al.,* 1998). For example, a survey study in primary care patients revealed that 45.5% of the patient suffering from chronic pain, reported sleep disorders (Jank *et al.,* 2017). Subjective complaints are of great importance and in the end, they are what need to be solved by the potential treatments. However, to understand the root of these complaints there is a need to find objective measures correlating with them, and that can be tested for causality. This is where PSG can be helpful.

Polysomnography in patients. PSG studies in chronic pain patients are the solution to investigate this aspect, but a large variability is observed between them and they gave rise to contradictory results (Bjurstrom & Irwin, 2016). More recently, a meta-analysis (Mathias *et al.,*

2018) helped to disentangle these results over PSG studies in various chronic pain populations. From 22 studies and despite a high level of variability, they concluded that patients shared the following noteworthy objective measures; sleep continuity was affected with less total sleep time, longer sleep onset latency and more time awake after sleep onset. Sleep architecture was slightly affected with proportionally more time spend in NREM 1 sleep, but same percentage of the other sleep phases NREMS 2, 3 and REMS. Sleep fragmentation was increased, with more full transitions to wakefulness, but no significant difference in the amount of microarousals. They also observed more episodes of sleep apnea in patients, which could be the cause of the sleep fragmentation. This meta-analysis however highlights some possible biases in the different measures. One example is in the use of opioid treatment in chronic pain patient. Indeed, such treatment is known to increase the occurrence of sleep apnea events and subsequent sleep fragmentation (Guilleminault *et al.,* 2010). The fact of sleeping in a laboratory or at home also had a significant impact on some measures, among which total sleep time. Moreover, a screen for sleep disorders predating the onset of chronic pain was often not assessed, which might inflate some of the results (Mathias *et al.,* 2018) (*Table 1*).

	Sleep Variable	$N_{studies}$	$N_{participants}$		Hedges *g*	*p*	N_{ES}	Heterogeneity		Study References
			CP	HC				*Q*	I^2	
Sleep continuity	Total Sleep Time (mins)	19	629	503	**-0.69**	0.01	47	284.58*	93.67	7-8, 14-15, 17, 25-27, 34, 39, 48, 50, 61, 71, 84, 86, 88, 90, 94
	Sleep Onset Latency (mins)	14	476	365	**-0.79**	0.001	41	118.65*	89.04	1, 7-8, 15, 17, 25, 34, 39, 48, 50, 71, 86, 89, 90
	REM Latency (mins)	8	204	179	-0.07	0.51	0	4.99	0.00	1, 7, 15, 27, 39, 48, 64, 71
	Sleep Efficiency (%)	18	557	433	**-1.24**	<0.001	94	224.63*	92.43	1, 7-8, 14-15, 25-27, 39, 48, 50, 61, 71, 84, 89, 90, 94, 97
	Wake After Sleep Onset (mins)	11	400	312	**-1.08**	<0.001	48	115.38*	91.33	7, 14-15, 25-26, 34, 39, 48, 71, 86, 90
Sleep architecture	NREM 1 (%)	18	495	435	-0.47	0.01	24	97.18*	82.51	1, 7-8, 14-15, 17, 25, 27, 34, 39, 48, 61, 71, 84, 86, 89, 94, 97
	NREM 2 (%)	18	495	435	0.07	0.65	0	81.84*	79.23	1, 7-8, 14-15, 17, 25, 27, 34, 39, 48, 61, 71, 84, 86, 89, 94, 97
	NREM 3 (%)	19	519	455	-0.38	0.06	17	150.11*	88.01	1, 7-8, 14-15, 17, 25, 27, 34, 39, 48, 61, 71, 84, 86, 88, 89, 94, 97
	REM (%)	18	508	444	0.06	0.60	0	49.51*	65.66	1, 7-8, 14-15, 17, 25, 27, 34, 39, 48, 61, 71, 84, 86, 88, 89, 94
Sleep fragmentation	Stage Shifts (total)	4	79	59	-0.43	0.01	5	2.34	0.00	14, 26-27, 97
	Awakenings (total)	6	284	194	**-0.96**	<0.001	23	17.55*	71.51	7-8, 25, 39, 48, 90
	Arousal Index	9	239	186	-0.74	0.06	24	110.27*	92.75	1, 8, 15, 27, 71, 84, 88-89, 94
	Apnea-Hypopnea Index	9	241	207	-0.34	0.01	6	13.93	42.59	1, 8, 14-15, 27, 34, 39, 88, 94,
	Periodic Limb Movement Index	7	208	177	**-0.51**	0.03	11	26.86*	77.66	1, 8, 15, 27, 34, 39, 71

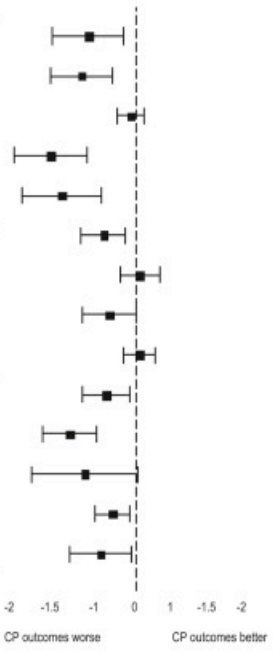

Table 1. Obtained from table 3 in Mathias et al., 2018. Summary of the differences in PSG-measured sleep variables between chronic pain patients and healthy controls.

Sleep studies in chronic pain patients therefore helped to pinpoint specific sleep alterations and could conclude that patients suffer from an objectively poorer sleep compared to controls, despite the high variability and possible biases. This intrinsic variability in patients

and between the type of chronic pain conditions render attempts at objectively describing sleep alterations very difficult and often not successful. In opposition, poor perceived sleep and subjective complaints are reliably observed in patients (Jank *et al.,* 2017) and their causes should be investigated within the quality of each sleep stages and not just their proportion and transitions.

4.2 Paradoxical insomnia

Introductory remark. A subgroup of insomnia disorder, the paradoxical insomnia (Edinger & Krystal, 2003) illustrates well the dissociation between measured and perceived sleep. Patients suffering from paradoxical insomnia feel unrested in the morning despite no visible sleep architecture alterations. Therefore, objective sleep alterations could represent only the visible and non-obligatory consequences of a deeper problem, which could explain part of the discrepancies in chronic pain PSG studies.

Spectral changes and substates. The spectral power and dynamics of the EEG in sleep can help to identify and distinguish substates. For example, frequencies in the theta (4–8 Hz), alpha (8–12 Hz) and beta range (14–35 Hz), normally associated with information processing in wakefulness were elevated, opposed to a reduction in delta power (1–4 Hz) in patients (Feige *et al.,* 2013; M. L. Perlis *et al.,* 2001; M. T. Perlis *et al.,* 2001). More recently, another study distinguished substates within the dynamic of the EEG spectral composition. Using machine learning, they revealed that data-driven classification in 6 stages, with possible co-occurrence from deep N3 sleep to wakefulness were necessary to reveal the appearance of a wake-related stages in what would be considered sleep in insomnia disorder patients (Christensen *et al.,* 2019).

Interestingly, differences in sleep stage quality can already be identified in the normal population. A study from the center of investigation and research on sleep CIRS at the CHUV compared a cohort of normal sleepers, although having a habit of underestimating their time asleep, with a cohort of people correctly estimating their sleep. The under-estimators displayed a higher prevalence of beta power (18–30 Hz) and a diminution of delta power (1–4 Hz), best represented by the activation index which is the ratio of high over low frequencies (Lecci *et al.,* 2020). Reminiscent of what is observed in paradoxical insomnia patients, this imbalance, correlate of the feeling of unrest in the morning, could represent an early marker for insomnia.

Sleep stages as we describe them are therefore not sufficient and further distinction is needed to explore their heterogeneity. This would help to understand which sleep parameter is affected in many diseases which still resist and present too much variability for classical PSG measures.

4.3 Animal studies on sleep and pain

Introductory remark. As presented individually above, the research on animal models greatly improved the understanding of the mechanisms involved in the sleep-wake control system and the nociceptive system. Particularly the transition from acute to chronic pain states (Burma *et al.,* 2017), and the associated remodeling of the central and peripheral nervous system and its consequences are well documented (Kuner & Kuner, 2020). However, despite the parallel advances in these two fields, sleep studies on chronic pain models are not numerous, assessing mainly architectural changes in sleep and sometimes contradict each other.

Architecture studies and limitations. For example, a group found severe changes in sleep architecture in rats with CCI, such as reduced sleep efficiency, increase number of full arousals from day 2 to day 10 and again from day 20 after surgery (Andersen & Tufik, 2003). However, another group concluded on the same year that rats with CCI had no sleep alteration from day 13 to 146 (Kontinen *et al.,* 2003). Later, an interesting result was found when a group added an environmental condition to the experiment. Rats with CCI were showing no sleep alteration, until they were housed on sandpaper instead of pellets. In contrast, the sham animals were sleeping as much as before in this condition (Tokunaga *et al.,* 2007). These results suggest that sleep is indeed perturbed in animal models, however to a degree that is not obvious at the level of the architecture. This highlights the need to assess sleep at the qualitative level and look within the states as it is already done in patients with insomnia disorders. That direction was taken already in a study that did not rely on sleep scoring, but on an automatic state classification method (Gervasoni *et al.,* 2004). They discovered that the classification was highlighting more transitions between the wake-like and sleep-like state, that were not necessarily obvious at the architectural level (Cardoso-Cruz *et al.,* 2011). Animal model therefore could help understanding the direct effect of pain on sleep, without the eventual confounding factors encountered in human, such as mood related sleep disturbances, previous conditions, and environmental factors.

My own study. My thesis pursues this question by analyzing sleep in SNI compared to sham animals, focusing on NREMS. Indeed, with the knowledge that sleep can be altered without noticeable effects onto scored sleep architecture, I have designed specific analysis and measures relying on frequency dynamics and heart rate variations at specific fragile moments of NREMS, where it would be likely to identify such disturbances and fragmentation. Moreover, I pointed out above that sleep can vary locally. This information coupled with the alteration in some brain areas after SNI, specifically in the loss of inhibitory drive (Cichon *et al.,* 2017), and the increased gamma frequency (Tan *et al.,* 2019), lead us to hypothesize that sleep could be altered only in some area related to pain, such as S1 or prelimbic cortex. Finally, as we suspected a fragile sleep facing external stimulus, I designed a method to assess arousability in response to vibrations based on a closed-loop system able to target continuous or fragile moments within NREMS.

Results

Study I:

Coordinated infra-slow neural and cardiac oscillations mark fragility and offline periods in mammalian sleep

Sandro Lecci, Laura M. J. Fernandez, Frederik D. Weber, Romain Cardis, Jean-Yves Chatton, Jan Born, Anita Lüthi

Sci Adv. 2017 Feb 8;3(2):e1602026.

Sleep is a state of relative disconnection from the close by environment. This disconnection seems essential to complete the restorative, memory consolidation and metabolite clearance functions of sleep. However, to protect the individual against potential threats, some attention to stimulus must remain and be permitted to trigger an arousal. Therefore, sleep should be continuous and fragile. How are these two contradictory aspects reconciled?

In this study we used PSG in mice and human to explore the heterogeneity of NREMS and find markers predicting moment of higher or lower arousability facing auditory stimuli. NREMS is characterized by specific power band such as SWA (0.75–4 Hz) and sigma (10–15 Hz). We investigated the temporal dynamics of the power of these two bands in mice, in continuous bouts of NREMS.

We found that sigma power displayed a cyclic pattern of rising and falling on an infraslow timescale of around 50 s per cycle. This infraslow rhythm was specific to sigma as it was not found in SWA activity and decreased in amplitude in the adjacent frequency bands theta (5–10 Hz) and beta (15–25 Hz). A similar observation was subsequently made in human stage 2 NREMS, by following the dynamics of the individual fast spindle peak frequency. We then tested if the phases of this infraslow rhythm timed difference in arousal threshold. We exposed the sleeping mice to threshold-level non-biologically relevant stimuli (white noise, 20 s-long, 90 dB SPL) and scored each stimulus as sleep-through or wake-up. When the sound was played in ascending phase, mice tend to sleep through and when the sound was played in descending phase, mice tend to wake up. We noted that continuity periods displayed an increase in ripple activity, suggesting offline memory processing, and a reduced sympathetic drive detected through heart rate measure from the EMG electrodes. In opposition, fragility periods displayed a reduced hippocampal ripple activity and correlated with signs of increased sympathetic drive. Finally, in human subject the higher the oscillating power of their fast spindle band in the infraslow range during the night, the better they were in a declarative memory task on the next day.

In summary we identified a novel infraslow fluctuation in sigma power that correlate with sympathetic and parasympathetic activity as well as memory consolidation processes. This rhythm essentially subdivided NREMS in alternating periods of 20–25 s of continuity and fragility.

Personal meaning and contribution

I arrived at a period when this publication was close to be completed. It represents the work of Sandro Lecci, my friend and first mentor during my PhD. This was my entry point into signal analysis and the study of sleep. I completed the datasets with new animals, which helped me learn how to perform the EEG/EMG implantation surgery. My contribution was mostly on the link between the heart rate fluctuation and the 0.02 Hz-fluctuation. I helped in designing the method for heartbeat extraction from the EMG data and reproduced the various analysis they had developed in Igor, using MATLAB.

Study II:

Cortico-autonomic local arousals and heightened somatosensory arousability during NREM sleep of mice in neuropathic pain

Romain Cardis, Sandro Lecci, Laura M.J. Fernandez, Alejandro Osorio-Forero, Paul Chu Sin Chung, Stephany Fulda, Isabelle Decosterd, Anita Lüthi

BioRxiv: https://doi.org/10.1101/2021.01.04.425347, Currently under revision at Elife.

Chronic pain patients complain about troubled sleep in the form of difficulties to fall asleep, frequent awakenings and daily fatigue. Improving the quality of sleep is beneficial on pain sensitivity, but the neurophysiological mechanisms causing sleep disturbances from chronic pain are unclear. Chronic pain is known to cause high-frequency electrical activity within the pain matrix, which could in turn disturb the normal generation of low-frequency sleep rhythm.

In this study we assessed sleep architecture in SNI animal compared to Sham. Moreover, we explored specific frequency band dynamics at moment of highest NREMS fragility, detected through a novel marker of sleep continuity-fragility, the 0.02 Hz fluctuation.

We found that SNI animals have a preserved sleep architecture compared to Sham animals but display hallmarks of hyper alertness in the form of elevated heart rate and imbalance between low and high frequencies within the S1 hindlimb (S1HL) cortex during NREMS. Then, by exploring NREMS in the light of the 0.02 Hz-fluctuation, we determined the fragility period as a moment of highest sensitivity to perturbation. With that in mind, we probed for novel form of perturbations and found a new kind of spontaneous local microarousal within the S1HL cortex, without phasic EMG activity but accompanied by heart rate increases. Interestingly, these local perturbations were more numerous in SNI compared to Sham. Finally, using a novel arousability assay based on closed-loop delivery of mild vibrational stimuli restricted to continuity or fragility periods, we determined that SNI animals had an overall higher propensity to wake-up facing external stimuli.

Sleep in SNI thus appears preserved in conventional measures but showed an elevated amount of local spontaneous perturbations and an increased evoked arousability. We developed here a novel moment-to-moment probing of NREMS fragility which helped in the proposal that chronic pain induced sleep complaints arise from perturbed arousability.

Personal meaning and contribution

This is the study that I realized during my thesis and that contain a condensed version of the various tools that I developed. For this study I designed and performed the implantation surgeries compatible with our (at the time) newly acquired Intan recording system. I developed the acquisition softwares with or without a closed-loop layer. I designed and performed the signal analysis, produced the figures and the statistical analysis.

Study III:

Infraslow locus coeruleus activity coordinates spindle rhythms and heart rate to gate fluctuating non-REM sleep substates

Alejandro Osorio-Forero, Romain Cardis, Gil Vantomme, Aurélie Guillaume-Gentil, Georgia Katsioudi, Laura M.J. Fernandez, Anita Lüthi

BioRxiv: https://doi.org/10.1101/2021.03.08.434399

The continuity of NREMS is essential for the function accomplished in that state. The disconnection from the environment can however pose a threat to the sleeping organisms. To address this problem, NREMS shows recurring moments of heightened sensory awareness to maintain environmental vigilance. The neuronal mechanisms behind the alternance of these continuity and fragility periods is yet unknown. This alternation could be related to previously described variation of activity within NREMS of the locus coeruleus (LC), the major contributor of the noradrenergic system.

In this study we used EEG/LFP/EMG recordings, fiber photometric measures of norepinephrine (NE) release and locus coeruleus optogenetic manipulation to interrogate the role of the LC in timing continuity and fragility periods in NREMS. We used a closed-loop method to target specifically the continuity or fragility periods.

We demonstrated that the LC is necessary and sufficient to generate the 0.02 Hz-fluctuation. Its activation using optogenetic during the continuity periods or fragility periods respectively suppressed and entrained the 0.02 Hz-fluctuation. In opposition, bilateral LC inhibition using a Jaws opsin during the continuity periods or fragility periods respectively entrained and suppressed it. These changes were accompanied by modification of spindle clustering, themselves being the main contributor of the 0.02 Hz-fluctuation. Changes in heart rate fluctuation was as well following the sigma dynamic imposed by the LC. This result was mediated by thalamic circuits and not cortical, as the effect was reproduced by activating optogenetically LC projections within the thalamus and not within the cortex. Moreover, through fiber photometry, the LC was shown to release NE into the thalamus at an exact anticorrelation with the 0.02 Hz-fluctuation in sigma power.

The LC therefore coordinates brain and bodily state during NREMS and by its timed activation, orchestrate the occurrence of the fragility periods of NREMS. This result confirms the LC as an important player in the physiology of the reconnection to the outside world happening during awakenings and as a target in sleep disorders related to abnormal arousability.

Personal meaning and contribution

This study is the main work of Alejandro Osorio-Forero, friend and source of inspiration during my PhD. For this work I designed the acquisition software with a closed-loop layer system based on machine learning recognition of fragility and continuity periods. I was as well mentoring Georgia Katsioudi, student in the lab at the time, in the data gathering and analysis of the peripheral pharmacological experiment on the heart rate relationship with sigma power fluctuation.

Discussion

The major results of my thesis are four-fold in the neurobiology of sleep and the understanding and the relevance of the 0.02 Hz-fluctuation of NREMS, in physiological and pathophysiological conditions. First, I contributed to its original description in the Lecci 2017 paper, in which we identified it to be present in NREMS of both mice and human. We indeed showed that this fluctuation divided NREMS into periods of continuity defined by low arousability and accompanied by markers of memory consolidation, and periods of fragility, associated with increased arousability to sound stimuli. Second, we advanced on the relevance of this fluctuation by associating it not only to evoked arousability, but as well to spontaneous arousability, as we demonstrated that it was regulating the appearance of microarousals in our Cardis 2021 pain/sleep paper. Third, this last information, by highlighting when NREMS was the most fragile, helped to identify a novel type of microarousal in mice that is distinct from conventional microarousals in that (i) it occurs locally in terms of EEG correlates of arousal (ii) it goes without any sign of muscle activity, but is accompanied by heart rate increases. Fourth, we have identified the neuronal mechanisms underlying the generation of the 0.02 Hz-fluctuation. Indeed, by using precisely timed optogenetic stimulations of LC activity, we were able to perturb or entrain the 0.02 Hz-fluctuation effectively demonstrating the LC necessity and sufficiency for its generation.

My thesis also extends into novel aspects of sleep pathophysiology. My results provided valuable insights on how nerve injury perturb sleep in an experimental model of neuropathic pain, the SNI. First, I demonstrated in this model that the brain and body were showing physiological correlates of pain states perduring into NREMS. Second, I found that sleep in neuropathic pain-like conditions appeared mostly unchanged at the architectural level measured through global EEG/EMG parameters. Third, I highlighted that that the above mentioned local microarousals were more numerous in the S1 cortex of our SNI model of neuropathic pain, which proved the usefulness of the 0.02 Hz-fluctuation in identifying relevant marker of sleep perturbation. And Fourth, that these mice presented an overall lower arousal threshold in NREMS, when facing external vibration stimuli.

In the following discussion, I would like to develop two major aspects of my thesis. First, I will give evidence for the relevance of the 0.02 Hz-fluctuation as a fundamental organizer of NREMS. I will summarize the findings by comparing to existing literature on infraslow phenomena in sleep and indicate what this rhythm may represent in the lights of our 2017 study and our latest Osorio-Forero 2021 study. Second, I will discuss the findings on the sleep perturbations in SNI animals, what they could represent and what translational information we can extract from them. Finally, for each part, I will mention limitations and give future perspectives.

1. The 0.02 Hz-fluctuation, a marker of sleep fragility/continuity

One aspect of sleep I introduced is the need to reconcile conflicting needs to be disconnected from the environment, while maintaining the ability to answer to external stimuli (Andrillon & Kouider, 2020). The 0.02 Hz fluctuation in human and mice that we described in our 2017 paper qualifies as a hallmark for how this continuity and fragility of sleep are reconciled. Several characteristics associated with the fluctuating levels of sigma power, its defining feature, support this claim. First, the period of rising sigma power is accompanied by several hallmarks of sleep protection and consolidation. Its frequency in the sigma range (10–15 Hz), is associated to spindles which are themselves hallmarks of thalamic sensory gating. Then, ripple activity in the hippocampus is increasing during the continuity period, highlighting a likely memory consolidation function taking place during this consolidated state. Conversely the period of declining sigma power encompasses markers of sleep perturbations. We observe a modulation of autonomic status with the heart rate increase and an increased arousability facing external stimulus. While we first provided evidence for variable arousability in a retrospective classification of sounds randomly played in NREMS, I corroborated this in a hypothesis-driven manner by targeting specifically rising and declining periods with vibrations in a closed-loop experiment. This confirms that sleep is indeed more fragile in these descending periods, justifying their description as fragility periods, as opposed to the rising continuity periods. Accumulated evidence, to which my thesis contributes in critical ways supports the idea that the 0.02 Hz-fluctuation provides a measurable temporal scale of mammalian NREMS, during which both continuity with beneficial aspects of sleep, and fragility with environmental reactivity are balanced.

Here, I will mention what we effectively measure on a shorter time scale when we extract the fluctuation. I will then propose a role for the 0.02 Hz-fluctuation as a fundamental organizer of NREMS. To support this, I will continue with an in-depth description of the continuity and fragility periods, speculating on their possible roles and how they are timing exits out of NREMS. Continuing, I will analyze our result in the light of the CAP sequences and k-complexes observed in human and speculate on how these processes relate to the described 0.02 Hz-fluctuation. I will then address a limitation of our studies, which is the current lack of clear link to REMS transitions in a dedicated part. For that purpose, I will discuss recently published and unpublished results. Finally, I will mention the main limitations and possible future experiments and outcomes to unravel more about this fundamental NREMS dynamic.

1.1 The 0.02 Hz-fluctuation is composed of spindle-rich and spindle-poor periods

The results of the 2017 study on the discovery of the 0.02 Hz-fluctuation and the one on its likely generation by the LC gave great insights on what gives rise to the measure of the 0.02 Hz-fluctuation on this slow timescale. The 10–15 Hz frequency contains sleep spindles, which are a thalamocortically generated obvious hallmark of NREMS in mice and human (L. M. J. Fernandez & Lüthi, 2020). The infraslow fluctuating pattern of this band is the result of the clustering of discrete spindle events within tens of seconds periods. Spindles indeed are known to last from 1 to 3 seconds and to have a recurring interval from 3 to 10 seconds (Steriade *et al.,* 1993). Several of our results support the fact that the fluctuation is the smoothed measure of individual spindles. First, in the 2017 study, following the narrower individual fast spindle band in human gave the highest infraslow oscillatory power measured with FFT. Second, in the 2021 LC study in mice, the individual spindles automatically detected in the S1 cortex were clustered at the peaks of the fluctuation. In human, it was as well shown by another group that the spindles are appearing in clusters giving rise to this fluctuation (Lazar *et al.,* 2019). These results together clearly indicate that the spindles themselves are the main contributor of the slow fluctuation in the sigma (10–15 Hz) range. However, adjacent bands to sigma, theta (5–10 Hz) and beta (15–20 Hz) also show a smaller 0.02 Hz-fluctuation which indicates that other players than the spindles might contribute to the final smoothed output that we measure as the 0.02 Hz fluctuation. Still, it should be clearly mentioned that more work will be needed to clarify the manifestations of the 0.02 Hz-fluctuation in human sleep. The presence of slow and fast spindle and the grater variability of the strength of the 0.02 Hz-fluctuation in human promises to complicate its characterization compared to our results in mice.

1.2 The 0.02 Hz-fluctuation provides a fundamental organizational time scale for NREMS

Our finding demonstrated that the human brain fluctuation was present in NREMS 2 in human and in the whole of NREMS in mice. This presence in two mammalian species with very different sleep behavior and sleep architecture needs further investigation. However, as mice display a constant 0.02 Hz-fluctuation even in the deepest form of NREMS after sleep deprivation for example, we could speculate that they sleep only in what we call NREMS 2 in human, making this state a fundamental for sleep functions. We demonstrated the importance of NREMS 2 and the advantage of its organization by the presence of the 0.02 Hz-fluctuation, by correlating its oscillatory power with the score on an overnight declarative memory consolidation task. Moreover, close to our 2017 publication, a group demonstrated the presence of periods where the triggering of cues for targeted memory reactivation was more efficient. These periods were within refractory time in between spindles, which would correspond what we describe as the fragility period, when the sleeper is more perceptive of its surrounding (Antony *et al.,* 2018).

One remarkable aspect of the 0.02 Hz oscillation is the conservation of its rhythmicity between mice and human, even though NREMS is different in term of duration and architecture between the two species. This around 50 s periodicity seems to be a constant that predate the separation of mice and human in the evolutionary tree. Although the infraslow time interval is arguably very broad, it is repeatedly mentioned in sleep studies on diverse mammalian species. Cats and ferrets for example show cluster of spindles recurring at interval from 10 to 40 seconds (Steriade *et al.,* 1993). Rats as well, present a slow periodicity in LC activity on a similar timescale (Aston-Jones & Bloom, 1981). More recently, this fluctuation was indeed confirmed in rats and was shown to correlate with dendritic and cortical column activity measured through calcium imaging (Seibt *et al.,* 2017). Similar rhythmicity has even been observed in reptiles and birds that seem to switch between two distinct states within this timescale (Libourel *et al.,* 2018). In human, such slow periodicity is as well found for cycling blood oxygen level revealed by functional neuroimaging in the resting state network (Mantini *et al.,* 2007; Palva & Palva, 2012). Moreover, it was discovered that the human brain in NREMS exhibited waves of cerebrospinal fluid at a similar timescale, likely providing metabolite clearance at recurring periods (Fultz *et al.,* 2019). The definitive link between these infraslow rhythms observations and the 0.02 Hz-fluctuation described here remain to be established, however the shared frequency suggests an evolutionarily conserved time frame that coordinate NREMS 2 in achieving its functions in the appropriate order.

1.3 The continuity period, when NREMS beneficial aspects happen

Our results demonstrated, with the observation of the 0.02 Hz-fluctuation, the recurrent appearance of spindle-rich periods with lowered arousability facing external stimulus, and the almost absence of spontaneous microarousals. This period was accompanied by a decrease in heart rate and an increase in hippocampal ripple activity (*figure 6*). Ripple activity being linked to offline memory consolidation (Maingret *et al.,* 2016), their presence in that moment, concomitant with spindles, could underly the functional relevance of that period. Moreover, the more pronounced was the 0.02 Hz-oscillation in human, the better they were at an overnight declarative memory consolidation task. This indicates that restricting spindle events to limited time periods improves performance. Based on our result, we can speculate that these periods represent specific units of necessary functional activity responsible for memory consolidation. As such and linked to their duration (~25 s) they would explain why a minimal period of uninterrupted sleep (30 to 60 s) seems to be necessary for memory consolidation (Rolls *et al.,* 2011). This is also supported by the fact that the spindle rich period in human a less efficient moment for targeted memory reactivation (TMR) (Antony *et al.,* 2018).

The presence of a ~50 s infraslow time scale in sleep that links to arousability can give grounds to speculation as to its evolutionary origins and optimization. I can speculate that longer offline periods would represent an increased danger, however I would expect a different timescale in carnivorous and prey species, which is not the case. I would risk going as far as thinking that NREMS is a form of sleep that progressively slips into a deeper and deeper state the longer it lasts, and that the depth limit before an irreversible level is reached is situated around 25 seconds. This is a scary perspective as it would mean that our brain triggers a fall and timely catch us back before coma once every minute or so. However, rest assured, our results on optogenetic inhibition of LC during the fragility period, which often caused a prolongation of the continuity periods never induced a coma in our animals. This hypothesis is therefore either wrong, or the brain possess other failsafe mechanisms to catch us back early enough. Furthermore, in human we observe NREMS 3, which indicates that a continuity period uninterrupted by a fragility periods could ultimately lead to that state before coma.

1.4 The fragility period as a checkpoint for NREMS continuation

In our study of 2017 on the discovery of the 0.02 Hz-fluctuation and our 2021 study on pain and sleep, we highlighted that the descending phase of the 0.02 Hz-fluctuation was a moment of heightened arousability when facing external stimulus. Although this observation remains to be tested in human, we have in the meantime found enhanced arousability in the fragility period using two different sensory modalities in a closed-loop experimental design. Moreover, another study recently linked the pupil diameter to the phase of sigma power proposing that the larger pupil size in fragility would result in an increased sampling of visual information (Yüzgeç *et al.,* 2018) (*Figure 6*). What exactly makes this period more fragile is still open to debate, however we can speculate that it is likely linked to at least two parameters. First, the absence of sleep spindles themselves renders that substate free of thalamocortical gating control. Second, the norepinephrine (NE) release revealed through fiber-photometry measures suggests a heightened LC activity during these periods, which has been linked to heightened arousability (Hayat *et al.,* 2020).

I consider one of my major results the findings that spontaneous microarousals without obvious stimulus where preferentially occurring in the fragility periods as well. I find this result so important because it brings additional insight into the fragility period as a brain state that is vulnerable to not only external, but also internal, types of stimuli, the nature of which is still to be determined. Moreover, given that many types of sleep disorders, in particular insomnia, go along with spontaneous arousals that can result from aberrant activity due to stress or emotional states, my results could pave the way for a better characterization of abnormal arousability more generally.

Of course, my result on spontaneous microarousals could be explained following the same logic as for the increased stimulus evoked arousability and especially by the increased LC activity. One concern here it that knowing that microarousals can occur as a protective reaction to external stimulus, we cannot exclude that these events where partly caused by intermittent noise from the neighboring animals or reaching the recording room. However, by comparing the proportion of observed microarousals in fragility periods over continuity periods, we reach a much higher ratio compared to the one of evoked arousability facing vibration in continuity over fragility periods. We would therefore expect more observed microarousals in continuity periods if they were exclusively due to outside events. I thus believe that these microarousals were for the most part spontaneously generated in the fragility period. Their presence here, in this moment of heightened sensory perception could be due to a similar heightened perception of internal cues. Indeed, cues such as elevated carbon dioxide are known to induce microarousals (Kaur & Saper, 2019). It is therefore likely that other internal cues could be probed by the sleeping brain during this period, and that the microarousals would be the protective answer to them. I can speculate on possible internal cues. It was already proposed that untimed REMS transitions or an excessive deepening of sleep could trigger microarousals (Dos Santos Lima *et al.,* 2019). This would make the fragility period a recurring checkpoint for both internal and external cues in between functionally important disconnected periods of NREMS.

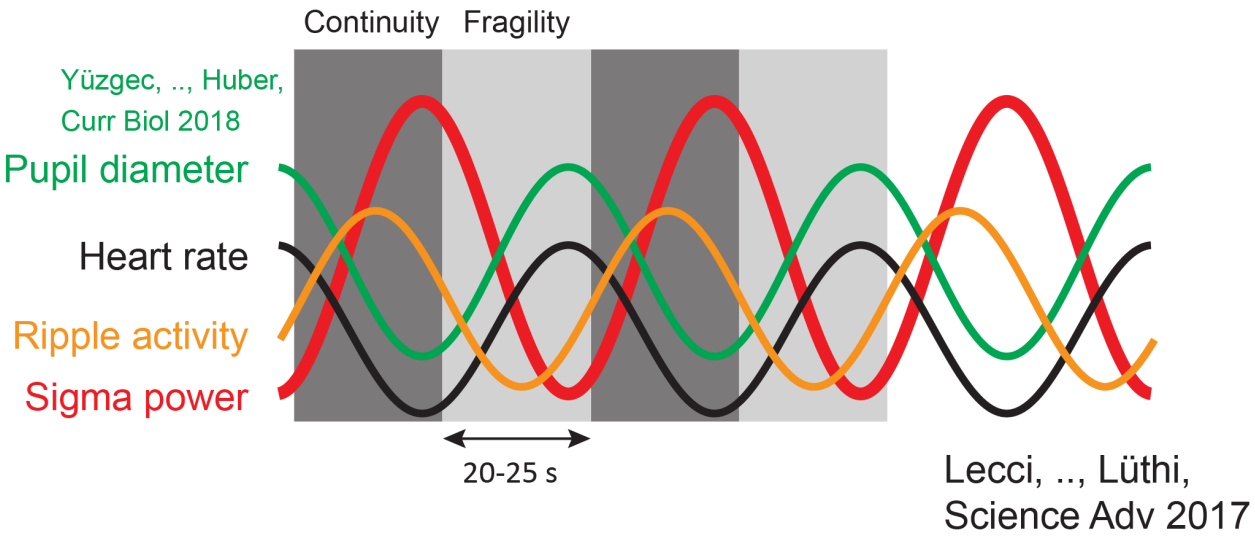

Figure 6. The different parameters fluctuating together with sigma power and defining the continuity and fragility periods

1.5 A link to the CAP

A recurrent question keeps being the relation between the 0.02 Hz-oscillation in mouse and the peculiar human sleep signature referred to as CAP (Manconi *et al.,* 2017). Indeed, cyclic periods of perturbations highlighted by the 0.02 Hz-fluctuation are undoubtably reminiscent of the observed CAP sequences in human which occur naturally but can highlight a pathological condition when overrepresented within sleep (Terzano & Parrino, 2000). There are however fundamental differences between the two. First, the 0.02 Hz-fluctuation is present in human in NREMS 2 only, whereas CAP sequences can occur throughout every sleep stage, as is the case for microarousals. Second, CAP sequences are a marker of sleep perturbation containing visible effects of the disturbances in the form of k-complexes and microarousals. The 0.02 Hz-oscillation is not constituted of sleep perturbation per-se, it allows to probe for them at appropriate times. This does not exclude a link between the two, as the 0.02 Hz-fluctuation likely times the occurrence of CAP sequences, giving them their cyclicity in NREMS 2, but it is important to see them as two co-occurring separated processes. One dictating the timing, and the other reflecting a detected perturbation.

Studies on K-complexes and CAP sequences highlighted a very important point concerning sleep perturbations. The progression of the CAP sequences from A1 to A3, with the first containing attempts at deepening sleep in response to a perturbation, and the latter a fail attempt translated into a microarousal, allows us to speculate on what is happening within the fragility periods. Indeed, in our study on the relation between sleep and pain, we clearly noticed that delta power (1–4 Hz) presented an upstroke in the fragility periods devoid of microarousals, whereas it is was falling in the periods containing one. This mean upward dynamic of the delta band may represent a form of k-complex or delta burst in a subgroup of fragility periods as a response to the decreased arousal threshold observed there. Moreover, the dynamic across the light phase of these fragility periods containing an upstroke of delta power was reminiscent of the one of the k-complexes in human (Peter Halasz & Bódizs, 2013), with a higher proportion at the beginning of the resting phase and a progressive diminution towards its end.

This would require a finer analysis of these moments, but this result could represent the first evidence of graded CAP sequences in animals and confirm the 0.02 Hz-oscillation as the orchestrator of this recuring measure.

1.6 The 0.02 Hz-fluctuation and REMS transitions

Finally, to really characterize the 0.02 Hz-fluctuation as an orchestrator of NREMS, we lack a definitive link to one of the most important NREMS features, its ability to transit into REMS. This is a question that came a lot during my thesis, and we have unpublished results that

constitute a good start to show this link. First, with a similar approach as for the microarousals in the pain-sleep paper, I extracted the phase of the 0.02 Hz-fluctuation at which REMS transitions, detected on hippocampus LFP recordings, occurred. Interestingly, these transitions were happening at the onset of the fragility period, slightly before the preferred phase for microarousals. It thus seems that these two events share the same time window for their occurrence. Second, increasing REMS pressure by selectively waking up the animals with a vibration at REMS onset reduced the amount of microarousal as more and more fragility periods were occupied by REMS transition attempts. Third, the optogenetic activation of LC during the fragility periods was markedly diminishing the amount of REMS transitions, without increasing the amount of microarousals. The opposite held true with the inhibition of LC in fragility period, which increased the amount of REMS transitions.

In my view, these results provide a proof of concept that REMS transitions, or at least attempts, are timed lock to the fragility period and can indeed represent internal disruptive cues able to provoke a microarousal.

1.7 Limitations and future perspectives

A further subdivision. There are still open questions about the role and the capacity of the 0.02 Hz-fluctuation at timing specific events in NREMS. For the case of the enhanced arousability in fragility versus continuity period for example. We indeed considered these two substates of NREMS as homogenous. However, a very clear aspect of sleep that I perceived during my thesis is that homogeneity is only rarely present within sleep states. It is thus very likely that at least the continuity period presents variation of arousability within itself. First, the presence of spindles would undoubtedly modify the momentary arousal threshold and second, if we indeed observe a deepening of sleep along this period, the arousal threshold should reflect it. To answer these questions, we could in the future play randomly placed short vibration stimuli within NREMS across many light phases and construct a phase of the 0.02 Hz-fluctuation/arousability curve that would give information on the composition of the continuity and fragility themselves.

Arousability in human. To go further into arousability facing external stimuli, I already mentioned that although we demonstrated it twice in mice, it was never shown in human. The 50 s time scale figures prominently in sleep-related breathing and movement disorders, but the link to evoked arousability should be tested specifically. Such experiment would surely strengthen the link between the two species. The design of the experiment should however not be the same as for mice. Indeed, the stimuli, being a sound, or a mechanic one, should be carefully selected to control for saliency and not induce an awakening at every presentation.

Sound mimicking everyday unimportant events would be appropriate as they have been shown to sometime induce a wake up, and sometimes not (Dang-Vu *et al.,* 2010; Rudzik *et al.,* 2020).

LC link to arousability. In the 2021 Osorio-Forero study, we speculated that the LC activity was responsible for part of the increased arousability observed in the fragility period. Although this is likely, we only observed a temporal co-occurrence of increased LC activity and increased arousability. To definitely confirm this in our conditions, we would need to link LC activity with wake-ups when facing our vibration stimuli. An optogenetic approach would be suited as we already demonstrated that the 1 Hz optogenetic activation of LC induced artificial fragility periods. By coupling this activation with a vibration, we would answer the question in the most direct way possible.

2. Chronic neuropathic pain, a threat to sleep continuity

As I introduced, chronic pain is a major burden for the individual, its surrounding and to another level, the society in general. Sleep disturbances associated to chronic pain states are known to further aggravate the pain sensitivity and together, they constitute a vicious circle. In my study we teased apart the pain-sleep associations by focusing on the specific aspects of sleep that are perturbed by chronic pain at an early time point of pain chronicity. Day 20 after SNI indeed constitute a moment when the increased sensitivity is established and stable, and when we do not yet find major depressive of mood-related symptoms (Guida *et al.,* 2020). By identifying these first consequences of pain on sleep, we hoped to frame the first causes of the amplification of the symptoms observed in patients.

In this part I will discuss our main findings starting with the surprising lack of a difference in sleep architecture between SNI and Sham animals. I will give possible explanation why this specific aspect observed in patient could not be reproduced in our animal model and compare it with what is known from animal literature. Then I will come back on the evidence that the wakefulness pain signatures are locally intruding into NREMS of SNI mice and what could be the causes and consequences of these changes. I will then dedicate a part to the novel described local microarousal, why they could be considered as such and where they position themselves in the arousal diversity. Moreover, I will speculate on their increased representation in SNI and what translational information we can extract from this result. I will next proceed to our evoked arousability result and explain how it relates to the spontaneous one. I will speculate on why we observed an overall increase in this form of arousability and not one restricted to the fragility periods. Finally, based on common observations between mice and human, I will try and answer to the question: do SNI animals suffer from insomnia? As in the previous chapter I will then wrap-up by mentioning some limitations and future perspectives on our results.

2.1 SNI animals are resilient enough to not show sleep disturbances without challenge

Our first experiment was simply to obtain a measure of sleep architecture in SNI animals and compare it to the one going through Sham surgery. According to the literature on chronic pain patients, we were expecting a reduced time asleep and more fragmentation. However, we found that there was no difference in these measures. Indeed, the time spent in NREMS was even slightly higher in both SNI and Sham 20 day after surgery compared to baseline. Moreover, the NREMS and REMS bout length distributions were the same in both groups, highlighting a remarkable absence of fragmentation. Complementary to that result, the number of microarousals were not different. This is surprising as the quantification of arousal from NREMS is central to estimate the severity of a sleep disorder. The time spent in REMS equal in both

groups also suggests that our animals were not experiencing excessive stress (Nollet *et al.,* 2019). It thus seems that SNI animals at day 20 do not experience particularly marked sleep disturbances.

As global measure of sleep duration can hide smaller homeostatic or circadian dependent changes, and that sleep deprivation is known to increase pain sensitivity (Alexandre *et al.,* 2017), we explored their sleep distribution over the light-dark cycle and their homeostatic response to sleep deprivation. Again, we did not notice striking modifications in sleep architecture. Delta power (1–4 Hz) was reliably increased after the 6 h-long sleep deprivation and the recovery period showed a classic sleep rebound and similar delta power discharge between the two groups. The proportion of microarousals and their distribution within NREMS was unchanged. Regarding the 0.02 Hz-fluctuation, we did not find a difference in its manifestation or in its capacity to time NREMS events in SNI, highlighting the resilience of this fundamental rhythm to pathological conditions. This was particularly helpful as we could rely on it to define moments of highest fragility and successfully find discrete perturbations.

Based on these results, we assumed that sleep in normal condition and challenged by one sleep deprivation is visibly not affected by an injury to the nerve. As the literature on rats with CCI suggested, such absence of effect is not without precedent (Kontinen *et al.,* 2003). Sleep in nerve injury conditions seems to require an additional external challenge to show its fragility, as suggested by the study showing sleep architecture changes only when CCI rats were sleeping on sandpaper (Tokunaga *et al.,* 2007). Moreover, the magnitude of the sleep architecture changes in CCI rats has been shown to correlate with their social response to an intruder in their home cage (Monassi *et al.,* 2003). Together and based on these various observations, we speculate that our animals, C57BL/6J mice, were likely resilient enough and that their sleep was not challenged sufficiently to show architectural changes.

2.2 The waking pain signatures perdure in NREMS of SNI animals

With the previous result in mind, we however looked for evidence of sleep fragility that could represent the basis of architectural disturbances when challenged. Given the numerous findings on pain-related rhythms in literature, we specifically explored the higher power bands and indeed found an increase of the gamma band (60–80 Hz) only, in the EEG of SNI animal compared to their baseline. Although this effect was present in both wakefulness and NREMS, it was not pronounced and only visible compared to baseline, and not between the two groups. This highlights a possible limitation of the use of EEG recording to show spectral modifications, as it essentially samples the whole hemisphere. It was however shown that a compensatory equilibrium exists between areas displaying wake-like pattern and areas displaying sleep-like pattern at least in human (Nobili *et al.,* 2011). We therefore expected that these small changes

could hide a bigger effect at a local level. We confirmed this in our LFP recordings aiming specifically for the S1HL cortex. Here, we demonstrated a tonic increase of beta (16–25 Hz) and low gamma (26–40 Hz) bands during NREMS. Moreover, and not shown in the current version of the paper, we also highlighted an increase of the theta band (5–10 Hz) in S1HL during wakefulness, although only within epochs of low muscular activity, likely corresponding to moments of immobility. This last result is particularly relevant, as such measures have been related to chronic pain on several occasions by another group (LeBlanc, Bowary, *et al.,* 2016; LeBlanc *et al.,* 2017; LeBlanc *et al.,* 2014). On top of these local frequency changes, we observed an increase in heart rate in NREMS compared to baseline in SNI animals. Together, this suggests a higher sympathetic tonus during sleep and an overall state of hyperarousal in NREMS in these animals, in which a supposed correlate of pain appears during wakefulness.

The causes of this hyperarousal state are unclear. However, the shared frequency bands are suggestive of the cortical oscillatory activity evoked with acute painful stimuli. Could it be that nociceptive inputs continue to arrive in the cortex during NREMS and generate excessive excitation? The fact that there are evidences of ectopic peripheral activity in SNI would suggest as much (Devor, 2009; Wall & Devor, 1983), even though other possibilities cannot be excluded. The profound changes observed in cortical circuits happening in chronic pain central sensitization could be a likely cause of the appearance of high frequencies for example. Indeed, the reduced inhibitory drive (Blom *et al.,* 2014; Cichon *et al.,* 2017) might prevent the complete expression of NREMS rhythms and wake-like activity would transpire more easily within it.

Interestingly, although the PrL area is concerned with signaling emotional discomfort in several forms of chronic pain in humans (May *et al.,* 2019; Nickel *et al.,* 2017; Schulz *et al.,* 2015), we did not find any alteration in the frequency bands observed. This absence of effect however may not be that surprising. The PrL, unlike the ACC or the S1 area that both show a decreased inhibitory drive, has been shown to display an increased inhibitory drive from PV interneurons after nerve injury (Z. Zhang *et al.,* 2015). This does not exclude that we could have find other type of frequency alteration, and more cellular studies would be necessary to understand the absence of effect within this area.

2.3 The discrete spontaneous arousals

Our results showing spontaneous arousal like events within S1 cortex is complementary to our previous observation of this hyperarousal state in SNI animals. Not without similarity to the NREMS-wake transitions previously observed in rats with CCI, in their locality and high frequency content (Cardoso-Cruz *et al.,* 2011), these events can be characterized as spontaneous arousals for several reasons. First, they appear in moments of highest fragility within NREMS, as they are within the fragility periods previously described in our studies. Second, they are

composed of a sudden decrease of delta (1–4 Hz) power and an increase of higher frequencies, which is a dynamic observed in classical microarousals clearly defined by their phasic EMG activity. Third, they are accompanied by a marked increase in heart rate, to a level that is not attained within fragility periods devoid of perturbation. And fourth, their regulation across the light phase is similar to that of the microarousal themselves.

Interestingly, although they experience more of them, not only the SNI animal display such local arousals. They were clearly present in sham animals suggesting that they are part of a normal sleep reaction to a possible perturbative cue. In human and as I introduced, it is now clear that arousals are not ubiquitous and that they display a graded response. The intensity of their hallmarks such as the EEG desynchronization and heart rate increases are indeed known to vary from one type of arousal to another (Azarbarzin *et al.,* 2014; Sforza *et al.,* 2000). Here and based on our result, I speculate that the local arousal that we found could constitute an early form of sleep fragmentation able to give rise to a full-fledged arousal if the perturbation continues or is assessed as salient enough to induce a wake up. Indeed, as I mentioned in the first part on my discussion, we cannot exclude that the increase in delta power observed in some fragility periods represent an attempt at sleep consolidation. As discussed before, this period is particularly sensitive to perturbation, internal or external, likely because of the increased LC activity. Interestingly, the mean dynamic of delta power in SNI animals within this period is lacking the upstroke observed in Sham. This could highlight an impossibility for SNI animals to rapidly generate the delta power increase in S1HL that would help them to stay in NREMS despite disturbances. The local microarousals, which would constitute the next step of the expression of the perturbation, would thus appear more often and bring the S1HL cortex closer to an actual awakening, as one protective mechanism is lacking. The impossibility to generate a delta power response is not that farfetched, as one observation preceding a cortical down state is an increase in somatostatin interneuron activity (Niethard *et al.,* 2018), which are known to be impaired in nerve injury conditions in the S1 cortex (Cichon *et al.,* 2017).

In summary, the fragility periods in nerve injury conditions, because of the lack of protective mechanism, would represent moments where internal signals would have a free access to the cortex and result in local sleep fragmentation (*figure 7*). As painful stimuli already represent a special kind of challenge (Claude *et al.,* 2015), it is likely that the wrong signals misinterpreted as pain could constitute such internal perturbations. Observing more of this form of sleep fragmentation in SNI could highlight the source of the perceived lack of rest in patients. Indeed, sleep fragmentation is the primary cause for daytime fatigue and cognitive deficits. By itself, it has also been associated with long term heart deficiency (M. Bonnet *et al.,* 1992; Silvani, 2019). This aspect is therefore of particular importance and can now constitute a very interesting lead for translational approaches.

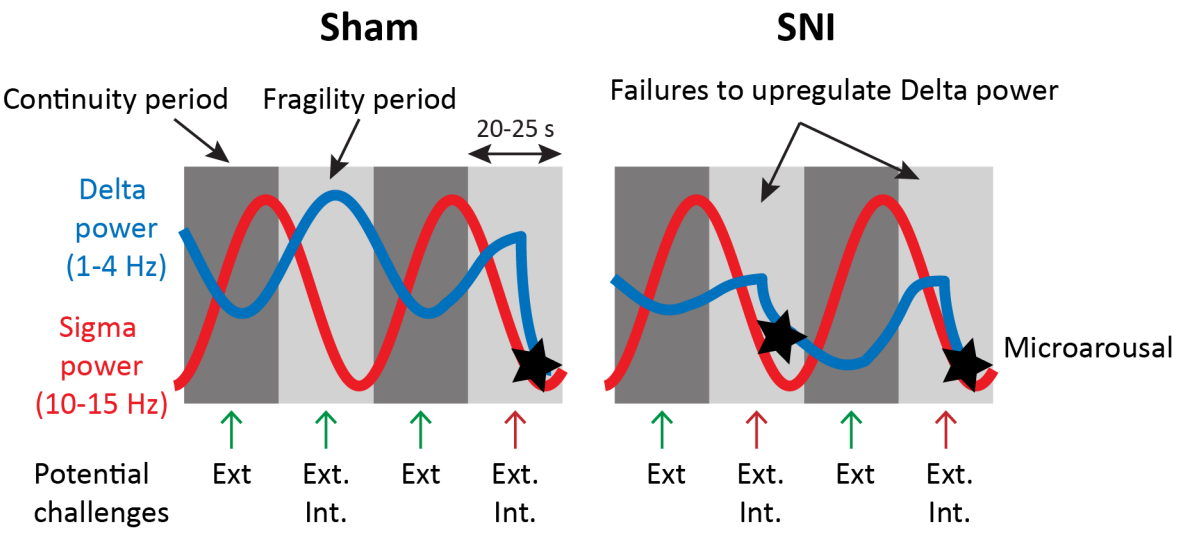

Figure 7 Proposed mechanisms for increased arousability in SNI animals. Ext: exterior; Int: internal potential challenges. The internal challenges would be probed only in fragility period whereas the external one in both continuity and fragility. The supposed inability to upregulate delta power in SNI would result in an increased perception of both external and internal potential challenges.

2.4 The external challenges confirm the increased sensitivity

On top of the spontaneous arousal-like activity that we observed in the fragility periods of our animals, we also demonstrated that they were overall more prone to wake up facing an external stimulus. The vibration system that I developed to investigate this aspect of arousability is particularly suited for such question. First, the vibrations being perceived by the somatosensory cortex, we can correlate the findings with the hyperarousal state that we found in this area. This of course do not assure causality but allows to speculate on mechanisms and build hypotheses. Second, the vibrations are perceived only by the animal to which they are targeted. Unlike sounds, this allows for specific individual closed-loop settings of several animals at the same time. This last point is of particular interest as it allowed us to specifically test whether only the fragility periods where more sensitive, or sleep in general.

The result that both continuity and fragility are more sensitive to external stimulus in SNI, although preserving the classical relationship with more arousals in fragility, is of great interest. This confirms that although the reaction to them is similar, internal or external challenges are not treated the same way during sleep. I can speculate that if NREMS can take the luxury to probe for internal challenges only every about 25 seconds, it would indeed be too dangerous to wait for that long to probe for a potential immediate external danger. This could explain why we still observe awakenings facing vibrations in continuity periods in our animals, despite observing almost no spontaneous microarousals there. Although this would merit further analysis, it could

explain why, due to their increased arousability, we observe more spontaneous hallmarks of arousals only in fragility, but more arousal facing external challenges in both fragility and continuity periods in SNI.

This results as well constitute an interesting lead for translational studies. From this observation, we can hypothesize that chronic pain patients experience worse sleep because of a heightened perception of their immediate environment. An extra care should therefore be taken to assure the comfort and the potential disturbing factors.

2.5 Do SNI mice suffer from insomnia?

Our results are in some parts reminiscent of what is objectively observed in paradoxical insomnia patients and in people underestimating their time asleep (Lecci *et al.,* 2020). This raises the question of whether our animals experience similar misperception of their time asleep. Although this would be quite complicated to assess, as to conclude that they suffer from insomnia we would need their own subjective assessment, we can speculate based on the similarities between the two conditions in between species. We observe a regionally restricted tonic imbalance between low and high frequencies in our animals. The people underestimating their time asleep showed similar imbalance over sensorimotor areas, and paradoxical insomnia patient in a widespread manner over several brain regions (Lecci *et al.,* 2020). Specifically, higher beta power has been linked to patients remaining hypervigilant or excessively ruminating before sleep, preventing the transition (M. L. Perlis *et al.,* 2001). These similitudes indicate that mice with SNI might indeed experience a sleep that could be subjectively more apparent to wakefulness. The more frequent spontaneous local microarousal in S1HL would most likely contribute to this feeling and the increased response to external stimulus confirms this state of hypervigilance. Another aspect that should be reproduce is the daytime sleepiness. Whether our animals experience it is uncertain, but napping time during the dark phase did not show an over increased delta power compared to Sham, suggesting that they accumulate sleep pressure in a similar way. However, and interestingly, animals with nerve injury have deficits in working and declarative memories (Guida *et al.,* 2020), which could be direct consequences of unrested sleep. In summary it is impossible to conclude firmly that our animals are feeling awake during NREMS, but several aspects of the two conditions are undoubtedly shared.

2.6 Limitations and future perspectives

<u>Comparative studies between mice and human.</u> One of the main limitations is paradoxically as well one of the strengths of my study. The use of animal model indeed provides a much-needed condition control during sleep studies which is not achieved in human and allows

for the dissociation of the effect on sleep from other comorbidities associated to chronic pain. However, if the effect of chronic pain on sleep is indissociable from these comorbidities, we might lose a part of the relevance in our search. Moreover, mice are prey animals with strong survival instinct, harsh social exclusion rules and high resilience. It is likely that they would not have the "luxury" to experience a highly perturbed sleep for long periods of time, or to ruminate about it. It would surely be interesting to measure sleep in SNI animals after a longer period. Heightened pain hypersensitivity remains at least for one year, it would thus be interesting to probe sleep later when other comorbidities appear (Guida *et al.,* 2020).

Limited localization. As mentioned above, the use of EEG measure in mice is a great tool to assess momentary global state but lack a very important aspect in the locality of the signals. Human high-density EEG has proved to be most useful in the study of sleep and neuropsychiatric disorders and demonstrated the importance of signal source localization (Lustenberger & Huber, 2012). One alternative in animal is the LFP which gain in localization what it loses in density. The choice of an area of interest allows for an in-depth characterization of the spectral components and individual events there but biases the results as only a limited amount of other nearby areas can be sampled. In my case, we noticed differences in S1HL, but we cannot exclude that such differences extend to the whole S1 area and nearby motor areas. In addition, The PrL that did not show any changes in SNI compared to Sham, is located just below the ACC which was proved to be modified as well by central sensitization (Blom *et al.,* 2014). One intermediate solution is the use of silicon probes (Jun *et al.,* 2017) or surface electrode array (Jonak *et al.,* 2018) which allow for the measure of several neighboring areas at the same time. Further sleep characterization using such technology would surely help to disentangle our results. On top of these experiments in mice, a translational study in human using high density EEG would help to address this limitation together with the previous one.

Sensory modalities. Another limitation which is somehow linked to the above-mentioned lack of localization is that our result on increased arousability in SNI is limited to somatosensory stimuli in the form of vibrations. While it provided us a very practical and efficient experimental design, this modality is not the only one able to induce a wake up. In our case, we correlated the changes observed in the S1HL area with the increased arousability to vibrations, but it would be a very interesting complement to measure other areas such as A1 cortex and try a sound stimuli arousability experiment. Are the changes observed in SNI common to all sensory areas or restricted to S1? As well, would such rhythms in sleep in a specific primary sensory area increase only the corresponding stimulus chance to wake up? A very interesting experiment to answer this would be to imprint a specific area with a beta rhythm using optogenetic and play the corresponding modality. In one animal we would be able to stimulate S1 and play alternatively sounds and vibrations, and in a second period, stimulate A1 and play again both modalities. This

would certainly unravel a lot about our previous result and could definitively link the oscillatory changes in the cortex with a potential modality specific increased arousability.

Vibrant artifacts. The vibration stimulus unfortunately has another limitation. While they are on, the motors are creating a big artifact in the recording. Thankfully a 2 s-long stimulation at full power is already enough to reliably wake the animal up, restricting the time from which we cannot extract information. However, in the case of wake-ups and sleep-throughs, it would have been very interesting to analyze the direct response to the onset of a vibration. Indeed, in the case of spontaneous arousability within the fragility period, we noticed the absence of delta power upstroke in SNI compared to Sham. If such absence reflects an inability in SNI to generate sleep protective delta rhythms like the k-complexes in human, it would be interesting to see if sleep-through facing vibrations; (i) provoke such delta increase in mice and (ii) is impaired in SNI. Using shorter vibrations or sound stimuli would help to answer this in a specifically designed experiment.

Two deltas. Regarding delta power, it was recently confirmed that two bands (slow delta 0.75–1.75 Hz and fast 2.5–3.5 Hz) with separate homeostatic dynamic exist (Hubbard *et al.,* 2020). My results however encompass both delta bands as I considered delta power from 1 to 4 Hz. As my result suggest an inability to compensate internal and external perturbations with delta power increases, it would certainly be interesting to analyze again my data with this separation in mind. In addition, as it has already been shown in rats, K-complex-like events exist. As in human, they are dynamically non-distinguishable from slow waves (Deibel *et al.,* 2020). Whether what we observe is more of a slow wave or a delta burst is thus unclear. I can speculate that it is more of a delta wave process for two reason. First, with inhibition of thalamic reticular nucleus using DREADD, we demonstrated in 2018 that NREMS would locally switch from spindle rich power to delta rich power, suggesting an opposite relationship (L. M. Fernandez *et al.,* 2018). Second, the band that I used (1–4 Hz) is clearly more prone to sample delta waves than slow oscillations.

Assessment of spontaneous pain. Finally, in a mindset of reducing to the maximum the additional sleep perturbation in our animals, we did not test for pain sensitivity during our recordings. The stress associated to the behavioral tests could indeed have consequences on SNI only and not Sham, and we wanted to avoid any possible stress bias to be able to attribute our results to nerve injury only. However, although the SNI model is known for its reliable increase in sensitivity (Guida *et al.,* 2020), we do not have the possibility to firmly conclude that our results are due to spontaneous pain, as is the case in patients. Testing the sensitivity as it is classically done using von-Frey monofilaments or plantar test would not help in that regard, as it does not mean that the animals are experiencing spontaneous pain. Beside the already observed increase in theta power in quiet wakefulness in our animal, an observation of supposed spontaneous pain through grimace scale or condition place preference upon analgesia (Akintola *et al.,* 2017; Larson

et al., 2019) would help to begin to answer that complicated question that is often present in pain study in animal models.

Conclusion

Recently, the advances in both sleep and pain research and the common techniques used in both fields allowed to couple the knowledge and disentangle the important relationship between the two. I believe that there is still a lot to unravel about this complicated relationship, both in the direction that impaired sleep increases pain, and in the one I studied, where pain is disturbing sleep. My study represents only a part of the answer, but we provided important leads and novel approach to the question. The developing knowledge on the 0.02 Hz-fluctuation indeed already showed the value of considering it in sleep research in physiological and pathophysiological conditions. In my case, the subdivision of NREMS, and knowing where to probe for internal perturbations, helped to distinguish between spontaneous and evoked arousability and lead to the discovery of partial local arousal events accompanied by autonomic changes. These newly described arousal events find their place in the graded diversity of arousals between the k-complexes and the microarousals. Moreover, the development of closed-loop techniques and a strong dose of DIY electronics allowed to address questions in a precise and efficient manner. To achieve my work, I walked on the bumpy paved road that represent science. I hope that my study can find its place within this road and help future researcher in finding their own path.

Bibliography

Abel, T., Havekes, R., Saletin, J. M., & Walker, M. P. (2013). Sleep, plasticity and memory from molecules to whole-brain networks. *Curr Biol, 23*(17), R774-788. doi:10.1016/j.cub.2013.07.025

Akeju, O., & Brown, E. N. (2017). Neural oscillations demonstrate that general anesthesia and sedative states are neurophysiologically distinct from sleep. *Current Opinion in Neurobiology, 44*, 178-185. doi:10.1016/j.conb.2017.04.011

Akintola, T., Raver, C., Studlack, P., Uddin, O., Masri, R., & Keller, A. (2017). The grimace scale reliably assesses chronic pain in a rodent model of trigeminal neuropathic pain. *Neurobiol Pain, 2*, 13-17. doi:10.1016/j.ynpai.2017.10.001

Alexandre, C., Latremoliere, A., Ferreira, A., Miracca, G., Yamamoto, M., Scammell, T. E., & Woolf, C. J. (2017). Decreased alertness due to sleep loss increases pain sensitivity in mice. *Nat Med, 23*(6), 768-774. doi:10.1038/nm.4329

Alexandrou, A. J., Brown, A. R., Chapman, M. L., Estacion, M., Turner, J., Mis, M. A., . . . Stevens, E. B. (2016). Subtype-Selective Small Molecule Inhibitors Reveal a Fundamental Role for Nav1.7 in Nociceptor Electrogenesis, Axonal Conduction and Presynaptic Release. *PLoS One, 11*(4), e0152405. doi:10.1371/journal.pone.0152405

Alshelh, Z., Di Pietro, F., Youssef, A. M., Reeves, J. M., Macey, P. M., Vickers, E. R., . . . Henderson, L. A. (2016). Chronic Neuropathic Pain: It's about the Rhythm. *J Neurosci, 36*(3), 1008-1018. doi:10.1523/JNEUROSCI.2768-15.2016

Andersen, M. L., & Tufik, S. (2003). Sleep patterns over 21-day period in rats with chronic constriction of sciatic nerve. *Brain Res, 984*(1-2), 84-92. doi:10.1016/s0006-8993(03)03095-6

Andrillon, T., & Kouider, S. (2020). The vigilant sleeper: neural mechanisms of sensory (de)coupling during sleep. *Current Opinion in Physiology, 15*, 47-59. doi:10.1016/j.cophys.2019.12.002

Antony, J. W., Piloto, L., Wang, M., Pacheco, P., Norman, K. A., & Paller, K. A. (2018). Sleep Spindle Refractoriness Segregates Periods of Memory Reactivation. *Curr Biol, 28*(11), 1736-1743 e1734. doi:10.1016/j.cub.2018.04.020

Arce-Santana, E. R., Alba, A., Mendez, M. O., & Arce-Guevara, V. (2020). A-phase classification using convolutional neural networks. *Med Biol Eng Comput, 58*(5), 1003-1014. doi:10.1007/s11517-020-02144-6

Aston-Jones, G., & Bloom, F. E. (1981). Activity of norepinephrine-containing locus coeruleus neurons in behaving rats anticipates fluctuations in the sleep-waking cycle. *J Neurosci, 1*(8), 876-886. Retrieved from https://www.ncbi.nlm.nih.gov/pubmed/7346592

Axelrod, F. B., & Hilz, M. J. (2003). Inherited autonomic neuropathies. *Semin Neurol, 23*(4), 381-390. doi:10.1055/s-2004-817722

Azarbarzin, A., Ostrowski, M., Hanly, P., & Younes, M. (2014). Relationship between arousal intensity and heart rate response to arousal. *Sleep, 37*(4), 645-653. doi:10.5665/sleep.3560

Bastuji, H., Perchet, C., Legrain, V., Montes, C., & Garcia-Larrea, L. (2008). Laser evoked responses to painful stimulation persist during sleep and predict subsequent arousals. *Pain, 137*(3), 589-599. doi:10.1016/j.pain.2007.10.027

Beas, B. S., Wright, B. J., Skirzewski, M., Leng, Y., Hyun, J. H., Koita, O., . . . Penzo, M. A. (2018). The locus coeruleus drives disinhibition in the midline thalamus via a dopaminergic mechanism. *Nature Neuroscience, 21*(7), 963-+. doi:10.1038/s41593-018-0167-4

Belenky, G., Wesensten, N. J., Thorne, D. R., Thomas, M. L., Sing, H. C., Redmond, D. P., . . . Balkin, T. J. (2003). Patterns of performance degradation and restoration during sleep restriction and subsequent recovery: a sleep dose-response study. *J Sleep Res, 12*(1), 1-12. doi:10.1046/j.1365-2869.2003.00337.x

Bellesi, M., Riedner, B. A., Garcia-Molina, G. N., Cirelli, C., & Tononi, G. (2014). Enhancement of sleep slow waves: underlying mechanisms and practical consequences. *Front Syst Neurosci, 8*, 208. doi:10.3389/fnsys.2014.00208

Benchenane, K., Tiesinga, P. H., & Battaglia, F. P. (2011). Oscillations in the prefrontal cortex: a gateway to memory and attention. *Curr Opin Neurobiol, 21*(3), 475-485. doi:10.1016/j.conb.2011.01.004

Berna, C., Cojan, Y., Vuilleumier, P., & Desmeules, J. (2011). [Analgesic placebo effect: contribution of the neurosciences]. *Rev Med Suisse, 7*(301), 1390-1393. Retrieved from https://www.ncbi.nlm.nih.gov/pubmed/21815494

Bernardi, G., Siclari, F., Handjaras, G., Riedner, B. A., & Tononi, G. (2018). Local and Widespread Slow Waves in Stable NREM Sleep: Evidence for Distinct Regulation Mechanisms. *Frontiers in Human Neuroscience, 12*. doi:ARTN 248

10.3389/fnhum.2018.00248

Berry, R. B., Brooks, R., Gamaldo, C., Harding, S. M., Lloyd, R. M., Quan, S. F., . . . Vaughn, B. V. (2017). AASM Scoring Manual Updates for 2017 (Version 2.4). *J Clin Sleep Med, 13*(5), 665-666. doi:10.5664/jcsm.6576

Berta, T., Perrin, F. E., Pertin, M., Tonello, R., Liu, Y. C., Chamessian, A., . . . Decosterd, I. (2017). Gene Expression Profiling of Cutaneous Injured and Non-Injured Nociceptors in SNI Animal Model of Neuropathic Pain. *Sci Rep, 7*(1), 9367. doi:10.1038/s41598-017-08865-3

Besedovsky, L., Lange, T., & Born, J. (2012). Sleep and immune function. *Pflugers Arch, 463*(1), 121-137. doi:10.1007/s00424-011-1044-0

Bjurstrom, M. F., & Irwin, M. R. (2016). Polysomnographic characteristics in nonmalignant chronic pain populations: A review of controlled studies. *Sleep Med Rev, 26*, 74-86. doi:10.1016/j.smrv.2015.03.004

Blake, H., & Gerard, R. W. (1937). Brain potentials during sleep. *Am J Physiol, 119*, 692-703.

Blom, S. M., Pfister, J. P., Santello, M., Senn, W., & Nevian, T. (2014). Nerve injury-induced neuropathic pain causes disinhibition of the anterior cingulate cortex. *J Neurosci, 34*(17), 5754-5764. doi:10.1523/JNEUROSCI.3667-13.2014

Blume, C., Del Giudice, R., Wislowska, M., Heib, D. P. J., & Schabus, M. (2018). Standing sentinel during human sleep: Continued evaluation of environmental stimuli in the absence of consciousness. *Neuroimage, 178*, 638-648. doi:10.1016/j.neuroimage.2018.05.056

Bonnet, M., Carley, D., Carskadon, M., Easton, P., Guilleminault, C., Harper, R., . . . Westbrook, P. (1992). The Atlas Task Force. EEG arousals: Scoring rules and examples. *Sleep, 15*, 173-184.

Bonnet, M. H., Johnson, L. C., & Webb, W. B. (1978). The reliability of arousal threshold during sleep. *Psychophysiology, 15*(5), 412-416. doi:10.1111/j.1469-8986.1978.tb01407.x

Borbely, A. A., Tobler, I., & Hanagasioglu, M. (1984). Effect of sleep deprivation on sleep and EEG power spectra in the rat. *Behav Brain Res, 14*(3), 171-182. doi:10.1016/0166-4328(84)90186-4

Bourquin, A. F., Süveges, M., Pertin, M., Gilliard, N., Sardy, S., Davison, A. C., . . . Décosterd, I. (2006). Assessment and analysis of mechanical allodynia-like behavior induced by spared nerve injury (SNI) in the mouse. *Pain, 122*(1-2), 14 e11-14. doi:10.1016/j.pain.2005.10.036

Braun, A. R., Balkin, T. J., Wesenten, N. J., Carson, R. E., Varga, M., Baldwin, P., . . . Herscovitch, P. (1997). Regional cerebral blood flow throughout the sleep-wake cycle. An H2(15)O PET study. *Brain, 120 (Pt 7)*, 1173-1197. doi:10.1093/brain/120.7.1173

Burma, N. E., Leduc-Pessah, H., Fan, C. Y., & Trang, T. (2017). Animal models of chronic pain: Advances and challenges for clinical translation. *J Neurosci Res, 95*(6), 1242-1256. doi:10.1002/jnr.23768

Bushnell, M. C., Duncan, G. H., Hofbauer, R. K., Ha, B., Chen, J. I., & Carrier, B. (1999). Pain perception: is there a role for primary somatosensory cortex? *Proc Natl Acad Sci U S A, 96*(14), 7705-7709. doi:10.1073/pnas.96.14.7705

Campbell, S. S., & Tobler, I. (1984). Animal sleep: a review of sleep duration across phylogeny. *Neurosci Biobehav Rev, 8*(3), 269-300. doi:10.1016/0149-7634(84)90054-x

Cardoso-Cruz, H., Sameshima, K., Lima, D., & Galhardo, V. (2011). Dynamics of circadian thalamocortical flow of information during a peripheral neuropathic pain condition. *Front Integr Neurosci, 5*, 43. doi:10.3389/fnint.2011.00043

Cash, S. S., Halgren, E., Dehghani, N., Rossetti, A. O., Thesen, T., Wang, C., . . . Ulbert, I. (2009). The human K-complex represents an isolated cortical down-state. *Science, 324*(5930), 1084-1087. doi:10.1126/science.1169626

Challa, S. R. (2015). Surgical animal models of neuropathic pain: Pros and Cons. *Int J Neurosci, 125*(3), 170-174. doi:10.3109/00207454.2014.922559

Chiu, I. M., Pinho-Ribeiro, F. A., & Woolf, C. J. (2016). Pain and infection: pathogen detection by nociceptors. *Pain, 157*(6), 1192-1193. doi:10.1097/j.pain.0000000000000559

Christensen, J. A. E., Wassing, R., Wei, Y., Ramautar, J. R., Lakbila-Kamal, O., Jennum, P. J., & Van Someren, E. J. W. (2019). Data-driven analysis of EEG reveals concomitant superficial sleep during deep sleep in insomnia disorder. *Front Neurosci, 13*, 598. doi:10.3389/fnins.2019.00598

Cichon, J., Blanck, T. J. J., Gan, W. B., & Yang, G. (2017). Activation of cortical somatostatin interneurons prevents the development of neuropathic pain. *Nat Neurosci, 20*(8), 1122-1132. doi:10.1038/nn.4595

Claude, L., Chouchou, F., Prados, G., Castro, M., De Blay, B., Perchet, C., . . . Bastuji, H. (2015). Sleep spindles and human cortical nociception: a surface and intracerebral electrophysiological study. *J Physiol, 593*(22), 4995-5008. doi:10.1113/JP270941

Colrain, I. M. (2005). The K-complex: a 7-decade history. *Sleep, 28*(2), 255-273. doi:10.1093/sleep/28.2.255

Da Rosa, A. C., Kemp, B., Paiva, T., Lopes da Silva, F. H., & Kamphuisen, H. A. (1991). A model-based detector of vertex waves and K complexes in sleep electroencephalogram. *Electroencephalogr Clin Neurophysiol, 78*(1), 71-79. doi:10.1016/0013-4694(91)90021-u

Dang-Vu, T. T., McKinney, S. M., Buxton, O. M., Solet, J. M., & Ellenbogen, J. M. (2010). Spontaneous brain rhythms predict sleep stability in the face of noise. *Curr Biol, 20*(15), R626-627. doi:10.1016/j.cub.2010.06.032

De Felice, M., & Ossipov, M. H. (2016). Cortical and subcortical modulation of pain. *Pain Manag, 6*(2), 111-120. doi:10.2217/pmt.15.63

De Gennaro, L., Ferrara, M., & Bertini, M. (2000). The spontaneous K-complex during stage 2 sleep: is it the 'forerunner' of delta waves? *Neurosci Lett, 291*(1), 41-43. doi:10.1016/s0304-3940(00)01366-5

de Lecea, L., Carter, M. E., & Adamantidis, A. (2012). Shining light on wakefulness and arousal. *Biol Psychiatry, 71*(12), 1046-1052. doi:10.1016/j.biopsych.2012.01.032

Decosterd, I., & Woolf, C. J. (2000). Spared nerve injury: an animal model of persistent peripheral neuropathic pain. *Pain, 87*(2), 149-158. doi:10.1016/s0304-3959(00)00276-1

Deibel, S. H., Rota, R., Steenland, H. W., Ali, K., McNaughton, B. L., Tatsuno, M., & McDonald, R. J. (2020). Assessment of Sleep, K-Complexes, and Sleep Spindles in a T21 Light-Dark Cycle. *Front Neurosci, 14*, 551843. doi:10.3389/fnins.2020.551843

Devor, M. (2009). Ectopic discharge in Abeta afferents as a source of neuropathic pain. *Exp Brain Res, 196*(1), 115-128. doi:10.1007/s00221-009-1724-6

Dolensek, N., Gehrlach, D. A., Klein, A. S., & Gogolla, N. (2020). Facial expressions of emotion states and their neuronal correlates in mice. *Science, 368*(6486), 89-94. doi:10.1126/science.aaz9468

Dos Santos Lima, G. Z., Lobao-Soares, B., Corso, G., Belchior, H., Lopes, S. R., de Lima Prado, T., . . . Ivanov, P. C. (2019). Hippocampal and cortical communication around micro-arousals in slow-wave sleep. *Sci Rep, 9*(1), 5876. doi:10.1038/s41598-019-42100-5

Drewes, A. M., Nielsen, K. D., Arendt-Nielsen, L., Birket-Smith, L., & Hansen, L. M. (1997). The effect of cutaneous and deep pain on the electroencephalogram during sleep--an experimental study. *Sleep, 20*(8), 632-640. doi:10.1093/sleep/20.8.632

Dubin, A. E., & Patapoutian, A. (2010). Nociceptors: the sensors of the pain pathway. *J Clin Invest, 120*(11), 3760-3772. doi:10.1172/JCI42843

Edinger, J. D., & Krystal, A. D. (2003). Subtyping primary insomnia: is sleep state misperception a distinct clinical entity? *Sleep Med Rev, 7*(3), 203-214. doi:10.1053/smrv.2002.0253

Ermis, U., Krakow, K., & Voss, U. (2010). Arousal thresholds during human tonic and phasic REM sleep. *J Sleep Res, 19*(3), 400-406. doi:10.1111/j.1365-2869.2010.00831.x

Esser, S. K., Hill, S., & Tononi, G. (2009). Breakdown of effective connectivity during slow wave sleep: investigating the mechanism underlying a cortical gate using large-scale modeling. *J Neurophysiol, 102*(4), 2096-2111. doi:10.1152/jn.00059.2009

Eto, K., Wake, H., Watanabe, M., Ishibashi, H., Noda, M., Yanagawa, Y., & Nabekura, J. (2011). Inter-regional contribution of enhanced activity of the primary somatosensory cortex to the anterior cingulate cortex accelerates chronic pain behavior. *J Neurosci, 31*(21), 7631-7636. doi:10.1523/JNEUROSCI.0946-11.2011

Feige, B., Baglioni, C., Spiegelhalder, K., Hirscher, V., Nissen, C., & Riemann, D. (2013). The microstructure of sleep in primary insomnia: an overview and extension. *Int J Psychophysiol, 89*(2), 171-180. doi:10.1016/j.ijpsycho.2013.04.002

Fernandez, A., Kirsch, I., Noel, L., Rodondi, P. Y., Kaptchuk, T. J., Suter, M. R., . . . Berna, C. (2019). A test of positive suggestions about side effects as a way of enhancing the analgesic response to NSAIDs. *PLoS One, 14*(1), e0209851. doi:10.1371/journal.pone.0209851

Fernandez, L. M., Vantomme, G., Osorio-Forero, A., Cardis, R., Béard, E., & Lüthi, A. (2018). Thalamic reticular control of local sleep in sensory cortex. *Elife*, e39111. doi:doi: 10.7554/eLife.39111

Fernandez, L. M. J., & Lüthi, A. (2020). Sleep Spindles: Mechanisms and Functions. *Physiol Rev, 100*(2), 805-868. doi:10.1152/physrev.00042.2018

Ferri, R., Koo, B. B., Picchietti, D. L., & Fulda, S. (2017). Periodic leg movements during sleep: phenotype, neurophysiology, and clinical significance. *Sleep Med, 31*, 29-38. doi:10.1016/j.sleep.2016.05.014

Finan, P. H., Goodin, B. R., & Smith, M. T. (2013). The association of sleep and pain: an update and a path forward. *J Pain, 14*(12), 1539-1552. doi:10.1016/j.jpain.2013.08.007

Finnerup, N. B., Kuner, R., & Jensen, T. S. (2021). Neuropathic pain: from mechanisms to treatment. *Physiol Rev, 101*(1), 259-301. doi:10.1152/physrev.00045.2019

Franken, P., Dijk, D. J., Tobler, I., & Borbely, A. A. (1991). Sleep deprivation in rats: effects on EEG power spectra, vigilance states, and cortical temperature. *Am J Physiol, 261*(1 Pt 2), R198-208. doi:10.1152/ajpregu.1991.261.1.R198

Franken, P., Malafosse, A., & Tafti, M. (1999). Genetic determinants of sleep regulation in inbred mice. *Sleep, 22*(2), 155-169. Retrieved from https://www.ncbi.nlm.nih.gov/pubmed/10201060

Fries, P. (2015). Rhythms for Cognition: Communication through Coherence. *Neuron, 88*(1), 220-235. doi:10.1016/j.neuron.2015.09.034

Fultz, N. E., Bonmassar, G., Setsompop, K., Stickgold, R. A., Rosen, B. R., Polimeni, J. R., & Lewis, L. D. (2019). Coupled electrophysiological, hemodynamic, and cerebrospinal fluid oscillations in human sleep. *Science, 366*(6465), 628-631. doi:10.1126/science.aax5440

Garcia-Larrea, L., Frot, M., & Valeriani, M. (2003). Brain generators of laser-evoked potentials: from dipoles to functional significance. *Neurophysiol Clin, 33*(6), 279-292. doi:10.1016/j.neucli.2003.10.008

Garland, E. L. (2012). Pain processing in the human nervous system: a selective review of nociceptive and biobehavioral pathways. *Prim Care, 39*(3), 561-571. doi:10.1016/j.pop.2012.06.013

Gattlen, C., Clarke, C. B., Piller, N., Kirschmann, G., Pertin, M., Decosterd, I., . . . Suter, M. R. (2016). Spinal Cord T-Cell Infiltration in the Rat Spared Nerve Injury Model: A Time Course Study. *Int J Mol Sci, 17*(3), 352. doi:10.3390/ijms17030352

Gattlen, C., Deftu, A. F., Tonello, R., Ling, Y., Berta, T., Ristoiu, V., & Suter, M. R. (2020). The inhibition of Kir2.1 potassium channels depolarizes spinal microglial cells, reduces their proliferation, and attenuates neuropathic pain. *Glia, 68*(10), 2119-2135. doi:10.1002/glia.23831

Gerrans, P. (2020). Pain Asymbolia as Depersonalization for Pain Experience. An Interoceptive Active Inference Account. *Front Psychol, 11*, 523710. doi:10.3389/fpsyg.2020.523710

Gervasoni, D., Lin, S. C., Ribeiro, S., Soares, E. S., Pantoja, J., & Nicolelis, M. A. (2004). Global forebrain dynamics predict rat behavioral states and their transitions. *J Neurosci, 24*(49), 11137-11147. doi:10.1523/JNEUROSCI.3524-04.2004

Groh, A., Krieger, P., Mease, R. A., & Henderson, L. (2018). Acute and Chronic Pain Processing in the Thalamocortical System of Humans and Animal Models. *Neuroscience, 387*, 58-71. doi:10.1016/j.neuroscience.2017.09.042

Gross, J., Schnitzler, A., Timmermann, L., & Ploner, M. (2007). Gamma oscillations in human primary somatosensory cortex reflect pain perception. *PLoS Biol, 5*(5), e133. doi:10.1371/journal.pbio.0050133

Guida, F., De Gregorio, D., Palazzo, E., Ricciardi, F., Boccella, S., Belardo, C., . . . Maione, S. (2020). Behavioral, biochemical and electrophysiological changes in spared nerve injury model of neuropathic pain. *Int J Mol Sci, 21*(9). doi:10.3390/ijms21093396

Guilleminault, C., Cao, M., Yue, H. J., & Chawla, P. (2010). Obstructive sleep apnea and chronic opioid use. *Lung, 188*(6), 459-468. doi:10.1007/s00408-010-9254-3

Haack, M., Simpson, N., Sethna, N., Kaur, S., & Mullington, J. (2020). Sleep deficiency and chronic pain: potential underlying mechanisms and clinical implications. *Neuropsychopharmacology, 45*(1), 205-216. doi:10.1038/s41386-019-0439-z

Haas, H., & Panula, P. (2003). The role of histamine and the tuberomamillary nucleus in the nervous system. *Nat Rev Neurosci, 4*(2), 121-130. doi:10.1038/nrn1034

Halasz, P. (1998). Hierarchy of micro-arousals and the microstructure of sleep. *Neurophysiologie Clinique-Clinical Neurophysiology, 28*(6), 461-475. doi:Doi 10.1016/S0987-7053(99)80016-1

Halasz, P. (2005). K-complex, a reactive EEG graphoelement of NREM sleep: an old chap in a new garment. *Sleep Med Rev, 9*(5), 391-412. doi:10.1016/j.smrv.2005.04.003

Halasz, P. (2016). The K-complex as a special reactive sleep slow wave - A theoretical update. *Sleep Med Rev, 29*, 34-40. doi:10.1016/j.smrv.2015.09.004

Halasz, P., & Bódizs, R. b. (2013). *Dynamic structure of NREM sleep*. London ; New York: Springer.

Halasz, P., Terzano, M., Parrino, L., & Bodizs, R. (2004). The nature of arousal in sleep. *Journal of Sleep Research, 13*(1), 1-23. doi:DOI 10.1111/j.1365-2869.2004.00388.x

Hartmann, S., Bruni, O., Ferri, R., Redline, S., & Baumert, M. (2020). Characterization of cyclic alternating pattern during sleep in older men and women using large population studies. *Sleep, 43*(7). doi:10.1093/sleep/zsaa016

Hauck, M., Lorenz, J., & Engel, A. K. (2007). Attention to painful stimulation enhances gamma-band activity and synchronization in human sensorimotor cortex. *J Neurosci, 27*(35), 9270-9277. doi:10.1523/JNEUROSCI.2283-07.2007

Hayat, H., Regev, N., Matosevich, N., Sales, A., Paredes-Rodriguez, E., Krom, A. J., . . . Nir, Y. (2020). Locus coeruleus norepinephrine activity mediates sensory-evoked awakenings from sleep. *Sci Adv, 6*(15), eaaz4232. doi:10.1126/sciadv.aaz4232

Heid, C., Mouraux, A., Treede, R. D., Schuh-Hofer, S., Rupp, A., & Baumgartner, U. (2020). Early gamma-oscillations as correlate of localized nociceptive processing in primary sensorimotor cortex. *J Neurophysiol, 123*(5), 1711-1726. doi:10.1152/jn.00444.2019

Hu, L., Peng, W., Valentini, E., Zhang, Z., & Hu, Y. (2013). Functional features of nociceptive-induced suppression of alpha band electroencephalographic oscillations. *J Pain, 14*(1), 89-99. doi:10.1016/j.jpain.2012.10.008

Huang, Z. L., Mochizuki, T., Qu, W. M., Hong, Z. Y., Watanabe, T., Urade, Y., & Hayaishi, O. (2006). Altered sleep-wake characteristics and lack of arousal response to H3 receptor antagonist in histamine H1 receptor knockout mice. *Proc Natl Acad Sci U S A, 103*(12), 4687-4692. doi:10.1073/pnas.0600451103

Hubbard, J., Gent, T. C., Hoekstra, M. M. B., Emmenegger, Y., Mongrain, V., Landolt, H. P., . . . Franken, P. (2020). Rapid fast-delta decay following prolonged wakefulness marks a phase of wake-inertia in NREM sleep. *Nat Commun, 11*(1), 3130. doi:10.1038/s41467-020-16915-0

Ibrahim, M. M., Deng, H., Zvonok, A., Cockayne, D. A., Kwan, J., Mata, H. P., . . . Malan, T. P., Jr. (2003). Activation of CB2 cannabinoid receptors by AM1241 inhibits experimental neuropathic pain: pain inhibition by receptors not present in the CNS. *Proc Natl Acad Sci U S A, 100*(18), 10529-10533. doi:10.1073/pnas.1834309100

Imeri, L., & Opp, M. R. (2009). How (and why) the immune system makes us sleep. *Nat Rev Neurosci, 10*(3), 199-210. doi:10.1038/nrn2576

Inostroza, M., & Born, J. (2013). Sleep for preserving and transforming episodic memory. *Annu Rev Neurosci, 36*, 79-102. doi:10.1146/annurev-neuro-062012-170429

Ioannides, A. A., Liu, L., & Kostopoulos, G. K. (2019). The Emergence of Spindles and K-Complexes and the Role of the Dorsal Caudal Part of the Anterior Cingulate as the Generator of K-Complexes. *Front Neurosci, 13*, 814. doi:10.3389/fnins.2019.00814

Jahnke, K., von Wegner, F., Morzelewski, A., Borisov, S., Maischein, M., Steinmetz, H., & Laufs, H. (2012). To wake or not to wake? The two-sided nature of the human K-complex. *Neuroimage, 59*(2), 1631-1638. doi:10.1016/j.neuroimage.2011.09.013

Jank, R., Gallee, A., Boeckle, M., Fiegl, S., & Pieh, C. (2017). Chronic Pain and Sleep Disorders in Primary Care. *Pain Res Treat, 2017*, 9081802. doi:10.1155/2017/9081802

Jensen, K. B., Kaptchuk, T. J., Kirsch, I., Raicek, J., Lindstrom, K. M., Berna, C., . . . Kong, J. (2012). Nonconscious activation of placebo and nocebo pain responses. *Proc Natl Acad Sci U S A, 109*(39), 15959-15964. doi:10.1073/pnas.1202056109

Jonak, C. R., Lovelace, J. W., Ethell, I. M., Razak, K. A., & Binder, D. K. (2018). Reusable Multielectrode Array Technique for Electroencephalography in Awake Freely Moving Mice. *Front Integr Neurosci, 12*, 53. doi:10.3389/fnint.2018.00053

Jones, B. E. (2003). Arousal systems. *Front Biosci, 8*, s438-451. doi:10.2741/1074

Jun, J. J., Steinmetz, N. A., Siegle, J. H., Denman, D. J., Bauza, M., Barbarits, B., . . . Harris, T. D. (2017). Fully integrated silicon probes for high-density recording of neural activity. *Nature, 551*(7679), 232-236. doi:10.1038/nature24636

Kato, T., Montplaisir, J. Y., & Lavigne, G. J. (2004). Experimentally induced arousals during sleep: a cross-modality matching paradigm. *J Sleep Res, 13*(3), 229-238. doi:10.1111/j.1365-2869.2004.00409.x

Kaur, S., & Saper, C. B. (2019). Neural Circuitry Underlying Waking Up to Hypercapnia. *Front Neurosci, 13*, 401. doi:10.3389/fnins.2019.00401

Keene, A. C., & Duboue, E. R. (2018). The origins and evolution of sleep. *Journal of Experimental Biology, 221*(11). doi:ARTN jeb159533

10.1242/jeb.159533

Kehlet, H., Jensen, T. S., & Woolf, C. J. (2006). Persistent postsurgical pain: risk factors and prevention. *Lancet, 367*(9522), 1618-1625. doi:10.1016/S0140-6736(06)68700-X

Kelly, G. A., Blake, C., Power, C. K., O'Keeffe, D., & Fullen, B. M. (2011). The association between chronic low back pain and sleep: a systematic review. *Clin J Pain, 27*(2), 169-181. doi:10.1097/AJP.0b013e3181f3bdd5

Kennedy, C., Gillin, J. C., Mendelson, W., Suda, S., Miyaoka, M., Ito, M., . . . Sokoloff, L. (1982). Local cerebral glucose utilization in non-rapid eye movement sleep. *Nature, 297*(5864), 325-327. doi:10.1038/297325a0

Kontinen, V. K., Ahnaou, A., Drinkenburg, W. H., & Meert, T. F. (2003). Sleep and EEG patterns in the chronic constriction injury model of neuropathic pain. *Physiol Behav, 78*(2), 241-246. doi:10.1016/s0031-9384(02)00966-6

Krueger, J. M., Frank, M. G., Wisor, J. P., & Roy, S. (2016). Sleep function: Toward elucidating an enigma. *Sleep Med Rev, 28*, 46-54. doi:10.1016/j.smrv.2015.08.005

Kucyi, A., & Davis, K. D. (2015). The dynamic pain connectome. *Trends Neurosci, 38*(2), 86-95. doi:10.1016/j.tins.2014.11.006

Kuner, R., & Kuner, T. (2020). Cellular circuits in the brain and their modulation in acute and chronic pain. *Physiol Rev*. doi:10.1152/physrev.00040.2019

Langford, D. J., Bailey, A. L., Chanda, M. L., Clarke, S. E., Drummond, T. E., Echols, S., . . . Mogil, J. S. (2010). Coding of facial expressions of pain in the laboratory mouse. *Nat Methods, 7*(6), 447-449. doi:10.1038/nmeth.1455

Largo, R., Lopes, M. C., Spruyt, K., Guilleminault, C., Wang, Y. P., & Rosa, A. C. (2019). Visual and automatic classification of the cyclic alternating pattern in electroencephalography during sleep. *Braz J Med Biol Res, 52*(3), e8059. doi:10.1590/1414-431X20188059

Larson, C. M., Wilcox, G. L., & Fairbanks, C. A. (2019). The Study of Pain in Rats and Mice. *Comp Med, 69*(6), 555-570. doi:10.30802/AALAS-CM-19-000062

Latremoliere, A., & Woolf, C. J. (2009). Central Sensitization: A Generator of Pain Hypersensitivity by Central Neural Plasticity. *Journal of Pain, 10*(9), 895-926. doi:10.1016/j.jpain.2009.06.012

Lavigne, G., Brousseau, M., Kato, T., Mayer, P., Manzini, C., Guitard, F., & Monplaisir, J. (2004). Experimental pain perception remains equally active over all sleep stages. *Pain, 110*(3), 646-655. doi:10.1016/j.pain.2004.05.003

Lavigne, G., Zucconi, M., Castronovo, C., Manzini, C., Marchettini, P., & Smirne, S. (2000). Sleep arousal response to experimental thermal stimulation during sleep in human subjects free of pain and sleep problems. *Pain, 84*(2-3), 283-290. doi:10.1016/s0304-3959(99)00213-4

Lazar, Z. I., Dijk, D. J., & Lazar, A. S. (2019). Infraslow oscillations in human sleep spindle activity. *J Neurosci Methods, 316*, 22-34. doi:10.1016/j.jneumeth.2018.12.002

LeBlanc, B. W., Bowary, P. M., Chao, Y. C., Lii, T. R., & Saab, C. Y. (2016). Electroencephalographic signatures of pain and analgesia in rats. *Pain, 157*(10), 2330-2340. doi:10.1097/j.pain.0000000000000652

LeBlanc, B. W., Cross, B., Smith, K. A., Roach, C., Xia, J., Chao, Y. C., . . . Saab, C. Y. (2017). Thalamic bursts down-regulate cortical theta and nociceptive behavior. *Sci Rep, 7*(1), 2482. doi:10.1038/s41598-017-02753-6

LeBlanc, B. W., Lii, T. R., Huang, J. J., Chao, Y. C., Bowary, P. M., Cross, B. S., . . . Saab, C. Y. (2016). T-type calcium channel blocker Z944 restores cortical synchrony and thalamocortical connectivity in a rat model of neuropathic pain. *Pain, 157*(1), 255-263. doi:10.1097/j.pain.0000000000000362

LeBlanc, B. W., Lii, T. R., Silverman, A. E., Alleyne, R. T., & Saab, C. Y. (2014). Cortical theta is increased while thalamocortical coherence is decreased in rat models of acute and chronic pain. *Pain, 155*(4), 773-782. doi:10.1016/j.pain.2014.01.013

Lecci, S., Cataldi, J., Betta, M., Bernardi, G., Heinzer, R., & Siclari, F. (2020). EEG changes associated with subjective under- and overestimation of sleep duration. *Sleep, 43*, zsaa094. doi:10.1093/sleep/zsaa094

Legrain, V., Crombez, G., Verhoeven, K., & Mouraux, A. (2011). The role of working memory in the attentional control of pain. *Pain, 152*(2), 453-459. doi:10.1016/j.pain.2010.11.024

Leknes, S., Berna, C., Lee, M. C., Snyder, G. D., Biele, G., & Tracey, I. (2013). The importance of context: when relative relief renders pain pleasant. *Pain, 154*(3), 402-410. doi:10.1016/j.pain.2012.11.018

Léna, C., Popa, D., Grailhe, R., Escourrou, P., Changeux, J. P., & Adrien, J. (2004). β2-containing nicotinic receptors contribute to the organization of sleep and regulate putative micro-arousals in mice. *J Neurosci, 24*(25), 5711-5718. doi:10.1523/JNEUROSCI.3882-03.2004

Liberati, G., Klocker, A., Algoet, M., Mulders, D., Maia Safronova, M., Ferrao Santos, S., . . . Mouraux, A. (2018). Gamma-Band Oscillations Preferential for Nociception can be Recorded in the Human Insula. *Cereb Cortex, 28*(10), 3650-3664. doi:10.1093/cercor/bhx237

Libourel, P. A., Barrillot, B., Arthaud, S., Massot, B., Morel, A. L., Beuf, O., . . . Luppi, P. H. (2018). Partial homologies between sleep states in lizards, mammals, and birds suggest a complex evolution of sleep states in amniotes. *PLoS Biol, 16*(10), e2005982. doi:10.1371/journal.pbio.2005982

Llinas, R. R., Ribary, U., Jeanmonod, D., Kronberg, E., & Mitra, P. P. (1999). Thalamocortical dysrhythmia: A neurological and neuropsychiatric syndrome characterized by magnetoencephalography. *Proc Natl Acad Sci U S A, 96*(26), 15222-15227. doi:10.1073/pnas.96.26.15222

Lo, C. C., Chou, T., Penzel, T., Scammell, T. E., Strecker, R. E., Stanley, H. E., & Ivanov, P. (2004). Common scale-invariant patterns of sleep-wake transitions across mammalian species. *Proc Natl Acad Sci U S A, 101*(50), 17545-17548. doi:10.1073/pnas.0408242101

Loomis, A. L., Harvey, E. N., & Hobart, G. A. (1937). Cerebral states during sleep, as studied by human brain potentials. *Journal of Experimental Psychology, 21*, 127-144. doi:DOI 10.1037/h0057431

Lorenz, J., & Garcia-Larrea, L. (2003). Contribution of attentional and cognitive factors to laser evoked brain potentials. *Neurophysiol Clin, 33*(6), 293-301. doi:10.1016/j.neucli.2003.10.004

Lustenberger, C., & Huber, R. (2012). High density electroencephalography in sleep research: potential, problems, future perspective. *Front Neurol, 3*, 77. doi:10.3389/fneur.2012.00077

Maingret, N., Girardeau, G., Todorova, R., Goutierre, M., & Zugaro, M. (2016). Hippocampo-cortical coupling mediates memory consolidation during sleep. *Nat Neurosci, 19*(7), 959-964. doi:10.1038/nn.4304

Manconi, M., Silvani, A., & Ferri, R. (2017). Commentary: Coordinated infraslow neural and cardiac oscillations mark fragility and offline periods in mammalian sleep. *Front Physiol, 8*, 847. doi:10.3389/fphys.2017.00847

Mantini, D., Perrucci, M. G., Del Gratta, C., Romani, G. L., & Corbetta, M. (2007). Electrophysiological signatures of resting state networks in the human brain. *Proc Natl Acad Sci U S A, 104*(32), 13170-13175. doi:10.1073/pnas.0700668104

Martinac, B. (2012). Mechanosensitive ion channels: an evolutionary and scientific tour de force in mechanobiology. *Channels (Austin), 6*(4), 211-213. doi:10.4161/chan.22047

Massimini, M., Ferrarelli, F., Huber, R., Esser, S. K., Singh, H., & Tononi, G. (2005). Breakdown of cortical effective connectivity during sleep. *Science, 309*(5744), 2228-2232. doi:10.1126/science.1117256

Massimini, M., Rosanova, M., & Mariotti, M. (2003). EEG slow (approximately 1 Hz) waves are associated with nonstationarity of thalamo-cortical sensory processing in the sleeping human. *J Neurophysiol, 89*(3), 1205-1213. doi:10.1152/jn.00373.2002

Mathias, J. L., Cant, M. L., & Burke, A. L. J. (2018). Sleep disturbances and sleep disorders in adults living with chronic pain: a meta-analysis. *Sleep Med, 52*, 198-210. doi:10.1016/j.sleep.2018.05.023

Mátyás, F., Komlósi, G., Babiczky, Á., Kocsis, K., Barthó, P., Barsy, B., . . . Acsády, L. (2018). A highly collateralized thalamic cell type with arousal-predicting activity serves as a key hub for graded state transitions in the forebrain. *Nat Neurosci, 21*(11), 1551-1562. doi:10.1038/s41593-018-0251-9

May, E. S., Butz, M., Kahlbrock, N., Hoogenboom, N., Brenner, M., & Schnitzler, A. (2012). Pre- and post-stimulus alpha activity shows differential modulation with spatial attention during the processing of pain. *Neuroimage, 62*(3), 1965-1974. doi:10.1016/j.neuroimage.2012.05.071

May, E. S., Nickel, M. M., Ta Dinh, S., Tiemann, L., Heitmann, H., Voth, I., . . . Ploner, M. (2019). Prefrontal gamma oscillations reflect ongoing pain intensity in chronic back pain patients. *Hum Brain Mapp, 40*(1), 293-305. doi:10.1002/hbm.24373

McCormick, D. A., & Bal, T. (1994). Sensory gating mechanisms of the thalamus. *Curr Opin Neurobiol, 4*(4), 550-556. doi:10.1016/0959-4388(94)90056-6

McEntire, D. M., Kirkpatrick, D. R., Dueck, N. P., Kerfeld, M. J., Smith, T. A., Nelson, T. J., . . . Agrawal, D. K. (2016). Pain transduction: a pharmacologic perspective. *Expert Rev Clin Pharmacol, 9*(8), 1069-1080. doi:10.1080/17512433.2016.1183481

McKenna, J. T., Thankachan, S., Uygun, D. S., Shukla, C., McNally, J. M., Schiffino, F. L., . . . Basheer, R. (2020). Basal forebrain parvalbumin neurons mediate arousals from sleep induced by hypercarbia or auditory stimuli. *Curr Biol, 30*(12), 2379-2385 e2374. doi:10.1016/j.cub.2020.04.029

Melzack, R. (1999). Pain--an overview. *Acta Anaesthesiol Scand, 43*(9), 880-884. doi:10.1034/j.1399-6576.1999.430903.x

Mendez, M. O., Chouvarda, I., Alba, A., Bianchi, A. M., Grassi, A., Arce-Santana, E., . . . Parrino, L. (2016). Analysis of A-phase transitions during the cyclic alternating pattern under normal sleep. *Med Biol Eng Comput, 54*(1), 133-148. doi:10.1007/s11517-015-1349-9

Menefee, L. A., Cohen, M. J. M., Anderson, W. R., Doghramji, K., Frank, E. D., & Lee, H. (2000). Sleep disturbance and nonmalignant chronic pain: A comprehensive review of the literature. *Pain Medicine, 1*(2), 156-172. doi:DOI 10.1046/j.1526-4637.2000.00022.x

Misra, G., Wang, W. E., Archer, D. B., Roy, A., & Coombes, S. A. (2017). Automated classification of pain perception using high-density electroencephalography data. *J Neurophysiol, 117*(2), 786-795. doi:10.1152/jn.00650.2016

Moldofsky, H. (2001). Sleep and pain. *Sleep Medicine Reviews, 5*(5), 387-398. doi:10.1053/smrv.2001.0179

Monassi, C. R., Bandler, R., & Keay, K. A. (2003). A subpopulation of rats show social and sleep-waking changes typical of chronic neuropathic pain following peripheral nerve injury. *Eur J Neurosci, 17*(9), 1907-1920. doi:10.1046/j.1460-9568.2003.02627.x

Morin, C. M., Gibson, D., & Wade, J. (1998). Self-reported sleep and mood disturbance in chronic pain patients. *Clin J Pain, 14*(4), 311-314. doi:10.1097/00002508-199812000-00007

Neckelmann, D., & Ursin, R. (1993). Sleep stages and EEG power spectrum in relation to acoustical stimulus arousal threshold in the rat. *Sleep, 16*(5), 467-477. Retrieved from https://www.ncbi.nlm.nih.gov/pubmed/8378687

Nickel, M. M., May, E. S., Tiemann, L., Postorino, M., Ta Dinh, S., & Ploner, M. (2017). Autonomic responses to tonic pain are more closely related to stimulus intensity than to pain intensity. *Pain, 158*(11), 2129-2136. doi:10.1097/j.pain.0000000000001010

Niethard, N., Ngo, H. V., Ehrlich, I., & Born, J. (2018). Cortical circuit activity underlying sleep slow oscillations and spindles. *Proc Natl Acad Sci U S A, 115*(39), E9220-E9229. doi:10.1073/pnas.1805517115

Nilius, B., & Honore, E. (2012). Sensing pressure with ion channels. *Trends Neurosci, 35*(8), 477-486. doi:10.1016/j.tins.2012.04.002

Nir, Y., Vyazovskiy, V. V., Cirelli, C., Banks, M. I., & Tononi, G. (2015). Auditory responses and stimulus-specific adaptation in rat auditory cortex are preserved across NREM and REM sleep. *Cereb Cortex, 25*(5), 1362-1378. doi:10.1093/cercor/bht328

Nobili, L., Ferrara, M., Moroni, F., De Gennaro, L., Russo, G. L., Campus, C., . . . De Carli, F. (2011). Dissociated wake-like and sleep-like electro-cortical activity during sleep. *Neuroimage, 58*(2), 612-619. doi:10.1016/j.neuroimage.2011.06.032

Nollet, M., Hicks, H., McCarthy, A. P., Wu, H., Moller-Levet, C. S., Laing, E. E., . . . Winsky-Sommerer, R. (2019). REM sleep's unique associations with corticosterone regulation, apoptotic pathways, and behavior in chronic stress in mice. *Proc Natl Acad Sci U S A, 116*(7), 2733-2742. doi:10.1073/pnas.1816456116

Palva, J. M., & Palva, S. (2012). Infra-slow fluctuations in electrophysiological recordings, blood-oxygenation-level-dependent signals, and psychophysical time series. *Neuroimage, 62*(4), 2201-2211. doi:10.1016/j.neuroimage.2012.02.060

Perlis, M. L., Merica, H., Smith, M. T., & Giles, D. E. (2001). Beta EEG activity and insomnia. *Sleep Med Rev, 5*(5), 363-374. doi:10.1053/smrv.2001.0151

Perlis, M. T., Smith, M. T., Andrews, P. J., Orff, H., & Giles, D. E. (2001). Beta/Gamma EEG activity in patients with primary and secondary insomnia and good sleeper controls. *Sleep, 24*(1), 110-117. doi:10.1093/sleep/24.1.110

Perrin, F., Garcia-Larrea, L., Mauguiere, F., & Bastuji, H. (1999). A differential brain response to the subject's own name persists during sleep. *Clin Neurophysiol, 110*(12), 2153-2164. doi:10.1016/s1388-2457(99)00177-7

Piéron, H. (1913). Le problème physiologique du sommeil.

Ploner, M., Sorg, C., & Gross, J. (2017). Brain rhythms of pain. *Trends Cogn Sci, 21*(2), 100-110. doi:10.1016/j.tics.2016.12.001

Portas, C. M., Krakow, K., Allen, P., Josephs, O., Armony, J. L., & Frith, C. D. (2000). Auditory processing across the sleep-wake cycle: simultaneous EEG and fMRI monitoring in humans. *Neuron, 28*(3), 991-999. doi:10.1016/s0896-6273(00)00169-0

Rasch, B., & Born, J. (2013). About Sleep's Role in Memory. *Physiological Reviews, 93*(2), 681-766. doi:10.1152/physrev.00032.2012

Rechtschaffen, A., Hauri, P., & Zeitlin, M. (1966). Auditory awakening thresholds in REM and NREM sleep stages. *Percept Mot Skills, 22*(3), 927-942. doi:10.2466/pms.1966.22.3.927

Riedner, B. A., Hulse, B. K., Murphy, M. J., Ferrarelli, F., & Tononi, G. (2011). Temporal dynamics of cortical sources underlying spontaneous and peripherally evoked slow waves. *Prog Brain Res, 193*, 201-218. doi:10.1016/B978-0-444-53839-0.00013-2

Rolls, A., Colas, D., Adamantidis, A., Carter, M., Lanre-Amos, T., Heller, H. C., & de Lecea, L. (2011). Optogenetic disruption of sleep continuity impairs memory consolidation. *Proc Natl Acad Sci U S A, 108*(32), 13305-13310. doi:10.1073/pnas.1015633108

Rosa, R. R., Bonnet, M. H., & Warm, J. S. (1983). Recovery of performance during sleep following sleep deprivation. *Psychophysiology, 20*(2), 152-159. doi:10.1111/j.1469-8986.1983.tb03281.x

Rudzik, F., Thiesse, L., Pieren, R., Heritier, H., Eze, I. C., Foraster, M., . . . Cajochen, C. (2020). Ultradian modulation of cortical arousals during sleep: effects of age and exposure to nighttime transportation noise. *Sleep, 43*(7). doi:10.1093/sleep/zsz324

Sakai, K., Crochet, S., & Onoe, H. (2001). Pontine structures and mechanisms involved in the generation of paradoxical (REM) sleep. *Archives Italiennes De Biologie, 139*(1-2), 93-107. Retrieved from <Go to ISI>://WOS:000167021100010

Samuels, E. R., & Szabadi, E. (2008). Functional neuroanatomy of the noradrenergic locus coeruleus: its roles in the regulation of arousal and autonomic function part II: physiological and pharmacological manipulations and pathological alterations of locus coeruleus activity in humans. *Curr Neuropharmacol, 6*(3), 254-285. doi:10.2174/157015908785777193

Sarnthein, J., Stern, J., Aufenberg, C., Rousson, V., & Jeanmonod, D. (2006). Increased EEG power and slowed dominant frequency in patients with neurogenic pain. *Brain, 129*(Pt 1), 55-64. doi:10.1093/brain/awh631

Schabus, M., Dang-Vu, T. T., Heib, D. P., Boly, M., Desseilles, M., Vandewalle, G., . . . Maquet, P. (2012). The Fate of Incoming Stimuli during NREM Sleep is Determined by Spindles and the Phase of the Slow Oscillation. *Front Neurol, 3*, 40. doi:10.3389/fneur.2012.00040

Schieber, J. P., Muzet, A., & Ferriere, P. J. (1971). [Phases of spontaneous transitory activation during normal sleep in humans]. *Arch Sci Physiol (Paris), 25*(4), 443-465. Retrieved from https://www.ncbi.nlm.nih.gov/pubmed/4345798

Schulz, E., May, E. S., Postorino, M., Tiemann, L., Nickel, M. M., Witkovsky, V., . . . Ploner, M. (2015). Prefrontal gamma oscillations encode tonic pain in humans. *Cereb Cortex, 25*(11), 4407-4414. doi:10.1093/cercor/bhv043

Seibt, J., Richard, C. J., Sigl-Glöckner, J., Takahashi, N., Kaplan, D., Doron, G., . . . Larkum, M. E. (2017). Cortical dendritic activity correlates with spindle-rich oscillations during sleep in rodents. *Nat Commun, 8*(1), 684. doi: 10.1038/s41467-017-00735-w

Sforza, E., Jouny, C., & Ibanez, V. (2000). Cardiac activation during arousal in humans: further evidence for hierarchy in the arousal response. *Clin Neurophysiol, 111*(9), 1611-1619. doi:10.1016/s1388-2457(00)00363-1

Shang, Y., Griffith, L. C., & Rosbash, M. (2008). Light-arousal and circadian photoreception circuits intersect at the large PDF cells of the Drosophila brain. *Proc Natl Acad Sci U S A, 105*(50), 19587-19594. doi:10.1073/pnas.0809577105

Siclari, F., Baird, B., Perogamvros, L., Bernardi, G., LaRocque, J. J., Riedner, B., . . . Tononi, G. (2017). The neural correlates of dreaming. *Nat Neurosci, 20*(6), 872-878. doi:10.1038/nn.4545

Siegel, J. M. (2005). Clues to the functions of mammalian sleep. *Nature, 437*(7063), 1264-1271. doi:10.1038/nature04285

Silvani, A. (2019). Sleep disorders, nocturnal blood pressure, and cardiovascular risk: A translational perspective. *Auton Neurosci, 218*, 31-42. doi:10.1016/j.autneu.2019.02.006

Stepanski, E., Lamphere, J., Badia, P., Zorick, F., & Roth, T. (1984). Sleep fragmentation and daytime sleepiness. *Sleep, 7*(1), 18-26. doi:10.1093/sleep/7.1.18

Steriade, M., McCormick, D. A., & Sejnowski, T. J. (1993). Thalamocortical oscillations in the sleeping and aroused brain. *Science, 262*(5134), 679-685. doi:10.1126/science.8235588

Stern, J., Jeanmonod, D., & Sarnthein, J. (2006). Persistent EEG overactivation in the cortical pain matrix of neurogenic pain patients. *Neuroimage, 31*(2), 721-731. doi:10.1016/j.neuroimage.2005.12.042

Stuck, B. A. (2010). [Chemosensory processing during sleep]. *HNO, 58*(6), 564-568. doi:10.1007/s00106-009-2071-4

Stuck, B. A., Moutsis, T. T., Bingel, U., & Sommer, J. U. (2016). Chemosensory stimulation during sleep - Arousal responses to gustatory stimulation. *Neuroscience, 322*, 326-332. doi:10.1016/j.neuroscience.2016.02.044

Stuck, B. A., Stieber, K., Frey, S., Freiburg, C., Hormann, K., Maurer, J. T., & Hummel, T. (2007). Arousal responses to olfactory or trigeminal stimulation during sleep. *Sleep, 30*(4), 506-510. doi:DOI 10.1093/sleep/30.4.506

Sun, G., Wen, Z., Ok, D., Doan, L., Wang, J., & Chen, Z. S. (2021). Detecting acute pain signals from human EEG. *J Neurosci Methods, 347*, 108964. doi:10.1016/j.jneumeth.2020.108964

Takahashi, K., Kayama, Y., Lin, J. S., & Sakai, K. (2010). Locus coeruleus neuronal activity during the sleep-waking cycle in mice. *Neuroscience, 169*(3), 1115-1126. doi:10.1016/j.neuroscience.2010.06.009

Tan, L. L., Oswald, M. J., Heinl, C., Retana Romero, O. A., Kaushalya, S. K., Monyer, H., & Kuner, R. (2019). Gamma oscillations in somatosensory cortex recruit prefrontal and descending serotonergic pathways in aversion and nociception. *Nat Commun, 10*(1), 983. doi:10.1038/s41467-019-08873-z

Terzano, M. G., & Parrino, L. (2000). Origin and Significance of the Cyclic Alternating Pattern (CAP). REVIEW ARTICLE. *Sleep Med Rev, 4*(1), 101-123. doi:10.1053/smrv.1999.0083

Terzano, M. G., Parrino, L., Sherieri, A., Chervin, R., Chokroverty, S., Guilleminault, C., . . . Walters, A. (2001). Atlas, rules, and recording techniques for the scoring of cyclic alternating pattern (CAP) in human sleep. *Sleep Med, 2*(6), 537-553. doi:10.1016/s1389-9457(01)00149-6

Terzano, M. G., Parrino, L., Smerieri, A., De Carli, F., Nobili, L., Donadio, S., & Ferrillo, F. (2005). CAP and arousals are involved in the homeostatic and ultradian sleep processes. *Journal of Sleep Research, 14*(4), 359-368. doi:DOI 10.1111/j.1365-2869.2005.00479.x

Tobler, I., Gaus, S. E., Deboer, T., Achermann, P., Fischer, M., Rulicke, T., . . . Manson, J. C. (1996). Altered circadian activity rhythms and sleep in mice devoid of prion protein. *Nature, 380*(6575), 639-642. doi:10.1038/380639a0

Tokunaga, S., Takeda, Y., Shinomiya, K., Yamamoto, W., Utsu, Y., Toide, K., & Kamei, C. (2007). Changes of sleep patterns in rats with chronic constriction injury under aversive conditions. *Biol Pharm Bull, 30*(11), 2088-2090. doi:10.1248/bpb.30.2088

Tononi, G., & Cirelli, C. (2014). Sleep and the price of plasticity: from synaptic and cellular homeostasis to memory consolidation and integration. *Neuron, 81*(1), 12-34. doi:10.1016/j.neuron.2013.12.025

Topham, L., Gregoire, S., Kang, H., Salmon-Divon, M., Lax, E., Millecamps, M., . . . Stone, L. S. (2020). The transition from acute to chronic pain: dynamic epigenetic reprogramming of the mouse prefrontal cortex up to 1 year after nerve injury. *Pain, 161*(10), 2394-2409. doi:10.1097/j.pain.0000000000001917

Tracey, I., & Mantyh, P. W. (2007). The cerebral signature for pain perception and its modulation. *Neuron, 55*(3), 377-391. doi:10.1016/j.neuron.2007.07.012

Treede, R. D., Rief, W., Barke, A., Aziz, Q., Bennett, M. I., Benoliel, R., . . . Wang, S. J. (2019). Chronic pain as a symptom or a disease: the IASP Classification of Chronic Pain for the International Classification of Diseases (ICD-11). *Pain, 160*(1), 19-27. doi:10.1097/j.pain.0000000000001384

Tyree, S. M., & de Lecea, L. (2017). Optogenetic Investigation of Arousal Circuits. *Int J Mol Sci, 18*(8). doi:10.3390/ijms18081773

Usoskin, D., Furlan, A., Islam, S., Abdo, H., Lonnerberg, P., Lou, D., . . . Ernfors, P. (2015). Unbiased classification of sensory neuron types by large-scale single-cell RNA sequencing. *Nat Neurosci, 18*(1), 145-153. doi:10.1038/nn.3881

Van der Werf, Y. D., Witter, M. P., & Groenewegen, H. J. (2002). The intralaminar and midline nuclei of the thalamus. Anatomical and functional evidence for participation in processes of arousal and awareness. *Brain Res Brain Res Rev, 39*(2-3), 107-140. doi:10.1016/s0165-0173(02)00181-9

Van Dongen, H. P., Belenky, G., & Krueger, J. M. (2011). A local, bottom-up perspective on sleep deprivation and neurobehavioral performance. *Curr Top Med Chem, 11*(19), 2414-2422. doi:10.2174/156802611797470286

Vanneste, S., Song, J. J., & De Ridder, D. (2018). Thalamocortical dysrhythmia detected by machine learning. *Nature Communications, 9*. doi:ARTN 1103

10.1038/s41467-018-02820-0

Wall, P. D., & Devor, M. (1983). Sensory afferent impulses originate from dorsal root ganglia as well as from the periphery in normal and nerve injured rats. *Pain, 17*(4), 321-339. doi:10.1016/0304-3959(83)90164-1

Woodworth, R. S., & Sherrington, C. S. (1904). A pseudaffective reflex and its spinal path. *J Physiol, 31*(3-4), 234-243. doi:10.1113/jphysiol.1904.sp001034

Woolf, C. J., & Salter, M. W. (2000). Neuronal plasticity: increasing the gain in pain. *Science, 288*(5472), 1765-1769. doi:10.1126/science.288.5472.1765

Yam, M. F., Loh, Y. C., Tan, C. S., Khadijah Adam, S., Abdul Manan, N., & Basir, R. (2018). General Pathways of Pain Sensation and the Major Neurotransmitters Involved in Pain Regulation. *Int J Mol Sci, 19*(8). doi:10.3390/ijms19082164

Yue, L., Iannetti, G. D., & Hu, L. (2020). The Neural Origin of Nociceptive-Induced Gamma-Band Oscillations. *J Neurosci, 40*(17), 3478-3490. doi:10.1523/JNEUROSCI.0255-20.2020

Yüzgeç, O., Prsa, M., Zimmermann, R., & Huber, D. (2018). Pupil size coupling to cortical states protects the stability of deep sleep via parasympathetic modulation. *Curr Biol, 28*(3), 392-400 e393. doi:10.1016/j.cub.2017.12.049

Zerbi, V., Floriou-Servou, A., Markicevic, M., Vermeiren, Y., Sturman, O., Privitera, M., . . . Bohacek, J. (2019). Rapid Reconfiguration of the Functional Connectome after Chemogenetic Locus Coeruleus Activation. *Neuron, 103*(4), 702-718 e705. doi:10.1016/j.neuron.2019.05.034

Zhang, Z., Gadotti, V. M., Chen, L., Souza, I. A., Stemkowski, P. L., & Zamponi, G. W. (2015). Role of prelimbic GABAergic circuits in sensory and emotional aspects of neuropathic pain. *Cell Rep, 12*(5), 752-759. doi:10.1016/j.celrep.2015.07.001

Zhang, Z. G., Hu, L., Hung, Y. S., Mouraux, A., & Iannetti, G. D. (2012). Gamma-band oscillations in the primary somatosensory cortex--a direct and obligatory correlate of subjective pain intensity. *J Neurosci, 32*(22), 7429-7438. doi:10.1523/JNEUROSCI.5877-11.2012

Zhao, R., Zhou, H., Huang, L., Xie, Z., Wang, J., Gan, W. B., & Yang, G. (2018). Neuropathic pain causes pyramidal neuronal hyperactivity in the anterior cingulate cortex. *Front Cell Neurosci, 12*, 107. doi:10.3389/fncel.2018.00107

CORRECTED 29 JUNE 2017; SEE ERRATUM

SCIENCE ADVANCES | RESEARCH ARTICLE

NEUROSCIENCE

Coordinated infraslow neural and cardiac oscillations mark fragility and offline periods in mammalian sleep

Sandro Lecci,[1] Laura M. J. Fernandez,[1]* Frederik D. Weber,[2]* Romain Cardis,[1] Jean-Yves Chatton,[1] Jan Born,[2] Anita Lüthi[1]†

Rodents sleep in bouts lasting minutes; humans sleep for hours. What are the universal needs served by sleep given such variability? In sleeping mice and humans, through monitoring neural and cardiac activity (combined with assessment of arousability and overnight memory consolidation, respectively), we find a previously unrecognized hallmark of sleep that balances two fundamental yet opposing needs: to maintain sensory reactivity to the environment while promoting recovery and memory consolidation. Coordinated 0.02-Hz oscillations of the sleep spindle band, hippocampal ripple activity, and heart rate sequentially divide non–rapid eye movement (non-REM) sleep into offline phases and phases of high susceptibility to external stimulation. A noise stimulus chosen such that sleeping mice woke up or slept through at comparable rates revealed that offline periods correspond to raising, whereas fragility periods correspond to declining portions of the 0.02-Hz oscillation in spindle activity. Oscillations were present throughout non-REM sleep in mice, yet confined to light non-REM sleep (stage 2) in humans. In both species, the 0.02-Hz oscillation predominated over posterior cortex. The strength of the 0.02-Hz oscillation predicted superior memory recall after sleep in a declarative memory task in humans. These oscillations point to a conserved function of mammalian non-REM sleep that cycles between environmental alertness and internal memory processing in 20- to 25-s intervals. Perturbed 0.02-Hz oscillations may cause memory impairment and ill-timed arousals in sleep disorders.

INTRODUCTION

All mammals benefit from sleep in fundamental aspects for brain and body (*1*, *2*). For sleep to be beneficial, it must be of sufficient duration and physiological continuity. Conversely, sleep needs to retain a certain degree of fragility, because all sleeping organisms remain capable of a behavioral arousal response to salient stimuli and potential threats. To date, it is unclear how sleep generates advantageous effects while maintaining sensory responsiveness and how the two opposite needs for continuity and fragility are balanced. Recently, given the enormous differences in sleep fragmentation between mammalian species (*3*), the idea of universal beneficial functions of sleep for all mammals has even been challenged (*4*).

Ongoing electrical rhythms in the thalamocortical loops of the sleeping brain are central to disrupt sensory information processing. Among these, sleep spindles are particularly efficient in attenuating the likelihood that sensory stimuli arrive in cortex (*5*, *6*). Spindles are electroencephalographic hallmarks of non–rapid eye movement (non-REM) sleep in the sigma (10 to 15 Hz) power range that occur preferentially during human "light" sleep (*7*) and that last for ~0.5 to 3 s throughout mammals (*8*). Sensory processing thus varies momentarily along with the spectral dynamics of thalamocortical rhythms and contributes to sleep fragility (*9*). Non-REM sleep is also accompanied by marked changes in the autonomic system, notably including decreases in heart rate that recover before transitions to REM sleep or awakening (*10*). Therefore, periods of sleep fragility, during which awakenings are more likely to occur, should involve the autonomic system. To date, however, an analysis of sleep fragility periods based on a combined assessment of sensory processing, spectral dynamics, and autonomic parameters has not been carried out. Moreover, how fragility phases interchange with phases of continuity and how these concur with hallmarks of memory processing during sleep remain open questions.

[1]Department of Fundamental Neurosciences, University of Lausanne, 1005 Lausanne, Switzerland. [2]Institute of Medical Psychology and Behavioral Neurobiology, University of Tübingen, 72076 Tübingen, Germany.
*These authors contributed equally to this work.
†Corresponding author. Email: anita.luthi@unil.ch

RESULTS

Undisturbed non-REM sleep in mice shows a 0.02-Hz oscillation in sigma power

To examine whether mouse non-REM sleep shows microarchitectural dynamics indicative of variable fragility, we used polysomnography [electroencephalography (EEG)/electrocorticography (ECoG) and electromyography (EMG)] in freely moving mice (*11*) and inspected the temporal evolution of two major spectral bands characteristic for non-REM sleep: the slow-wave activity (SWA; 0.75 to 4 Hz) and the sigma (10 to 15 Hz) power band (*8*). Epochs of non-REM sleep were selected during the first 100 min after onset of the light phase [zeitgeber time 0 (ZT0)], during which mice slept ~63% of their time (n = 18 mice). During this period, non-REM sleep occurred in bouts ranging from 8 to >512 s in duration, with a mean length of 108.6 ± 8.1 s. Both sigma power and SWA were elevated during non-REM sleep and decreased during waking or REM sleep (Fig. 1A and fig. S1). Unexpectedly, we noticed that sigma power, but not SWA, displayed marked variations that recurred periodically in both short and long non-REM sleep bouts (Fig. 1B and fig. S1). We assessed the dynamics of sigma power across time for consolidated non-REM sleep periods ≥96 s (mean duration, 180.4 ± 8.8 s) (fig. S2). This revealed a predominant frequency of 0.021 ± 0.001 Hz (Fig. 1C) in a fast Fourier transform (FFT), corresponding to a cycle length of 47.6 ± 2.1 s. In contrast, such a prominent peak was not present for the SWA time course (Fig. 1C), and it was markedly weaker in frequency bands adjacent to the sigma band (n = 18; Friedman's test, $P = 7.9 \times 10^{-5}$; Fig. 1D). Further analyses and computational simulations confirmed that sigma power oscillated robustly in the 0.02-Hz frequency range (fig. S3). First, a 0.02-Hz oscillation emerged when the analysis was restricted to long non-REM sleep bouts (≥192 s, corresponding to 32.08% of all the

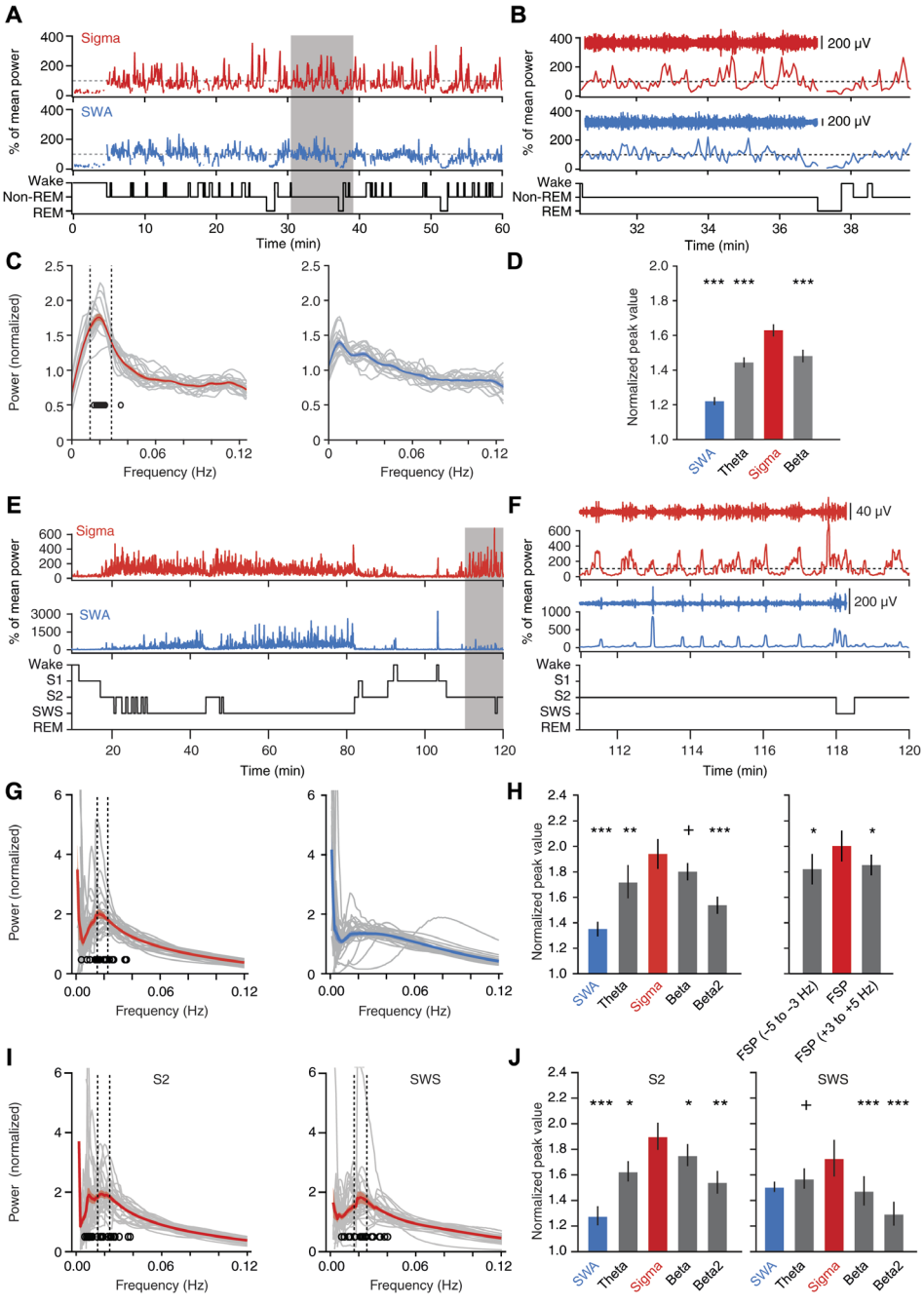

Fig. 1. The 0.02-Hz oscillation in sigma power in undisturbed non-REM sleep of mice and humans. (**A** to **D**) Sleep analysis in freely moving mice (n = 18). (A and B) Sigma (red; 10 to 15 Hz) and SWA (blue; 0.75 to 4 Hz) power time course for a single mouse, with hypnograms shown below. Gray-shaded area in (A) is expanded in (B), with aligned band-pass–filtered ECoG traces. (C) FFT of power time course for sigma (left) and SWA (right) for individual mice (gray traces, n = 18) and for the average across mice (color + shading, means ± SEM). Open circles denote FFT peaks obtained from Gaussian fits (their SD was 0.015 Hz). Vertical dotted lines indicate mean peak frequency ± 0.5 SD. Minor ticks are added to indicate the 0.02-Hz value on the frequency axis. (D) Mean peak values from (C) for sigma power, SWA, theta (6 to 10 Hz), and beta (16 to 20 Hz) bands (Friedman rank sum test; $P = 4.9 \times 10^{-8}$, post hoc Wilcoxon signed-rank tests relative to sigma power, $P = 7.63 \times 10^{-6}$ for SWA; $P = 3.81 \times 10^{-5}$ for theta; $P = 1.53 \times 10^{-5}$). (**E** to **J**) Sleep analysis in humans (n = 27). (E and F) Same as (A) and (B) for a single human subject (sigma, 10 to 15 Hz; SWA, 0.5 to 4 Hz). (G) Power spectral profiles for sigma power and SWA time course during non-REM sleep (S2 + SWS) graphed as in (C). The open circles indicate the peak of Gaussian fits, which show an SD of 0.008 Hz. (H) Left: Same as (D), calculated over all non-REM sleep (theta, 4 to 8 Hz; beta, 16 to 20 Hz; beta2, 20 to 24 Hz). Same statistics as (D): $P = 3.5 \times 10^{-4}$; post hoc Wilcoxon signed-rank tests with $P = 9.5 \times 10^{-6}$ for SWA; $P = 0.009$ for theta; $P = 0.095$ for beta; $P = 4.3 \times 10^{-4}$ for beta2. Right: Individual fast spindle power peaks (FSP ± 1 Hz) and adjacent frequency bands. Same statistics as in (C): $P = 0.034$ for Friedman rank sum test; $P = 0.015$ for −5 to −3 Hz; $P = 0.032$ for +3 to +5 Hz. (I) Same analysis as (G), restricted to S2 or to SWS and sigma power. (J) Left: Power analysis as in (H) restricted to S2 sleep revealed a prominent peak for sigma power over other frequency bands (n = 27; Friedman rank sum test, $P = 8.5 \times 10^{-6}$, followed by Wilcoxon signed-rank tests with respect to sigma power; $P = 2.5 \times 10^{-6}$ for SWA; $P = 0.023$ for theta; $P = 0.011$ for beta; $P = 0.002$ for beta2). Right: As left for SWS only (same statistics as the left panel: $P = 1.8 \times 10^{-4}$; $P = 0.11$ for SWA; $P = 0.052$ for theta; $P = 6 \times 10^{-4}$ for beta; $P = 1.6 \times 10^{-4}$ for beta2). $^{+}P < 0.1$, $^{*}P < 0.05$, $^{**}P < 0.01$, $^{***}P < 0.001$.

bouts ≥96 s) (fig. S3, A to F), demonstrating that sigma power cycles on a 50-s time scale during consolidated non-REM sleep. Second, computational simulations indicated that a true sinusoidal component at ~0.02 Hz rather than scale-free power dynamics underlay the peak in the FFT (fig. S3, G to J). Third, autocorrelations displayed side peaks with a periodicity of 52.6 ± 0.83 s (paired *t* test compared to shuffled data, $t = 3.82$, $P = 0.0015$; fig. S4, A and B). These combined results demonstrate that mouse non-REM sleep contains a 0.02-Hz oscillation of sigma power dynamics, corresponding to a periodicity of ~50 s.

Undisturbed non-REM sleep in humans shows a 0.02-Hz oscillation in sigma power

To explore whether this infraslow 0.02-Hz oscillation exists in higher mammals, we carried out a comparable power analysis for human sleep (fig. S5). As expected, sigma power was high during stage 2 (S2) sleep (light sleep) and declined during slow-wave sleep (SWS; "deep" sleep) (*7*) when SWA emerged (Fig. 1E and fig. S6). The 0.02-Hz oscillation was present in the sigma power band (10 to 15 Hz) with maximal amplitudes comparable to those in mice (Fig. 1F and fig. S7) but was attenuated in the SWA band (Fig. 1, G and H). When analyzed across all non-REM sleep (S2 + SWS), human sigma power oscillations had a periodicity of 0.019 ± 0.001 Hz ($n = 27$), corresponding to a cycle length of 52.6 ± 2.6 s, comparable to mice. The sigma power band showed the most pronounced dynamics of around 0.02 Hz, while adjacent frequency bands displayed distinctly weaker periodicity ($n = 27$; Friedman's test, $P < 3.5 \times 10^{-4}$; Fig. 1H). Furthermore, SWA lacked prominent infraslow dynamics and showed a minor spectral peak (Fig. 1H). In humans, there are fast (12 to 15 Hz) and slow spindles (9 to 12 Hz), with the former being prevalent during S2 and providing a distinct peak in individual power spectra (*12*). When focusing our analysis on the fast spindles, we found that 0.02-Hz oscillations emerged strongest in a 2-Hz band around the fast spindle peak (FSP; 13.16 ± 0.12 Hz) and fell off in adjacent bands (Fig. 1H). The 0.02-Hz oscillation of sigma power appeared to be more prominent in S2 than in SWS (Fig. 1, I and J). Autocorrelations confirmed the oscillatory nature of sigma power dynamics, displaying side peaks with a periodicity of 53.0 ± 2.73 s (Wilcoxon signed-rank test for periodicity, $P = 0.026$; fig. S4, C and D). Together, these data unravel a 0.02-Hz oscillation common to both human and mouse non-REM sleep that is prevalent for sigma power and most prominent for fast spindles in human non-REM sleep.

The 0.02-Hz oscillation shows regional specificity in both mice and humans

To assess whether 0.02-Hz oscillations were present in local cortical circuits, we performed multisite referential local field potential (LFP) recordings across four cortical areas in combination with polysomnography in sleeping head-fixed mice ($n = 6$). Under these recordings conditions, the three major vigilance states wake, non-REM, and REM sleep showed spectral profiles comparable to those of freely moving animals (fig. S8). The 0.02-Hz oscillation in sigma power of non-REM sleep was present in the simultaneously recorded EEG and LFP signals (Fig. 2, A and B), yet the latter showed that the amplitude of the oscillation depended on cortical area [$n = 6$ mice; repeated-measures (RM) analysis of variance (ANOVA) for factors "frequency" and "area"; $F_{1,5} = 145.8$, $P = 6.88 \times 10^{-5}$; $F_{4,20} = 19.23$, $P = 1.25 \times 10^{-6}$; Fig. 2C]. Primary (SI) and secondary (SII) somatosensory cortices showed a major 0.02-Hz peak in the sigma compared to the SWA power time course ($n = 6$; paired *t* test, $t = 17.88$, $P = 1.01 \times 10^{-5}$ for SI; $t = 5.72$, $P = 0.0023$ for SII; Fig. 2D), yet this peak was minor in auditory cortex (AC) and medial prefrontal cortex (mPFC) ($n = 6$; paired *t* test, $t = 2.83$, $P = 0.037$ for AC; $t = 2.02$, $P = 0.1$ for mPFC).

The topography of 0.02-Hz oscillations in humans was assessed in an additional group of $n = 24$ subjects with full-night polysomnographic recordings (Fig. 3A and fig. S6). These data confirmed that the 0.02-Hz oscillation in sigma power was more pronounced during S2 than SWS. Furthermore, the 2-Hz band around the FSP was the strongest oscillatory component in these comparisons (fig. S6C). The 0.02-Hz oscillations showed a maximum over parietal derivations for power in both the sigma and the FSP band and declined toward anterior central and frontal areas. However, the relative dominance of the 0.02-Hz oscillation in the sigma and FSP bands over adjacent frequency bands and SWA persisted along the parietofrontal axis (Fig. 3B).

The 0.02-Hz oscillation divides non-REM sleep into periods of high and low fragility to acoustic noise

If 0.02-Hz oscillations are relevant for sleep fragility and continuity, then they should be accompanied by a varying arousability of mice in response to external stimuli. We chose acoustic stimuli such that they lasted half a cycle of the 0.02-Hz oscillation (20 s). This long-duration noise would probe the propensity to arouse over the sustained periods of low and high sigma power and hence reveal whether these corresponded to states of distinct fragility. A white noise stimulus of 90-dB sound pressure level (SPL) yielded an arousal success rate of 38.7 ± 8.6% ($n = 10$), as assessed by polysomnography (Fig. 4A), and trials were post hoc–classified on the basis of ECoG (EEG)/EMG data in "wake-up" or "sleep-through" trials (Fig. 4B). Noise was played as soon as the mouse was in consolidated non-REM sleep (for ≥40 s) and at most once every 4 min, without knowledge of the oscillation phase. In a wake-up trial from a single mouse, sigma power was at its maximum before noise onset, such that noise exposure fell within a phase of declining power. In contrast, for a sleep-through trial of the same mouse, sigma power had just exited the trough, and noise was played within the phase of incrementing power (Fig. 4C). This phase difference between wake-up and sleep-through trials was robust when calculated across trials and mice (wake-up, $n = 9$ mice; sleep-through, $n = 10$ mice; RM ANOVA for factors "time" and "behavioral outcome"; $F_{4.78,81.27} = 3.81$, $P < 0.0042$, after Greenhouse-Geisser correction; Fig. 4D, left). Moreover, the time course corresponded to the 0.02-Hz oscillations during undisturbed sleep (Fig. 4D, right; see also Fig. 1), whereas SWA time course was indistinguishable between the wake-up and sleep-through trials (wake-up, $n = 9$ mice; sleep-through, $n = 10$ mice; RM ANOVA for factors "time" and "behavioral outcome"; $F_{4.84,82.20} = 1.86$, $P = 0.11$, after Greenhouse-Geisser correction; Fig. 4E). Therefore, as shown schematically in Fig. 4F, the 0.02-Hz sigma power oscillations seem to divide mouse non-REM sleep into alternating periods of successive high and low responsiveness to external stimuli. To test this hypothesis, we analyzed the phases of the 0.02-Hz oscillation before noise onset and found that values for the wake-up and sleep-through trials fell onto opposite halves in a polar plot of oscillation phases (Fig. 4, G and H). Therefore, wake-ups and sleep-throughs occur during declining and rising sigma power levels, respectively. As wake-ups took place either early or late during the 20-s noise exposure, we asked whether the declining sigma power phase could be further subdivided according to the occurrence of wake-ups. Sigma power was significantly lower for early (taking place within <8 s after noise onset) than for late (12 to 16 s after noise onset) wake-ups (early arousals, $n = 6$; late arousals, $n = 9$; RM ANOVA for factors "time" and "behavioral

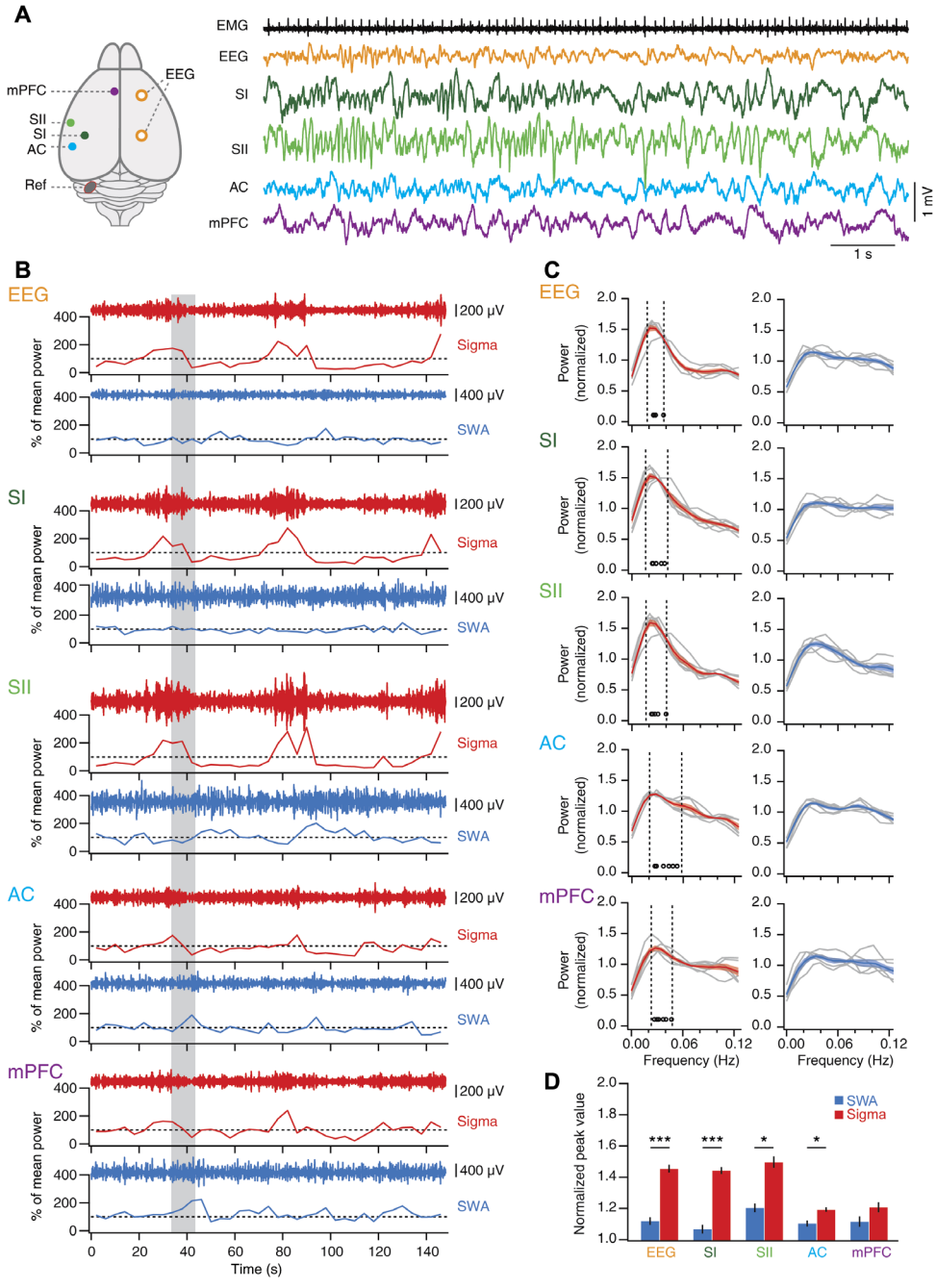

Fig. 2. The 0.02-Hz oscillation is present in local cortical areas and predominates in somatosensory cortex. (**A**) Top view of mouse brain with indication of recording sites and with corresponding representative traces obtained during non-REM sleep scored on the basis of EEG/EMG recordings. (**B**) Sigma (red) and SWA (blue) power time course for a single non-REM sleep bout recorded simultaneously from all areas. The gray-shaded area indicates the time corresponding to the traces in (A). Dotted lines indicate 100%. (**C**) FFT of power time course for sigma (left) and SWA (right) for individual mice (gray traces, $n = 6$) and for the average across mice (color + shading, means ± SEM). Open circles denote FFT peaks obtained from Gaussian fits. Vertical dotted lines indicate mean peak frequency ± 0.5 SD. (**D**) Mean peak values from (C) for sigma power and SWA for all brain areas and EEG recordings, analyzed as in Fig. 1D. RM ANOVA with factors "area" and "frequency"; area, $P = 1.25 \times 10^{-6}$; frequency, $P = 6.88 \times 10^{-5}$; post hoc paired t tests; EEG, $t = 11.19$, $P = 9.93 \times 10^{-5}$; SI, $t = 17.88$, $P = 1.01 \times 10^{-5}$; SII, $t = 5.72$, $P = 0.0023$; AC, $t = 2.83$, $P = 0.037$; mPFC, $t = 2.02$, $P = 0.1$; $^{*}P < 0.01$, $^{***}P < 0.001$. SI and SII, primary and secondary somatosensory cortex; AC, auditory cortex; mPFC, medial prefrontal cortex; Ref, reference.

outcome"; $F_{4,52} = 2.72$, $P = 0.04$; fig. S9), suggesting a phase advancement for early over late arousals. The progression into the declining sigma power period thus reflects the entry into a period of sleep fragility. Last, we asked whether the total duration of the non-REM sleep before noise exposure affected responsiveness. Both wake-up and sleep-through trials were broadly distributed across the range of non-REM sleep bout durations in mice (fig. S10), ruling out bout duration as a determinant of behavioral outcome to noise exposure.

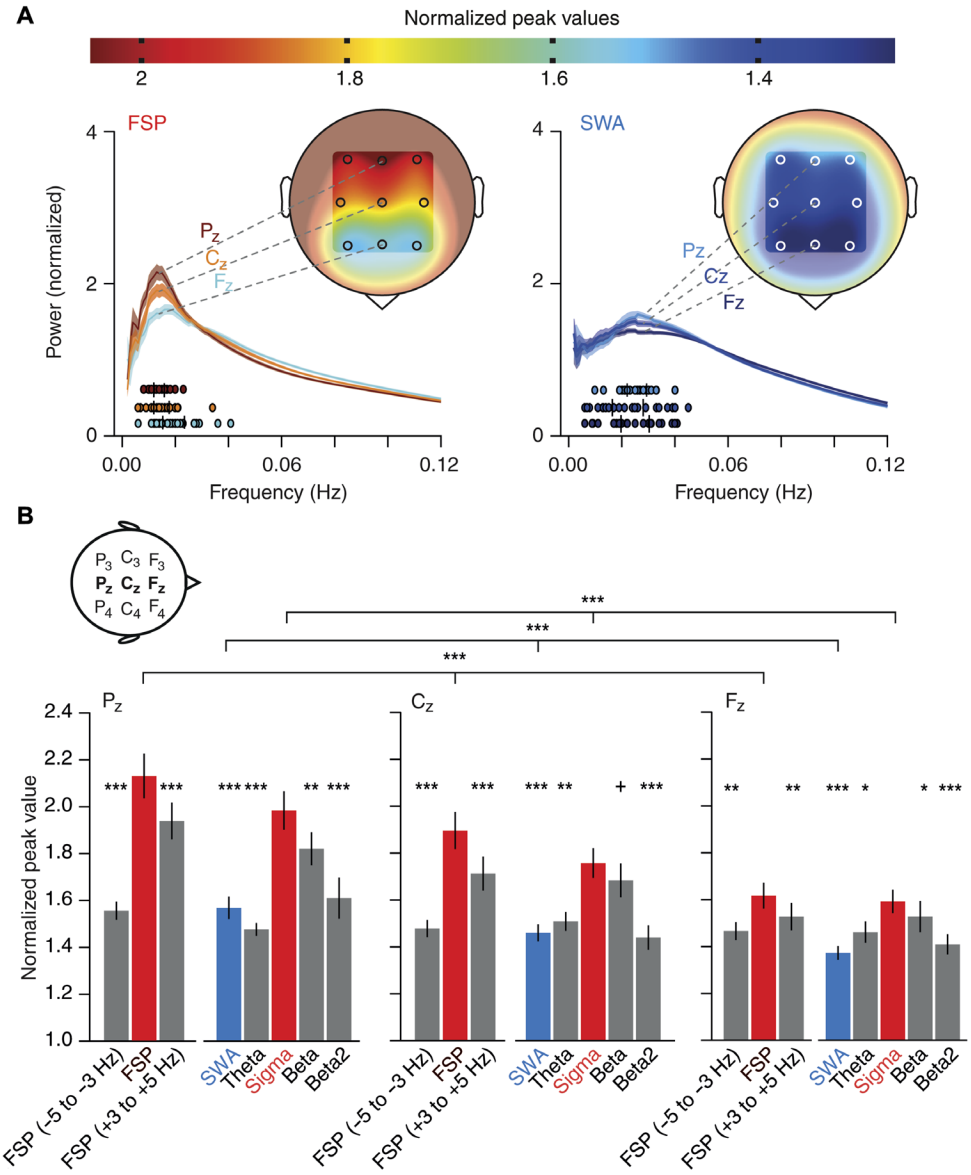

Fig. 3. Regional cortical topology of the 0.02-Hz oscillation in humans. (**A**) Top: Color scale that indicates the mean normalized power values calculated from the average 0.02-Hz oscillation band (±0.5 SD around average peak values) during non-REM sleep. Bottom: The power spectral profiles for the FSP band (FSP ± 1 Hz, ~13 Hz, left) and the SWA band (right) averaged across subjects (color + shading, means ± SEM) displayed for representative midline electrodes (F_Z, C_Z, and P_Z); analysis as in Fig. 1G. Coloring for power spectral profiles and each subject's 0.02-Hz oscillation peak (filled circles underneath the power spectral profiles) corresponds to normalized peak values in the color scale. Insets show human head with an approximate topography of the mean normalized peak power values for all nine EEG electrodes (F_3, F_Z, F_4, C_3, C_Z, C_4, P_3, P_Z, and P_4). (**B**) Mean (±SEM) normalized peak values for FSP band and adjacent frequency bands (FSP −5 to −3 Hz and FSP +3 to +5 Hz), as well as sigma power (10 to 15 Hz), SWA (0.5 to 4 Hz), theta (4 to 8 Hz), beta (16 to 20 Hz), and beta2 (20 to 24 Hz) bands separate for the three midline electrodes (F_Z, C_Z, and P_Z); analysis as in Fig. 1H with data from the participants of the memory study ($n = 24$). Additional Friedman rank sum test between three midline electrodes for FSP band ($P = 3.5 \times 10^{-8}$), sigma ($P = 6.35 \times 10^{-9}$), and SWA ($P = 2.8 \times 10^{-6}$) (top three horizontal lines), with post hoc–paired comparisons along decreases from P_z to C_z as well as C_z to F_z separate for those three frequency bands (Wilcoxon signed-rank test, all $P_s < 0.0036$). For consistency with the core study analyses, which relied on nonparametric statistics, the same statistical tests were performed here. $^{+}P < 0.1$, $^{*}P < 0.05$, $^{**}P < 0.01$, $^{***}P < 0.001$ for Wilcoxon signed-rank test relative to FSP band (left bar groups) and relative to the sigma band (right bar groups).

The offline periods are coordinated with hippocampal ripples

We further characterized the 0.02-Hz oscillation by examining the timing of ripples (150 to 250 Hz) in the CA1 area of the hippocampus, which represent an established index for offline memory processing (*13*). Sigma power and ripple power were correlated such that ripple activity augmentations preceded sigma power rises by ~4 s ($n = 6$; fig. S11). Thus, hippocampal ripple activity was high during periods of increasing sigma power, during which mice maintained sleep while being exposed to noise. This suggests that more pronounced 0.02-Hz oscillations strengthen offline consolidation of hippocampus-dependent memory.

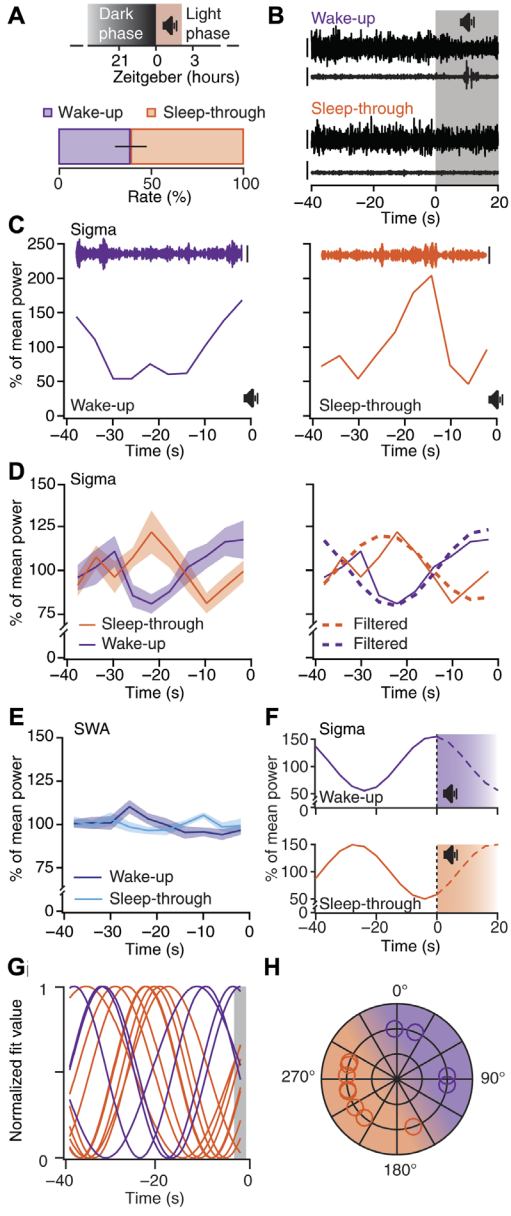

Fig. 4. The 0.02-Hz oscillation imposes periods of high and low fragility to acoustic noise. (**A**) Top: Acoustic stimulation protocol. Bottom: Percentage (means ± SEM) of wake-up and sleep-through trials (n = 10 mice). (**B**) Representative EEG (ECoG) (upper trace)/EMG (lower trace) traces from wake-up and sleep-through trials. Gray-shaded area indicates period of noise exposure. Scale bars, 400 and 80 μV for EEG(ECoG)/EMG. (**C**) Time course of sigma power for the 40 s of non-REM sleep before noise onset for a wake-up (violet) and a sleep-through (orange) trial [same data as (B)]. Insets show corresponding band-pass–filtered (10 to 15 Hz) EEG (ECoG) traces. Scale bars, 200 μV. (**D**) Left: Means ± SEM sigma power time course for wake-up and sleep-through trials (n = 9 and 10, respectively; RM ANOVA for factors "time" and "behavioral outcome", Greenhouse-Geisser–corrected, $P < 0.0042$). Right: Overlay of the traces from the left, once unfiltered (continuous line) and once band-pass–filtered (dotted lines) for the frequencies corresponding to 0.02-Hz oscillation peak ± 1 width (see Fig. 1C). (**E**) Means ± SEM SWA time course as in (D) [same statistics as in (D), $P = 0.11$]. (**F**) Projected time course of sigma power during noise exposure for wake-up and sleep-through trials. (**G**) Waveforms for average wake-up (n = 4) and sleep-through (n = 8) trials obtained through sinusoidal fits. (**H**) Polar representation of sigma power phases decoded from (G) (shaded area; 0°, peak), with shading of corresponding intervals for high (purple) and low (orange) responsiveness to stimulation.

The strength of the 0.02-Hz oscillation correlates with overnight consolidation of declarative memory in humans

To explore the role of 0.02-Hz oscillations in memory consolidation, we correlated the explicit postsleep recall on an episodic memory task (presented before sleep) in humans with oscillation peaks and conventional measures of spindle density (*14*). Recall correlated with the individual peak of 0.02-Hz oscillations in the fast spindle band during all-night non-REM sleep (r = 0.45, P = 0.027; n = 24; Fig. 5A), while correlation was absent for SWA (r = −0.24; Fig. 5B). The correlation episodic memory recall appeared to be most robust for the 0.02-Hz oscillation over centroparietal sites (C_4, C_Z, P_4, and P_Z; $P_s < 0.043$). The 0.02-Hz oscillation peak also correlated with the mean fast spindle density (r = 0.51, P = 0.011; Fig. 5C), but not with overall spindle count ($P > 0.38$). Spindle measures per se (such as spindle density and spindle count) in this analysis were not significantly correlated with episodic memory recall (all $P_s > 0.15$). These data are the first indications that the periodic clustering of spindle activity on a 50-s time scale is a critical determinant for offline memory consolidation.

The online periods are coordinated with heart rate changes

To test our hypothesis that changes in heart rate accompany the period of fragility to external stimuli, we monitored heart rate along with non-REM sleep in both mice and humans. In mice, through measuring interbeat intervals from the nuchal EMG (fig. S12), we found that heart rate increased and fluctuated around elevated values when sigma power oscillations were declining (Fig. 6, A and B), yielding a cross-correlation function with a prominent negative peak at ~0 s (Fig. 6, B and E). In humans, heart rate alterations also correlated with sigma power, but with a clear time lag. Here, heart rate declined rapidly once sigma power had reached a peak and increased gradually during sigma power minima (Fig. 6, C and D), before subsequent sigma peaks by ~5 s (Fig. 6F). Thus, although with different phase relations that could be related to differences in the kinetics and mechanisms of neural coupling to the heart in both species, cardiovascular activity is coordinated with brain oscillations that mark arousability.

DISCUSSION

Sleep has to reconcile the needs for continuity and fragility. Here, we uncovered a 0.02-Hz oscillation in mouse and human non-REM sleep with characteristics that qualify it as a hallmark for how sleep balances these conflicting needs. First, the 0.02-Hz oscillation is most prominent in a frequency band that contains neural rhythms associated with the gating of sensory information during sleep. Second, it is coordinated with an established physiological correlate of offline memory processing and with modulation of autonomic status. Third, the 0.02-Hz oscillation phase is linked to wake-up from sleep in mice and to the extent of overnight memory consolidation in humans. This dual behavioral relevance in two different species suggests that the 0.02-Hz oscillation provides a unitary temporal scale of mammalian non-REM sleep over which both beneficial effects and maintained reactivity to the environment are balanced.

The 0.02-Hz oscillation in sigma power results from a periodic recurrence of sleep spindles

The 10- to 15-Hz frequency band analyzed here contains sleep spindles, a well-described sleep rhythm that is a thalamocortically generated and visually obvious hallmark of the non-REM sleep EEG in

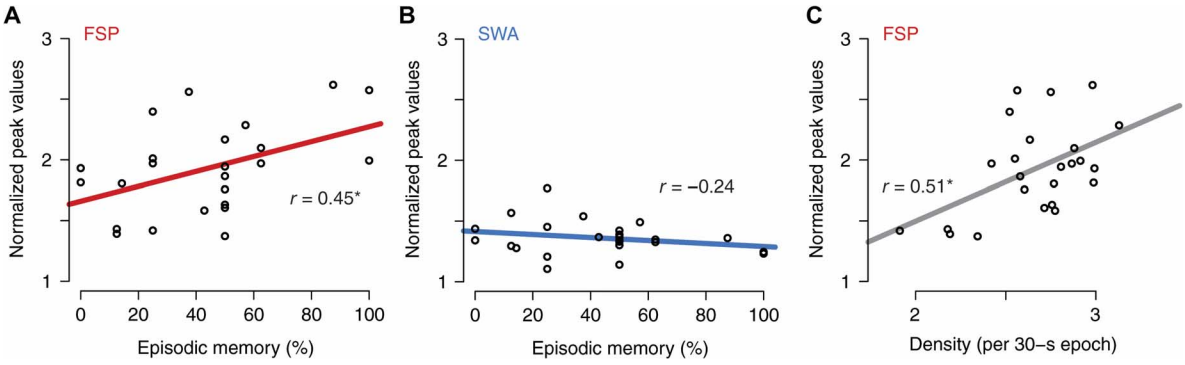

Fig. 5. Sleep benefit in episodic memory correlates with the strength of the 0.02-Hz oscillation in the FSP band (FSP ± 1 Hz). (**A**) Correlation of episodic memory recall (that is, recall of objects in their spatiotemporal context) with normalized peak values of FSP band. Pearson's *r* values are given in all panels (*P = 0.027). (**B**) Same for SWA band (P = 0.26). (**C**) Normalized power in FSP band was positively associated with the density of fast spindles (*P = 0.011). Analyses were performed on the average of all parietocentral EEG electrodes (C_3, C_Z, C_4, P_3, P_Z, and P_4) for the FSP band, and across frontal electrodes (F_3, F_Z, and F_4) for the SWA band, as these sites correspond to the locations with the highest overall power in the respective bands.

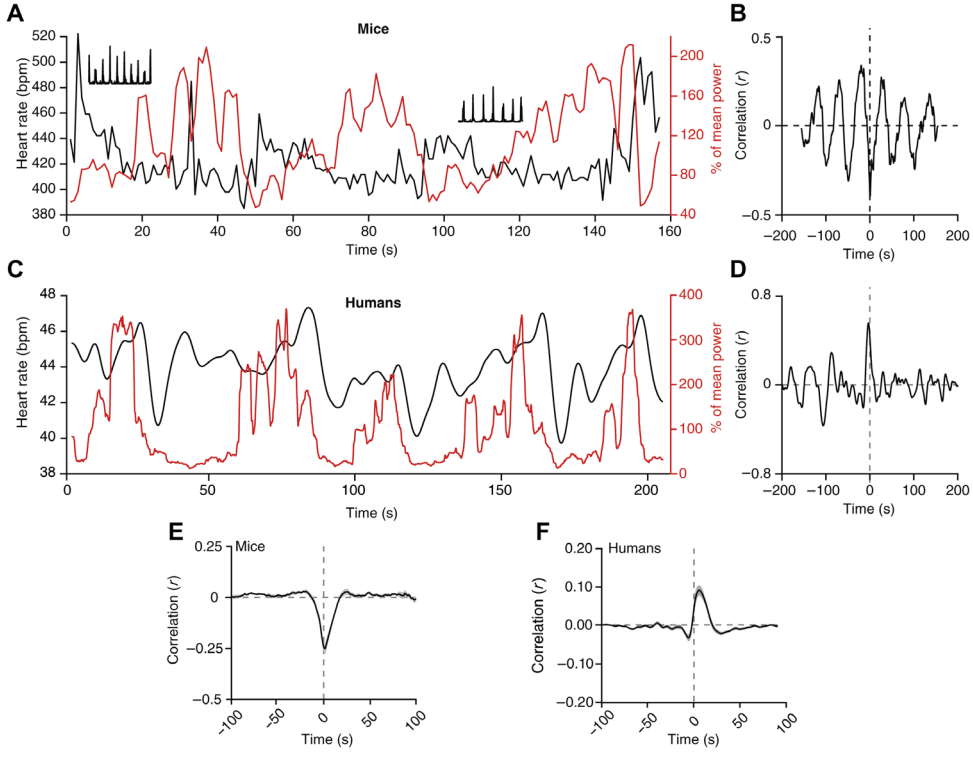

Fig. 6. The 0.02-Hz oscillation aligns with heart rate changes in both mice and humans. (**A**) Representative non-REM sleep bout with simultaneous recording of sigma power (red trace) and heart rate [black trace; in beats per minute (bpm)]. Insets show 1-s period of corresponding raw data (squared) to illustrate R-wave detection in EMG traces. (**B**) Cross-correlogram between sigma power and heart rate for traces in (A). (**C**) Same as (A) for a single human subject. (**D**) Corresponding cross-correlogram as (B). (**E** to **F**) Mean cross-correlogram for mice (n = 12) (E) and humans (n = 27) (F). Shadowing represents means ± SEM.

humans and carnivores between ~8 and 16 Hz (*7*, *15*). Mouse EEG traces show a more continuous and graded activity in the 9- to 18-Hz band that is best quantified through mean power levels (*11*). For species comparisons, we focused here on power dynamics in the 10- to 15-Hz band. The oscillatory pattern we found accords with the slow recurrence of discrete spindles over intervals of tens of seconds in humans and carnivores (*16*, *17*). Moreover, the much narrower individualized fast spindle band (around 13 Hz) oscillated most vigorously on a 0.02-Hz scale and correlated with the density of discrete spindles. Therefore, sleep spindles and fast spindles in particular are primary constituents of the 0.02-Hz oscillation. As adjacent frequency bands also show clear yet weaker 0.02-Hz oscillations, neural rhythm generators other than the thalamocortical spindle-generating circuits could contribute. In this context, it is noteworthy that the 8- to 13-Hz alpha band was recently associated with enhanced fragility of non-REM sleep in humans (*9*).

The 0.02-Hz time scale is a fundamental property of mammalian non-REM sleep

Aside from shared spectral hallmarks and regulatory mechanisms, mouse and human non-REM sleep are strikingly different, in particular with

respect to their architecture. In this study, we have now identified a temporal scale that is relevant for both S2 in humans and non-REM sleep in mice. We also have shown that mouse non-REM sleep shares several of the basic neural and autonomic characteristics of S2. These similarities will undoubtedly contribute to emerging questions on the specific benefits provided by S2 to sleep and in particular to sleep-dependent memory consolidation. We exemplify this here through demonstrating that the 0.02-Hz amplitude of fast spindles is a predictor of overnight declarative memory consolidation. Recent human research specifically linking S2 to strengthened hippocampal-cortical connectivity (*18*) and to procedural memory (*19*) is now open for reassessment in rodents in terms of novel temporal and spatial aspects of spindle organization.

The 0.02-Hz oscillation likely acts to provide an organizational time scale for non-REM sleep in other mammalian species. Carnivores, such as cats and ferrets, show periodically recurring spindle events at intervals of 10 to 40 s (*16*). Slow periodicities occur in brainstem arousal systems in sleeping rats (*20*). Beyond mammals, the Australian reptile *Pogona vitticeps* sleeps in alternating low (<4 Hz)– and high-frequency (10 to 30 Hz)–dominated states in cycles of 60 to 80 s (*21*).

The infraslow frequency of 0.02 Hz is strikingly similar to the periodicity found for cycling blood oxygen level–dependent imaging signals observed in brain subnetworks during rest (*22*) and non-REM sleep (*23*) that are conserved across rodents, monkeys, and humans (*24*) and that result from varying brain integration during sleep (*25*). Although the link between infraslow periodicities in electrophysiological and functional magnetic resonance imaging signals remains to be established, the shared oscillation frequency suggests that it represents an evolutionarily conserved time frame over which neural and hemodynamic sleep rhythms are coordinated.

The 0.02-Hz oscillation renders human sleep S2 a functionally unique sleep stage

The predominance of 0.02-Hz oscillations for fast spindles in S2 of human non-REM sleep functionally sets S2 apart from SWS. Over a 50-s time scale, an S2-specific spindle amassment in parietal areas yields a qualitatively different spatiotemporal spindle pattern than in SWS, where cortically driven spindle grouping predominates (*8*). It remains to be determined how these diverse organizational hierarchies contribute to the differential alignment of fast and slow spindles with slow waves (*12*). To what extent the 0.02-Hz oscillation will be important for observed differences in local versus global recurrence of spindles during S2 and SWS (*26*), as well as for proposed frameworks on active systems consolidation (*27*), remains an additional area of future investigation.

The online period of the 0.02-Hz oscillation facilitates wake-up in response to acoustic stimuli

Cortical responses to acoustic stimuli show an enhanced late inhibitory component of the evoked sensory responses during spindles (*6*, *28*), which is a neural correlate for disrupted cortical processing. The fragility period of the 0.02-Hz oscillation, corresponding to low spindle occurrence, could thus be accompanied by a suppression of these inhibitory components. However, the transition to full-blown awakening additionally requires an activation of brainstem arousal systems, such as the noradrenergic locus coeruleus that effectively arouses the thalamocortical system (*29*) and discharges phasically during alerting stimuli (*30*). Periodicities in sleep's fragility to acoustic stimuli could be modulated through periodic patterns in excitability of this and/or additional subcortical arousal-promoting systems, which so far have not been investigated with respect to infraslow rhythms in activity during non-REM sleep (*20*).

Although a protective function of sleep spindles for arousals is well established, the role of the 0.02-Hz oscillation for arousability in humans will need to be ascertained to more comprehensively address the parallels between human sleep S2 and mouse non-REM sleep reported here. However, we caution here against a simple transfer of approaches between species. Not only do mice and humans differ in terms of subcortical and cortical mechanisms of sensory processing; stimulus attributes such as frequency composition also have different ecological valence (*31*). In humans, exposure to sounds mimicking those found in everyday life was previously used to assess resilience to sleep disruption and therefore seems suitable to address the role of the 0.02-Hz oscillation for sleep fragility in humans (*9*, *32*).

The offline period of the 0.02-Hz oscillation promotes memory consolidation

The observed offline periods with reduced responsiveness to external noise might favor internal memory processing, as they coincide with enhanced ripple power, a sign for memory replay of recently experienced episodes (*13*). Human fast spindles predominate in sensorimotor areas and augment following learning (*33*) together with hippocampal ripples (*34*–*36*), a phenomenon that is crucial for memory consolidation (*1*, *37*). Our findings reveal the alignment of ripples and spindles within 25-s intervals that concur during periods of low fragility to noise. These data support the idea of a minimally required unit of uninterrupted sleep and provides a compelling explanation why optogenetically fragmenting non-REM sleep to periods shorter than 30 to 60 s disrupts memory consolidation (*38*). Corroborating the link to memory consolidation, we present the first evidence in humans that more pronounced 0.02-Hz oscillations in the spindle band correlated with enhanced hippocampus-dependent episodic memory after sleep. This further substantiates the idea that the temporal grouping of spindles, rather than their overall occurrence, is central to sleep-dependent memory consolidation.

Alternative roles of the 0.02-Hz oscillation in non-REM sleep

Several facets of the 0.02-Hz oscillation support a role in subdividing sleep into fragility and offline periods, yet it undoubtedly serves roles that could complement or add to the ones presented here. These additional roles could include promotion of oscillatory signaling in signaling pathways in neurons and astrocytes, with implications for sleep-dependent gene transcription and synapse function. More generally, slow metabolic or energetic processes that result from, or contribute to, modified neuronal excitability during sleep (*39*) could evolve over infraslow time scales. Notably, oscillations in the 0.02-Hz range have also been reported in the EEG alpha and theta band activity during waking rest periods in humans (*40*). Furthermore, infraslow oscillations were observed in a broader frequency range (0.01 to 0.1 Hz) during a somatosensory detection task carried out in fully awake subjects (*41*), raising the possibility that neural variations on a 50-s time scale may be common to several vigilance states.

Infraslow periodicities observed in clinical settings

Important clinical clues to infraslow periodicities in sleep fragility come from the "cyclic alternating pattern" (CAP) that is prominent in sleep disorder patients, consisting of visually identifiable alternations in EEG synchrony over periods of 10 to 60 s (*42*). Similar to

the 0.02-Hz oscillation, these are coordinated with autonomic parameters and signs of elevated arousability, such as body movements. However, unlike the 0.02-Hz oscillation, the CAP occurs throughout all non-REM sleep stages with wide variations in its spectral composition. Infra-slow periodicities on a broader frequency range (0.01–0.1 Hz) have also been observed in the occurrence of epileptic seizures in humans (*43*), and hippocampal interneuron discharges in sleeping rats (*44*).

CONCLUSIONS

In conclusion, the 0.02-Hz infraslow oscillation reflects sleep's arbitration between maintaining readiness for arousal and continuity for offline processing. The oscillation provides a supraordinate temporal framework that, as we show here, controls sleep's alternation between fragility and continuity, and which might likewise explain previously established links between sleep EEG rhythms, cardiac activity, hemodynamic fluctuations, and offline memory consolidation mechanisms (*22*, *23*, *45*) that occur on a 50-s time scale during sleep. Hypothalamic and brainstem circuits coordinating autonomic output with cortical state, possibly through diencephalic relays, are likely generators of the infraslow rhythm, which could affect cortical excitability (*46*, *47*). Therefore, we speculate that the 0.02-Hz infraslow oscillation reflects an inverse bottom-up oscillatory control between online and offline states, counterbalancing cortically driven faster sleep rhythms that organize brain activity in a top-down manner.

MATERIALS AND METHODS

Animal husbandry and experimental groups

Mice were housed in a temperature- and humidity-controlled environment with a 12-hour light/dark cycle (lights on from 9:00 a.m. to 9:00 p.m.). Food and water were administered ad libitum. Surgery for combined EEG (ECoG)/EMG electrode implantation was performed on a total of 26 5- to 7-week-old male C57BL/6J mice, bred in our colonies, as previously described by Wimmer *et al.* (*11*). For head-fixed conditions, eight C57BL/6J male mice of the same age were implanted for the EEG/EMG/LFP recordings. All experimental procedures complied with the Swiss National Institutional Guidelines on Animal Experimentation and were approved by the Swiss Cantonal Veterinary Office Committee for Animal Experimentation.

Surgeries for polysomnography and LFP recordings in mice

For EEG (ECoG)/EMG surgeries, mice were anesthetized with isoflurane (1 to 2%, O_2 and N_2O mixture), and two gold-plated screws (1.1-mm diameter) (*48*) were gently inserted into the skull over the right hemisphere to obtain a frontoparietal derivation; four additional screws were inserted for implant stabilization. Two gold wires were inserted into the neck muscle for EMG recordings. A male-to-female connector was soldered to EEG (ECoG) and EMG electrodes, and the implant was covered with two-component epoxy glue (RelyX, 3M ESPE Dental Products; or G-CEM, GC Corporation) and dental cement (Paladur, Heraeus Kulzer GmbH). Paracetamol (2 mg/ml) was diluted into the drinking water for at least 10 days of recovery after the surgery, and an additional week of adaptation was given after the animals were tethered to a commutator (Dragonfly Inc.) via custom-made counterbalanced cables. Surgery for head-fixed LFP electrode implantation was performed under isoflurane anesthesia (1 to 2%, O_2 and N_2O mixture) on eight mice (*49*). Above the left hemisphere, small craniotomies were drilled (<0.5-mm diameter) to chronically implant LFP tungsten microelectrodes (FHC; 10 to 12 megohms) in the following areas of interest: AC (bregma posterior, −2.5 mm; lateral, 3.9 mm; surface depth, 1.0 mm), SI (bregma posterior, −1.7 mm; lateral, 3.0 mm; surface depth, 0.9 mm), SII (bregma posterior, −0.7 mm; lateral, 4.2 mm; surface depth, 1.0 mm), mPFC (prelimbic and infralimbic area: bregma anterior, +1.8 mm; lateral, 0.3 mm; surface depth, 1.85 mm), and CA1 (bregma posterior, −2.5 mm; lateral, 2 mm; surface depth, 1.3 mm). A silver wire (Harvard Apparatus) was positioned in contact with the bone above the cerebellum and used as a neutral reference to record referential LFP signals. Over the right hemisphere, a light metal implant was glued to the bone, and two EEG gold-plated wires were chronically implanted to record differential frontoparietal EEG signals similar to those of the freely moving animals. For EMG electrodes, two gold pellets were inserted into the neck. Carprofen (5 mg/kg subcutaneously) and paracetamol were provided during recovery from surgery. Mice were daily habituated by gradually increasing the amount of time in the head-fixed condition and by rewarding with sweet water after each session.

Mouse polysomnographic and LFP recordings

EEG (ECoG)/EMG signals were recorded in freely moving mice, acquired and amplified using an Embla amplifier (gain 2000×), digitized at 2 kHz, and down-sampled to 200 Hz using Somnologica version 3.3.1 software (Embla System). The EEG (ECoG) and EMG traces were high-pass–filtered at 0.7 and 10 Hz, respectively. A 48-hour baseline sleep-wake recording under undisturbed conditions was obtained for every animal, and only the 100 min after light onset for the two consecutive days was used for further analysis to assess a data set homogeneous with respect to time of day. Recordings of LFPs were obtained from head-fixed mice habituated to sleep (fig. S8). The EEG (ECoG)/EMG signals allowed to assess the behavioral state during the sleep-wake cycle recordings and, together with LFP signals, were amplified (1000×) and acquired through Plexon Systems (16-channel Multiple Acquisition Processor system). More specifically, the signals were sampled at 1 kHz, high-pass–filtered at 0.8 Hz, and low-pass–filtered at 300 Hz. LFP electrode positions were labeled at the end of all recordings through electrocoagulation before transcardiac perfusion with 4% paraformaldehyde in 0.1 M phosphate buffer (under pentobarbital anesthesia, 60 mg/kg), through current injections (50 μA, 8 s), and post hoc compared to the stereotactic atlas after coronal slicing (100-μm sections) (fig. S8). Mice with an unprecise electrode localization were excluded from specific analyses. Head-fixed mice were not exposed to noise stimuli.

Scoring of rodent polysomnographic and LFP data

All sessions involving freely moving animals were visually scored using a 4-s epoch resolution, and power spectra were determined as previously described by Wimmer *et al.* (*11*). Whenever an abnormal discharge was present or the behavioral state was unclear, the epoch was scored as an artifact corresponding to the closest behavioral state and was omitted for any spectral analysis. For any 4-s epoch to be included in the spectral time course, it had to be preceded and followed by another epoch belonging to the same behavioral state excluding artifacts. A vigilance state file and a spectral file (FFT, 0.75 to 90 Hz with 0.25-Hz steps) were exported from Somnologica for every 4-s epoch and for every recording session. Under the head-fixed condition, scoring was based on combined EEG/EMG/LFP data and involved the selection of consolidated non-REM sleep bouts ≥45 s, excluding transitional periods to REM sleep or waking. Power spectra were calculated with a 4-s window resolution. Scoring of

EEG/LFP/EMG signals was performed using Igor Pro version 6.3 (WaveMetrics Inc.) customized semiautomated routines.

Human subjects and sleep recordings

Human data obtained from 27 healthy men (22.5 ± 0.49 years of age; range, 18 to 28 years of age) who participated in a previous pharmacological study included overnight polysomnographic and electrocardiographic (ECG) recordings (*50*) (further referred to as "core study") (the core analyses are presented in Figs. 1 and 6, and figs. S3, S4, S6A, and S7). Data for Figs. 3 and 5, and fig. S6 (B and C) were obtained from a sample that included 14 subjects taking part in a memory study (*14*) that was extended by 10 more subjects (n = 24, further referred to as "memory study"). The memory study also included standard polysomnographic full-night EEG recordings with a higher density of electrode sites.

All subjects had a regular sleep-wake pattern, did not take any medications at the time of the experiments, and were nonsmokers. Acute and chronic illness was excluded by medical history, routine laboratory investigation, and additional physical examination in the core study. The subjects of the core study were synchronized by daily activities and nocturnal rest with a more fixed sleep schedule, whereas the subjects of the memory study were instructed to keep their regular sleep schedule. Memory tasks were timed according to their regular sleeping time. All subjects spent one adaptation night in the laboratory to habituate to the experimental setting. For the core study, only data from placebo nights were included in the analysis. For the memory study, only the sleep group subjects were included. All participants gave written informed consent before participating, and both studies were approved by the local ethics committee.

Polysomnographic recordings included EEG from C_3 and C_4 electrode sites (International 10–20 system; reference: linked electrodes at the mastoids, ground at F_{pz}), EMG (*musculus mentalis*), and electrooculography (around the eyes), with the memory study data set using additional EEG sites (F_3, F_Z, F_4, C_3, C_Z, C_4, P_3, P_Z, and P_4). Electrode impedances were kept below 5 kilohms. Signals were amplified (BrainAmp, Brain Products), digitized (sampling rate >200 Hz), and filtered (EEG and electrooculogram between 0.3 and 35 Hz and EMG between 10 and 100 Hz).

Scoring of human EEG data and sleep EEG parameter analyses

Sleep stages were scored offline in 30-s epochs by an experienced scorer according to standard criteria (*51*). Further analysis of the core study was focused on the first 210 min starting with sleep onset of undisturbed sleep that was expected to contain long uninterrupted epochs rich in S2 as well as SWS and good cardiac recording quality. The analysis of the memory study used the entire sleep period. The proportion of stage 1, S2, SWS (the sum of stage 3 and stage 4), non-REM sleep (sum of S2 and SWS), REM sleep, wakefulness after sleep onset, movement time, and sleep latencies was determined. Sleep onset was defined with reference to lights off by the first occurrence of an S1 sleep epoch followed by S2 sleep. For simplicity, EEG analysis focused on C_3 channel mainly used for sleep scoring in the core study, whereas analyses in the memory group used all nine recording sites. Data of subsequent analyses were down-sampled to 100 Hz to facilitate computation. Analysis was performed in MATLAB 2013b (MathWorks) using custom-made scripts, FieldTrip (www.ru.nl/neuroimaging/fieldtrip) (*52*), and for analysis of standard sleep parameters including spindle and SWA analysis using the SpiSOP tool (www.spisop.org). For the correlation of the standard sleep parameters with memory and with the strength of the 0.02-Hz oscillation, the average of all parietocentral EEG electrodes (C_3, C_Z, C_4, P_3, P_Z, and P_4) was taken for the spindle band analyses, and the average of the frontal electrodes (F_3, F_Z, and F_4) was taken for the SWA band analysis, because these locations correspond to the sites with the highest overall power in the respective bands.

Briefly, power spectral analyses of non-REM sleep were calculated on consecutive artifact-free 5-s segments of non-REM sleep, which overlapped in time by 4 s along the entire recording period. Each segment was tapered by a single Hanning window before applying an FFT that resulted in interval power spectra with a frequency bin resolution of 0.2 Hz. Power spectra were then averaged across all segments (Welch's method). Mean power density from the spectra was calculated in the frequency band for slow waves (0.5 to 4 Hz) and in the sigma band (10 to 15 Hz). Concrete fast spindles and slow waves during non-REM sleep were analyzed according to previously published algorithms (*12*, *54*). For each individual and channel, their densities (per 30-s epoch of non-REM sleep), counts, mean amplitudes, and lengths were calculated.

For the identification of slow waves, the signal in each channel during non-REM sleep epochs was filtered between 0.5 and 3.5 Hz (−3 dB roll-off) using a digital finite impulse response (FIR) filter (Butterworth, order of 4). Next, all intervals of time with consecutive positive-to-negative zero crossings were marked as putative slow waves if their durations corresponded to a frequency between 0.5 and 1.11 Hz (*53*), yet these were excluded in case their amplitude was >1000 μV (as these were considered artifacts) or when both negative and positive half-wave amplitudes lay between −15 and +10 μV. A slow wave was identified if its negative half-wave peak potential was lower than the mean negative half-wave peak of all putatively detected slow oscillations in the respective EEG channel, and also only if the amplitude of the positive half-wave peak was larger than the mean positive half-wave amplitude of all other putatively detected slow waves within this channel.

For the detection of fast spindles, the EEG signal was filtered with a band-pass around the individual FSP (see "Analysis of 0.02-Hz oscillations in humans") with a ±1-Hz range (−3 dB cutoff). Then, using a sliding window with a size of 0.2 s, the root mean square (RMS) was computed, and the resulting signal was smoothed in the same window with a moving average. A spindle was detected when the smoothed RMS signal exceeded an individual amplitude threshold by 1.75 × SD of the filtered signal in this channel at least once and additionally exceeded a lower threshold of 1.5 × SD for 0.5 to 3 s. The crossings of the lower threshold marked the beginning and end of each spindle and quantified their length. Spindle amplitude was defined by the voltage difference between the largest trough and the largest peak. Spindles were excluded for amplitudes >200 μV.

Analysis of 0.02-Hz oscillations in mice

The scheme in fig. S2 summarizes the analysis steps for undisturbed non-REM sleep in mice. From the scored data, all non-REM sleep bouts ≥24 epochs (each epoch corresponding to 4 s, thus ≥96 s of uninterrupted non-REM sleep) were selected in the first 100 min at ZT0 for two consecutive light phases, regardless of the amount of non-REM sleep (fig. S2A). The spectral files of all 4-s epoch across all non-REM sleep (red lines in hypnogram in fig. S2A) were then used to calculate an arithmetic mean FFT per mouse. In recordings from head-fixed sleeping mice, an average non-REM sleep spectral

profile was calculated across the entire recording for each mouse (810 to 3210 s).

Figure S2B shows how the time course of spectral power was analyzed in 4-s bins for the following frequency bands: SWA (0.75 to 4 Hz), theta (6 to 10 Hz), sigma (10 to 15 Hz), and beta (16 to 20 Hz). To do this, the power values from the 4-s FFTs for each frequency band were normalized to the average non-REM sleep FFT calculated across all non-REM sleep (fig. S2A) and plotted against time, yielding the line graphs in Figs. 1 (A and B) and 6A, and figs. S1, S2B, and S12.

The spectral profiles of these power time courses of each non-REM sleep bout were obtained through calculating an FFT (fig. S2C) with Hamming window method, which revealed all power values in the infraslow frequency range (<0.125 Hz). The choice of a minimal bout length of 24 epochs, corresponding to ≥96 s, preserved at least two cycles of the 0.02-Hz oscillation detected here. A mean spectral profile was calculated for every mouse through averaging across the interpolated absolute FFTs obtained from each power profile of each non-REM sleep bout (fig. S2C, right).

Control analyses were carried out to ensure the robustness of peak detection (as shown in fig. S3). For the analysis of scale-free behavior, similar FFT calculations for a simulated scale-free power profile ($1/f$) with equal bout length distribution did not yield a peak unless a 0.02-Hz sine wave was added (fig. S3, G to J). Before FFT calculation, the average power value for each frequency band was subtracted from each non-REM sleep bout to prevent large power increases at extremely small frequencies; however, the 0.02-Hz peaks were also present without this offset. Autocorrelations were calculated for original and shuffled sigma power data of these long non-REM bouts for each mouse (fig. S4, A and B).

The mean FFT obtained per mouse was normalized to its own mean. Similarly, in EEG (ECoG)/LFP recordings, the FFTs over the power data mentioned above were obtained for each non-REM sleep bout using a Hamming window and means calculated as before (Fig. 2). Leaving out the Hamming window did not affect the result.

Last, to determine peak and SDs of the FFTs, we performed a Gaussian fit (one term). Peak location and SD values were obtained from the fitted curve and used to calculate the average peak value in the range (peak ± 0.5 × SD). These values were used to calculate average peak values in all other frequency bands (Fig. 1D). By choosing a mean that is determined not only by the single data point of the peak but also by the spread of values around 1 full SD, we take into account that the exact peaks might not be identical for all frequency bands.

The peak ± SD frequencies of the FFT for sigma power were also used to calculate a band-pass (FIR)–filtered trace of sigma power time course before noise onset (Fig. 4D) and to reconstruct the oscillations in Fig. 4F. The peak ± SD frequencies of the FFT for sigma power were also used for the phase analysis in Fig. 4 (G and H). Here, the sigma power time courses in the prestimulus period were fit to a sinus function with a frequency constrained by these limits. The phase of these sinusoids was read for the wake-up and sleep-through trials in which both a peak and a trough lay within the fitted period. This was the case for 4 of 9 wake-up and 8 of 10 sleep-through sigma power time courses.

In noise exposure experiments, the time courses of sigma power and SWA in the 40-s prestimulus period were averaged across animals after sorting the trials on the basis of their outcome (wake-up or sleep-through trials). For any successful trial, the values in both sigma and SWA frequency bands were expressed in percentage with respect to the average non-REM sleep power spectrum in the 40-s prestimulus period (Fig. 4, C and E). Because of this normalization, 0.02-Hz oscillations had smaller amplitudes than those in Fig. 1. A total of $n = 1$ of 10 animals did not wake up in any of the noise exposures and did not contribute to the power calculations (Fig. 4, D and E). Later analysis showed that, in this mouse, only two noise exposures were successful, and both of these fell onto the rising phase of the sigma power oscillation. Analysis of phase was carried out with phase convention peak of 0° and trough of 180°, as described above.

Ripple activity time course was quantified from the LFP recording in the CA1 area. The signal was first filtered between 150 and 250 Hz and then squared. The values were averaged in a 4-s bin, and a cross-correlation was performed against the corresponding sigma power from channel SI (resampled at 1 Hz) using the ripple activity trace as "source wave."

Analysis of 0.02-Hz oscillations in humans

The scheme in fig. S5 summarizes the analysis steps for human non-REM sleep. An analysis similar to that in mice was performed on consecutive 30-s intervals of non-REM sleep EEG (further referred to as bouts) of the first 210 min of sleep and free of artifacts or movement arousals for the core study data set (fig. S5A) and was extended to the full-night sleep in the memory group data set (Figs. 3 and 5). The analysis differed from that in mice to account for dissimilarities in sleep patterns of humans (for example, longer bouts). For each EEG signal of a bout, the power spectra were calculated every 0.1 s in the 0.5- to 24-Hz range in steps of 0.2 Hz with a continuous wavelet transform using Morlet wavelets with length of four cycles. At every time point, the average power in the bands was calculated in frequency bands equivalent to mice: SWA (0.5 to 4 Hz), theta (4 to 8 Hz), sigma (10 to 15 Hz), individual beta (16 to 20 Hz), and beta2 (20 to 24 Hz). This resulted in a detailed power time course for each respective frequency band (fig. S5B).

After visual confirmation that the power time course in the sigma and SWA bands corresponded to real spindle and SWA activity, the temporal resolution was reduced to highlight activity changes in the infraslow periodicity. Therefore, a symmetric moving average was applied in a 4-s time window to match the resolution of the mouse data. As in mice, the average absolute values of the non-REM sleep spectral composition were used for normalization by setting them to 100% (Fig. 1, E and F). The first 100 min of concatenated non-REM sleep was used for this normalization to account for interindividual differences in the amount of non-REM sleep and to match the time interval used for the analysis in mice [fig. S5, A (bottom) and C].

To establish the spectral profile of these power time courses, the spectra of the power time courses for each frequency band were obtained for all non-REM sleep bouts lasting ≥120 s (≥4 epochs) (fig. S5A, bottom). For this, a Morlet wavelet analysis was performed in each interval on the previously calculated power time courses for respective frequency bands that aimed for a frequency resolution of 0.001 Hz in the range 0.001 to 0.12 Hz with time steps of 0.5 s. To obtain one power spectrum for each bout, we then averaged the resulting signal across time steps along the duration of the bout (fig. S5D).

Last, the spectral profile of the 0.02-Hz oscillation of all frequency bands for all non-REM sleep was calculated by averaging the spectral values across all the non-REM sleep bouts of the subject, weighted by their duration. As in mice, the spectral profile obtained per subject was normalized to its own mean. To determine peak and

SDs of each power spectrum, a Gaussian fit (three terms) was performed on the normalized power from single subjects. The peak location and SD values were obtained from the fitted curve and used to calculate the average peak value in the range (peak ± 0.5 × SD) (Fig. 1, G and H). Accounting for the larger variability in individual peak values between human subjects and frequency bands as compared to mice, the respective range of each frequency band was used to approximate the highest possible average peak values. Using the range from the sigma band for averaging of peak values in all frequency bands essentially yielded the same results reported here.

To address specificity of the 0.02-Hz oscillation to spindles, we repeated the analysis for a frequency band tailored to the individual spindle band of each subject. Thus, for each subject, the frequency band was centered to its FSP that was determined according to previously described standard methods (*12*, *54*), and that is specified here briefly. Power spectra containing the sigma band (8 to 18 Hz) were calculated in the same way as reported above but using consecutive artifact-free 10-s intervals of non-REM sleep, which overlapped in time by 5 s with a frequency resolution of 0.1 Hz. The FSP was visually identified for each subject from the individual power spectra of non-REM sleep epochs as power maxima within the sigma band (*12*). Although slow spindles contribute to the sigma band, they were not considered because of their prevalence mainly during SWS and tight temporal association with fast spindles (*12*).

Control analyses for humans in figs. S3 and S4 including using minimal bout lengths of double (≥240 s; fig. S3, D to F) or triple the length (≥360 s), changing Morlet wavelet cycle length to seven cycles for better frequency resolution, skipping the normalization steps, or comparing the power fluctuations in the full spectrum (in smaller bands of 1 Hz from 1 to 24 Hz, instead of broader specific bands) essentially yielded the same results reported here. Autocorrelations were calculated as in mice for original and shuffled sigma power profile data of non-REM sleep. To more closely match the respective analyses in mice, the data were split in all possible continuous 240-s segments and down-sampled to 1 Hz (this analysis is referred to as 240-s bouts; see fig. S4, C and D).

White noise exposure during polysomnographic recordings in sleeping mice

A subset of 10 mice implanted for polysomnography was habituated to the experimental noise stimulus during the period of tethering after surgery through playing noises six to eight times per light phase. During the experimental trials, animals were exposed, four at a time, to white noise pulses of 90-dB SPL lasting 20 s, generated through custom-written LabVIEW procedure (National Instruments Corporation). The duration of the noise was chosen such that it covered half a cycle of the 0.02-Hz oscillation and because mice woke up or slept through it at comparable rates. The arousal success rate was defined as the fraction of wake-up trials within all accepted trials. In a preliminary experimental series, a 20-s pulse at 80 dB was found to lead to an insufficient number of wake-up trials, with the arousal success rate <30%, whereas a 4-s pulse at 100 dB led to arousals in more than 90% of the cases. Noise was played randomly in the first 100 min at ZT0, but the following conditions had to be fulfilled: At least one of the four mice was in non-REM sleep for ≥40 s, as assessed through online monitoring of EEG (ECoG)/EMG traces, and the previous noise had been played ≥4 min before. The experimenter was blind to the spectral composition of non-REM sleep during the noise exposure experiment, such that noises were played without knowledge of the sigma power phase. Wake-ups were identified on the basis of characteristic alterations of EEG/EMG signals, namely, the decrease in amplitude and increase in frequency for the EEG trace, combined with the detection of muscular activity from the EMG electrodes (Fig. 4B). The animals were exposed several times to the noise in each recording session. The 20-s pulse was played 14.0 ± 0.3 (minimally 9) times per mouse, of which 8.6 ± 0.4 (minimally two per mouse) trials were successful, meaning that the mouse did not wake up in the prestimulus period or in the first 4 s of noise exposure. EEG (ECoG)/EMG traces were scored blind with respect to noise exposure times.

Study procedures and memory assessment in humans

In the core study, subjects arrived at the laboratory at 9:00 p.m. for experimental preparation, and sleep was allowed between 11:00 p.m. (lights off) and 7:00 a.m. Subjects underwent blood sampling via an intravenous forearm catheter, which was connected to a long thin tube and enabled blood collection from an adjacent room without disturbing the subject's sleep and unnoticed by all subjects (*14*).

The memory study demonstrated a twofold better recall of episodic memory when task performance was followed by nocturnal sleep compared to postlearning daytime wakefulness (*14*). Here, we only used the subjects of the sleep group, for which the procedures were as follows: Encoding of the memory task took place in the evening (between ~8:00 p.m. and 11:00 p.m.). One hour after encoding, and in accordance with their usual sleep habits, participants went to bed (lights off) for an 8-hour sleep period in the laboratory with polysomnographic recordings. The retrieval phase started 1 hour after awakening. The episodic memory task described in detail by Weber *et al.* (*14*) required the encoding of faces (events) embedded in a spatial context (that is, different locations on a screen) and a temporal context (that is, different faces at the different locations were presented in two experimental episodes separated by a 1-hour interval). During encoding, participants remained unaware that the task was aimed at memory testing but were instructed to keep focused on the experimental episodes presented on the screen.

For recall testing during the retrieval phase after sleep, old and novel faces were presented, and the subjects had to indicate (by mouse clicks) whether a face was new or presented during one of the task episodes, and for the latter, whether it occurred in the first or second episode and at which location it occurred. Episodic memory, that is, "what-where-when" memory, was determined by the percentage of the faces that were correctly identified as occurring in one of the episodes (that is, "what"), and for which the participant also correctly indicated the episode (that is, "what-when") and the location (that is, "what-where") it occurred, minus the locations for which the participant had forgotten that they were occupied with any face in a final separate recall test (false "where-when" memory).

Analysis of heart rate in mice and humans

The instantaneous heart rate was extracted from the nuchal EMG recording in freely moving or head-fixed mice and calculated from the ECG recordings in humans. In $n = 12$ mice (eight freely moving and four head-fixed), the heart rate was quantified through detection of R waves in the EMG trace filtered between 20 and 300 Hz. Reliability of this signal was confirmed through standard ECG recording in one mouse (fig. S12) (*55*). Peak or threshold detections were used, with equal results. In the latter case, threshold was set as

the mean + 3.5 × SD of the EMG signal. We then calculated the interval between two successive peaks (R-R interval) for all consolidated non-REM sleep bouts ≥45 s. Occasionally, R waves were classified as aberrant because they were either below threshold or artifactual because of muscle twitches, which corresponded to 1.41% of all intervals. In freely moving animals, all non-REM sleep bouts ≥96 s were used. The number of non-REM sleep bouts per head-fixed animal included in the analysis ranged from 10 to 42 bouts (mean number of bouts, 22.3 ± 7.2). The R-R intervals were then binned (1 s) and converted into beats per minute. In humans, the heart rate was determined across artifact-free consecutive non-REM sleep intervals on the basis of R-R intervals. R waves were detected by first filtering the ECG signal with a high-pass filter of 20 Hz [infinite impulse response (IIR); designed for a stopband of 15 Hz with −100-dB attenuation, with two filter passings and no time shift] and then applying a low-pass filter at 45 Hz (IIR; filter order of 4, with two filter passings and no time shift). To obtain a clear signal amplitude envelope describing the R wave, we calculated the absolute values of the Hilbert transform of the signal. Then, the signal was down-sampled to 100 Hz to facilitate computation. R-wave peaks were automatically identified as maxima in the envelope signal if they were at least 0.2 s apart (minimal heart refractory period) and reached above a threshold of 2 SDs from overall envelope signal values. This method was visually confirmed in each subject to validate correct R-wave peak detection in all epochs. Instantaneous heart rate at every R-wave peak was then determined by duration between consecutive R-R intervals.

For cross-correlating time courses of heart rate (in beats per minute) and sigma power in mice, the sigma power trace was interpolated to match the 1-Hz sampling rate of the heart rate trace. In humans, it was smoothed in a 4-s moving symmetric time window, and both sigma power and heart rate traces were resampled at 100 Hz by interpolation. The 120-s intervals were z-transformed (by subtracting the mean and dividing by the SD). In both mice and humans, the cross-correlation was performed using the heart rate signal as source wave. In both species, the cross-correlograms were first averaged within and then across subjects. In humans, all of the above procedures were repeated separately for S2 and SWS epochs instead of non-REM sleep epochs but reported solely for the oscillation peak analysis.

Experimental design and statistics

Group size in mice matched the minimum required to obtain a statistical power of 0.8. Power analyses were carried out on the basis of effect sizes obtained from preliminary data sets. Group size in humans was chosen to obtain a statistical power of 0.95 for similar effect sizes, as observed in mice. Statistical power was calculated using G*Power version 3.1.9.2. Data normality was tested using the Shapiro-Wilk W test, and parametric or nonparametric statistical tests were chosen accordingly. The Wilcoxon signed-rank test was used for nonparametric matched pair comparisons, whereas paired two-tailed Student's t tests (referred to as t test in text and legends) were used as parametric statistical tests. RM ANOVA was used as parametric statistical test to study the within-subjects effect of behavioral outcome and/or the between-subjects effect. To assess equality of variances for the RM ANOVA, we calculated the Mauchly's test of sphericity. Whenever equality of variances was rejected, the univariate adjusted Greenhouse-Geisser correction was applied. Friedman rank sum test was used as a nonparametric test to study within-subjects effect in case parametric model parameters of an ANOVA violated assumptions of normality. Statistical tests were calculated using JMP version 10.0.0 (SAS Institute Inc.), Igor Pro, and the R programming language (2.15.0, R Core Team) [The R Development Core Team, The R Foundation for Statistical Computing (www.r-project.org/foundation), 2007]. $P < 0.05$ was considered statistically significant. If not mentioned otherwise, P values were reported uncorrected for multiple comparisons, as taking these into account did not alter the main results. For the purpose of comparison between mice and humans, all data in bar graphs are presented as means ± SEM, even if not normally distributed (Fig. 1, D, H, and J). All indications of n refer to either mice or humans. Time course graphs, as well as data in the main text, are presented as means ± SEM.

SUPPLEMENTARY MATERIALS

Supplementary material for this article is available at http://advances.sciencemag.org/cgi/content/full/3/2/e1602026/DC1

fig. S1. The 0.02-Hz oscillation is prominent for sigma power throughout both short and long non-REM sleep bouts in mice.
fig. S2. Scheme of analysis for 0.02-Hz oscillations in mice.
fig. S3. The 0.02-Hz oscillation is robust against the choice of non-REM sleep bout length for analysis and does not result from an 1/f power dependence.
fig. S4. The sigma power dynamics in both mice and humans show a periodicity on a 0.02-Hz time scale, as assessed through autocorrelations.
fig. S5. Scheme of analysis for 0.02-Hz oscillations in humans.
fig. S6. Sleep parameters for the participants of the studies in humans and predominance of 0.02-Hz oscillations in S2 sleep.
fig. S7. The 0.02-Hz oscillation is prominent for sigma power throughout early non-REM sleep in humans.
fig. S8. Sleep in head-fixed animals reproduces the three major vigilance states and their spectral characteristics found in freely moving animals.
fig. S9. Acoustic stimuli causing early or late wake-ups fall onto late or early portions of the declining sigma power phase, respectively.
fig. S10. Wake-up and sleep-through trials do not depend on previous sleep duration.
fig. S11. Ripple power increases precede sigma power elevations.
fig. S12. Nuchal EMG recordings faithfully detect the R-waves of the heartbeat in mice.

REFERENCES AND NOTES

1. B. Rasch, J. Born, About sleep's role in memory. *Physiol. Rev.* **93**, 681–766 (2013).
2. J. M. Krueger, M. G. Frank, J. P. Wisor, S. Roy, Sleep function: Toward elucidating an enigma. *Sleep Med. Rev.* **28**, 46–54 (2016).
3. S. S. Campbell, I. Tobler, Animal sleep: A review of sleep duration across phylogeny. *Neurosci. Biobehav. Rev.* **8**, 269–300 (1984).
4. J. M. Siegel, Sleep viewed as a state of adaptive inactivity. *Nat. Rev. Neurosci.* **10**, 747–753 (2009).
5. T. T. Dang-Vu, M. Bonjean, M. Schabus, M. Boly, A. Darsaud, M. Desseilles, C. Degueldre, E. Balteau, C. Phillips, A. Luxen, T. J. Sejnowski, P. Maquet, Interplay between spontaneous and induced brain activity during human non-rapid eye movement sleep. *Proc. Natl. Acad. Sci. U.S.A.* **108**, 15438–15443 (2011).
6. M. Elton, O. Winter, D. Heslenfeld, D. Loewy, K. Campbell, A. Kok, Event-related potentials to tones in the absence and presence of sleep spindles. *J. Sleep Res.* **6**, 78–83 (1997).
7. D. Aeschbach, A. A. Borbély, All-night dynamics of the human sleep EEG. *J. Sleep Res.* **2**, 70–81 (1993).
8. S. Astori, R. D. Wimmer, A. Lüthi, Manipulating sleep spindles—Expanding views on sleep, memory, and disease. *Trends Neurosci.* **36**, 738–748 (2013).
9. S. M. McKinney, T. T. Dang-Vu, O. M. Buxton, J. M. Solet, J. M. Ellenbogen, Covert waking brain activity reveals instantaneous sleep depth. *PLOS ONE* **6**, e17351 (2011).
10. E. Sforza, C. Jouny, V. Ibanez, Cardiac activation during arousal in humans: Further evidence for hierarchy in the arousal response. *Clin. Neurophysiol.* **111**, 1611–1619 (2000).
11. R. D. Wimmer, S. Astori, C. T. Bond, Z. Rovó, J.-Y. Chatton, J. P. Adelman, P. Franken, A. Lüthi, Sustaining sleep spindles through enhanced SK2-channel activity consolidates sleep and elevates arousal threshold. *J. Neurosci.* **32**, 13917–13928 (2012).
12. M. Mölle, T. O. Bergmann, L. Marshall, J. Born, Fast and slow spindles during the sleep slow oscillation: Disparate coalescence and engagement in memory processing. *Sleep* **34**, 1411–1421 (2011).
13. G. Buzsáki, Hippocampal sharp wave-ripple: A cognitive biomarker for episodic memory and planning. *Hippocampus* **25**, 1073–1188 (2015).
14. F. D. Weber, J. Wang, J. Born, M. Inostroza, Sleep benefits in parallel implicit and explicit measures of episodic memory. *Learn. Mem.* **21**, 190–198 (2014).

15. D. Contreras, A. Destexhe, T. J. Sejnowski, M. Steriade, Spatiotemporal patterns of spindle oscillations in cortex and thalamus. *J. Neurosci.* **17**, 1179–1196 (1997).
16. M. Steriade, D. A. McCormick, T. J. Sejnowski, Thalamocortical oscillations in the sleeping and aroused brain. *Science* **262**, 679–685 (1993).
17. E. Werth, P. Achermann, D.-J. Dijk, A. A. Borbély, Spindle frequency activity in the sleep EEG: Individual differences and topographical distribution. *Electroencephalogr. Clin. Neurophysiol.* **103**, 535–542 (1997).
18. K. C. Andrade, V. I. Spoormaker, M. Dresler, R. Wehrle, F. Holsboer, P. G. Sämann, M. Czisch, Sleep spindles and hippocampal functional connectivity in human NREM sleep. *J. Neurosci.* **31**, 10331–10339 (2011).
19. S. Laventure, S. Fogel, O. Lungu, G. Albouy, P. Sévigny-Dupont, C. Vien, C. Sayour, J. Carrier, H. Benali, J. Doyon, NREM2 and sleep spindles are instrumental to the consolidation of motor sequence memories. *PLOS Biol.* **14**, e1002429 (2016).
20. G. Aston-Jones, F. E. Bloom, Activity of norepinephrine-containing locus coeruleus neurons in behaving rats anticipates fluctuations in the sleep-waking cycle. *J. Neurosci.* **1**, 876–886 (1981).
21. M. Shein-Idelson, J. M. Ondracek, H.-P. Liaw, S. Reiter, G. Laurent, Slow waves, sharp waves, ripples, and REM in sleeping dragons. *Science* **352**, 590–595 (2016).
22. D. Mantini, M. G. Perrucci, C. Del Gratta, G. L. Romani, M. Corbetta, Electrophysiological signatures of resting state networks in the human brain. *Proc. Natl. Acad. Sci. U.S.A.* **104**, 13170–13175 (2007).
23. M. Fukunaga, S. G. Horovitz, P. van Gelderen, J. A. de Zwart, J. M. Jansma, V. N. Ikonomidou, R. Chu, R. H. R. Deckers, D. A. Leopold, J. H. Duyn, Large-amplitude, spatially correlated fluctuations in BOLD fMRI signals during extended rest and early sleep stages. *Magn. Reson. Imaging* **24**, 979–992 (2006).
24. H. Lu, Q. Zou, H. Gu, M. E. Raichle, E. A. Stein, Y. Yang, Rat brains also have a default mode network. *Proc. Natl. Acad. Sci. U.S.A.* **109**, 3979–3984 (2012).
25. M. Boly, V. Perlbarg, G. Marrelec, M. Schabus, S. Laureys, J. Doyon, M. Pélégrini-Issac, P. Maquet, H. Benali, Hierarchical clustering of brain activity during human nonrapid eye movement sleep. *Proc. Natl. Acad. Sci. U.S.A.* **109**, 5856–5861 (2012).
26. Y. Nir, R. J. Staba, T. Andrillon, V. V. Vyazovskiy, C. Cirelli, I. Fried, G. Tononi, Regional slow waves and spindles in human sleep. *Neuron* **70**, 153–169 (2011).
27. L. Genzel, M. C. W. Kroes, M. Dresler, F. P. Battaglia, Light sleep versus slow wave sleep in memory consolidation: A question of global versus local processes? *Trends Neurosci.* **37**, 10–19 (2014).
28. M. Schabus, T. T. Dang-Vu, D. P. J. Heib, M. Boly, M. Desseilles, G. Vandewalle, C. Schmidt, G. Albouy, A. Darsaud, S. Gais, C. Degueldre, E. Balteau, C. Phillips, A. Luxen, P. Maquet, The fate of incoming stimuli during NREM sleep is determined by spindles and the phase of the slow oscillation. *Front. Neurol.* **3**, 40 (2012).
29. M. E. Carter, O. Yizhar, S. Chikahisa, H. Nguyen, A. Adamantidis, S. Nishino, K. Deisseroth, L. De Lecea, Tuning arousal with optogenetic modulation of locus coeruleus neurons. *Nat. Neurosci.* **13**, 1526–1533 (2010).
30. K. Takahashi, Y. Kayama, J. S. Lin, K. Sakai, Locus coeruleus neuronal activity during the sleep-waking cycle in mice. *Neuroscience* **169**, 1115–1126 (2010).
31. K. K. Ohlemiller, S. M. Jones, K. R. Johnson, Application of mouse models to research in hearing and balance. *J. Assoc. Res. Otolaryngol.* **17**, 493–523 (2016).
32. T. T. Dang-Vu, S. M. McKinney, O. M. Buxton, J. M. Solet, J. M. Ellenbogen, Spontaneous brain rhythms predict sleep stability in the face of noise. *Curr. Biol.* **20**, R626–R627 (2010).
33. S. Gais, M. Mölle, K. Helms, J. Born, Learning-dependent increases in sleep spindle density. *J. Neurosci.* **22**, 6830–6834 (2002).
34. O. Eschenko, W. Ramadan, M. Mölle, J. Born, S. J. Sara, Sustained increase in hippocampal sharp-wave ripple activity during slow-wave sleep after learning. *Learn. Mem.* **15**, 222–228 (2008).
35. M. Mölle, O. Eschenko, S. Gais, S. J. Sara, J. Born, The influence of learning on sleep slow oscillations and associated spindles and ripples in humans and rats. *Eur. J. Neurosci.* **29**, 1071–1081 (2009).
36. Z. Clemens, M. Mölle, L. Erőss, R. Jakus, G. Rásonyi, P. Halász, J. Born, Fine-tuned coupling between human parahippocampal ripples and sleep spindles. *Eur. J. Neurosci.* **33**, 511–520 (2011).
37. N. Maingret, G. Girardeau, R. Todorova, M. Goutierre, M. Zugaro, Hippocampo-cortical coupling mediates memory consolidation during sleep. *Nat. Neurosci.* **19**, 959–964 (2016).
38. A. Rolls, D. Colas, A. Adamantidis, M. Carter, T. Lanre-Amos, H. C. Heller, L. de Lecea, Optogenetic disruption of sleep continuity impairs memory consolidation. *Proc. Natl. Acad. Sci. U.S.A.* **108**, 13305–13310 (2011).
39. F. Ding, J. O'Donnell, Q. Xu, N. Kang, N. Goldman, M. Nedergaard, Changes in the composition of brain interstitial ions control the sleep-wake cycle. *Science* **352**, 550–555 (2016).
40. P. Novak, V. Lepicovska, C. Dostalek, Periodic amplitude modulation of EEG. *Neurosci. Lett.* **136**, 213–215 (1992).
41. S. Monto, S. Palva, J. Voipio, J. M. Palva, Very slow EEG fluctuations predict the dynamics of stimulus detection and oscillation amplitudes in humans. *J. Neurosci.* **28**, 8268–8272 (2008).
42. L. Parrino, R. Ferri, O. Bruni, M. G. Terzano, Cyclic alternating pattern (CAP): The marker of sleep instability. *Sleep Med. Rev.* **16**, 27–45 (2012).
43. S. Vanhatalo, J. M. Palva, M. D. Holmes, J. W. Miller, J. Voipio, K. Kaila, Infraslow oscillations modulate excitability and interictal epileptic activity in the human cortex during sleep. *Proc. Natl. Acad. Sci. U.S.A.* **101**, 5053–5057 (2004).
44. M. Penttonen, N. Nurminen, R. Miettinen, J. Sirviö, D. A. Henze, J. Csicsvári, G. Buzsáki, Ultra-slow oscillation (0.025 Hz) triggers hippocampal afterdischarges in Wistar rats. *Neuroscience* **94**, 735–743 (1999).
45. R. Kaplan, M. H. Adhikari, R. Hindriks, D. Mantini, Y. Murayama, N. K. Logothetis, G. Deco, Hippocampal sharp-wave ripples influence selective activation of the default mode network. *Curr. Biol.* **26**, 686–691 (2016).
46. A. Silvani, R. A. L. Dampney, Central control of cardiovascular function during sleep. *Am. J. Physiol. Heart Circ. Physiol.* **305**, H1683–H1692 (2013).
47. E. V. Golanov, J. R. C. Christensen, D. J. Reis, Neurons of a limited subthalamic area mediate elevations in cortical cerebral blood flow evoked by hypoxia and excitation of neurons of the rostral ventrolateral medulla. *J. Neurosci.* **21**, 4032–4041 (2001).
48. G. M. Mang, P. Franken, Sleep and EEG phenotyping in mice. *Curr. Protoc. Mouse Biol.* **2**, 55–74 (2012).
49. L. M. Fernandez, J.-C. Comte, P. Le Merre, J.-S. Lin, P.-A. Salin, S. Crochet, Highly dynamic spatiotemporal organization of low-frequency activities during behavioral states in the mouse cerebral cortex. *Cereb. Cortex* 10.1093/cercor/bhw311 (2017).
50. L. Besedovsky, J. Born, T. Lange, Endogenous glucocorticoid receptor signaling drives rhythmic changes in human T-cell subset numbers and the expression of the chemokine receptor CXCR4. *FASEB J.* **28**, 67–75 (2014).
51. A. Rechtschaffen, A. Kales, *A Manual of Standardized Terminology, Techniques and Scoring System for Sleep of Human Subjects* (U.S. Department of Health, Education and Welfare, 1968).
52. R. Oostenveld, P. Fries, E. Maris, J.-M. Schoffelen, FieldTrip: Open source software for advanced analysis of MEG, EEG, and invasive electrophysiological data. *Comput. Intell. Neurosci.* **2011**, 156869 (2011).
53. H.-V. V. Ngo, T. Martinetz, J. Born, M. Mölle, Auditory closed-loop stimulation of the sleep slow oscillation enhances memory. *Neuron* **78**, 545–553 (2013).
54. M. Mölle, L. Marshall, S. Gais, J. Born, Grouping of spindle activity during slow oscillations in human non-rapid eye movement sleep. *J. Neurosci.* **22**, 10941–10947 (2002).
55. C. Jin, J. Zhang, X. Li, X. Yang, J. Li, J. Liu, Injectable 3-D fabrication of medical electronics at the target biological tissues. *Sci. Rep.* **3**, 3442 (2013).

Acknowledgments: We are grateful to all laboratory members for constructive discussions and detailed reading of the manuscript. We thank N. Liaudet for help with MATLAB, R. Kraftsik for help with statistical analysis, L. Besedovsky for providing the human sleep recordings, and J.-Y. Wang for providing sleep and memory data in humans. We are grateful to P. Franken, D. McCormick, and P. Salin for the critical input; M. Tafti and R. Gervais for the stimulating discussions; and J. Brumberg, M. Celio, P. Franken, S. Fulda, M. Tafti, and E. Welker for the careful reading of earlier versions of the manuscript. Basic Igor Pro routines were provided by S. Crochet. This work was possible thanks to the Physiology Department of the University of Lausanne, which provided the room for the mouse sleep experimentation, and the Werner Reichardt Centre for Integrative Neuroscience within the University of Tübingen, which provided computational infrastructure. **Funding:** Funding was provided by the Swiss National Science Foundation (grants 31003A_146244 and 31003A_166318) and the Etat de Vaud and the Deutsche Forschungsgemeinschaft (SFB 654 "Plasticity and Sleep"). **Author contributions:** S.L. and A.L. conceived the original study in mice, which was extended and rewritten in interaction with F.D.W. and J.B., who contributed the human findings. L.M.J.F. performed the LFP recordings and developed the analyses. S.L. performed all mouse experiments. R.C. contributed to the polysomnographic recordings in undisturbed mice. J.-Y.C. developed the noise generator in LabVIEW. S.L., L.M.J.F., F.D.W., R.C., and A.L. analyzed the data. S.L., L.M.J.F., F.D.W., and R.C. prepared the figures. A.L. wrote the manuscript together with S.L., F.D.W., L.M.J.F., and J.B. **Competing interests:** The authors declare that they have no competing interests. **Data and materials availability:** All data needed to evaluate the conclusions in the paper are present in the paper and/or the Supplementary Materials. Additional data related to this paper may be requested from the authors. Computer codes used to generate the results can be provided upon request. Code for spindle (peak) and slow wave detection as well as general power analysis of human data is publicly available at www.spisop.org.

Submitted 25 August 2016
Accepted 19 December 2016
Published 8 February 2017
10.1126/sciadv.1602026

Citation: S. Lecci, L. M. J. Fernandez, F. D. Weber, R. Cardis, J.-Y. Chatton, J. Born, A. Lüthi, Coordinated infraslow neural and cardiac oscillations mark fragility and offline periods in mammalian sleep. *Sci. Adv.* **3**, e1602026 (2017).

Science Advances

Coordinated infraslow neural and cardiac oscillations mark fragility and offline periods in mammalian sleep

Sandro Lecci, Laura M. J. Fernandez, Frederik D. Weber, Romain Cardis, Jean-Yves Chatton, Jan Born and Anita Lüthi

Sci Adv **3** (2), e1602026.
DOI: 10.1126/sciadv.1602026

Coordinated infraslow neural and cardiac oscillations mark fragility and offline periods in mammalian sleep

Sandro Lecci, Laura M. J. Fernandez, Frederik D. Weber, Romain Cardis, Jean-Yves Chatton, Jan Born and Anita Lüthi

Sci Adv **3** (2), e1602026.
DOI: 10.1126/sciadv.1602026

Cortico-autonomic local arousals and heightened somatosensory arousability during NREM sleep of mice in neuropathic pain

Romain Cardis[1,2], Sandro Lecci[1], Laura M.J. Fernandez[1], Alejandro Osorio-Forero[1], Paul Chu Sin Chung[1,2], Stephany Fulda[3,*], Isabelle Decosterd[1,2,*], Anita Lüthi[1,*]

*shared senior authorship and correspondence

Address:

[1]Department of Fundamental Neurosciences, Rue du Bugnon 9, CH-1005 Lausanne

[2]Pain Center, Department of Anesthesiology, Lausanne University Hospital (CHUV), Lausanne, Switzerland

[3]Sleep and Epilepsy Center, Neurocenter of Southern Switzerland, Civic Hospital (EOC) of Lugano, Lugano, Switzerland.

Manuscript info:

Number of figures: 7

Number of Supplementary figures: 4

Number of words in abstract: 149

Number of words in main text including legends: 9,579

Number of words in legends: 3,093

Number of references: 85

Abstract

Chronic pain patients frequently suffer from sleep disturbances. Improvement of sleep quality alleviates pain, but neurophysiological mechanisms underlying sleep disturbances require clarification to advance therapeutic strategies. Chronic pain causes high-frequency electrical activity in pain-processing cortical areas that could disrupt the normal process of low-frequency sleep rhythm generation. We found that the spared-nerve-injury (SNI) mouse model, mimicking human neuropathic pain, had preserved sleep-wake behavior. However, when we probed spontaneous arousability based on infraslow continuity-fragility dynamics of non-rapid-eye-movement sleep (NREMS), we found more numerous local cortical arousals accompanied by heart rate increases in hindlimb primary somatosensory, but not in prelimbic, cortices of SNI mice. Closed-loop mechanovibrational stimulation revealed higher sensory arousability in SNI. Sleep in chronic pain thus looked preserved in conventional measures but showed elevated spontaneous and evoked arousability. Our findings develop a novel moment-to-moment probing of NREMS fragility and propose that chronic pain-induced sleep complaints arise from perturbed arousability.

Introduction

Pain causes functional impairment, displeasure and stress and can impede even the simplest daily life routines, including sleep. If not treated, pain has the ability to outlast its original cause, producing chronic pain that is generally difficult to treat (Finnerup *et al.*, 2015; Treede *et al.*, 2019). Current estimates are that more than two out of three individuals suffering from chronic pain also show diverse symptoms characteristic for insomnia disorders, such as lower sleep efficiency, more time awake after sleep onset and frequent brief awakenings during the night (Bjurstrom & Irwin, 2016; Mathias *et al.*, 2018). The relation between chronic pain and sleep disruptions is complex and bidirectional, but accurate assessment of sleep problems is considered critical to antagonize the perpetuation of pain (Bjurstrom & Irwin, 2016). Therefore, key mechanisms associating pain with sleep disturbance need to be clarified.

Animal models of chronic pain that mimic clinical symptoms of human patients have been critical to understand the pathophysiological mechanisms producing chronic pain states (Burma *et al.*, 2017). Neuropathic pain is caused by damage to the somatosensory nervous system (Finnerup *et al.*, 2021) and induced in rodents by surgically lesioning peripheral nerves, such as the sciatic nerve (Decosterd & Woolf, 2000; Bourquin *et al.*, 2006). Neuropathic pain causes maladaptive structural and functional remodeling of the central and peripheral nervous systems, shifting brain circuits towards pain hypersensitivity and aversive behavioral states (Kuner & Kuner, 2020). Hyperexcitability and an abnormal activity in a broad range of gamma frequencies (30—100 Hz) in pain-processing cortical areas were found to be primary culprits for the elevated sensitivity to painful stimuli and for aversive behaviors (Tan *et al.*, 2019), a finding that is in line with observations in human (Ploner *et al.*, 2017). In contrast to these advances, sleep studies on chronic pain models are scarce, used relatively simple sleep measures, and produced variable results (Andersen & Tufik, 2003; Kontinen *et al.*, 2003; Tokunaga *et al.*, 2007; Cardoso-Cruz *et al.*, 2011; Leys *et al.*, 2013). Therefore, it is currently open whether these animal models are also suited to address the sleep complaints of human patients.

One possibility is that current approaches have so far failed to uncover the full profile of the sleep disruptions caused by chronic pain. Studies in insomnia disorders indeed suggest that changes in traditional sleep parameters often seem not in line with the severity of the sleep complaints (Feige *et al.*, 2013; van Someren, 2020). Standard polysomnography describes sleep as a sequence of discrete states and distinguishes between non-rapid-eye-movement sleep (NREMS) and rapid-eye-movement sleep (REMS), with the former further subdivided into transitional (N1), light (N2) and deep (N3) stages (Iber *et al.*, 2007). Many reports on human patients find little change in the absolute or relative times spent in

these stages and/or their principal spectral characteristics (Salin-Pascual *et al.*, 1992; Perlis *et al.*, 2001b; Buysse *et al.*, 2008; Wei *et al.*, 2017; Feige *et al.*, 2018; Christensen *et al.*, 2019; Lecci *et al.*, 2020). Instead, cortical activity patterns are abnormally enriched in the alpha (8—12 Hz) (Krystal *et al.*, 2002; Riedner *et al.*, 2016), beta (18—30 Hz) (Krystal et al., 2002; Spiegelhalder *et al.*, 2012; Maes *et al.*, 2014; Riedner et al., 2016; Lecci et al., 2020) and/or low-gamma bands (30—45 Hz) (Perlis et al., 2001b; Lecci et al., 2020), in one or more NREMS stages and/or in REMS (Spiegelhalder et al., 2012; Christensen et al., 2019; Lecci et al., 2020) and/or in restricted brain areas (St-Jean *et al.*, 2012; Riedner et al., 2016; Lecci et al., 2020). Such high-frequency electrical rhythms during sleep are part of a physiological state referred to as "hyperarousal" (Feige et al., 2013; van Someren, 2020; Vargas *et al.*, 2020) that has been related to less restorative sleep (Moldofsky *et al.*, 1975; Krystal & Edinger, 2008), to misperceiving sleep as wakefulness (Perlis et al., 2001b; Lecci et al., 2020), and to higher heart rates (Maes et al., 2014), all of which are key features of insomnia disorders in humans. Other studies applied various metrics and proposed more spontaneous arousals and/or easier wake-ups in response to sensory stimulation (Parrino *et al.*, 2009; Forget *et al.*, 2011; Wei et al., 2017; Feige et al., 2018). Taken together, the presence of high-frequency electrical activity, combined with diverse measures of arousability, has been useful in clarifying the pathophysiological mechanisms underlying insomnia disorders. To date, however, such measures have not been applied to study sleep in chronic pain in humans and mice, and there is still a paucity of comparative studies between sleep in chronic pain patients and in primary insomniacs (Bjurstrom & Irwin, 2016). Therefore, it is currently unclear whether chronic pain is accompanied by high-frequency cortical activity during NREMS and whether this affects spontaneous and evoked arousability (Mathias et al., 2018; Kuner & Kuner, 2020).

This study pursues this question through implementing a real-time tracking method for spontaneous and evoked arousability in the mouse spared-nerve-injury (SNI) model of neuropathic pain (Bourquin et al., 2006). We start from previously described fragility-continuity dynamics of NREMS in mice and humans that indicate variable arousability on the ~50-sec time scale (Lecci *et al.*, 2017). The fragility-continuity dynamics are present while NREMS remains polysomnographically continuous and manifest in fluctuating activity of several brain and peripheral parameters, notably in the power of sleep spindles (10—15 Hz) in the global EEG and the local field potential (LFP) signals. On this close-to-minute timescale, we show here that we are capable of tracking spontaneous and evoked arousability across NREMS in the resting (light) phase. We find that the sleep disruptions in SNI animals concern both, altered spontaneous and evoked arousability. In particular, we identify a novel, previously undescribed cortico-autonomic

arousal that pairs EEG desynchronization with increased heart rate and that occurs more frequently in SNI animals.

Results

SNI mice show normal sleep-wake behavior

SNI mice and Sham controls (n = 18 each) were first analyzed for their sleep-wake behavior using standard polysomnography. EEG/EMG measurements were carried out prior to SNI and Sham surgery and at post-surgical days 22-23 (D20+), a time point at which chronic pain is established (Decosterd & Woolf, 2000; Bourquin et al., 2006). At both time points, recordings lasted for 48 h under undisturbed conditions. Based on these data, SNI and Sham controls spent similar amounts of time asleep in the 12 h-light and dark phases, during both baseline and at D20+ (***Figure 1A***). Both treatment groups showed minor increases (2.4-3 %) in NREMS time at the expense of wakefulness at D20+ compared to baseline in both dark and light phases (mixed-model ANOVAs with factors 'treatment' and 'day', $p = 0.0013$ in light phase, $p = 8.5 \times 10^{-6}$ in dark phase for 'day', $p > 0.8$ for 'treatment' for either light or dark phase, no interaction). Moreover, cumulative distributions of NREMS and REMS bout lengths at D20+ were similar for Sham and SNI, with only a minor shift toward smaller values in SNI for both NREMS (***Figure 1B***, -2.3 s; Kolmogorov-Smirnov (KS) test, $p = 0.015$) and REMS (-3 s; KS test, $p = 0.026$). When subdivided into short, intermediate and long bouts for the light phase, there were no significant differences between Sham and SNI for both NREMS and REMS (***Figure 1B***, mixed-model ANOVAs for 'treatment' x 'bout length', $p = 0.79$ for NREMS, $p = 0.23$ for REMS).

Furthermore, sleep onset latency (***Figure 1C***) and NREMS fragmentation by brief movement-associated microarousals (MAs, defined in mouse as <= 16 s awakenings accompanied by movement activity seen in the EMG, measured over 48 h) (***Figure 1D***) (Franken *et al.*, 1999), were not altered by treatment or time post-surgery (mixed-model ANOVA with factors 'treatment' and 'day', for sleep onset latency, $p = 0.42$ and $p = 0.94$, no interactions; for number of MAs, $p = 0.79$ and $p = 0.43$, no interactions).

We next investigated the mean spectral properties of each vigilance state through constructing normalized power spectral densities (Vassalli & Franken, 2017) for the full 48 h-long recordings. Both NREMS and REMS showed the respective characteristic spectral peaks at delta (1—4 Hz) and at theta frequencies (5—10 Hz), respectively. These were indistinguishable between the two groups of animals and from baseline to D20+ (***Figure 1E***).

We specifically evaluated power in the high-gamma frequency (60—80 Hz) range, a frequency band linked to pain sensations when optogenetically induced in mouse (Tan et al., 2019). We found that relative gamma power was increased in SNI at D20+ compared to baseline both in wake and in NREMS (***Figure 1F***, 1-sample *t*-test for wake and NREMS in SNI, p = 0.011 and p = 0.0092, respectively). The heart rate was also higher in NREMS of SNI animals at D20+ compared to baseline (***Figure 1G***, mixed-model ANOVA with factors 'treatment' x 'state' x 'day' with interaction, p = 0.02, *post-hoc* paired *t*-test for SNI in NREMS, p = 0.002, with Bonferroni-corrected α = 0.0125). A tendency was also evident in REMS, during which heart rate was already elevated (***Figure 1G***, effect of 'state' in the ANOVA, p = 0.003, paired *t*-test in SNI in REMS, p = 0.027). There were no correlations between relative changes in gamma power and alterations in sleep architecture in individual mice (change in the number of MAs per h of NREMS x change in gamma power; pairwise linear correlation R^2 = 0.09, p = 0.08; change in total NREMS time x change in gamma power; R^2 = 0.02, p = 0.36).

These data indicate that SNI animals do not suffer from major alterations in sleep-wake behaviors. Still, pain-related pathological changes in brain and periphery continued to be present in sleep. This is consistent with a state of "hyperarousal" whereby high-frequency power components are disproportionately elevated during sleep that is normally dominated by low-frequency rhythms (van Someren, 2020; Vargas et al., 2020), and where heart rate also remains elevated. As such alterations could affect arousability, we asked when and where in the brain this abnormal activity appeared. Furthermore, we developed an approach to systematically quantify alterations in both, spontaneous and evoked, types of arousability from NREMS during the resting phase.

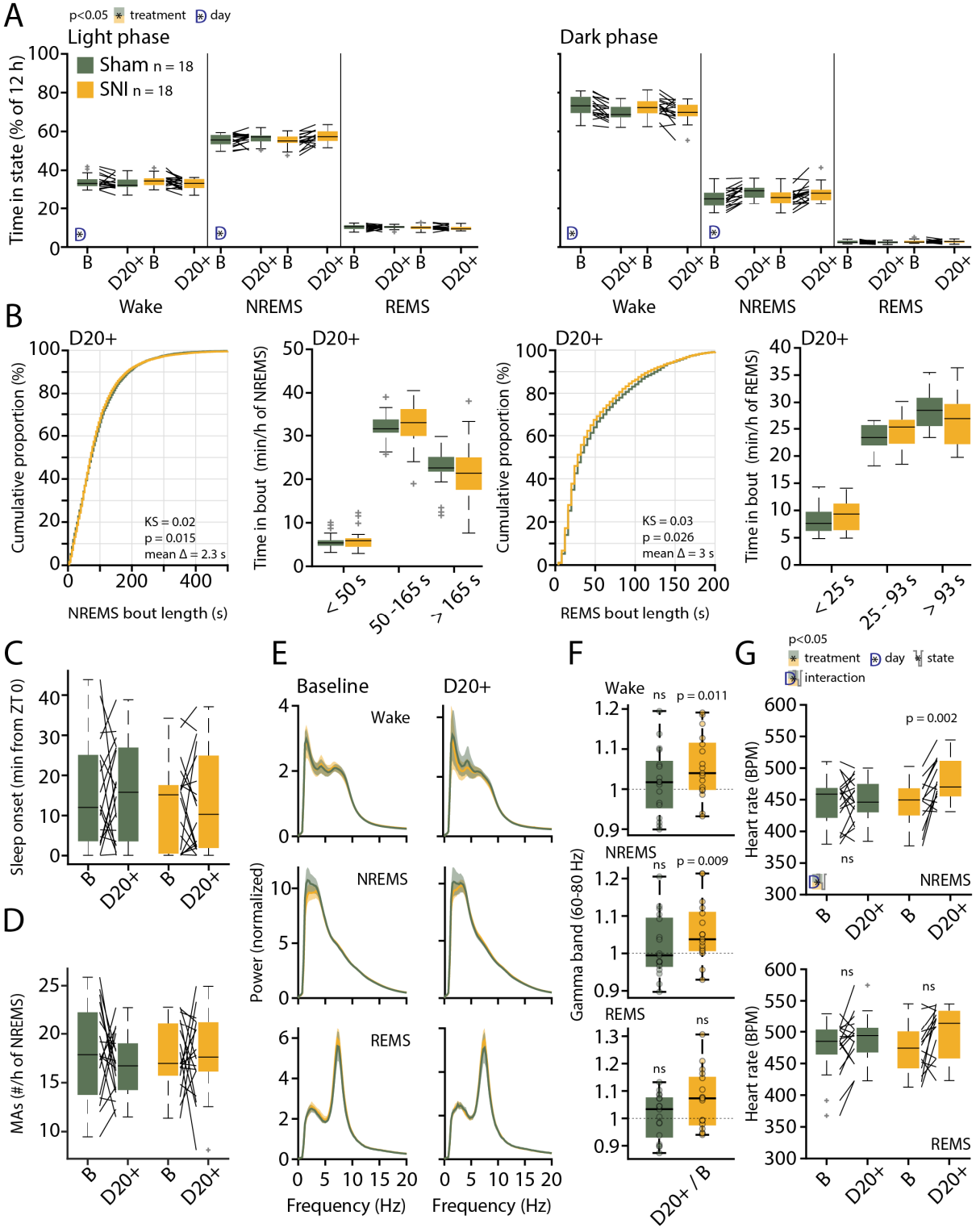

Figure 1 – Preserved sleep-wake behavior and spectral properties in SNI animals. (**A**) Mean percentage of total time spent in the three main vigilance states for Sham (n = 18) and SNI (n = 18) animals in light (left) and dark phase (right) in baseline (B) and at day 20+ (D20+) after surgery. Black lines connect data from single animals. The significant main effects and interactions from the ANOVAs are shown using

pictograms for factors and interaction. *Post-hoc* tests were done once interactions were significant. Mixed-model ANOVA for non-rapid-eye-movement sleep (NREMS) in light phase**:** $F_{(1,34)} = 0.048$, $p = 0.82$ for 'treatment'; $F_{(1,34)} = 12.24$, $p = 0.0013$ for 'day'; $F_{(1,34)} = 2.5$, $p = 0.12$ for interaction. Mixed-model ANOVA for NREMS in dark phase**:** $F_{(1,34)} = 0.009$, $p = 0.92$ for 'treatment'; $F_{(1,34)} = 27.409$, $p = 8.5\text{x}10^{-6}$ for 'day'; $F_{(1,34)} = 0.379$, $p = 0.54$ for interaction. There were no significant effects in rapid-eye-movement sleep (REMS). (**B**) Bout size cumulative distribution, (with Kolmogorov Smirnov (KS) test results) and time spent in short, intermediate and long bouts for NREMS (left) and REMS (right) between Sham and SNI at D20+. Mixed-model ANOVA for time in bouts (log transform for normality criteria) for NREMS: $F_{(2,68)} = 0.23$, $p = 0.79$ for interaction, for REMS: $F_{(2,68)} = 1.5$, $p = 0.23$ for interaction. (**C**) Mean latency to sleep onset (first consolidated NREMS). Mixed-model ANOVA $F_{(1,34)} = 0.7$, $p = 0.4$ for 'treatment'; $F_{(1,34)} = 0.006$, $p = 0.94$ for 'day'; $F_{(1,34)} = 0.021$, $p = 0.88$ for interaction. (**D**) Number of microarousals (MAs) per h of NREMS in light phase; Mixed-model ANOVA $F_{(1,34)} = 0.067$, $p = 0.8$ for 'treatment'; $F_{(1,34)} = 0.63$, $p = 0.43$ for 'day'; $F_{(1,34)} = 0.61$, $p = 0.44$ for interaction. (**E**) Normalized power spectrum for Sham and SNI for wake, NREMS and REMS at baseline (left) and D20+ (right). Shaded errors are 95 % confidence intervals (CIs) of the means. (**F**) High-gamma power (60—80 Hz) for D20+ relative to baseline (from the spectra shown in E). One-sample *t*-test for wake in Sham: $t_{(16)} = 0.86$, $p = 0.4$; for wake in SNI: $t_{(16)} = 2.8$, $p = 0.011$. One-sample *t*-test for NREMS in Sham: $t_{(16)} = 0.97$, $p = 0.34$; for NREMS in SNI: $t_{(16)} = 2.96$, $p = 0.0092$. One-sample *t*-test for REMS in Sham: $t_{(16)} = 0.46$, $p = 0.64$; for REMS in SNI: $t_{(16)} = 2.62$, $p = 0.0184$. $\alpha = 0.0167$. (**G**) Heart rate in NREMS (top) and REMS (bottom) from animals with suitable EMG signal, Sham (n = 17) and SNI (n = 14). Mixed-model three-way ANOVA: $F_{(1,29)} = 0.5$, $p = 0.47$ for 'treatment'; $F_{(1,29)} = 70.4$, $p = 3\text{x}10^{-9}$ for 'state', $F_{(1,29)} = 9.79$, $p = 0.003$ for 'day'; $F_{(1,1,29)} = 5.37$, $p = 0.02$ for interaction between the three factors; *post-hoc* paired *t*-test in NREMS for baseline *vs* D20+ in Sham: $t_{(16)} = -0.4$, $p = 0.69$; SNI: $t_{(13)} = -3.75$, $p = 0.002$; paired *t*-test in REMS for baseline *vs* D20+ in Sham: $t_{(16)} = -1.9$, $p = 0.07$; SNI: $t_{(13)} = -2.4$, $p = 0.027$; $\alpha = 0.0125$.

The 0.02 Hz-fluctuation allows to probe variations in spontaneous arousability during NREMS

Arousability in sleeping rodent, measured via external stimuli or through spontaneous arousals, changes across the night (Neckelmann & Ursin, 1993; Wimmer *et al.*, 2012), and with variations in sleep pressure (Franken et al., 1999). For NREMS in early phases of the resting phase, we described a 0.02 Hz-fluctuation during NREMS that provides a minute-by-minute time raster to measure arousability driven by sensory stimuli. This fluctuation subdivides NREMS bouts into ~25 s-long periods of continuity and fragility that show low and high sensory-evoked arousability, respectively (Lecci et al., 2017; Yüzgeç *et al.*, 2018). To evaluate the utility of this fluctuation for measures of spontaneous arousability across the entire light phase, we first tested whether MAs associated with muscular activity (***Figure 2A***), well-established correlates for spontaneous arousability, were phase-locked to the 0.02 Hz-fluctuation in healthy mice (n = 30 mice with 9,476 MAs). The onset of MAs coincided with declining or low sigma power levels that followed a pronounced sigma power peak (***Figure 2B,C***), which is characteristic for a fragility period (Lecci et al., 2017; Fernandez & Lüthi, 2020). A spectral band typical for NREMS, such as delta (1—4 Hz) power,

showed a rapid decline preceding the MAs, indicating the momentary interruption of NREMS. The phase values of the 0.02 Hz-fluctuation, calculated via a Hilbert transform (***Figure 2 – figure supplement 1***), showed that MA onset times clustered around a mean preferred phase of 151.6° ± 1.1°, with 180° representing the sigma power trough (Rayleigh test, $p < 1x10^{-16}$). The majority of MAs (89 %) was clustered between 90—270°, which narrows the fragility period to the low values of sigma power around the trough (Lecci et al., 2017). The phase-locking was also observed when time points at 4, 8 and 12 s before the onset of a MA were quantified (***Figure 2D***). This shows that the onset of the fragility period preceded the MA. Fragility periods thus constitute moments during which MAs preferentially occur.

These phase relations persisted for all 1-h intervals across time-of-day (***Figure 2E***), although the density of MAs showed a characteristic increase towards the end of the light phase and was higher during the dark phase (***Figure 2F***). The peak frequency of the 0.02 Hz-fluctuation also remained relatively constant, with a minor decrease in power during the dark phase (***Figure 2G***). Across the 24-h cycle, a median of 33.6 % of all fragility periods were accompanied by a MA (***Figure 2H***). In sum, fragility periods are permissive windows for MAs. This means that MAs appeared predominantly during fragility periods, while a majority of fragility periods occurred with NREMS remaining consolidated.

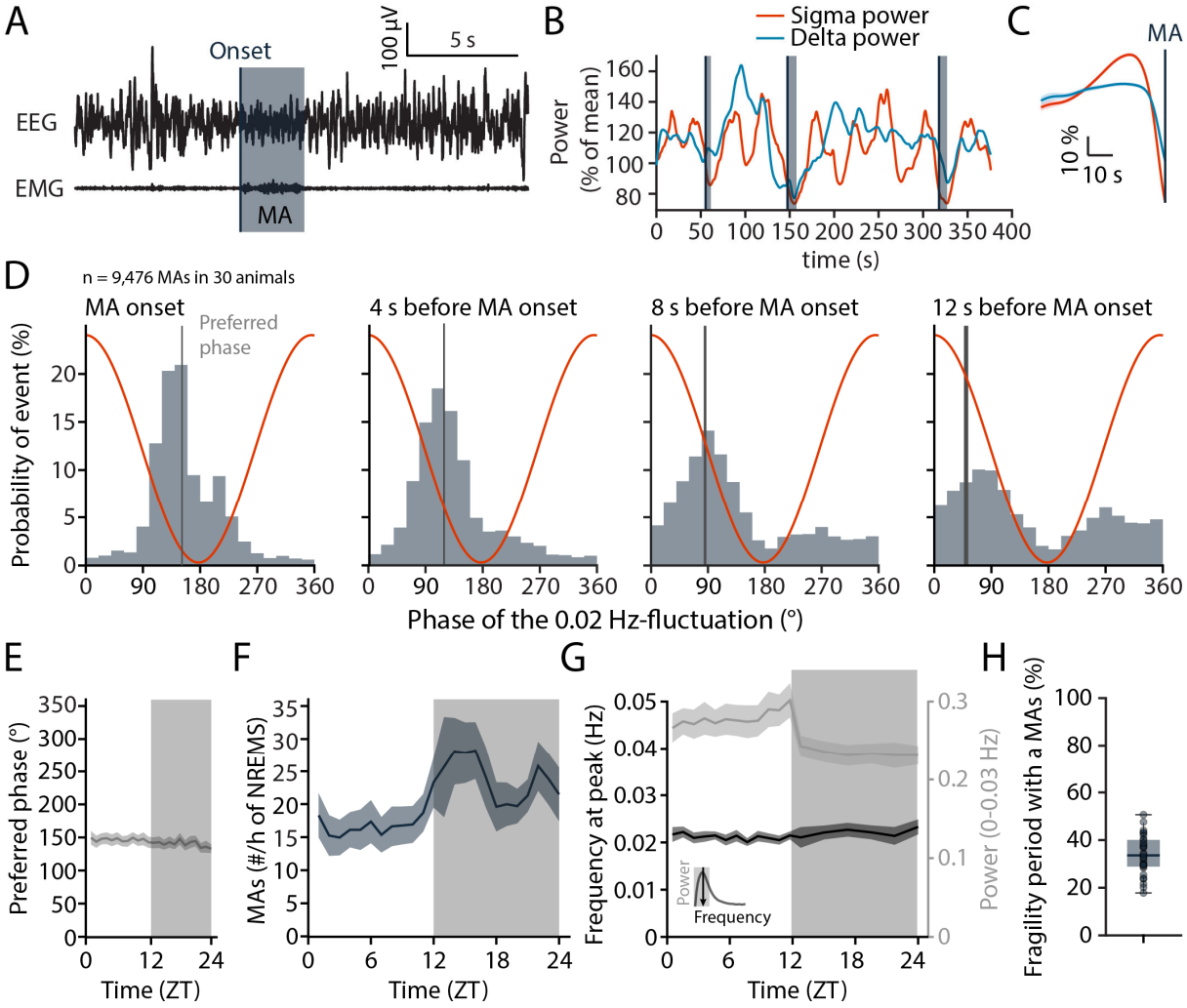

Figure 2 – MAs, indicating spontaneous arousability, are time-locked to the trough of the 0.02 Hz-fluctuation, corresponding to the NREMS fragility period. (**A**) Example of a MA (underlain in grey) defined by both a desynchronization in the EEG (top) and a burst of EMG activity (bottom) of length <16 s. The MAs were scored visually, and the onset was set at the beginning of phasic EMG activity (black vertical line). (**B**) Continuous sigma (red; 10—15 Hz) and delta (blue; 1—4 Hz) power in a NREMS period with MAs (grey-shading as in panel A). Note their occurrence during descending / low values of sigma power. (**C**) Mean sigma and delta power dynamics preceding the onset of a MA. (**D**) Histograms of the phase angle values of the 0.02 Hz-fluctuation at specific time points relative to the onset of a MA. The red line represents the corresponding phase of the fluctuation at each bin. A total of n = 9,476 MAs from 30 un-operated C57Bl/6J animals were included across the light-dark cycles for all analyses in this figure. Rayleigh tests and preferred phases ± 95% CI for MA onset: z = 4214.7, $p < 1x10^{-16}$, m = 151.5 ± 1.1°; for 4 s before MA onset: z = 3489, $p < 1x10^{-16}$, m = 119.1 ± 1.2°; for 8 s before MA onset: z = 1416, $p < 1x10^{-16}$, m = 85.3 ± 2.0°; for 12 s before MA onset: z = 548.163, $p < 1x10^{-16}$, m = 50.1 ± 3.3°. (**E**) Preferred phase of the 0.02 Hz-fluctuation at MA onset across time-of-day in hourly bins (dark phase, shaded, ZT, Zeitgeber time). (**F**) Density of MAs (per h of NREMS) across the light-dark cycle. (**G**) Parameters of the 0.02 Hz-fluctuation (frequency at peak and power, see inset for illustration) across the light-dark cycle. (**H**) Proportion of fragility periods (corresponding to values from 90 to 270°, see panel D) containing a MA.

NREMS in SNI conditions shows normal phase-coupling of MAs to the 0.02 Hz-fluctuation

We next evaluated SNI and Sham animals regarding the MAs and their coupling to the 0.02 Hz-fluctuation. The 0.02 Hz-fluctuation was not different between Sham and SNI (n = 18 for both groups) across the light phase. Thus, neither its amplitude nor frequency (***Figure 3A-C***), or, equivalently, the number of its cycles per h of NREMS, were different between the groups (***Figure 3D***). The phase-coupling to MAs was also unaltered (***Figure 3E***, mean angle ± 95% CI: 152.3 ± 1.4 for Sham and 150.4 ± 1.3 for SNI) and the distribution of fragility periods containing transitions to MAs, to REMS, or with continuation into NREMS was indistinguishable (***Figure 3F***).

It has been shown that sleep loss exacerbates pain (Alexandre *et al.*, 2017). Sleep could thus be relatively more disrupted in SNI animals after a period of sleep loss. We therefore carried out a 6 h-sleep deprivation (SD) at the beginning of the light phase as done previously in the lab (n = 12 for Sham and SNI each) (Kopp *et al.*, 2006). We confirmed a characteristic rebound of delta power (***Figure 3G,H***) and a decrease in the frequency of MAs (***Figure 3I,J***, mixed-model ANOVA with factors 'treatment' and 'SD', $p = 0.35$ and $p = 1.23 \times 10^{-7}$ with no interaction). The phase-coupling of MAs to the 0.02 Hz-fluctuation remained unaltered in both groups even with high sleep pressure (***Figure 3K***,***L***). Conditions of SNI thus left spontaneous MAs, their coupling to the 0.02 Hz-fluctuation, as well as homeostatic regulation of spontaneous arousability unaltered.

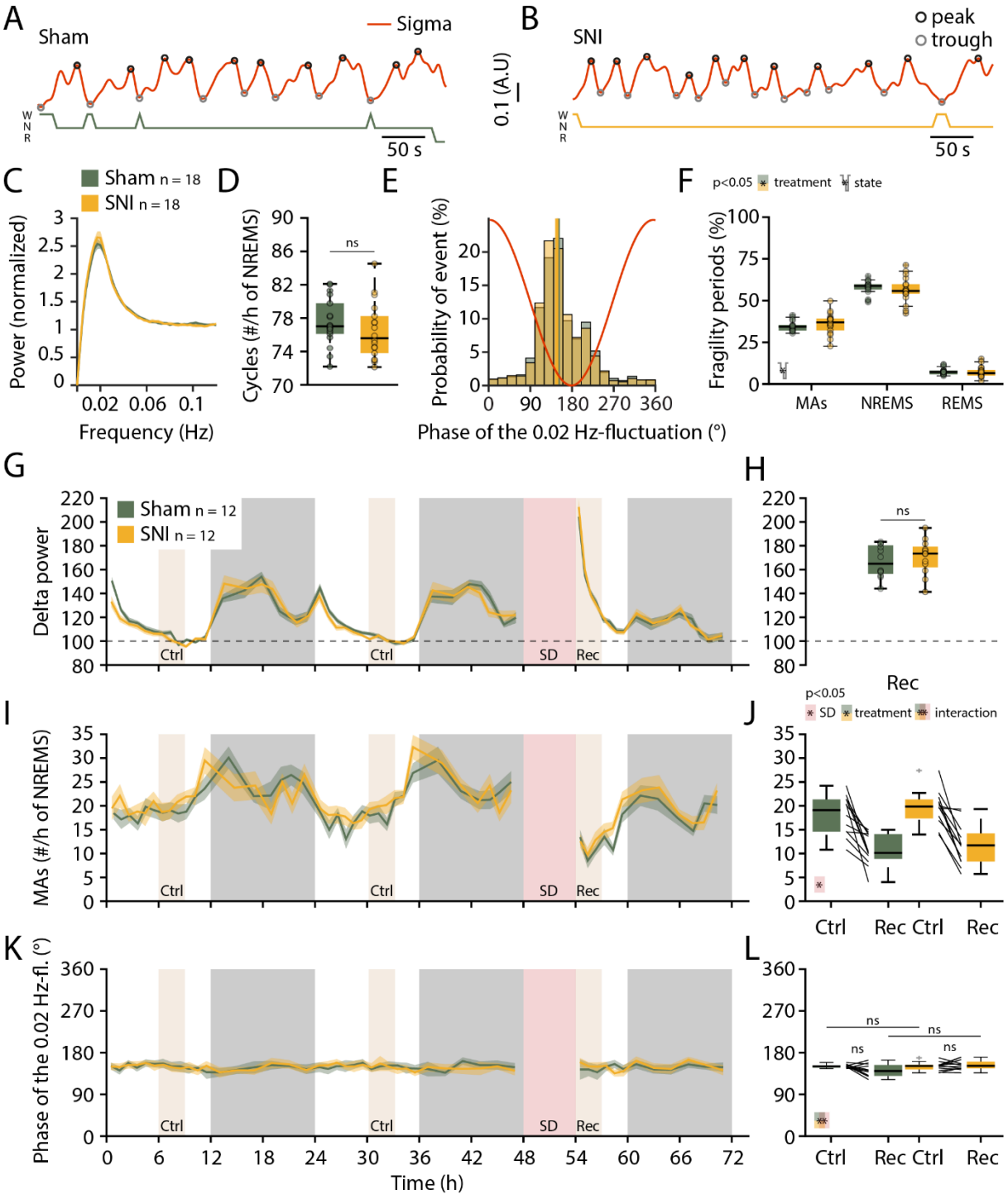

Figure 3 – The 0.02 Hz-fluctuation and its relationship to MAs were preserved in SNI animals, even when sleep pressure was high. (**A-B**) Representative traces of sigma power dynamics in a Sham (A) and a SNI (B) animal. Hypnograms shown below for W, wakefulness; N, NREMS; R, REMS. The circles represent the individual cycle detection used in D and F (see methods). (**C**) Power in the infraslow range for Sham and SNI (n = 18 each); shaded areas represent 95% CIs. (**D**) Another measure of the 0.02 Hz-fluctuation, calculated as number of cycles per h of NREMS. Data are shown for D20+ only, but baseline data points

were considered for statistical analysis. Mixed-model ANOVA: $F_{(1,34)} = 0.012$, $p = 0.91$ for 'treatment'; $F_{(1,34)} = 0.003$, $p = 0.95$ for 'day'; $F_{(1,34)} = 2.17$, $p = 0.14$ for the interaction. (**E**) Histograms of the phase values of the 0.02 Hz-fluctuation at MA onset for Sham and SNI, same as Figure 2D. Vertical lines denote mean direction ± 95% CI for Sham: 152.3 ± 1.4; SNI: 150.4 ± 1.3. (**F**) Proportion of fragility periods (defined by 0.02 Hz-fluctuation phase values of 90—270°) containing a MA, continuing into NREMS or containing a transition to REMS. Mixed-model ANOVA: $F_{(1,34)} = 0.17$, $p = 0.67$ for 'treatment'; $F_{(2,68)} = 550.8$, $p = 2x10^{-16}$ for 'state' ; $F_{(2,68)} = 0.59$, $p = 0.55$ for interaction. (**G**) Delta power dynamics across two light and dark phases and after a 6 h-sleep deprivation. SD, Sleep deprivation, Rec, Recovery period, Ctrl control periods with corresponding ZT values. Delta power values are normalized to the mean of those at ZT9-12. Shaded areas represent SEM. SD was carried on a subset of 12 Sham and 12 SNI from the 18 shown in A—F, directly following the D20+ recording. (**H**) Boxplot for delta power values during Rec. One-sample *t*-test for Sham: $t_{(11)} = 17.2$, $p = 2.6x10^{-9}$; SNI: $t_{(11)} = 16.48$, $p = 4.2x10^{-9}$; between Sham and SNI two-sample *t*-test: $t_{(22)} = -0.6$, $p = 0.52$; $\alpha = 0.0125$. (**I, J**) As panels G, H for the number of MAs per h of NREMS. (**J**) Mixed-model ANOVA: $F_{(1,22)} = 0.9$, $p = 0.35$ for 'treatment'; $F_{(1,22)} = 58.52$, $p = 1.2x10^{-7}$ for 'SD'; $F_{(1,22)} = 0.12$, $p = 0.72$ for interaction. (**K, L**) As panels G, H, for the preferred phase of the 0.02 Hz-fluctuation at MA onset. (**L**) Mixed-model ANOVA: $F_{(1,22)} = 3.08$, $p = 0.09$ for 'treatment'; $F_{(1,22)} = 1.45$, $p = 0.24$ for 'SD'; $F_{(1,22)} = 5.72$, $p = 0.025$ for interaction. No significance in paired *post-hoc t*-tests.

NREMS in SNI conditions shows a novel type of cortical local arousal

In human NREMS, spontaneous arousals are an important measure for the severity of sleep disorders and are primarily described by EEG desynchronization (Bonnet *et al.*, 1992; Azarbarzin *et al.*, 2014). In contrast, the scoring of a MA in mice requires concomitant muscular activity by convention (Franken et al., 1999). We hence tested whether the 0.02 Hz-fluctuation could serve to identify previously undescribed arousal types in mice with characteristics distinct from conventional MAs. For this, we generated spectral profiles of all cycles of the 0.02 Hz-fluctuation that were devoid of MAs. To take into account the possibility that there were local events delimited to certain cortical regions (Nobili *et al.*, 2011; St-Jean et al., 2012; Riedner et al., 2016; Lecci et al., 2017), we combined polysomnography with stereotaxically guided local field potential (LFP) recordings, as done previously in the lab (***Figure 4A,B***) (Fernandez *et al.*, 2018). We chose the S1 hindlimb (S1HL, 5 Sham and 9 SNI) cortex (***Figure 4C,D***) that is the site of sensory discrimination of pain and the prelimbic (PrL, 6 Sham and 8 SNI) cortex (***Figure 4I,J***) that is concerned with aversive pain feelings in rodents (Kuner & Kuner, 2020) and in its homologue in humans (Moisset & Bouhassira, 2007).

Local field potential recordings reliably reported on the 0.02 Hz-fluctuation in these two areas. Consistent with its predominant expression in sensory cortices (Lecci et al., 2017), the 0.02 Hz-fluctuation showed a higher peak in S1HL than in PrL (***Figure 4A,B***). The cycles of successive continuity and fragility periods were extracted (***Figure 2, figure supplement 1***) and their spectral dynamics plotted separately for

the relative contribution of power in the low-frequency delta (1—4 Hz) and the beta (16—25 Hz), low- (26—40 Hz) and high- (60—80 Hz) gamma bands (***Figure 4E-H*** for S1HL, ***Figure 4K-N*** for PrL). Average values for the infraslow phase angles between 90—270°, corresponding to the fragility period enriched in MAs (*see* ***Figure 2***), and for the continuity period (from 270—90°), were calculated. Such analysis revealed SNI- and region-specific alterations in the contributions of these bands to total power that were clearly present in S1HL, but not detectable in PrL. In S1HL, delta power levels were decreased compared to Sham (***Figure 4E***) whereas high-frequency components in the beta and the low-gamma range were elevated (***Figure 4F-G***). Remarkably, delta power differences between Sham and SNI varied between fragility and continuity periods (***Figure 4E***, mixed-model ANOVA with factors 'treatment' and 'period', $p = 0.001$ for the interaction). In Sham, there was a distinct rapid upstroke of power in this frequency band that reached a peak during the fragility periods (***Figure 4E,*** *post-hoc t*-test for delta power in fragility vs continuity period in Sham, $p = 0.001$). Fragility periods continuing into NREMS were thus clearly distinct from the ones associated with MAs during which there is muscular activity and a decrease in EEG delta power (see ***Figure 2C***). In SNI animals, in contrast to Sham, there was no detectable elevation in delta power during fragility periods continuing into NREMS (***Figure 4E,*** *post-hoc t*-test in SNI, $p = 0.44$). The high-frequency bands in the beta and low-gamma range instead showed a tonic increase in SNI that was present throughout continuity and fragility periods (***Figure 4F-G,*** mixed-model ANOVA with factors 'treatment' and 'period', for beta, $p = 0.01$, $p = 1.3 \times 10^{-9}$ and for low gamma, $p = 0.0053$, $p = 1.4 \times 10^{-10}$) and that was also present, although to a milder extent, in the high-gamma range (***Figure 4H***).

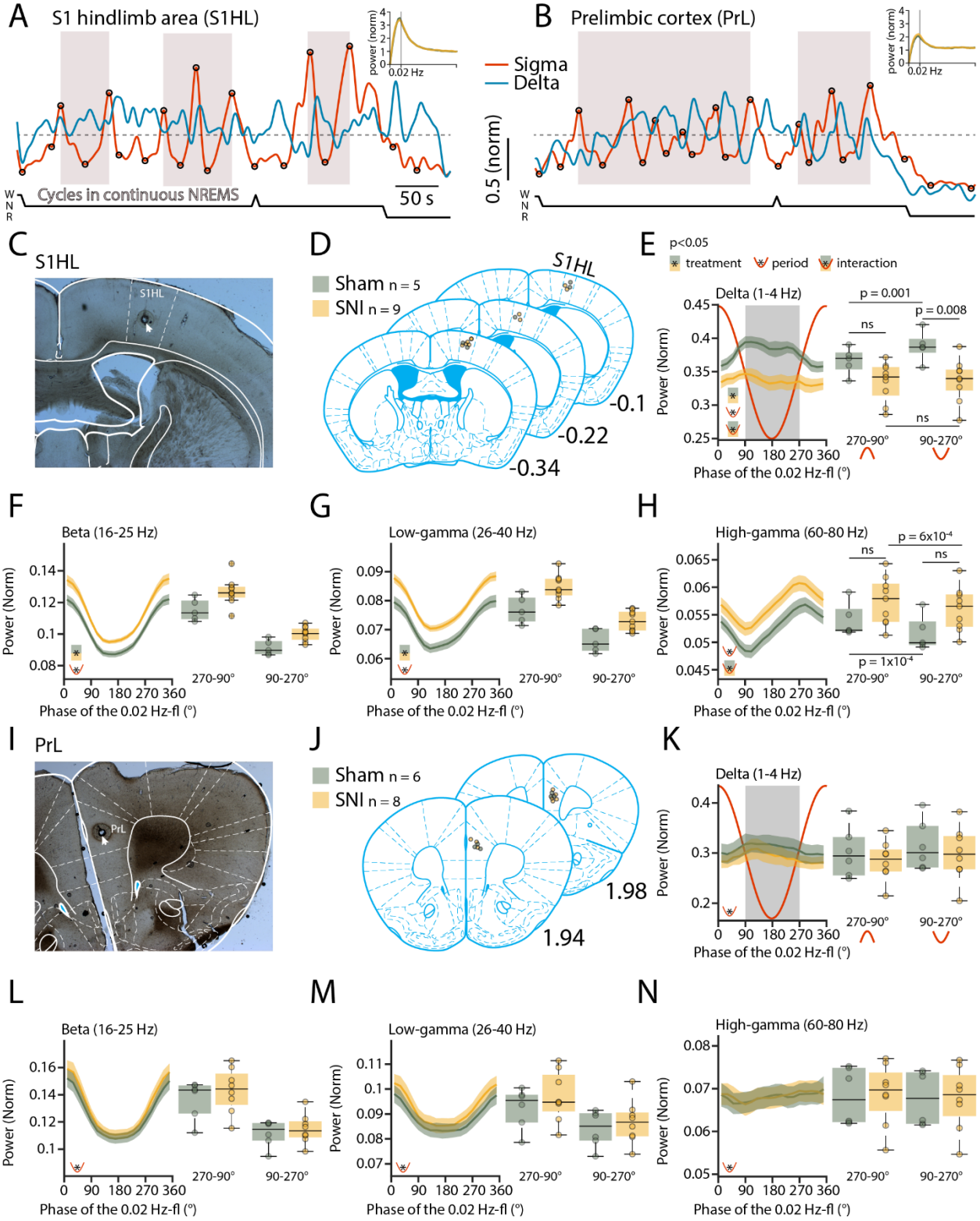

Figure 4 – SNI animals present locally disrupted spectral power dynamics during NREMS. (**A-B**) Sigma (10—15 Hz) and delta (1—4 Hz) dynamics during the same NREMS period in S1 hindlimb (HL) (A) and PrL (B) during a baseline recording. Hypnograms shown below. Circles represent peaks and troughs used to

detect the 0.02 Hz-fluctuation cycles (see Methods). Shaded areas indicate 0.02 Hz-fluctuation cycles that are continuing uninterrupted in NREMS. Insets: Power spectrograms in the infraslow range, with Sham and SNI overlapping. (**C**) Representative histological section confirming the location of recording site through post-mortem electrocoagulation (arrowhead). (**D**) Anatomical sections summarizing histological verification, with small circles showing recording sites for all animals included. Anteroposterior stereotaxic coordinates are given relative to Bregma. (**E-H**) Trajectories of power in specific frequency bands (indicated on top of graphs) across uninterrupted cycles of the 0.02 Hz-fluctuation, quantified in 20° bins. Red line shows the corresponding 0.02 Hz-fluctuation phase. Boxplots quantify spectral power within continuity (270—90°, red inverted U-shaped line) and fragility periods (90—270°, red U-shaped line). For all bands, mixed-model ANOVA with factors 'treatment' and 'period' were done, followed by *post-hoc t*-tests if applicable. Significance for main effects and/or interaction are shown by the presence of the corresponding pictograms at the bottom left. These yielded (**E**) for delta $F_{(1,12)} = 7.16$, $p = 0.02$ for 'treatment'; $F_{(1,12)} = 18.5$, $p = 0.001$ for 'period'; $F_{(1,12)} = 18.31$, $p = 0.001$ for interaction. *Post-hoc* for Sham *vs* SNI in continuity: $t_{(12)} = 2.11$, $p = 0.055$; fragility: $t_{(12)} = 3.13$, $p = 0.0085$; and across periods for Sham: $t_{(4)} = -7.9$, $p = 0.001$; SNI: $t_{(8)} = -0.8$, $p = 0.44$; $\alpha = 0.0125$; (**F**) for beta $F_{(1,12)} = 9.3$, $p = 0.01$ for 'treatment'; $F_{(1,12)} = 270.01$, $p = 1.3\text{x}10^{-9}$ for 'period'; $F_{(1,12)} = 1.01$, $p = 0.33$ for interaction. *Post-hoc* for Sham *vs* SNI in continuity: $t_{(12)} = -2.5$, $p = 0.025$; fragility: $t_{(12)} = -3.43$, $p = 0.004$; and across periods for Sham: $t_{(4)} = 14.7$, $p = 0.0001$; SNI: $t_{(8)} = 12.02$, $p = 2.1\text{x}10^{-6}$; $\alpha = 0.0125$; (**G**) for low-gamma $F_{(1,12)} = 11.49$, $p = 0.0053$ for 'treatment'; $F_{(1,12)} = 398.35$, $p = 1.4\text{x}10^{-10}$ for 'period'; $F_{(1,12)} = 0.75$, $p = 0.4$ for interaction. *Post-hoc* for Sham *vs* SNI in continuity: $t_{(12)} = -3.1$, $p = 0.008$; fragility: $t_{(12)} = -3.4$, $p = 0.0049$; and across periods for Sham: $t_{(4)} = 18.6$, $p = 4.9\text{x}10^{-5}$; SNI: $t_{(8)} = 14.39$, $p = 5.3\text{x}10^{-7}$; $\alpha = 0.0125$; (**H**) for high-gamma $F_{(1,12)} = 3.31$, $p = 0.09$ for 'treatment'; $F_{(1,12)} = 94.38$, $p = 4.8\text{x}10^{-7}$ for 'period'; $F_{(1,12)} = 5.83$, $p = 0.03$ for interaction. *Post-hoc* for Sham *vs* SNI in continuity: $t_{(12)} = -1.5$, $p = 0.14$; fragility: $t_{(12)} = -2.08$, $p = 0.059$; and across periods for Sham: $t_{(4)} = 14.17$, $p = 1.4\text{x}10^{-4}$; SNI: $t_{(8)} = 5.45$, $p = 6\text{x}10^{-4}$; $\alpha = 0.0125$. (**I-N**) Analogous presentation for PrL. Statistical analysis yielded: (**K**) For delta $F_{(1,12)} = 0.4$, $p = 0.5$ for 'treatment'; $F_{(1,12)} = 11.99$, $p = 0.004$ for 'period'; $F_{(1,12)} = 0.009$, $p = 0.92$ for interaction; (**L**) for beta $F_{(1,12)} = 0.56$, $p = 0.46$ for 'treatment'; $F_{(1,12)} = 127.5$, $p = 9.5\text{x}10^{-8}$ for 'period'; $F_{(1,12)} = 0.65$, $p = 0.43$ for interaction; (**M**) for low-gamma $F_{(1,12)} = 0.63$, $p = 0.44$ for 'treatment'; $F_{(1,12)} = 75.84$, $p = 1.5\text{x}10^{-6}$ for 'period'; $F_{(1,12)} = 0.93$, $p = 0.35$ for interaction; (**N**) for high-gamma $F_{(1,12)} = 0.004$, $p = 0.94$ for 'treatment'; $F_{(1,12)} = 9.49$, $p = 0.009$ for 'period'; $F_{(1,12)} = 2.6$, $p = 0.12$ for interaction.

We calculated an "activation index" (AI), defined by the ratio between the summed spectral power in the beta and low-gamma bands and the delta band power, to quantify alterations in spectral balance between high- and low-frequency power components, similarly to what has been done previously in studies on insomnia disorders (Lecci et al., 2020). The AI is a measure for the degree of EEG desynchronization and increases when NREMS moves closer to wakefulness. In the fragility periods continuing into NREMS and devoid of EMG activity, the AI decreased, consistent with NREMS remaining consolidated (***Figure 5A-C***). In SNI animals, however, the AI was higher compared to Sham specifically in the fragility periods (***Figure 5B***, mixed-model ANOVA with factors 'treatment' and 'period', $p = 0.039$ for interaction, *post-hoc t*-tests Sham vs SNI in fragility period, $p = 0.005$, in continuity period, $p = 0.027$, not

significant with α = 0.0125). Fragility periods during uninterrupted NREMS are thus specific moments during which the AI in SNI conditions was significantly higher compared to continuity periods.

Can such mean differences in cortical activation profiles during NREMS qualify as differences in cortical arousals? To address this, we compared the AI in fragility periods *with* a MA (associated with EMG increase). As expected, the AI showed an intermittent phasic peak (***Figure 5D-F***) in most cases (75.2 ± 4.1 %), which is explained by the strong decline in delta power (see ***Figure 2C***) and the appearance of higher frequencies associated with MAs. Therefore, we inspected individual fragility periods continuing into NREMS (without a MA) for the presence of similar phasic increases in AI. Indeed, we noticed that a subset of these did indeed contain an intermittent peak resembling the one found during MAs (***Figure 5G***) and not evident in the mean AI in ***Figure 5B***. The amplitudes of these peaks were higher in SNI, in accordance with the tonically higher AI in these animals, but in size comparable to the ones of MAs (***Figure 5H***, mixed-model ANOVA with factors 'treatment' and 'MA', p = 0.002 for 'treatment', p = 2.1×10^{-7} for 'MA', no interaction). Moreover, the half-widths of these peaks were only moderately smaller than the ones of MAs (***Figure 5I***, mixed-model ANOVA with factors 'treatment' and 'MA', p = 0.62 for 'treatment', p = 3.28×10^{-7} for 'MA', no interaction). These events could thus qualify as a local cortical arousal based on phasic spectral properties reminiscent of a MA. To further support our assumption that these AI peaks constituted arousals, we looked at heart rate increases known to accompany cortical arousals in human (Sforza *et al.*, 2000; Azarbarzin et al., 2014). The heart rate was distinctly higher during the fragility period for cycles containing an AI peak as opposed to the ones without such peak (**Figure 5J**, mixed-model ANOVA with factors 'treatment', 'period' and 'peak', p = 0.007 for the 'peak' x 'period' interaction). These events were more frequent in SNI animals and followed a similar time-of-day dependence as the classical MAs (***Figure 5K,L***, *t*-test Sham *vs* SNI, p = 0.02). Moreover, their increased occurrence was specific for S1HL while absent in PrL and in the contralateral EEG (***Figure 5 – figure supplement 2***). The presence of a subgroup of fragility periods continuing into NREMS, yet showing a cortical arousal, is noteworthy for several reasons. First, it demonstrates that rodent NREMS shows local cortical intrusion of wake-related activity in the absence of muscular activity. Second, these local cortical arousals in SNI showed intermittent peaks in AI that were close the ones of MAs, indicating comparable cortical desynchronization at the local level. Third, they were accompanied by heart rate increases that are sensitive hallmarks of arousal in human (Azarbarzin et al., 2014). Fourth, neuropathic pain goes along with a specific increase in the relative occurrence of fragility periods with such AI peaks specifically in the S1HL area. The systematic classification of fragility periods helped unravel these novel cortico-autonomic arousals and their similarity to MAs. Still, other arousal-like events outside fragility periods could exist.

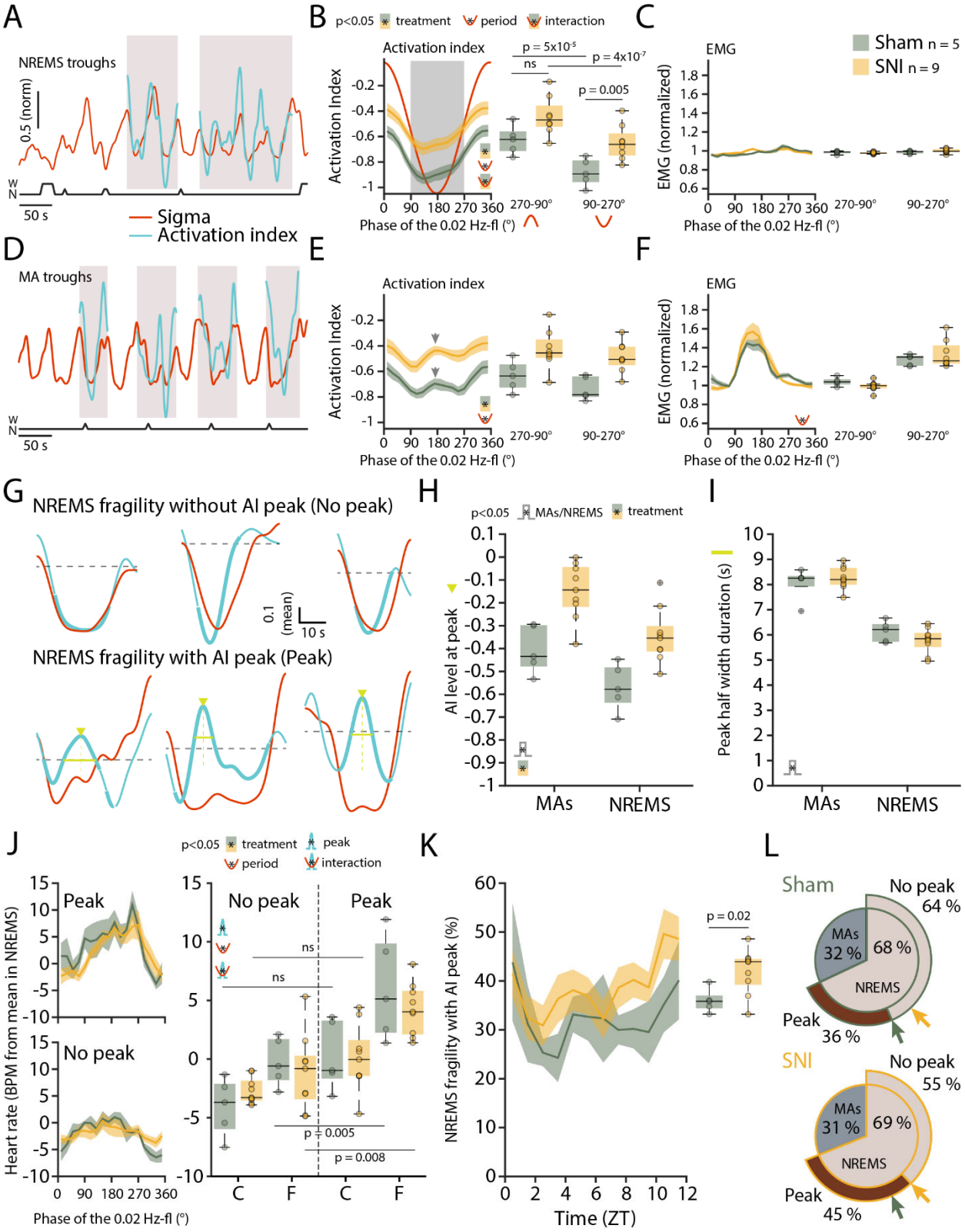

Figure 5 – Mice generate local cortical arousals during NREMS that appear more frequently in SNI. (**A**) Normalized dynamics of sigma (10—15 Hz) and activation indices (calculated as ln((beta + low-gamma)

/delta))). Hypnogram is shown below. Shaded areas show cycles of the 0.02 Hz-fluctuation continuing into NREMS. (**B**) Activation indices for cycles continuing into NREMS, with mean values shown in boxplots for continuity (270—90°) and fragility periods (90—270°). Mixed-model ANOVA $F_{(1,12)} = 8.9$, $p = 0.011$ for 'treatment'; $F_{(1,12)} = 470.6$, $p = 5.4x10^{-11}$ for 'period'; $F_{(1,12)} = 5.33$, $p = 0.039$ for interaction. *Post-hoc t*-test for Sham *vs* SNI in continuity: $t_{(12)} = -2.51$, $p = 0.027$; fragility: $t_{(12)} = -3.44$, $p = 0.005$; and across periods for Sham: $t_{(4)} = 17.98$, $p = 5.6x10^{-5}$; SNI: $t_{(8)} = 14.86$, $p = 4.1x10^{-7}$; $\alpha = 0.0125$. (**C**) Corresponding EMG values (normalized to the mean value in NREMS). Mixed-model ANOVA $F_{(1,12)} = 0.2$, $p = 0.65$ for 'treatment'; $F_{(1,12)} = 3.83$, $p = 0.07$ for 'period'; $F_{(1,12)} = 1.31$, $p = 0.27$ for interaction. (**D-F**) Same presentation as in panels A-C, for cycles of the 0.02 Hz-fluctuation associated with MAs. Shaded areas in panel D show cycles of the 0.02 Hz-fluctuation interrupted by a MA. Arrowhead in E denotes the peak of the intermittent increase in AI due to MA occurrence. Statistics for E: Mixed-model ANOVA $F_{(1,12)} = 11.26$, $p = 0.0057$ for 'treatment'; $F_{(1,12)} = 25.34$, $p = 2.9x10^{-4}$ for 'period'; $F_{(1,12)} = 2.61$, $p = 0.13$ for interaction. Statistics for F: Mixed-model ANOVA $F_{(1,12)} = 0.045$, $p = 0.83$ for 'treatment'; $F_{(1,12)} = 44.5$, $p = 2.3x10^{-5}$ for 'period'; $F_{(1,12)} = 0.91$, $p = 0.35$ for interaction. (**G**) Six individual cases in one sham animal illustrating sigma (red) and AI (blue) dynamics in uninterrupted cycles of the 0.02 Hz-fluctuation. Thick portions of the blue traces represent the AI during the fragility period. Top three examples show an AI without an intermittent peak, bottom three examples show an AI with a peak (Peak is denoted by green arrowheads and duration at half-maximum by the green line). The horizontal line (mean AI per cycle) represents the threshold for peak detection. (**H**) Values of AI at the intermittent peak for cycles with (left, MA) and without (right, NREMS) an interruption by a MA. Mixed-model ANOVA $F_{(1,12)} = 14.94$, $p = 0.0022$ for 'treatment'; $F_{(1,12)} = 110.29$, $p = 2.1x10^{-7}$ for 'MA'; $F_{(1,12)} = 0.76$, $p = 0.39$ for interaction. (**I**) Duration of the intermittent peak at half-maximum, for cycles with (left, MA) and without (right, NREMS) an interruption by a MA. Mixed-model ANOVA $F_{(1,12)} = 0.24$, $p = 0.62$ for 'treatment'; $F_{(1,12)} = 101.64$, $p = 3.28x10^{-7}$ for 'MA'; $F_{(1,12)} = 1.39$, $p = 0.26$ for interaction. (**J**) Left: Heart rate dynamics (compared to the mean heart rate in NREMS), for cycles continuing into NREMS. Cycles are divided in whether a peak in activation index (AI) was present (top) or not (bottom). Right: boxplot quantification of the heart rate values shown on the left for continuity (270—90°) and fragility periods (90—270°), for Sham and SNI in NREMS fragility periods without (left of the dotted line) or with (right of the dotted line) an AI peak. Mixed-model three-way ANOVA $F_{(1,12)} = 1.75$, $p = 0.21$ for 'treatment'; $F_{(1,12)} = 26.71$, $p = 2.3x10^{-4}$ for 'peak'; $F_{(1,12)} = 11.18$, $p = 0.005$ for 'period'; only significant interaction in 'peak' x 'period' $F_{(1,12)} = 10.7$; $p = 0.007$. *Post-hoc* cycles with AI peak vs cycles without AI peak for sham in continuity: $t_{(4)} = -4.01$, $p = 0.015$; Sham in fragility: $t_{(4)} = -4.61$, $p = 0.009$; SNI in continuity: $t_{(8)} = -2.82$, $p = 0.022$; SNI in fragility: $t_{(8)} = -3.51$, $p = 0.008$; $\alpha = 0.0125$. (**K**) Occurrence of fragility periods with intermittent peak in AI across the light phase, quantified in boxplots on the right (unpaired *t*-test for Sham *vs* SNI $t_{(12)} = -2.66$, $p = 0.02$). (**L**) Two level-pie plots for Sham (left) and SNI (right) representing the proportion of cycles containing a MA or continuing in NREMS. These latter fragility periods are further subdivided into the ones with intermittent peak ('Peak') and without intermittent peak ('No peak'). The arrows show the proportions for Sham (green) and SNI (yellow).

The 0.02 Hz-fluctuation allows to anticipate elevated spontaneous arousability during NREMS

We finally examined sensory arousability in SNI conditions, focusing on the somatosensory modality. To anticipate fragility and continuity periods in real-time in the sleeping animal, we trained a machine learning software to predict online periods of continuity and fragility based on EEG/EMG

recordings (***Figure 6A-E***). For the training, we used online-calculated 0.02 Hz-fluctuation estimates onto which fragility and continuity periods were labelled using peak-and-trough detection of sigma power dynamics (***Figure 6 – figure supplement 3***). To control for the accuracy of the online prediction, we visually scored MAs in 12 C57Bl/6J animals implanted only for polysomnography and verified their position in either online detected peak-to-trough ('online fragility') or trough-to-peak phases ('online continuity') (***Figure 6F***). We compared the online prediction to that generated by chance through randomly shuffling both online fragility and continuity point positions in the recordings. This showed that the MA proportions obtained with the real detection exceeded those obtained by chance prediction (***Figure 6G***, for online fragility periods, $p = 0.0004$, for online continuity periods, $p = 0.0028$). Online detection of peak-to-trough and trough-to-peak periods of the 0.02 Hz-fluctuation is thus a versatile method to probe variations of evoked arousability from NREMS.

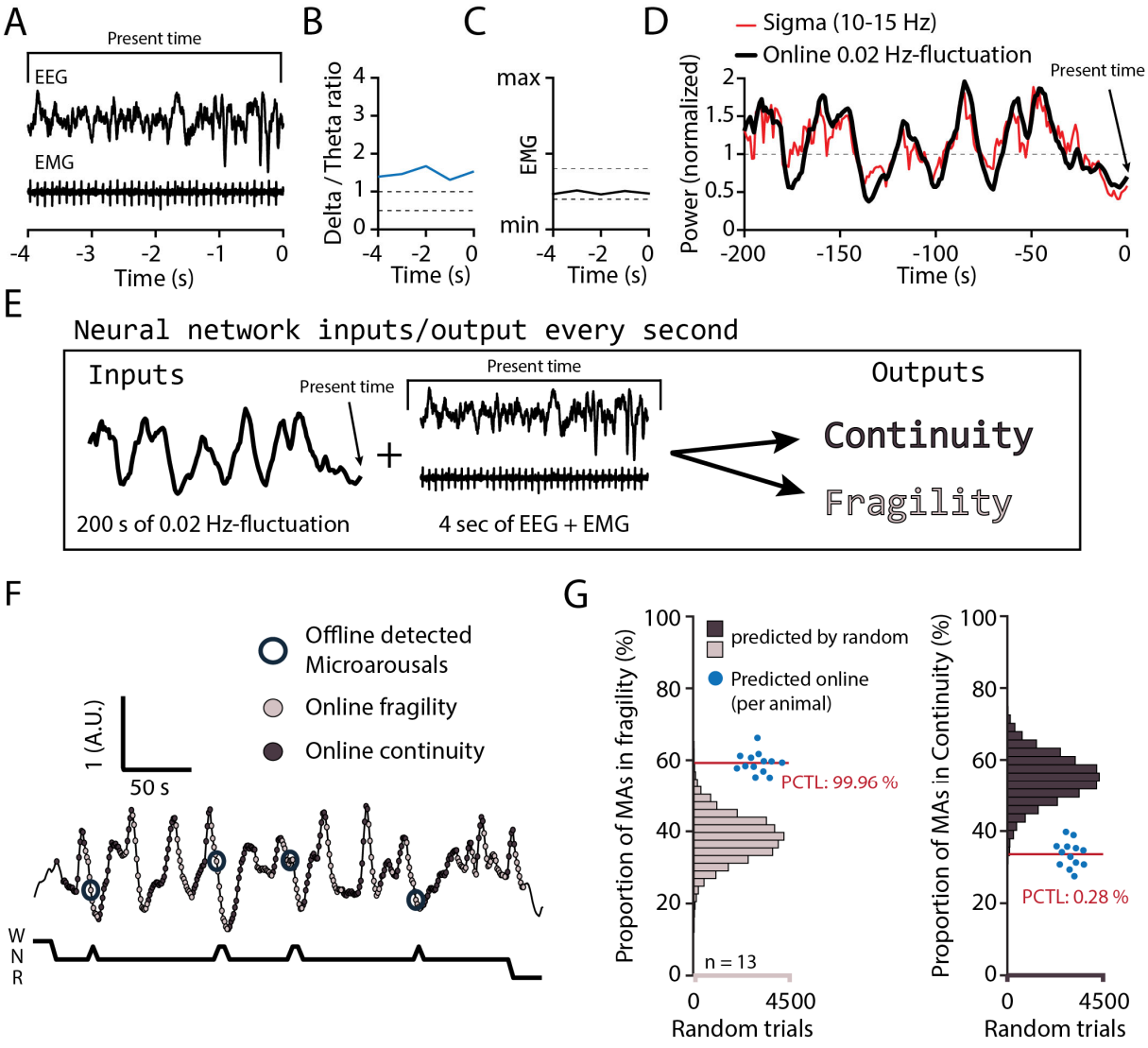

Figure 6 – On-line detection of fragility periods during mouse NREMS. (**A-E**) Input and output parameters for machine-learning of NREMS fragility and continuity periods. From the EEG and EMG up to the momentary time. (**A**) 4 last second of EEG and EMG at momentary time. (**B**) Ratio delta (1—4 Hz) over theta (5—10 Hz) from the FFT every s (**C**) normalized EMG levels. Together (B,C), are the variables for state decision using appropriate thresholds (dashed lines, see Methods). (**D**) The 0.02 Hz-fluctuation was estimated (black line) from sigma values (red) every s. The black line was constructed using the last point of a 9th order polynomial fit over the last 200 s of sigma power values. (**E**) The network was trained to use the last 200 s of online 0.02 Hz-fluctuation and the present window of EEG and EMG to determine whether the animal was in continuity or in fragility. The detection was carried out only when the animal was likely in NREMS. (**F**) Representative trace resulting from an online detection of fragility and continuity periods over a period of NREMS. Every s of detection is marked by a dark or light grey circle for online continuity and fragility periods, respectively. The hypnogram below represents the visual scoring done offline, blind to the online detection. The offline-detected MAs are indicated by open circles over the corresponding point of online detection. (**G**) Left, Proportion of MAs scored during online detected fragility. Right, proportion of MAs scored over online detected continuity, for 13 animals (blue dots). Horizontal

455 histograms represent the distribution of possible values of these proportions for randomly shuffled points
456 of fragility or continuity. The mean proportions for the 13 animals fell at percentile 99.96 % for fragility
457 and 0.28 % for continuity.

458

459 **SNI conditions produce elevated somatosensory-evoked arousability from NREMS**

460 Evoked arousability was probed through applying sensory stimuli either during online detected
461 fragility or continuity periods. To deliver somatosensory stimuli remotely while the animals were asleep,
462 we attached vibrational motors to their head implant that could be triggered to briefly vibrate (for 3 s) to
463 test the chance for wake-up (***Figure 7A***). These motors were calibrated to vibrate with the same low
464 intensity (~ 30% of full power) across animals (***Figure 7 – figure supplement 4***). Vibrations were applied
465 randomly with 25% probability during either online detected fragility or continuity periods, for at least
466 two complete light phases per condition (***Figure 7B***). Intensity was chosen such that Sham animals showed
467 approximately equal chances for wake-up or sleep-through in online continuity periods (***Figure 7C***).
468 Moreover, these vibrations produced wake-ups that were short, indicating that the sleeping animal felt
469 only mildly perturbed. Consistent with prior findings, similar stimuli applied during online fragility periods
470 showed consistently higher chances for wake-up (Lecci et al., 2017). In SNI, sensory arousability was
471 elevated for both continuity and fragility periods, leading to highest values during the online fragility
472 periods (***Figure 7D***, mixed-model ANOVA with factors 'treatment' and 'online period', $p = 0.0049$ for
473 'treatment', $p = 1.31 \times 10^{-8}$ for 'online period', no interaction). Interestingly, consistent with the tonic
474 increase in AI, this increase in sensory arousability in SNI was present across the whole light phase with a
475 conserved time of day dependence (***Figure 7E***).

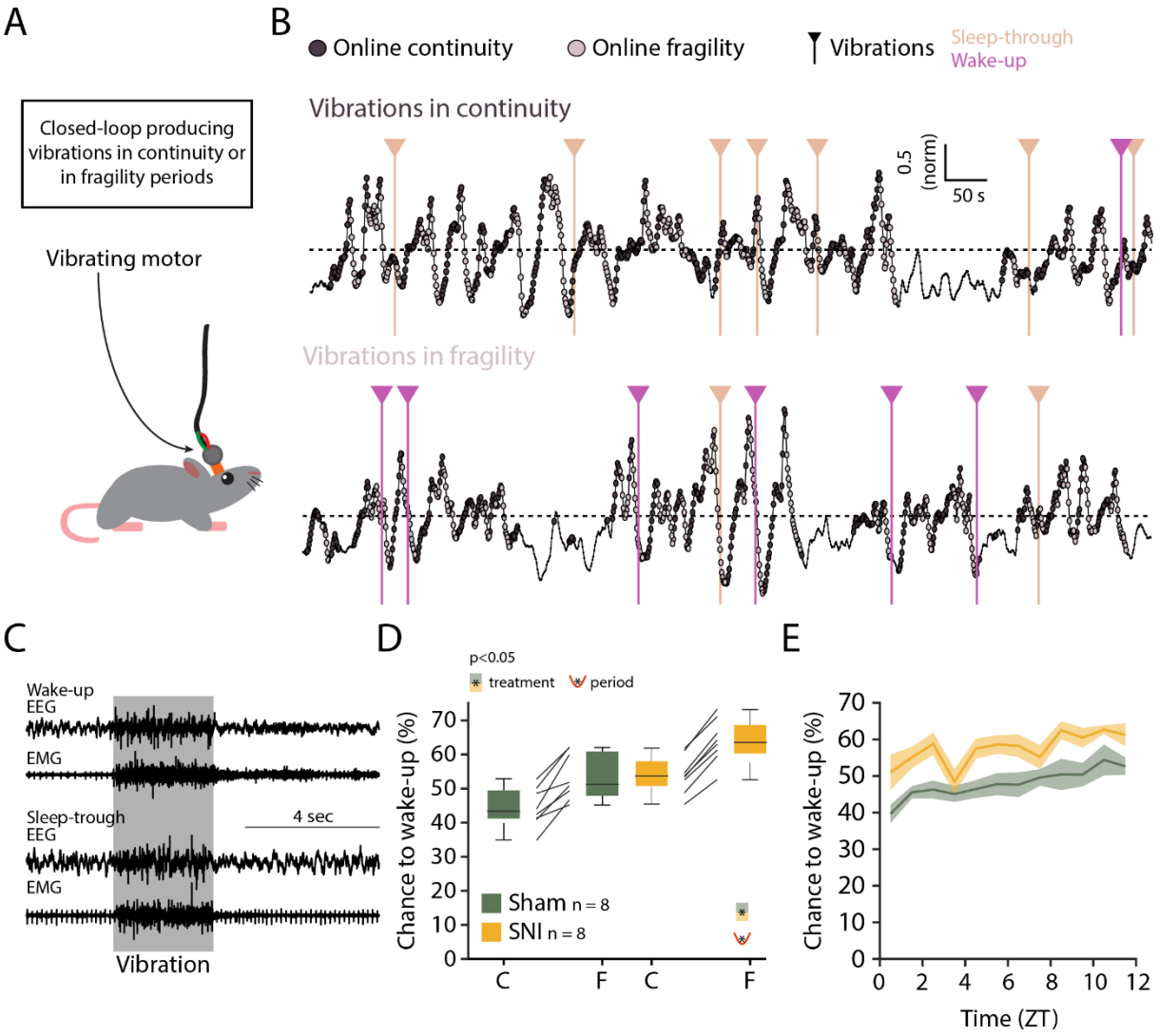

Figure 7 – Closed-loop probing of sensory-evoked arousability reveals a more fragile sleep in SNI. (**A**) Setup for delivering vibrating stimuli to the sleeping animal. A small vibrating motor was fixed at the end of the recording cable that was connected to the animal's headstage. When the algorithm presented in Figure 6 detected a change to an online fragility or continuity for > 4 s, a 3-s mild vibration (see Methods) was delivered with a chance of 25%. (**B**) Example of NREMS periods with vibrations over online continuity (top) or fragility (bottom) periods. Dark and light circles represent the online detection (see Figure 6F). Vertical lines represent the moments when the vibrations were delivered. Color-codes for wake-up or sleep-throughs. (**C**) Representative EEG/EMG recordings representing a wake-up (top) and a sleep-through (bottom). Time of stimulus delivery is shaded. The artifacts caused by the vibrations were not considered during automated wake-up or sleep-through detection (see Methods). (**D**) Chances to wake-up in response to a vibration in online continuity (C) or online fragility (F) periods. Mixed-model ANOVA $F_{(1,14)}$ = 11.07, p = 0.0049 for 'treatment'; $F_{(1,14)}$ = 136.58, p = 1.31×10^{-8} for 'period'; $F_{(1,14)}$ = 0.3, p = 0.58 for interaction. (**E**) Probability of wake-up (pooled continuity and fragility) for Sham and SNI over the light phase (ZT0-12). Shaded areas are SEMs.

Discussion

Chronic pain is a widespread and complex condition compromising sleep. As poor sleep further aggravates pain, therapeutic approaches to improve sleep quality have potential to attenuate disease progression. Here, in efforts to tease apart pain-sleep associations, we decided to focus on mechanisms of sleep disruptions at early stages of chronic pain. This study progresses on the sleep-pain association in four essential ways. First, we show that brain and autonomic signatures of pain states during the day intrude in a persistent manner into sleep in early phases of the disease. Second, sleep appeared nevertheless preserved in architecture, in dominant spectral band power, and in homeostatic regulation. Third, a previously undescribed spontaneous arousal during NREMS, showing local cortical activation with concomitant heart rate increases, appeared more frequently in SNI conditions. Fourth, we also demonstrate that fine mechanovibrational stimuli triggered brief wake-ups from NREMS more easily in SNI animals. In summary, chronic pain impacts on NREMS in terms of arousability, more specifically in the probability that NREMS transits towards diverse levels of wakefulness, either spontaneously, or with external stimuli. Chronic pain additionally instates a tonic regional elevation of high-frequency electrical activity. Both these consequences are not detectable in conventional measures of sleep. However, they bear resemblance to pathophysiological markers of insomnia disorders and, as we show here, produce elevated responsiveness to fine vibrational stimuli. The study further suggests that, amongst the many peripheral and central circuit alterations caused by chronic pain, the ones affecting the primary nociceptive sensory areas could serve as a site of entry to treat pain-related sleep disturbances directly at early states of the disease. For example, targeted interference by transcranial stimulation techniques has been proposed to modulate pain-related oscillations and could thus be probed to modify abnormal arousals (Shirvalkar *et al.*, 2018; Hohn *et al.*, 2019).

The quantification and classification of arousals from NREMS, both in terms of their physiological correlates and in their intensity, is central to estimate the severity of a sleep disorder. The fragmentation of sleep by arousals is the primary cause for daytime fatigue and for cognitive deficits and, in more severe cases, may constitute long-term risks for cardiovascular health (Bonnet et al., 1992; Silvani, 2019). Criteria for arousal scoring in humans are comparatively well established and there are strong indications that arousal intensity is graded, with EEG desynchronization and concomitant heart rate acceleration occurring independently of muscular activity (e.g. leg movements) (Sforza et al., 2000; Azarbarzin et al., 2014). In chronic pain patients, few systematic analyses on spontaneous arousals are currently available and a need for more polysomnographic assessments in well-controlled patient populations has been highlighted

(Bjurstrom & Irwin, 2016). In rodents, only few studies have described cortical desynchronization events without EMG activity, and these were not characterized with respect to autonomic correlates (Bergmann *et al.*, 1987; Franken, 2002; Léna *et al.*, 2004; Fulda, 2011). This relative lack of arousal characterization in mouse NREMS could have hampered the identification of models to replicate sleep disorders, as we found here to be the case for chronic pain models. To the best of our knowledge, our analysis of the SNI mouse is the first that qualifies as a rodent model replicating physiological correlates of insomnia disorders that are hidden behind a comparatively normal sleep and that could raise awareness for refined analysis of the diverse forms of sleep disruptions in chronic pain patients (Bjurstrom & Irwin, 2016). Our work also adds a novel variant to proposed insomnia models that provoked severe macroscopic sleep disruptions either through acute stress (Cano *et al.*, 2008; Li *et al.*, 2020) or by optogenetically enforced full awakenings to fragment NREMS (Rolls *et al.*, 2011).

This study proposes a novel type of arousal from NREMS in mouse that pairs cortical desynchronization with heart rate increases. Inclusion of this type of arousal is crucial to identify the exact sleep disruptions for the case of neuropathic pain. We departed here from previous observations on infraslow variations in sensory arousability during NREMS that take place over the minute time-scale (Lecci et al., 2017). We first demonstrated that spontaneous MAs, the only spontaneous arousal in rodent for which scoring criteria are widely established, occur remarkably clustered at phases for which sensory evoked arousals were most likely (Lecci et al., 2017). The high number of MAs and their remarkable clustering at phases > 90° and < 270°, allowed us to allocate the fragility periods to the phases with low sigma power. We consider this basic finding on MA timing in rodent NREMS significant for several reasons. First, it suggests that the infraslow 0.02 Hz-fluctuation is part of an overarching process that periodically sets a fragility of NREMS towards wake-promoting inputs, whether they arise from internal processes or external stimuli. Mechanistically, this points to an involvement of widely projecting neuromodulatory brain areas such as the locus coeruleus that remains active during NREMS (Aston-Jones & Bloom, 1981; Kjaerby *et al.*, 2020) and regulates sensory arousability (Hayat *et al.*, 2020). Second, the finding contributes to a long-standing uncertainty about the origin and the stochastic time-scales on which MAs are thought to occur (Lo *et al.*, 2004; Dvir *et al.*, 2018). We now calculate that MAs in consolidated NREMS occur with a mean ~35% probability on ~50-sec intervals, thus providing a temporal raster on which these can be anticipated with a measurable degree of certainty. MAs depend on activity in wake-promoting brain areas (Dvir et al., 2018), specifically on the histaminergic hypothalamus in mice (Huang *et al.*, 2006) and on cholinergic nicotinic receptors (Léna et al., 2004). This mechanistic origin of MAs is consistent with our observation that they occur at moments of NREMS during which sensory wake-ups occur preferentially.

We therefore consider the identification of fragility periods as time raster for MAs as key to reinforce mechanistic investigations into the origins of spontaneous arousals. This not only concerns MAs, but opens the opportunity to search for other arousal-like events that could be relevant to model pathological conditions of human patients.

The majority of this study was dedicated to providing a proof-of-concept for the usefulness of the infraslow fragility periods to scrutinize arousability. The chosen SNI model appeared particularly appropriate for this purpose because it produced a sensory deficit that could be exploited to specifically test somatosensory arousability. The separation of NREMS into fragility and continuity periods throughout the resting phase allowed us to sample and scrutinize the many fragility periods continuing apparently uninterrupted into NREMS. The fragility periods were also critical to determine when AI became most disparate between SNI and Sham and to identify previously undescribed cortico-autonomic arousals. During these, the activation index increased because of a phasic decrease in low-frequency delta power and an increase in high-frequency power. These events were more pronounced and more frequent in SNI because both these phasic power alterations were disrupted, with the deficits in delta power most pronounced. Without the raster provided by the fragility periods, the phasic differences amidst the tonically elevated high-frequency power would easily have gone undetected. To further ascertain that these detected events nevertheless constituted true arousals rather than accidental spectral fluctuations, we sought for independent physiological correlates. Inspired by the human literature (Sforza et al., 2000; Azarbarzin et al., 2014), we found that heart rate increases were consistently higher when calculated for cortical arousals with AI peak than for the ones without AI peak. Moreover, their distribution across the resting phase was similar to the one found for MAs and they were present in both S1HL and PrL. This result supports our interpretation that we have identified here a novel cortical-autonomic arousal subject to similar time-of-day-dependent regulatory mechanisms. Still, we cannot exclude that arousal subtypes outside the fragility periods went undetected that would require further characterization. We also remark here clearly that, aside from more frequent cortico-autonomic arousals, SNI animals suffered from a tonically elevated high-frequency power in S1HL that likely underlay the more elevated sensory arousability throughout continuity and fragility periods.

The lack of major sleep disruptions in the SNI mouse model was initially unexpected but seemed in line with other studies. We analyzed these animals at a time point when pain from the wound and associated inflammations are largely over (Guida *et al.*, 2020), both of which can strongly disrupt sleep (Landis *et al.*, 1989; Andersen & Tufik, 2003; Silva *et al.*, 2008). Moreover, the animals showed a preserved time spent in REMS, suggesting that they did not suffer from chronic mild stress-inflicted sleep disruptions

(Nollet *et al.*, 2019). Other studies on chronic pain also report diverse moderate effects on sleep (Kontinen et al., 2003; Leys et al., 2013). One study on rats at 2 and 10 days after SNI surgery suggested that brain states intermediate between NREMS and wakefulness during the resting phase exist (Cardoso-Cruz et al., 2011), which could in part reflect our observations. We also found no alterations in theta power or for shifts in theta peaks in wakefulness, as reported for other animal models of chronic pain (LeBlanc *et al.*, 2014) or for humans with severe neurogenic pain or arthritis (Sarnthein *et al.*, 2006). Analysis of sleep disruptions at later stages in the disease will help decide whether distinct phases of sleep disruptions mark distinct phases of pain chronicity when anxiety- and depression-related behaviors appear more strongly (Guida et al., 2020).

The spectral dynamics in two cortical regions we present here delineate possible areas of pathological neuronal activity that underlie the cortical arousals. The continued presence of high-frequency activity in S1HL is reminiscent of the cortical oscillatory activity evoked with acute painful stimuli, suggesting that nociceptive input continues to arrive in cortex during NREMS to generate excessive excitation. Indeed, it has been suggested that the SNI model does show spontaneous ectopic electrical activity in peripheral sensory neurons as a result of nerve injury (Wall & Devor, 1983; Devor, 2009). NREMS is thought to protect relatively weakly from nociceptive inputs (Claude *et al.*, 2015), therefore possibly allowing continued processing of spontaneous nociceptive activity that could explain the cortical spectral changes we detected. It has also been shown that optogenetic stimulation of the thalamic reticular nucleus, known to be implied in the balanced occurrence of delta and spindle waves during NREMS (Fernandez et al., 2018), can alleviate pain in SNI (LeBlanc et al., 2014). Suppressed TRN activity during NREMS could be implied in the attenuated delta dynamics observed in NREMS of SNI mice. In contrast, we found unperturbed local spectral dynamics in PrL during NREMS, although this area is concerned with signaling emotional discomfort in several forms of chronic pain in humans (Schulz *et al.*, 2015; Nickel *et al.*, 2017; May *et al.*, 2019) and is known to undergo strengthened synaptic inhibition in SNI (Zhang *et al.*, 2015; Radzicki *et al.*, 2017). Further cellular studies will be necessary to understand why these alterations seem not to perturb oscillatory activity in this area during NREMS.

Do SNI animals suffer from insomnia? Our objective measures of NREMS's spectral composition point to regionally restricted but tonic imbalances in the contribution of low- vs higher frequencies. Patients with insomnia show such imbalances over widespread brain regions that include sensorimotor areas (Lecci et al., 2020). Furthermore, higher power in the beta frequencies has been related to the patients remaining hypervigilant or excessively ruminating at sleep onset (Perlis *et al.*, 2001a), preventing the deactivation of cortical processes required for the loss of consciousness. Although insomnia also needs

subjective assessments that are not possible in animals, this phenomenological comparison suggests that SNI might suffer from similar experiences due to the tonically enhanced high-frequency oscillations. This interpretation is supported by the elevated wake-up rates in response to mild vibrational stimuli throughout the infraslow cycles, suggesting hyperalertness to environmental disturbance. On top of these tonic changes, there were more frequent cortico-autonomic arousals. Although these do not seem to elevate daytime sleepiness based on the mostly unchanged delta power dynamics across time-of-day, frequent increases in heart rate during the night could augment cardiovascular risk in the long-term (Silvani, 2019). To further analyze the animal's conditions during daytime, tests on their cognitive abilities in memory-dependent tasks while locally manipulating sleep in the affected hindlimb area could be considered. Deficits in working and declarative memories in rodents with SNI have been documented from early periods of chronic pain (Guida et al., 2020). Chemogenetic manipulation of neuronal populations proposed to be responsible for the gamma activity in chronic pain, restricted to sleep periods (Tan et al., 2019), seems a feasible approach to specifically suppress abnormal pain-related activity during sleep while testing performance in such tasks during wakefulness.

We provide here novel approaches to classify arousals in mouse NREMS that will help in the examination and validation of future candidates for rodent models of sleep disorders. We noted a remarkable stability of the 0.02 Hz-fluctuation across the resting phase that provided us with a temporal raster to screen the characteristics of fragility periods. These led us to identify a previously undescribed cortico-autonomic arousal in mouse NREMS that we also found more frequently in a chronic pain model. Together, this study presents NREMS as a state that is interwoven with arousals showing diverse combinations of physiological parameters with different graduations in intensity that can be the target of pathophysiological changes. Recognizing NREMS as a fluctuating state between fragility and continuity will thus further heighten awareness to arousability as a core component of sleep quality. In this study, we unraveled a so far undescribed sleep disruption in chronic pain that we hope will facilitate further research into the treatment of this devastating condition.

Materials and methods

Animal housing and experimental groups

Mice from the C57BL/6J line were singly housed in a temperature- and humidity-controlled environment with a 12-h/12 h light-dark cycle (lights on at 9:00 am, corresponding to ZT0), with access to food and water *ad libitum*. We first used 36 mice, 10-14 weeks-old and bred in our colonies in a conventional-clean

649 animal house, for polysomnography (combined EEG (ECoG)/EMG electrodes), followed by SNI or Sham
650 surgery (18 animals per Sham or SNI group). Mice were transferred from the animal house into the
651 recording room 2-3 d before surgery for polysomnography recording. We recorded a 48 h-long baseline
652 before SNI or Sham surgeries, followed by recording at 22-23 d after surgery (D20+). These data were used
653 for Figures 1 and 3. Total sleep deprivation in Figure 3 was done on 24 of these 36 animals (12 SNI, 12
654 Sham) within one day following the recording at D20+. The baseline data for Figure 2 were obtained from
655 the baseline recordings of 23 randomly selected animals from the previous 36, completed with 7 more
656 animals from previous baseline recording in the lab. For EEG (ECoG)/EMG/LFP recordings, 33 C57BL/6J
657 male mice of the same age were first operated for SNI or Sham (17 and 14, respectively) and 5 d later,
658 implanted for recordings from S1HL (4 Sham, 6 SNI) or PrL (3 Sham, 4 SNI) or both (3 Sham, 4 SNI). The
659 misplaced or non-functional electrodes were excluded. Recordings were carried on from day 20 to 35
660 after SNI or Sham surgery. These data were used for Figures 4 and 5. The data of 13 animals previously
661 recorded in the lab and otherwise not included in any dataset in this study were used to train the neural
662 network (EEG/EMG implantation, in *Figure 6*). The experiments on sensory evoked arousals (*Figure 7*)
663 were done on 16 animals (8 Sham, 8 SNI) out of which some (4 sham, 6 SNI) were used for Figures 4-5. All
664 experimental procedures complied with the Swiss National Institutional Guidelines on Animal
665 Experimentation and were approved by the Swiss Cantonal Veterinary Office Committee for Animal
666 Experimentation.

667 **Surgery for the SNI model of neuropathic pain**

668 The Sham and SNI surgeries were performed as previously described (Decosterd & Woolf, 2000). Briefly,
669 mice were kept under gas anesthesia (1—2 % isofluorane, mixed with O_2). The left hindleg was shaved
670 and the skin incised. The muscles were minimally cut until the sciatic nerve was exposed. Just below the
671 trifurcation between common peroneal, tibial and sural branches of the nerve, the common peroneal and
672 tibial branches were ligated and transected. The Sham animals, as controls, went through the same
673 surgery without the transection. The muscle and the skin were then stitched closed and the animals were
674 monitored via a score sheet established with the Veterinarian Authorities.

675 **Surgery for polysomnographic and LFP recordings in mice**

676 Surgeries were performed as recently described (Lecci et al., 2017; Fernandez et al., 2018). Animals were
677 maintained under gas anesthesia (1—2 % isofluorane, mixed with O_2). Small craniotomies were performed
678 in frontal and parietal areas over the right hemisphere and 2 gold-plated screws (1.1 mm diameter at their

679 base) (Mang & Franken, 2012) were gently inserted to serve as EEG electrodes. Careful scratching of the
680 skull surface with a blade strengthened the attachment of the implant by the glue, so that additional
681 stabilization screws were no longer necessary. Two gold wires were inserted into the neck muscle to serve
682 as EMG electrodes. In the case of LFP recordings, small craniotomies (0.2-0.3 mm) were performed to
683 implant high-impedance tungsten LFP microelectrodes (10–12 MΩ, 75-µm shaft diameter, FHC, Bowdoin,
684 ME) at the following stereotaxic coordinates relative to Bregma in mm, for S1HL: anteroposterior -0.7,
685 lateral -1.8, depth from surface -0.45; for PrL : +1.8, -0.3, -1.45). For the neutral reference for the LFP
686 recordings, a silver wire (Harvard Apparatus, Holliston, MA) was placed in contact with the bone within a
687 small grove drilled above the cerebellum. The electrodes were then soldered to a female connector and
688 the whole implant was covered with glue and dental cement. The animals were allowed 5 d of recovery,
689 while being monitored via a score sheet established with the Veterinarian Authorities, with access to
690 paracetamol (2mg/mL, drinking water). The paracetamol was removed when the animals were tethered
691 to the recording cable for another 5 d of habituation prior to the recording.

692 **Polysomnographic recording**

693 For sleep recordings, recording cables were connected to amplifier boards that were in turn connected to
694 a RHD USB interface board (C3100) using SPI cables (RHD recording system, Intan Technologies, Los
695 Angeles, CA). For EEG/EMG and/or LFP electrodes, signals were recorded through homemade adapters
696 connected to RHD2216 16-channel amplifier chips with bipolar input or RHD2132 32-channel amplifier
697 chips with unipolar inputs and common reference, respectively. Data were acquired at 1000 Hz via a
698 homemade Matlab recording software using the Intan Matlab toolbox. Each recording was then visually
699 scored in 4-s epochs into wake, NREMS, REMS, as described (Lecci et al., 2017) using a homemade Matlab
700 scoring software.

701 **Total sleep deprivation protocol**

702 Total SD was carried out from ZT0—ZT6 using the gentle handling method used previously in the lab (Kopp
703 et al., 2006), while animals remained tethered in their home cage. At ZT3, the cages were changed and,
704 from ZT5 to ZT6, new bedding material was provided. At ZT6, the animals were left undisturbed. The
705 recordings carried out during SD were visually scored to assure the absence of NREMS from ZT0 to ZT6.
706 There were no detected NREMS epochs during SD in the mice included in the analysis.

707 **Probing sensory arousability with vibration motors and automatic wake-up classification**

An online detection of continuity and fragility period (described below) was used in a closed-loop manner to time vibration stimuli during NREMS such that sensory arousability could be probed. Small vibrating motors (DC 3—4.2 V Button Type Vibration Motor, diameter 11 mm, thickness 3 mm) were fixed using double-sided tape, at the end of the recording cables, close to the animals' heads. The motors were driven using a Raspberry Pi 3B+ through a 3.3 V pulse-width modulation (PWM) signal. Each motor was calibrated to find the necessary PWM duty-cycle to output the same amount of mild vibration using a homemade vibration measurer equipped with a piezo sensor. A Python script was running on the Raspberry Pi to detect the voltage change sent by the digital-out channels on the Intan RHD USB interface board. Upon detecting a change from low to high, the Python script waited for an additional 4 s, and assessed the voltage again. In case the voltage was still high, it launched a 3 s vibration with 25% probability. To close the loop, the PWM signals from the Raspberry Pi driving the motors were as well fed into the analog-in channels of the Intan RHD USB interface board to detect the stimuli time-locked to the EEG/EMG signals. In the experiments, the voltage values were set to high during either continuity or fragility, using online detection as described in Data analysis. Four animals could be tested in parallel for their sensory arousability.

Histological verification of recording sites

After the *in vivo* LFP recordings, the animals were deeply anesthetized with pentobarbital (80 mg/kg) and electrode positions were marked through electro-coagulation (50 µA, 8—10 s). The animals were then transcardially perfused with 4 % paraformaldehyde (in 0.1 M phosphate buffer). After brain extraction and post-fixation for 24 h, 100 µm-thick coronal brain sections were cut and imaged in brightfield microscopy to verify correct electrode positioning.

Data analysis

Scoring and basic sleep measures

Scoring was done blind to the animal treatment according to standard scoring procedures (Fernandez et al., 2018). A MA was scored whenever the EEG presented a desynchronization time-matched with a burst of EMG activity lasting maximally 4 consecutive epochs (16 s). Latency to sleep onset was defined from ZT0 to the first appearance of 6 consecutive NREMS epochs (24 s). The bout size binning in short, intermediate and long bouts for NREMS and REMS was obtained from the pulled distribution of the bout sizes from all the animals. The edges of the intermediate bin were defined as: mean - ½ standard deviation to mean + 1 standard deviation.

Spectral power was computed on the raw EEG signal using a FFT on scored 4-s windows after offset correction through subtraction of the mean value of each epoch. The median power spectrum for each state was obtained for epochs non-adjacent to state transitions. The normalization was done through dividing by the average of mean power levels (from 0.75–47 Hz) for each vigilance state, ensuring that each state had the same weight in the averaging (Vassalli & Franken, 2017). This normalization was done separately for Baseline and D20+ recordings. Gamma power at D20+ was extracted through calculating mean power levels between 60—80 Hz. Data were normalized to corresponding baseline values.

The heart rate was extracted from the EMG signal as described previously (Lecci et al., 2017). Briefly, the EMG signal was highpass-filtered (>25 Hz) and squared. The R peaks of the heartbeats were detected using the Matlab 'Findpeaks' function. Only animals with clearly visible R peaks present in the EMG in NREMS were included in this analysis (Fernandez *et al.*, 2017).

For delta power time course, raw delta power (mean power between 1—4 Hz from FFT on mean-centered epochs) was extracted for each NREMS epoch non-adjacent to a state transition. Total NREMS time was divided into periods of equal amounts of NREMS (12 in light phases, 6 in dark phases) from which mean values for delta power were computed. The position in time of these periods was not different between groups. Normalization was done via mean values between ZT9—12, when sleep pressure is the lowest.

Wake-up and sleep-through events after vibration were scored automatically as follows. For each trial, the EEG and EMG signals were analyzed within time intervals from 5 s prior to 5 s after the vibrations. To distinguish wake-up and sleep-through events, three values were calculated: 1) The ratio theta (5-10 Hz)/ delta (1-4 Hz) for the 5 s before stimulation, 2) the difference in the low- / high-frequency ratios (1-4 Hz/ 100—500 Hz), before and after the stimulation, 3) the squared EMG amplitude ratio after/ before stimulation.

A trial was rejected when the ratio theta/delta was > 1 before stimulation or the EMG amplitude was larger before than after stimulation. In this way, trials starting in REMS or wakefulness were excluded. Wake-up events were scored when the difference in low/high ratios mentioned above decreased markedly after stimulation together with EMG activity. Occasionally, some wake-ups were also scored when EEG or EMG activity was very high while the other channel showed moderate changes. Appropriate thresholds were set upon visual inspection blinded to the animal's condition.

<u>Analyses related to the 0.02 Hz-fluctuation</u>

Extraction - The 0.02 Hz-fluctuation in sigma power (10–15 Hz) was extracted from EEG or LFP signals using a wavelet transform (Morlet wavelet, 4 cycles), calculated over 12 h recordings in 0.5-Hz bins. The resulting signal was down-sampled to 10 Hz and smoothed using an attenuating FIR filter (cutoff frequency 0.0125 Hz, order of 100, the low order allowing for frequencies above the cutoff). The mean of the datapoints within NREMS and MA epochs was used for normalization ***(Figure 2- figure supplement 1D***). The peak and frequency of the 0.02 Hz-fluctuation were calculated through a FFT on continuous NREMS bouts as described (Lecci et al., 2017). FFTs from individual bouts at frequency bins from 0 to 0.5 Hz were interpolated to 201 points before averaging across bouts to obtain a single measure per mouse. The angles of the phase of the 0.02 Hz-fluctuation were obtained through the Hilbert transform (Matlab signal processing toolbox). We set the troughs of the 0.02 Hz-fluctuation at 180°, the peaks at 0° ***(Figure 2- figure supplement 1G***).

In several instances (**Figures 3D, 4, 5**), instead of calculating FFTs in the infraslow frequency range, we needed to detect individual cycles of the 0.02 Hz-fluctuation. To do this, we applied the Matlab "Findpeaks" function, with the conditions that the peak values were > mean and the trough values < mean, each separated by > 20 s. With such parameters, the sequence trough-peak-trough appears only in NREMS and allows to count individual cycles.

Band-limited power dynamics during the 0.02 Hz-fluctuation - To calculate the power dynamics in different frequency bands, Morlet wavelet transforms were down-sampled to 10 Hz to match the sampling of the 0.02 Hz-fluctuation and normalized by the sum of their means in NREMS. The mean power of each band was then binned in 18 bins of 20° and a mean across cycles (with or without MAs) of power activity per phase bin was obtained per animal.

Analysis of activation index - AI was computed by the natural logarithm (ln) of the ratio between beta (16–25 Hz) + low gamma (26–40 Hz) over delta power (1–4 Hz), extracted as described above. Individual cycles from peak-to-peak were classified whether a MA was present in the fragility period or whether it continued into NREMS. To assess the presence of peaks in activation indices, the "findpeaks" function was used at phase values of 90–270°, with mean values used as a threshold.

Online detection of continuity and fragility periods - For the online detection of fragility and continuity periods during closed-loop sensory stimulation, a homemade software was generated with two layers of decision. The first one determined the likely current state of vigilance (wake, NREMS or REMS), whereas the second one made a machine learning-based decision between a continuity or a fragility period.

1 – Determination of vigilance state. This assessment was based on power band ratios characteristic for wake, NREMS and REMS using appropriate thresholds (***Figure 6B,C***). Every s, a FFT was calculated on the mean-centered last 4 s of EEG values and the power ratio between the delta (1–4 Hz) and the theta (5–10 Hz) was calculated.

Transitions out of wake: *1)* Switch to NREMS if the last 3 s of EMG were below a high threshold and at least 2 out of the 3 last s of ratio were above a high threshold. *2)* Switch to REMS if the full 5 s of EMG were below a low threshold and the full 5 s of ratio were above a high threshold.

Transitions out of NREMS: *1)* Switch to wake if the last s of EMG was above a high threshold. *2)* Switch to REMS if the last five s of EMG were below a low threshold and if among the last 5 s of ratio, at least 4 were below a low threshold and all 5 were below a high threshold.

Transitions out of REMS: *1)* Switch to wake if the last s of EMG were above a high threshold. *2)* Switch to NREMS if the ratio was above a high threshold for at least 4 out of 5 s.

2 – Continuity and fragility detection. From the previous step, the value of sigma (10—15 Hz) was kept every second. The mean sigma value in NREMS was dynamically updated if the likely state was determined as NREMS and used to normalize the incoming sigma power values. The last 200 s of sigma power regardless of the likely state were kept in memory. We heuristically found that a 9^{th}-order polynomial fit (Matlab 'polyfit' and 'polyval' functions) best approximated the 0.02 Hz-fluctuation. To train the network, we first generated online-estimated 0.02 Hz-fluctuation at 1 Hz for the 12 h of the light phase. We next applied offline cycle detection in NREMS periods. For simplicity, and in agreement with previous measures of sensory arousability (Lecci et al., 2017), we set the continuity periods from trough to peak and fragility from peak to trough. Then, we subdivided these recordings in chunks of 200 s (moving window of 1 s, as they would appear online) and keeping the label continuity, fragility or none for each of them. We could thus obtain 43,000 labelled chunks per 12 h of recording. We used 642,000 of these chunks from 13 animals to train a neural network (pattern recognition 'nprtool' from Matlab Statistics and Machine Learning Toolbox) 70 % of the for training, 15 % for validation and 15 % for testing. The network was composed of one hidden layer with 10 neurons and one output layer with the 3 different output. We then used the generated neural network online to take the decision between continuity, fragility or none.

Statistics

The statistics were done using Matlab R2018a and the R statistical language version 3.6.1. The normality and homogeneity of the variances (homoscedasticity) were assessed using the Shapiro-Wilk and the

Bartlett tests, respectively to decide for parametric statistics. In the cases where normality or homoscedasticity were violated, a log transformation was assessed at first and finally, non-parametric *post-hoc* tests were used (Wilcoxon rank sum test for unpaired and signed-rank test for paired data). The degrees of freedom and residuals for the F values are reported according to the R output. *Post-hoc* analyses were done only when the interaction between factors were significant ($p < 0.05$). Bonferroni's correction for multiple comparisons was applied routinely, and the corrected α values are given in the legends. The factors used in the ANOVAs are depicted with pictograms once the corresponding effects were significant. The factors used in the analysis were: 'treatment' with two levels: Sham and SNI; 'day' with two repeated levels: baseline and D20+; 'size' with three repeated levels: small, intermediate or long bouts; 'period' with two repeated levels: continuity or fragility; 'SD' with two repeated levels: control or recovery after sleep deprivation; 'state' with three repeated levels: wake, NREMS or REMS; 'MAs' with two levels: with or without MA in the fragility period; 'peak' with two repeated levels: cycles with or without a peak in AI during fragility periods. The circular statistics were done using the CircStat for Matlab toolbox (Berens, 2009).

Acknowledgements

All lab members provided critical input at all stages of this manuscript. The excellent animal caretaking headed by Michelle Blom and the Team of Animaliers, in particular Titouan Tromme, is highly appreciated. Expert veterinary support and advice was provided by Drs. Gisèle Ferrand and Laure Sériot. We thank Christiane Devenoges for support in histological analysis and Marie Pertin and Guylène Kirschmann for excellent technical support with SNI surgeries. Dr. Simone Astori and Dr. Marc Suter provided insightful comments on pre-final versions of the manuscript and Laura Solanelles Farré helped with careful proofreading. The useful discussions with Raquel Sandoval Adaia, Paul Franken, Thomas Nevian, Francesca Siclari and Raphaelle Winsky-Sommerer are gratefully acknowledged. This study was funded by The Swiss National Science Foundation (n° 310030_184759 to AL, n° 310030_179169 to ID, n° 320030-179194 to SF), and Etat de Vaud.

Competing interests

The authors declare no competing interests.

Author contributions

Romain Cardis, Conceptualization, Data collection, Data curation, Formal analysis, Software, Validation, Investigation, Visualization, Methodology, Figures, Writing—review and editing; Sandro Lecci, Conceptualization, Data collection, Data curation, Formal analysis, Methodology; Laura Fernandez, Methodology, Data curation; Alejandro Osorio-Forero, Methodology; Paul Chu Sin Chung, Editing; Stephany Fulda, Conceptualization, Data Validation, Writing—review and editing; Isabelle Decosterd and Anita Lüthi, Conceptualization, Data curation, Supervision, Funding acquisition, Validation, Visualization, Writing—original draft, Project administration, Writing—review and editing.

References

Alexandre, C., Latremoliere, A., Ferreira, A., Miracca, G., Yamamoto, M., Scammell, T. E., & Woolf, C. J. (2017). Decreased alertness due to sleep loss increases pain sensitivity in mice. *Nat Med, 23*(6), 768-774. doi: 10.1038/nm.4329

Andersen, M. L., & Tufik, S. (2003). Sleep patterns over 21-day period in rats with chronic constriction of sciatic nerve. *Brain Res, 984*(1-2), 84-92. doi: 10.1016/s0006-8993(03)03095-6

Aston-Jones, G., & Bloom, F. E. (1981). Norepinephrine-containing locus coeruleus neurons in behaving rats exhibit pronounced responses to non-noxious environmental stimuli. *J Neurosci, 1*(8), 887-900.

Azarbarzin, A., Ostrowski, M., Hanly, P., & Younes, M. (2014). Relationship between arousal intensity and heart rate response to arousal. *Sleep, 37*(4), 645-653. doi: 10.5665/sleep.3560

Berens, P. (2009). CircStat: A MATLAB toolbox for circular statistics. *J Stat Software, 31*(10), 1-21. doi: 10.18637/jss.v031.i10

Bergmann, B. M., Winter, J. B., Rosenberg, R. S., & Rechtschaffen, A. (1987). NREM sleep with low-voltage EEG in the rat. *Sleep, 10*(1), 1-11.

Bjurstrom, M. F., & Irwin, M. R. (2016). Polysomnographic characteristics in nonmalignant chronic pain populations: A review of controlled studies. *Sleep Med Rev, 26*, 74-86. doi: 10.1016/j.smrv.2015.03.004

Bonnet, M., Carley, D., Carskadon, M., Easton, P., Guilleminault, C., Harper, R., Hayes, B., Hirshkowitz, M., Ktonas, P., Keenan, S., Pressman, M., Roehrs, T., Smith, J., Walsh, J., Weber, S., & Westbrook, P. (1992). The Atlas Task Force. EEG arousals: Scoring rules and examples. *Sleep, 15*, 173-184.

Bourquin, A. F., Süveges, M., Pertin, M., Gilliard, N., Sardy, S., Davison, A. C., Spahn, D. R., & Décosterd, I. (2006). Assessment and analysis of mechanical allodynia-like behavior induced by spared nerve injury (SNI) in the mouse. *Pain, 122*(1-2), 14 e11-14. doi: 10.1016/j.pain.2005.10.036

Burma, N. E., Leduc-Pessah, H., Fan, C. Y., & Trang, T. (2017). Animal models of chronic pain: Advances and challenges for clinical translation. *J Neurosci Res, 95*(6), 1242-1256. doi: 10.1002/jnr.23768

Buysse, D. J., Germain, A., Hall, M. L., Moul, D. E., Nofzinger, E. A., Begley, A., Ehlers, C. L., Thompson, W., & Kupfer, D. J. (2008). EEG spectral analysis in primary insomnia: NREM period effects and sex differences. *Sleep, 31*(12), 1673-1682. doi: 10.1093/sleep/31.12.1673

894 Cano, G., Mochizuki, T., & Saper, C. B. (2008). Neural circuitry of stress-induced insomnia in rats. *J*
895 *Neurosci, 28*(40), 10167-10184. doi: 10.1523/JNEUROSCI.1809-08.2008
896 Cardoso-Cruz, H., Sameshima, K., Lima, D., & Galhardo, V. (2011). Dynamics of circadian thalamocortical
897 flow of information during a peripheral neuropathic pain condition. *Front Integr Neurosci, 5*, 43.
898 doi: 10.3389/fnint.2011.00043
899 Christensen, J. A. E., Wassing, R., Wei, Y., Ramautar, J. R., Lakbila-Kamal, O., Jennum, P. J., & Van
900 Someren, E. J. W. (2019). Data-driven analysis of EEG reveals concomitant superficial sleep
901 during deep sleep in insomnia disorder. *Front Neurosci, 13*, 598. doi: 10.3389/fnins.2019.00598
902 Claude, L., Chouchou, F., Prados, G., Castro, M., De Blay, B., Perchet, C., Garcia-Larrea, L., Mazza, S., &
903 Bastuji, H. (2015). Sleep spindles and human cortical nociception: a surface and intracerebral
904 electrophysiological study. *J Physiol, 593*(22), 4995-5008. doi: 10.1113/JP270941
905 Decosterd, I., & Woolf, C. J. (2000). Spared nerve injury: an animal model of persistent peripheral
906 neuropathic pain. *Pain, 87*(2), 149-158. doi: 10.1016/s0304-3959(00)00276-1
907 Devor, M. (2009). Ectopic discharge in Aβ afferents as a source of neuropathic pain. *Exp Brain Res,*
908 *196*(1), 115-128. doi: 10.1007/s00221-009-1724-6
909 Dvir, H., Elbaz, I., Havlin, S., Appelbaum, L., Ivanov, P. C., & Bartsch, R. P. (2018). Neuronal noise as an
910 origin of sleep arousals and its role in sudden infant death syndrome. *Sci Adv, 4*(4), eaar6277.
911 doi: 10.1126/sciadv.aar6277
912 Feige, B., Baglioni, C., Spiegelhalder, K., Hirscher, V., Nissen, C., & Riemann, D. (2013). The
913 microstructure of sleep in primary insomnia: an overview and extension. *Int J Psychophysiol,*
914 *89*(2), 171-180. doi: 10.1016/j.ijpsycho.2013.04.002
915 Feige, B., Nanovska, S., Baglioni, C., Bier, B., Cabrera, L., Diemers, S., Quellmalz, M., Siegel, M., Xeni, I.,
916 Szentkiralyi, A., Doerr, J. P., & Riemann, D. (2018). Insomnia-perchance a dream? Results from a
917 NREM/REM sleep awakening study in good sleepers and patients with insomnia. *Sleep, 41*(5).
918 doi: 10.1093/sleep/zsy032
919 Fernandez, L. M., Vantomme, G., Osorio-Forero, A., Cardis, R., Béard, E., & Lüthi, A. (2018). Thalamic
920 reticular control of local sleep in sensory cortex. *Elife*, e39111. doi: doi: 10.7554/eLife.39111
921 Fernandez, L. M. J., Lecci, S., Cardis, R., Vantomme, G., Béard, E., & Lüthi, A. (2017). Quantifying infra-
922 slow dynamics of spectral power and heart rate in sleeping mice. *J Vis Exp*(126). doi:
923 10.3791/55863
924 Fernandez, L. M. J., & Lüthi, A. (2020). Sleep Spindles: Mechanisms and Functions. *Physiol Rev, 100*(2),
925 805-868. doi: 10.1152/physrev.00042.2018

926 Finnerup, N. B., Attal, N., Haroutounian, S., McNicol, E., Baron, R., Dworkin, R. H., Gilron, I., Haanpaa, M.,
927 Hansson, P., Jensen, T. S., Kamerman, P. R., Lund, K., Moore, A., Raja, S. N., Rice, A. S.,
928 Rowbotham, M., Sena, E., Siddall, P., Smith, B. H., & Wallace, M. (2015). Pharmacotherapy for
929 neuropathic pain in adults: a systematic review and meta-analysis. *Lancet Neurol, 14*(2), 162-
930 173. doi: 10.1016/S1474-4422(14)70251-0
931 Finnerup, N. B., Kuner, R., & Jensen, T. S. (2021). Neuropathic pain: from mechanisms to treatment.
932 *Physiol Rev, 101*(1), 259-301. doi: 10.1152/physrev.00045.2019
933 Forget, D., Morin, C. M., & Bastien, C. H. (2011). The role of the spontaneous and evoked K-complex in
934 good-sleeper controls and in individuals with insomnia. *Sleep, 34*(9), 1251-1260. doi:
935 10.5665/SLEEP.1250
936 Franken, P. (2002). Long-term vs. short-term processes regulating REM sleep. *J Sleep Res, 11*(1), 17-28.
937 Franken, P., Malafosse, A., & Tafti, M. (1999). Genetic determinants of sleep regulation in inbred mice.
938 *Sleep, 22*(2), 155-169.
939 Fulda, S. (2011). Idiopathic REM sleep behavior disorder as a long-term predictor of neurodegenerative
940 disorders. *EPMA J, 2*(4), 451-458. doi: 10.1007/s13167-011-0096-8
941 Guida, F., De Gregorio, D., Palazzo, E., Ricciardi, F., Boccella, S., Belardo, C., Iannotta, M., Infantino, R.,
942 Formato, F., Marabese, I., Luongo, L., de Novellis, V., & Maione, S. (2020). Behavioral,
943 biochemical and electrophysiological changes in spared nerve injury model of neuropathic pain.
944 *Int J Mol Sci, 21*(9). doi: 10.3390/ijms21093396
945 Hayat, H., Regev, N., Matosevich, N., Sales, A., Paredes-Rodriguez, E., Krom, A. J., Bergman, L., Li, Y.,
946 Lavigne, M., Kremer, E. J., Yizhar, O., Pickering, A. E., & Nir, Y. (2020). Locus coeruleus
947 norepinephrine activity mediates sensory-evoked awakenings from sleep. *Sci Adv, 6*(15),
948 eaaz4232. doi: 10.1126/sciadv.aaz4232
949 Hohn, V. D., May, E. S., & Ploner, M. (2019). From correlation towards causality: modulating brain
950 rhythms of pain using transcranial alternating current stimulation. *Pain Rep, 4*(4), e723. doi:
951 10.1097/PR9.0000000000000723
952 Huang, Z. L., Mochizuki, T., Qu, W. M., Hong, Z. Y., Watanabe, T., Urade, Y., & Hayaishi, O. (2006).
953 Altered sleep-wake characteristics and lack of arousal response to H3 receptor antagonist in
954 histamine H1 receptor knockout mice. *Proc Natl Acad Sci U S A, 103*(12), 4687-4692. doi:
955 10.1073/pnas.0600451103

Iber, C., Ancoli-Israel, S., Chesson, A., & Quan, S. F. (2007). *The AASM manual for the scoring of sleep and associated events: rules, terminology and technical specifications.* Westchester, IL: American Academy of Sleep Medicine.

Kjaerby, C., Andersen, M., Hauglund, N., Ding, F., Wang, W., Xu, Q., Deng, S., Kang, N., Peng, S., Sun, Q., Dall, C., Jørgensen, P. K., Feng, J., Li, Y., Weikop, P., Hirase, H., & Nedergaard, M. (2020). Dynamic fluctuations of the locus coeruleus-norepinephrine system underlie sleep state transitions. *bioRxiv*, 2020.2009.2001.274977. doi: 10.1101/2020.09.01.274977

Kontinen, V. K., Ahnaou, A., Drinkenburg, W. H., & Meert, T. F. (2003). Sleep and EEG patterns in the chronic constriction injury model of neuropathic pain. *Physiol Behav, 78*(2), 241-246. doi: 10.1016/s0031-9384(02)00966-6

Kopp, C., Longordo, F., Nicholson, J. R., & Lüthi, A. (2006). Insufficient sleep reversibly alters bidirectional synaptic plasticity and NMDA receptor function. *J Neurosci, 26*(48), 12456-12465. doi: 10.1523/JNEUROSCI.2702-06.2006

Krystal, A. D., & Edinger, J. D. (2008). Measuring sleep quality. *Sleep Med, 9 Suppl 1*, S10-17. doi: 10.1016/S1389-9457(08)70011-X

Krystal, A. D., Edinger, J. D., Wohlgemuth, W. K., & Marsh, G. R. (2002). NREM sleep EEG frequency spectral correlates of sleep complaints in primary insomnia subtypes. *Sleep, 25*(6), 630-640.

Kuner, R., & Kuner, T. (2020). Cellular circuits in the brain and their modulation in acute and chronic pain. *Physiol Rev*. doi: 10.1152/physrev.00040.2019

Landis, C. A., Levine, J. D., & Robinson, C. R. (1989). Decreased slow-wave and paradoxical sleep in a rat chronic pain model. *Sleep, 12*(2), 167-177. doi: 10.1093/sleep/12.2.167

LeBlanc, B. W., Lii, T. R., Silverman, A. E., Alleyne, R. T., & Saab, C. Y. (2014). Cortical theta is increased while thalamocortical coherence is decreased in rat models of acute and chronic pain. *Pain, 155*(4), 773-782. doi: 10.1016/j.pain.2014.01.013

Lecci, S., Cataldi, J., Betta, M., Bernardi, G., Heinzer, R., & Siclari, F. (2020). EEG changes associated with subjective under- and overestimation of sleep duration. *Sleep, 43*, zsaa094. doi: 10.1093/sleep/zsaa094

Lecci, S., Fernandez, L. M., Weber, F. D., Cardis, R., Chatton, J. Y., Born, J., & Lüthi, A. (2017). Coordinated infraslow neural and cardiac oscillations mark fragility and offline periods in mammalian sleep. *Sci Adv, 3*(2), e1602026. doi: 10.1126/sciadv.1602026

Léna, C., Popa, D., Grailhe, R., Escourrou, P., Changeux, J. P., & Adrien, J. (2004). β2-containing nicotinic receptors contribute to the organization of sleep and regulate putative micro-arousals in mice. *J Neurosci, 24*(25), 5711-5718. doi: 10.1523/JNEUROSCI.3882-03.2004

Leys, L. J., Chu, K. L., Xu, J., Pai, M., Yang, H. S., Robb, H. M., Jarvis, M. F., Radek, R. J., & McGaraughty, S. (2013). Disturbances in slow-wave sleep are induced by models of bilateral inflammation, neuropathic, and postoperative pain, but not osteoarthritic pain in rats. *Pain, 154*(7), 1092-1102. doi: 10.1016/j.pain.2013.03.019

Li, S. B., Borniger, J. C., Yamaguchi, H., Hedou, J., Gaudilliere, B., & de Lecea, L. (2020). Hypothalamic circuitry underlying stress-induced insomnia and peripheral immunosuppression. *Sci Adv, 6*(37). doi: 10.1126/sciadv.abc2590

Lo, C. C., Chou, T., Penzel, T., Scammell, T. E., Strecker, R. E., Stanley, H. E., & Ivanov, P. (2004). Common scale-invariant patterns of sleep-wake transitions across mammalian species. *Proc Natl Acad Sci U S A, 101*(50), 17545-17548. doi: 10.1073/pnas.0408242101

Maes, J., Verbraecken, J., Willemen, M., De Volder, I., van Gastel, A., Michiels, N., Verbeek, I., Vandekerckhove, M., Wuyts, J., Haex, B., Willemen, T., Exadaktylos, V., Bulckaert, A., & Cluydts, R. (2014). Sleep misperception, EEG characteristics and autonomic nervous system activity in primary insomnia: a retrospective study on polysomnographic data. *Int J Psychophysiol, 91*(3), 163-171. doi: 10.1016/j.ijpsycho.2013.10.012

Mang, G. M., & Franken, P. (2012). Sleep and EEG phenotyping in mice. *Curr Protoc Mouse Biol, 2*(1), 55-74. doi: 10.1002/9780470942390.mo110126

Mathias, J. L., Cant, M. L., & Burke, A. L. J. (2018). Sleep disturbances and sleep disorders in adults living with chronic pain: a meta-analysis. *Sleep Med, 52*, 198-210. doi: 10.1016/j.sleep.2018.05.023

May, E. S., Nickel, M. M., Ta Dinh, S., Tiemann, L., Heitmann, H., Voth, I., Tolle, T. R., Gross, J., & Ploner, M. (2019). Prefrontal gamma oscillations reflect ongoing pain intensity in chronic back pain patients. *Hum Brain Mapp, 40*(1), 293-305. doi: 10.1002/hbm.24373

Moisset, X., & Bouhassira, D. (2007). Brain imaging of neuropathic pain. *Neuroimage, 37 Suppl 1*, S80-88. doi: 10.1016/j.neuroimage.2007.03.054

Moldofsky, H., Scarisbrick, P., England, R., & Smythe, H. (1975). Musculoskeletal symptoms and non-REM sleep disturbance in patients with "fibrositis syndrome" and healthy subjects. *Psychosom Med, 37*, 341-351.

Neckelmann, D., & Ursin, R. (1993). Sleep stages and EEG power spectrum in relation to acoustical stimulus arousal threshold in the rat. *Sleep, 16*(5), 467-477.

1018 Nickel, M. M., May, E. S., Tiemann, L., Postorino, M., Ta Dinh, S., & Ploner, M. (2017). Autonomic
1019 responses to tonic pain are more closely related to stimulus intensity than to pain intensity.
1020 *Pain, 158*(11), 2129-2136. doi: 10.1097/j.pain.0000000000001010
1021 Nobili, L., Ferrara, M., Moroni, F., De Gennaro, L., Russo, G. L., Campus, C., Cardinale, F., & De Carli, F.
1022 (2011). Dissociated wake-like and sleep-like electro-cortical activity during sleep. *Neuroimage,*
1023 *58*(2), 612-619. doi: 10.1016/j.neuroimage.2011.06.032
1024 Nollet, M., Hicks, H., McCarthy, A. P., Wu, H., Moller-Levet, C. S., Laing, E. E., Malki, K., Lawless, N.,
1025 Wafford, K. A., Dijk, D. J., & Winsky-Sommerer, R. (2019). REM sleep's unique associations with
1026 corticosterone regulation, apoptotic pathways, and behavior in chronic stress in mice. *Proc Natl*
1027 *Acad Sci U S A, 116*(7), 2733-2742. doi: 10.1073/pnas.1816456116
1028 Parrino, L., Milioli, G., De Paolis, F., Grassi, A., & Terzano, M. G. (2009). Paradoxical insomnia: the role of
1029 CAP and arousals in sleep misperception. *Sleep Med, 10*(10), 1139-1145. doi:
1030 10.1016/j.sleep.2008.12.014
1031 Perlis, M. L., Merica, H., Smith, M. T., & Giles, D. E. (2001a). Beta EEG activity and insomnia. *Sleep Med*
1032 *Rev, 5*(5), 363-374. doi: 10.1053/smrv.2001.0151
1033 Perlis, M. T., Smith, M. T., Andrews, P. J., Orff, H., & Giles, D. E. (2001b). Beta/Gamma EEG activity in
1034 patients with primary and secondary insomnia and good sleeper controls. *Sleep, 24*(1), 110-117.
1035 doi: 10.1093/sleep/24.1.110
1036 Ploner, M., Sorg, C., & Gross, J. (2017). Brain rhythms of pain. *Trends Cogn Sci, 21*(2), 100-110. doi:
1037 10.1016/j.tics.2016.12.001
1038 Radzicki, D., Pollema-Mays, S. L., Sanz-Clemente, A., & Martina, M. (2017). Loss of M1 receptor
1039 dependent cholinergic excitation contributes to mPFC deactivation in neuropathic pain. *J*
1040 *Neurosci, 37*(9), 2292-2304. doi: 10.1523/JNEUROSCI.1553-16.2017
1041 Riedner, B. A., Goldstein, M. R., Plante, D. T., Rumble, M. E., Ferrarelli, F., Tononi, G., & Benca, R. M.
1042 (2016). Regional patterns of elevated alpha and high-frequency electroencephalographic activity
1043 during nonrapid eye movement sleep in chronic insomnia: a pilot study. *Sleep, 39*(4), 801-812.
1044 doi: 10.5665/sleep.5632
1045 Rolls, A., Colas, D., Adamantidis, A., Carter, M., Lanre-Amos, T., Heller, H. C., & de Lecea, L. (2011).
1046 Optogenetic disruption of sleep continuity impairs memory consolidation. *Proc Natl Acad Sci U S*
1047 *A, 108*(32), 13305-13310. doi: 10.1073/pnas.1015633108

1048 Salin-Pascual, R. J., Roehrs, T. A., Merlotti, L. A., Zorick, F., & Roth, T. (1992). Long-term study of the
1049 sleep of insomnia patients with sleep state misperception and other insomnia patients. *Am J*
1050 *Psychiatry, 149*(7), 904-908. doi: 10.1176/ajp.149.7.904
1051 Sarnthein, J., Stern, J., Aufenberg, C., Rousson, V., & Jeanmonod, D. (2006). Increased EEG power and
1052 slowed dominant frequency in patients with neurogenic pain. *Brain, 129*(Pt 1), 55-64. doi:
1053 10.1093/brain/awh631
1054 Schulz, E., May, E. S., Postorino, M., Tiemann, L., Nickel, M. M., Witkovsky, V., Schmidt, P., Gross, J., &
1055 Ploner, M. (2015). Prefrontal gamma oscillations encode tonic pain in humans. *Cereb Cortex,*
1056 *25*(11), 4407-4414. doi: 10.1093/cercor/bhv043
1057 Sforza, E., Jouny, C., & Ibanez, V. (2000). Cardiac activation during arousal in humans: further evidence
1058 for hierarchy in the arousal response. *Clin Neurophysiol, 111*(9), 1611-1619. doi: 10.1016/s1388-
1059 2457(00)00363-1
1060 Shirvalkar, P., Veuthey, T. L., Dawes, H. E., & Chang, E. F. (2018). Closed-loop deep brain stimulation for
1061 refractory chronic pain. *Front Comput Neurosci, 12*, 18. doi: 10.3389/fncom.2018.00018
1062 Silva, A., Andersen, M. L., & Tufik, S. (2008). Sleep pattern in an experimental model of osteoarthritis.
1063 *Pain, 140*(3), 446-455. doi: 10.1016/j.pain.2008.09.025
1064 Silvani, A. (2019). Sleep disorders, nocturnal blood pressure, and cardiovascular risk: A translational
1065 perspective. *Auton Neurosci, 218*, 31-42. doi: 10.1016/j.autneu.2019.02.006
1066 Spiegelhalder, K., Regen, W., Feige, B., Holz, J., Piosczyk, H., Baglioni, C., Riemann, D., & Nissen, C.
1067 (2012). Increased EEG sigma and beta power during NREM sleep in primary insomnia. *Biol*
1068 *Psychol, 91*(3), 329-333. doi: 10.1016/j.biopsycho.2012.08.009
1069 St-Jean, G., Turcotte, I., & Bastien, C. H. (2012). Cerebral asymmetry in insomnia sufferers. *Front Neurol,*
1070 *3*, 47. doi: 10.3389/fneur.2012.00047
1071 Tan, L. L., Oswald, M. J., Heinl, C., Retana Romero, O. A., Kaushalya, S. K., Monyer, H., & Kuner, R. (2019).
1072 Gamma oscillations in somatosensory cortex recruit prefrontal and descending serotonergic
1073 pathways in aversion and nociception. *Nat Commun, 10*(1), 983. doi: 10.1038/s41467-019-
1074 08873-z
1075 Tokunaga, S., Takeda, Y., Shinomiya, K., Yamamoto, W., Utsu, Y., Toide, K., & Kamei, C. (2007). Changes
1076 of sleep patterns in rats with chronic constriction injury under aversive conditions. *Biol Pharm*
1077 *Bull, 30*(11), 2088-2090. doi: 10.1248/bpb.30.2088
1078 Treede, R. D., Rief, W., Barke, A., Aziz, Q., Bennett, M. I., Benoliel, R., Cohen, M., Evers, S., Finnerup, N.
1079 B., First, M. B., Giamberardino, M. A., Kaasa, S., Korwisi, B., Kosek, E., Lavand'homme, P.,

Nicholas, M., Perrot, S., Scholz, J., Schug, S., Smith, B. H., Svensson, P., Vlaeyen, J. W. S., & Wang, S. J. (2019). Chronic pain as a symptom or a disease: the IASP Classification of Chronic Pain for the International Classification of Diseases (ICD-11). *Pain, 160*(1), 19-27. doi: 10.1097/j.pain.0000000000001384

van Someren, E. J. W. (2020). Brain mechanisms of insomnia: new perspectives on causes and consequences. *Physiol Rev*, in press.

Vargas, I., Nguyen, A. M., Muench, A., Bastien, C. H., Ellis, J. G., & Perlis, M. L. (2020). Acute and chronic insomnia: what has time and/or hyperarousal got to do with it? *Brain Sci, 10*(2). doi: 10.3390/brainsci10020071

Vassalli, A., & Franken, P. (2017). Hypocretin (orexin) is critical in sustaining theta/gamma-rich waking behaviors that drive sleep need. *Proc Natl Acad Sci U S A, 114*(27), E5464-E5473. doi: 10.1073/pnas.1700983114

Wall, P. D., & Devor, M. (1983). Sensory afferent impulses originate from dorsal root ganglia as well as from the periphery in normal and nerve injured rats. *Pain, 17*(4), 321-339. doi: 10.1016/0304-3959(83)90164-1

Wei, Y., Colombo, M. A., Ramautar, J. R., Blanken, T. F., van der Werf, Y. D., Spiegelhalder, K., Feige, B., Riemann, D., & Van Someren, E. J. W. (2017). Sleep stage transition dynamics reveal specific stage 2 vulnerability in insomnia. *Sleep, 40*(9). doi: 10.1093/sleep/zsx117

Wimmer, R. D., Astori, S., Bond, C. T., Rovó, Z., Chatton, J. Y., Adelman, J. P., Franken, P., & Lüthi, A. (2012). Sustaining sleep spindles through enhanced SK2-channel activity consolidates sleep and elevates arousal threshold. *J Neurosci, 32*(40), 13917-13928. doi: 10.1523/JNEUROSCI.2313-12.2012

Yüzgeç, O., Prsa, M., Zimmermann, R., & Huber, D. (2018). Pupil size coupling to cortical states protects the stability of deep sleep via parasympathetic modulation. *Curr Biol, 28*(3), 392-400 e393. doi: 10.1016/j.cub.2017.12.049

Zhang, Z., Gadotti, V. M., Chen, L., Souza, I. A., Stemkowski, P. L., & Zamponi, G. W. (2015). Role of prelimbic GABAergic circuits in sensory and emotional aspects of neuropathic pain. *Cell Rep, 12*(5), 752-759. doi: 10.1016/j.celrep.2015.07.001

Supplementary figures

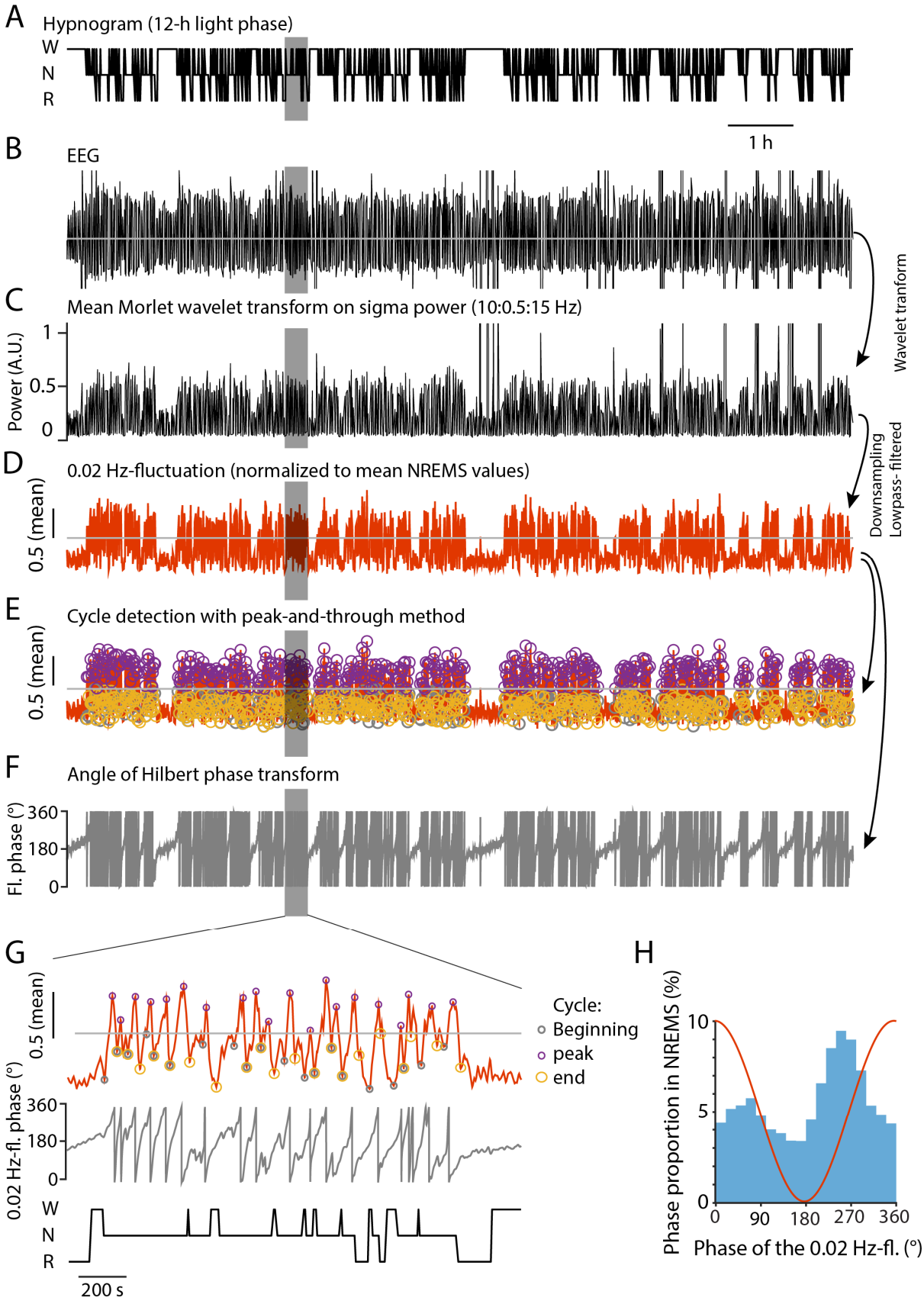

1112

Figure 2 – figure supplement 1 – Methodological illustration of how to extract the 0.02 Hz-fluctuation from raw signals, to detect individual cycles, and to calculate the angles of the Hilbert transform. (**A**) 12-h hypnogram obtained from visual scoring of EEG/EMG recordings. W, wakefulness; N, NREMS; R, REMS. (**B**) Corresponding EEG signal. (**C**) Corresponding mean Morlet wavelet transform, calculated in 0.5-Hz frequency bins from 10—15 Hz. (**D**) Corresponding 0.02 Hz-fluctuation, obtained through downsampling to 10 Hz and lowpass filtering. Normalization was done by dividing the signal by its mean value in NREMS. (**E**) Result of cycle detection on the signal shown in D, using the peak-and-trough detection approach described in the Methods. The beginning, peak and end of each cycle is shown with color-coded circles. (**F**) Angle of the Hilbert transform of the signal shown D. The values are wrapped around 360° with 180° representing the troughs of the fluctuation. (**G**) Expansion of the grey area highlighted for D, E, F and A. (**H**) Histogram showing the phase constitution of the 0.02 Hz-fluctuation. Note the prominence from 180—360°, indicating more time spent in ascending period compared to descending. A sinusoid would yield the same amount of points within each phase bin. Therefore, we now talk about 0.02 Hz-fluctuation and not oscillation as in (Lecci et al., 2017).

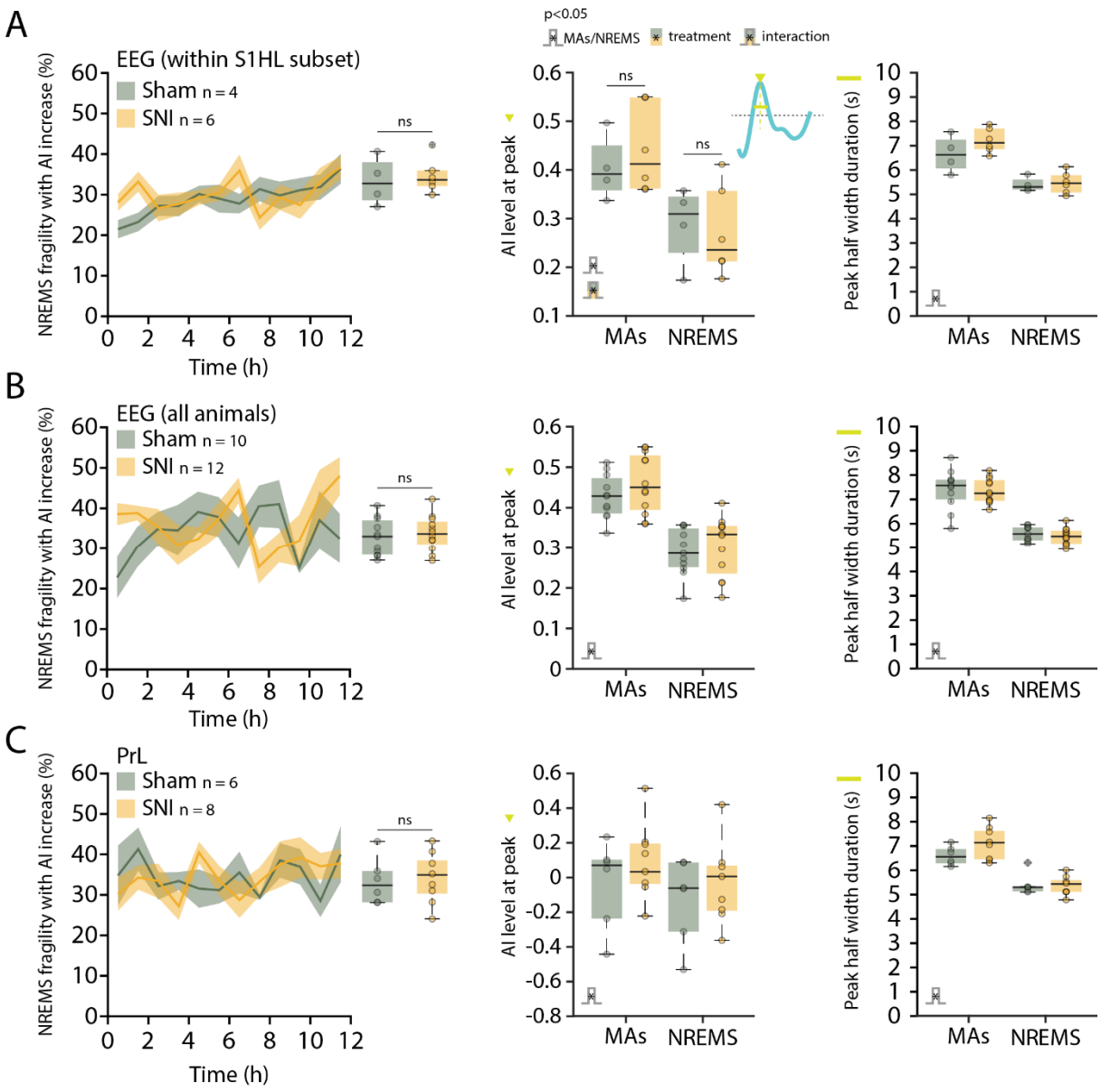

Figure 5 – figure supplement 2 – Activation index (AI) with peaks in fragility period are also present in EEG and PrL but occur in equal amounts in Sham or SNI. (**A**) Left, Proportion of fragility periods containing an AI peak over the 12-h light phase, detected in the frontoparietal EEG (contralateral to Sham or SNI surgeries) in the subset of animals from which the S1HL data were obtained in figure 5; sum rank test Sham vs SNI: W = 10, p = 0.76. The data from 1 Sham and 3 SNI animals were left out because the EEG was implanted ipsilateral to Sham or SNI surgeries. Middle: mean amplitude (green triangle in the inset) of the AI peaks in the EEG (S1HL subset), with or without the presence of a MA in the fragility period, in Sham and SNI. Mixed-model ANOVA: $F_{(1,8)}$ = 0.03, p = 0.85 for 'treatment'; $F_{(1,8)}$ = 224.9, p = 3.8×10^{-7} for 'MA'; $F_{(1,8)}$ = 6.83, p = 0.03 for interaction. *Post-hoc* rank sum test for Sham *vs* SNI for fragility periods with a MA: W = 9, p = 0.6; for fragility periods without a MA: W = 13, p = 0.91; signed rank test with *vs* without MA in Sham: V = 10, p = 0.12; in SNI: V = 21, p = 0.03 ; α = 0.0125. Right: half width duration (green line in the inset) of the AI peaks in the EEG (S1HL subset), with or without the presence of a MA in the fragility period, in Sham and SNI. Mixed-model ANOVA: $F_{(1,8)}$ = 2.06, p = 0.18 for 'treatment'; $F_{(1,8)}$ = 39.12, p = 2.4×10^{-4} for

'MA'; $F_{(1,8)}$ = 0.91, p = 0.36 for interaction. (**B**) Same layout as in A. Data from the frontoparietal EEG (contralateral to Sham or SNI surgeries) from all our animals; Left: proportion of fragility periods containing an AI peak, over time and 12 h quantification: unpaired *t*-tests Sham vs SNI: $t_{(21)}$ = -0.5, p = 0.62. Middle: mean amplitude of the AI peaks in the EEG with or without the presence of a MA in the fragility period, in Sham and SNI. Mixed-model ANOVA: $F_{(1,21)}$ = 0.81, p = 0.37 for 'treatment'; $F_{(1,21)}$ = 446.8, p = $1.23x10^{-15}$ for 'MA'; $F_{(1,21)}$ = 1.64, p = 0.21 for interaction. Right: duration at half-maximal amplitude of the AI peaks in the EEG, with or without the presence of a MA in the fragility period, in Sham and SNI. Mixed-model ANOVA: $F_{(1,21)}$ = 0.29, p = 0.59 for 'treatment'; $F_{(1,21)}$ = 174.9, p = $1.2x10^{-11}$ for 'MA'; $F_{(1,21)}$ = 0.03, p = 0.85 for interaction. (**C**) Same layout as in A and B. Data from the PrL cortex; Left: proportion of fragility periods containing an AI peak, over time and 12 h quantification: unpaired *t*-tests Sham vs SNI: $t_{(12)}$ = -0.23, p = 0.82. Middle: mean amplitude of the AI peaks in PrL with or without the presence of a MA in the fragility period, in Sham and SNI. Mixed-model ANOVA: $F_{(1,12)}$ = 0.89, p = 0.36 for 'treatment'; $F_{(1,12)}$ = 63.9, p = $3.7x10^{-6}$ for 'MA'; $F_{(1,12)}$ = 0.74, p = 0.4 for interaction. Right: duration at half-maximal amplitude of the AI peaks in the EEG, with or without the presence of a MA in the fragility period, in Sham and SNI. Mixed-model ANOVA: $F_{(1,12)}$ = 1.84, p = 0.19 for 'treatment'; $F_{(1,12)}$ = 50.26, p = $1.2x10^{-5}$ for 'MA'; $F_{(1,12)}$ = 1.71, p = 0.21 for interaction.

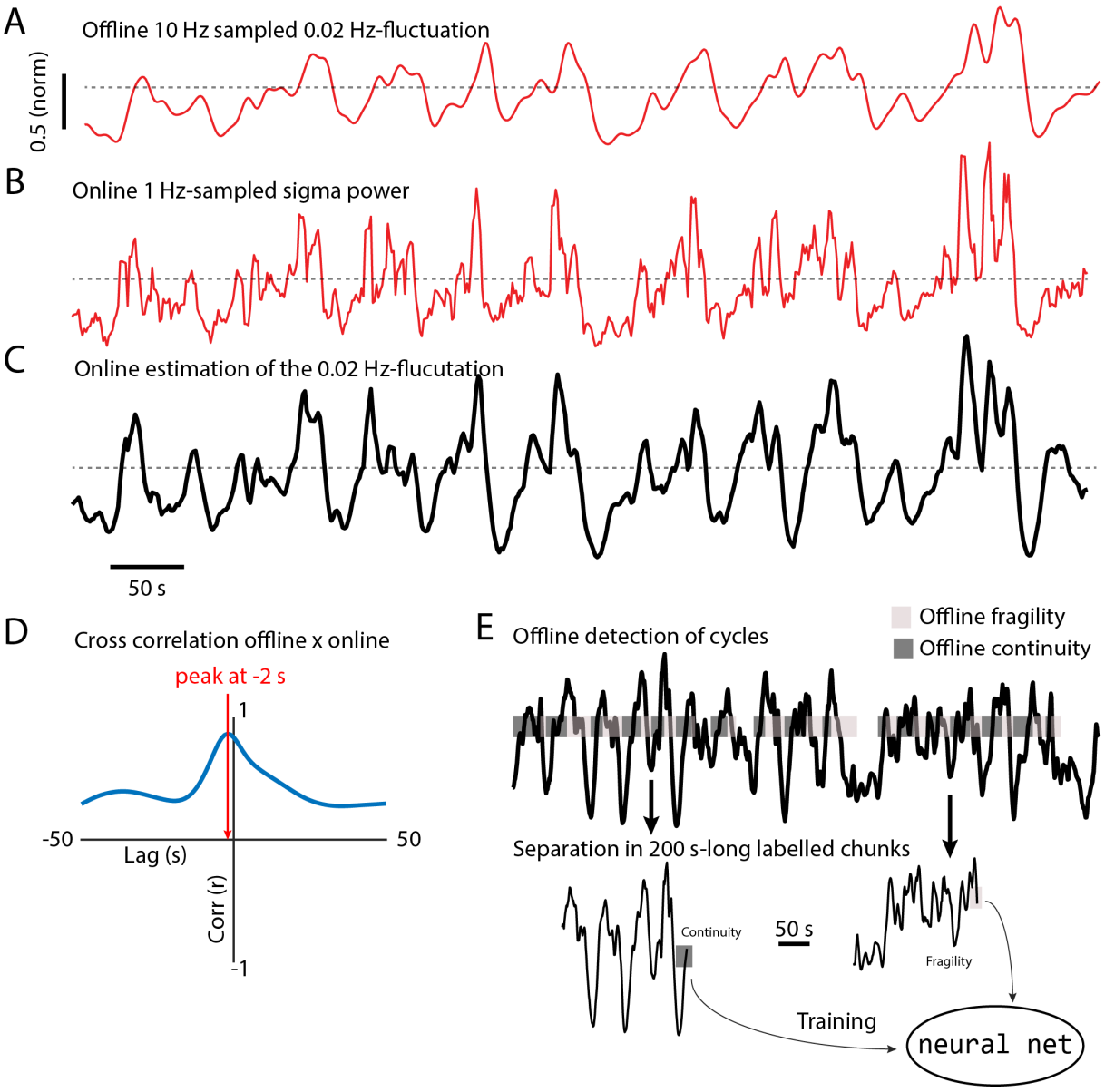

Figure 6 – figure supplement 3 – Online 0.02 Hz-fluctuation extraction and training of the neural network. (**A**) 0.02 Hz-fluctuation from a NREMS period extracted offline as described in ***Figure 2 - figure supplement 1***. (**B**) Corresponding sigma power values collected online at 1 Hz. (**C**) Corresponding online-estimated 0.02 Hz-fluctuation, based on a 9th order polynomial fit on the sigma values shown in B. (**D**) Validation of the online estimate through cross correlation with offline data from a 12 h recording from one animal. The red arrow indicates the position of the highest correlation, showing a minor lag (-2 s). (**E**) Illustration of data labeling to train the neural network. The cycle detection (see method) was used offline on the 0.02 Hz-fluctuation previously extracted online. Continuity was set to the ascending periods and fragility to the descending one. When conditions for complete cycles were not met, the label 'none' was applied. Then, 200 s-long chunks of this signal were extracted and labelled with continuity, fragility or none depending on the position of the last point.

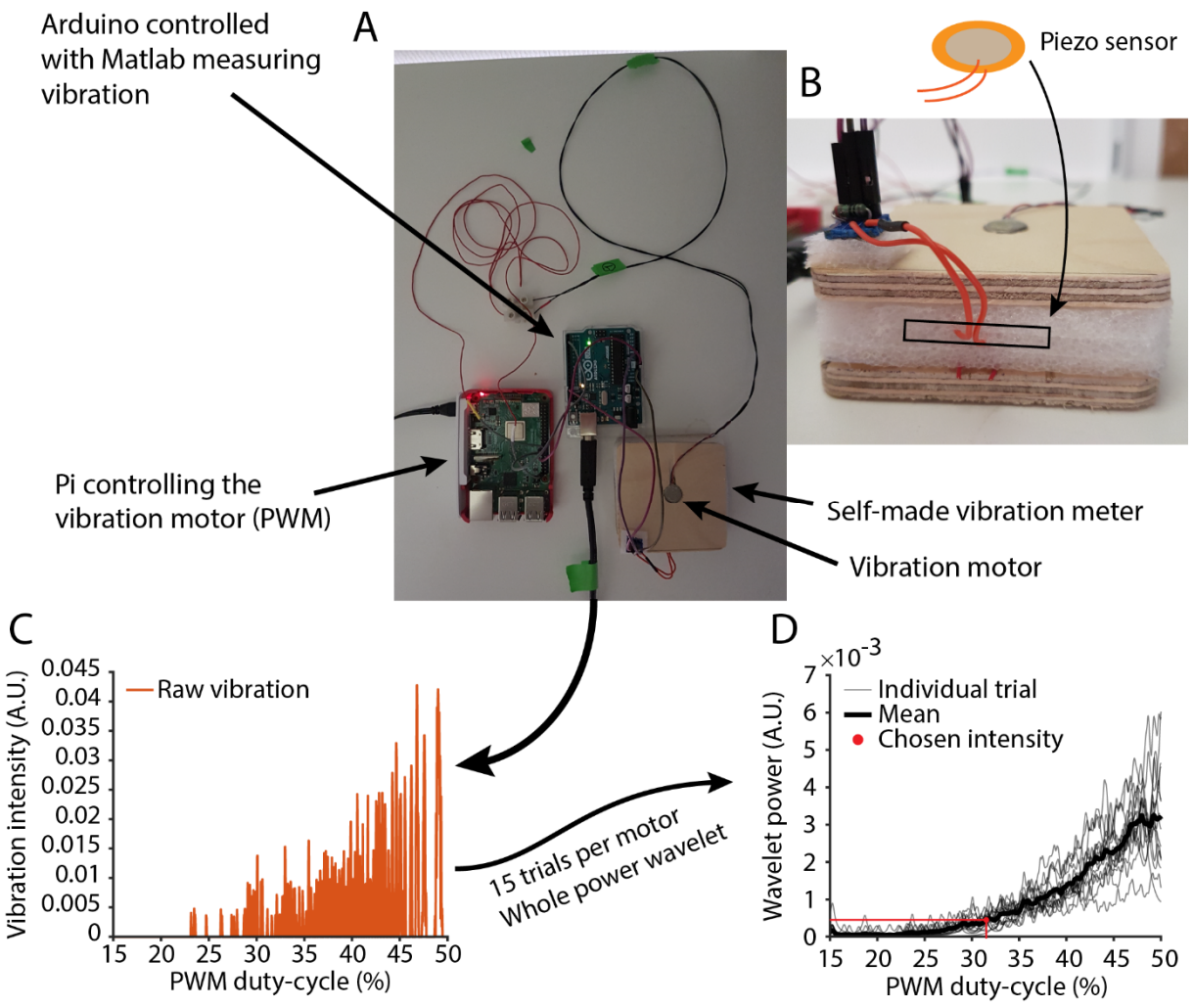

Figure 7 – figure supplement 4 – Vibration motor calibration for closed-loop somatosensory arousability testing. (**A**) Photo overview of the calibration setup, showing the vibration motor positioned onto a self-made piezometer containing the sensor (bottom right). The analog voltage generated by the sensor was measured by an Arduino and data fed into Matlab. To start vibrations, a raspberry pi sent a PWM signal to the vibration motor to modulate vibration intensity (achieved through increasing duty cycle from 15 to 50 %). A TTL signal sent from the raspberry pi to the Arduino initiated the trial. (**B**) Close-up view of the self-made piezometer. The piezometer was composed of protective foam sandwiched and glued between two thin wooden plates. The upper plate contained a hole the size of the vibration motors and the lower one was fixed to the table using two-sided adhesive tape. The piezo sensor was inserted inside the foam part and a resistance (1000 Ohm) was used in the circuit. (**C**) Plot of data received from one vibration measurement trial. The vibration curve was calculated from each trial using whole-power wavelet transform. (**D**) Calibration curve (mean of 15 trials) used to find the necessary duty-cycle value. The chosen intensity was the same for all the motors.

Infraslow locus coeruleus activity coordinates spindle rhythms and heart rate to gate fluctuating non-REM sleep substates

Alejandro Osorio-Forero, Romain Cardis, Gil Vantomme[1], Aurélie Guillaume-Gentil, Georgia Katsioudi[2], Laura M.J. Fernandez, Anita Lüthi[3]

Affiliation: Department of Fundamental Neurosciences, University of Lausanne, Rue du Bugnon 9, CH-1005 Lausanne, Switzerland

1 Present address: Department of Neurology, Wu Tsai Neurosciences Institute, Stanford University, 290 Jane Stanford Way, Stanford, CA94305, USA

2 Present address: Center for Integrative Genomics, University of Lausanne, Génopode, 1015 Lausanne, Switzerland

3 Corresponding author, e-mail: anita.luthi@unil.ch

Article Information:

Number of pages: 52

Total number of words (Introduction, Results, Discussion): 4,745

Number of Figures: 7

Number of words in Abstract: 150

Number of Supplementary Figures: 5

Number of references: 58 (+4 for Methods)

Keywords: continuity-fragility, arousability, parasympathetic, heart rate variability, targetted memory reactivation, hyperpolarization-activated cation channels

The continuity of non-rapid-eye-movement sleep (NREMS) is essential for its functions. However, many mammalian species, including humans, show NREMS fragility to maintain environmental vigilance. The neural substrates balancing NREMS continuity and fragility substates are unexplored. We show that the locus coeruleus (LC) is necessary and sufficient to generate infraslow (~50 s) continuity-fragility fluctuations in mouse NREMS. Through machine-learning-guided closed-loop optogenetic LC interrogation, we suppressed, locked, or entrained continuity-fragility fluctuations, as evident by LC-mediated regulation of sleep spindle clustering and heart rate variability. Noradrenergic modulation of thalamic but not cortical circuits was required for infraslow sleep spindle clustering and involved rapid noradrenaline increases that activated both α1- and β-adrenergic receptors to cause slowly decaying membrane depolarizations. The LC thus coordinates brain and bodily states during NREMS to engender continuity-fragility, accentuating its role in the physiology of sleep-related sensory uncoupling and as target in sleep disorders showing abnormal cortical and/or autonomic arousability.

Introduction

During sleep, behavioral interaction with the sensory environment is suppressed. The reduced response to external stimuli ensures a continuity of sleep in time that is necessary for its restorative and beneficial effects[1]. However, across the vertebrate kingdom, many species show adaptive mechanisms to continue monitoring their sensory environment while asleep. For example, unihemispheric sleep permits dolphins to continue surfacing to breathe or birds to engage in long-duration flights[2]. Sleeping humans also show sensory processing and cognitive elaboration of external stimuli during non-rapid-eye-movement sleep (NREMS) and REM sleep[3]. Incorporating sleep fragility to allow sensory vigilance could represent an adaptive strategy to trade-off between the benefits and risks of suppressed interactions with the environment. However, the neural implementations of such trade-off have not been pursued systematically. Therefore, it is unclear whether continuity-fragility dynamics are part of the design of vertebrate sleep-wake control circuits or reflect species-specific adaptations to particular ecological constraints.

Examinations of sensory arousability in rodent suggest that sensory isolation and environmental monitoring during NREMS occur, at least in part, sequentially in time. Based on monitoring arousability in response to auditory[4] or visual[5] stimuli, consolidated NREMS could be divided into substates of continuity and fragility that showed low and high arousability, respectively. Continuity-fragility substates alternated on an infraslow time scale of ~50 s (~0.02 Hz) and were accompanied by coordinated fluctuations in central and autonomic physiological correlates that were also found in human sleep[4]. These involved the electroencephalographic (EEG) spectral power component representing sleep spindles in the 10 – 15 Hz range, known to arise in thalamus and to be sleep-protective[3,6], and hippocampal ripples that are implied in sleep-dependent memory consolidation[7]. Moreover, both heart rate (HR) and pupil diameter co-varied such that increases coincided with low spindle occurrence. Infraslow variations are also prevalent in human NREMS, appearing in band-limited and full-band power EEG recordings, intracranial recordings, and in functional resonance imaging signals[4,8]. The time scale is also prominent in human cyclic alternating patterns, referred to as unstable sleep[9], in epilepsy and in abnormal arousal events in sleep-related movement and breathing disorders (reviewed in ref. [6]). However, the neural drives of infraslow

dynamics during NREMS have remained open, although neural and astrocytic mechanisms have been suggested[10].

Already the first recordings of action potentials in the sleeping animal indicated that wake-promoting brain areas retained some activity during NREMS[11-14]. The locus coeruleus (LC), the most dorsal of ten noradrenergic nuclei located in the pontine brain stem[11], ramifies widely within both the forebrain and the autonomic premotor nuclei[15] and coordinates neural and somatic conditions during wakefulness[16]. The LC discharges irregularly but continuously at 1 – 5 Hz when awake[11], but phasic discharges around 10 – 15 Hz precede autonomic and behavioral adaptations to unexpected stimuli in animals[17] and probably also in humans[18]. LC activity during NREMS coincides with the appearance of EEG or hippocampal sleep spindles[11,19,20] or cortical slow waves[21,22]. Opto- or chemogenetic LC stimulation in NREMS of rodents lowers auditory arousal thresholds[23] and increases resting state connectivity in salience networks[24], which is a signature of enhanced vigilance. Variations of LC activity during NREMS could thus be relevant for continuity-fragility fluctuations. Here, we used closed-loop real-time optogenetic modulation of LC activity in combination with global and local sleep recordings, HR monitoring, fiber photometric assessment of norepinephrine (NE) levels and the analysis of synaptic potentials generated by LC afferents in vitro. We demonstrate that infraslow activity variations in LC occur in natural undisturbed NREMS and coordinate central and autonomic physiological correlates underlying continuity-fragility fluctuations of NREMS.

Results

Noradrenergic signaling in thalamus is crucial for the clustering of sleep spindles during NREMS

Freely behaving mice sleep in NREM-REM sleep bouts interspersed by wakefulness during the light period (ZT0-12), which is their preferred resting phase. Figure 1a presents the sleep-wake behavior of a single mouse showing a hypnogram obtained from polysomnographic recordings between ZT1 and ZT9 and the corresponding time-frequency distribution derived from local field potential (LFP) recordings in the primary somatosensory cortex S1 (see Methods). From this distribution, power dynamics in two frequency bands characteristic for NREMS, the sigma (10 – 15 Hz) and the delta (1.5 – 4 Hz) frequency bands, were calculated. As shown previously[4], prominent power fluctuations in the sigma but not the delta

frequency band (10 – 15 Hz) determine NREMS continuity-fragility substates on an infraslow time interval with a peak around ~0.02 Hz (~50 s) (Fig. 1b). The sigma frequency band is populated by sleep spindles[6] that contribute to sensory decoupling during NREMS[3,6]. To determine whether sleep spindle density co-varied over 0.02 Hz, we used a previously developed sleep spindle detection algorithm[25] (Extended Data Fig. 1) and analyzed the phase-locking between sigma power and sleep spindle density in n = 33 mice (12 C57BL/6J and 21 dopamine-beta-hydroxylase (DBH)-Cre mice) recorded during the light phase. Sleep spindles clustered at the peak of the 0.02 Hz-fluctuation in sigma power, whereas they were rare in the troughs (Fig. 1c,d). Polar plots depicting the phase coupling of 168,097 spindles of 33 mice to the 0.02 Hz-fluctuation demonstrate the non-uniformity of this distribution (Fig. 1d; R of Rayleigh 0.51 ± 0.07; $P < 1.0*10^{-16}$). Sleep spindles thus cluster on the 50-s time scale during NREMS, in line with the infraslow fluctuation of sigma power and consistent with reports in mice and human[26,27].

To elucidate the role of noradrenergic signaling for infraslow variations in spindle density, we pharmacologically blocked noradrenergic receptors in thalamus, within which sleep spindles originate[6]. C57BL/6J mice implanted for polysomnography and S1 LFP recordings were injected with a mix of α1- and β- noradrenergic antagonists (0.1 mM Prazosine hydrochloride and 5 mM ((S)-(-)-atenolol, 150 nl, n = 6) or control artificial cerebrospinal fluid (ACSF, 150 nl, n = 6) locally into the somatosensory thalamus (see Methods). Noradrenergic antagonist but not ACSF injections resulted in a rapid and reversible reduction of the strength of the 0.02-Hz fluctuation in sigma power (Fig. 1e,f; Extended Data Fig. 2; P = 0.031). Moreover, instead of being clustered, sleep spindles now appeared irregularly and at a mean density that was ~2-fold higher (Fig. 1f; $P = 3.9*10^{-4}$). The properties of individual spindle events including amplitude, intra-spindle frequency, number of cycles and duration, showed minor changes (Extended Data Fig. 3). Noradrenergic signaling appears thus necessary for the generation of spindle-free periods resulting in their repeated clustering on the infraslow time scale.

Activity of the locus coeruleus is necessary and sufficient for the infraslow clustering of sleep spindles

To optogenetically interfere with the activity of the noradrenergic LC during NREMS in a time-controlled manner, we virally infected LC neurons of DBH-Cre mice to express excitatory (hChR2(H134R)

(ChR2); n = 11) or inhibitory (Jaws; n = 10) opsins. We then implanted these animals with EEG/EMG, an S1 LFP electrode and an optic fiber positioned uni- (for ChR2-injected animals) or bilaterally (for Jaws-injected animals) over the LC (Fig. 2a,b). Optimal fiber positioning was ensured through intra-surgical pupil diameter monitoring (Extended Data Fig 4). Using closed-loop monitoring of vigilance states, we first stimulated the LC specifically during NREMS at a low frequency (1 Hz) (Fig. 2c), and confirmed the successful expression of the opsins post mortem (Fig. 2d). The 1-Hz frequency is within the range of spontaneous LC unit activity during NREMS[19,21,28] and does not cause arousal when used to stimulate the LC optogenetically[19,29]. Stimulation sessions took place in the first 20 min of each hour during 8 h of the light phase (ZT1-9), with light or sham (during which the light source was turned off) stimulation alternating over successive recording days. Light stimulation in NREMS produced a rapid onset and almost complete suppression of sigma power and of sleep spindles. The effect lasted as long as light was present and instantly recovered once optogenetic stimulation stopped (Fig. 2e), decreasing the strength of the 0.02 Hz-fluctuation and sleep spindle density (Fig. 2f; n = 11, $P = 1.5*10^{-6}$ for the strength of the 0.02-Hz fluctuation, $P = 5.2*10^{-7}$ for spindle density). Conversely, continuous optogenetic inhibition according to the same experimental protocol locked sigma power at high levels and prolonged phases of high spindle occurrence (Fig. 2g,h; n = 10, $P = 2.0*10^{-3}$ for the strength of the 0.02-Hz fluctuation, $P = 2.0*10^{-3}$ for spindle density). These results demonstrate that LC activity is both necessary and sufficient for the 0.02 Hz-fluctuation and the clustering of sleep spindles.

To ensure that the LC interrogation did not disrupt NREMS, we quantified total times spent in the different vigilance states. We found that LC stimulation prolonged total time spent in NREMS at the expense of REM sleep and wakefulness (Fig. 2i), whereas LC inhibition had mild but opposite effects (Fig. 2j). These architectural alterations were not accompanied by significant changes in relative delta power (stimulation: increase by 13%, p = 0.10; inhibition: decrease <1%, p = 0.9). Therefore, low-frequency LC activity appears to consolidate NREMS without concomitant major changes in low-frequency spectral activity. This could be explained by the incompatibility of monoaminergic signaling with REM sleep, which would cause NREMS to continue[11,20,30].

Locus coeruleus fiber activation in thalamus but not in the cortex is relevant for sleep spindle clustering

From their thalamic site of origin, sleep spindle activity propagates to cortical circuits[6]. As LC innervates both thalamic and cortical brain areas[31], we tested the involvement of both innervation sites in the effects observed by direct LC stimulation. We placed the optic fiber over somatosensory thalamus or S1. For S1, the optic fiber stub was glued to the S1 LFP electrode at a distance of 800 – 1,200 µm over the tip. Light stimulation of thalamic LC afferents reproduced the suppressive effects observed with direct LC stimulation (Fig. 3 a,b; n = 6, $P = 5.6*10^{-4}$ for the strength of the 0.02-Hz fluctuation; $P = 0.014$ for spindle density). In contrast, cortical stimulation was ineffective (Fig. 3 c,d; n= 5, $P = 0.44$ for the strength of the 0.02-Hz fluctuation; $P = 0.63$ for spindle density). Thus, synaptic noradrenergic activity within the thalamus appears to sensitively control the clustering of sleep spindles measured in S1, in agreement with the pharmacological results in Fig 1.

Locus coeruleus activity fluctuates between high and low levels on an infraslow time scale

LC cells can discharge action potentials in both tonic and phasic modes during wakefulness, and both these modes have also been proposed to occur during NREMS[11,20,21]. To address whether time variations in LC activity were relevant for infraslow clustering of sleep spindles, we restricted the optogenetic manipulation of LC activity to distinct phases of the infraslow cycles. We detected these phases online through a machine-learning algorithm and triggered optogenetic activation based on whether sigma power started to rise or decline, thereby targetting large portions of fragility or continuity periods[32] (Fig. 4). When we optogenetically activated LC whenever sigma power started rising, the 0.02-Hz fluctuation was suppressed (Fig. 4 a,b; n = 9, $P = 4.4*10^{-9}$ for the strength of the 0.02-Hz fluctuation, $P = 2.2*10^{-6}$ for spindle density). This indicates that sigma increases, and sleep spindle generation, are not compatible with high LC activity. Conversely, when we inhibited LC when sigma power started declining, sigma power fluctuations became disrupted and tended to persist at high levels, thereby increasing sleep spindle density (Fig. 4 c,d; n = 10, $P = 2.0*10^{-3}$ for the strength of the 0.02-Hz fluctuation, $P = 5.9*10^{-3}$ for spindle density). The decline in sigma power thus required LC activity. These two results are best

compatible with LC activity showing an infraslow variation that is opposite to the one of the sigma power and sleep spindles, being high during the fragility periods and low during continuity periods, respectively.

Based on this result, we predicted that the converse experiment, stimulating LC during fragility or inhibiting it during continuity, would not disrupt infraslow dynamics. Intriguingly, when LC was activated while sigma power was declining, successive cycles of high sigma power kept appearing (Fig. 4e). Close inspection revealed that cycles appeared at shorter time intervals (sham: 52.9 ± 0.7 s, stim: 44.6 ± 1.7 s, n = 9, $P = 5.0*10^{-7}$, paired *t*-test) and were more regular, as evident by the decreased peak-to-peak variability (Fig. 4f; n = 9, $P = 5.2*10^{-5}$). Strengthening LC activity during fragility periods thus entrained a regular and faster infraslow fluctuation. When we specifically inhibited LC activity during online detected continuity periods, an entrainment was again observed, with interpeak intervals shortened (Fig. 4g; sham: 53.7 ± 2.6, inhibition: 50.8 ± 1.5 s, n = 9, $P = 3.6*10^{-3}$, paired *t*-test) and regularized (Fig. 4h; n = 10, $P = 0.049$). This indicates that a low level of LC activity remained during continuity periods that was inhibited by the light, thereby enforcing LC silency during sigma build-up and regularizing spindle appearance. Together, these results bring about a functionally relevant LC activity pattern during NREMS that interchanges between high, perhaps more phasic, and low, probably tonic, activity at infraslow timescales.

Rapid increases of noradrenaline levels in the thalamus precede the suppression of sleep spindles

High LC activity is expected to release NE within thalamus and to stimulate noradrenergic receptors as long as NE uptake is not completed. However, it is unclear how the time course of free NE and receptor signaling determine the time course of sleep spindle dis- and re-appearance. We used fiber photometry to measure free NE levels in thalamic nuclei across the sleep-wake cycle by expressing the newly developed fluorescent NE biosensor $GRAB_{NE1h}$[33] (see Methods). Mice expressing the NE biosensor in thalamus were implanted for sleep monitoring and fiber photometry. The fluorescence signals varied characteristically across the three vigilance states, including a pronounced decline during REM sleep, reminiscent of observations in prefrontal cortex (Fig. 5a)[20]. Focusing on NREMS bouts only, NE signals were inversely correlated with sigma power and showed recurrent negative peaks at infraslow intervals

(Fig. 5b). To resolve the time course of noradrenergic signaling on a cycle-to-cycle basis, we detected all infraslow sigma power cycles taking place during NREMS (excluding transitional periods) and examined the corresponding dynamics of free NE (Fig. 5c). Major increases in NE levels were detected before sigma power declined, consistent with the suppressant effects of LC activity. In contrast, NE levels were comparatively low as sigma power was rising at the beginning of the cycle. Therefore, NE increases suppress sigma power while NE decays seemed not tightly linked to the sigma power increases.

Ionic mechanisms underlying norepinephrine-induced infraslow membrane depolarizations

The effects of NE on neuronal excitability determine thalamic engagement in spindle-like rhythms[34], but the time range and actions of NE released by LC fibers on thalamic membrane potential and excitability are unknown. We hence combined patch-clamp recordings with optogenetic LC fiber stimulation to quantify cellular noradrenergic responses. We studied thalamocortical and thalamic reticular neurons, both of which are involved in sleep spindle generation[6]. From DBH-Cre mice expressing ChR2 in LC, we prepared coronal thalamic slices and recorded from cells in the ventrobasal complex, which contains the somatosensory thalamus. Thalamocortical cells had resting membrane potentials between -65 to -70 mV, and responded with rebound burst discharge upon negative current injection (Extended Data Fig. 5). Optogenetic stimulation generated a slow membrane depolarization for stimulation frequencies at 1, 3 and 10 Hz (Fig. 6a). Amplitudes of evoked potentials ranged between 0.8 – 4.5 mV with onset latencies of 1.25 – 6.9 s, and decayed with a slow time course lasting 66 – 106 s (Fig. 6b, Extended Data Fig. 5; n = 6 – 8). Only onset latency was modulated by stimulation frequency. The optogenetically evoked noradrenergic currents measured in cells voltage-clamped at -70 mV were blocked by atenolol (10 µM in bath, n = 5, $P = 0.049$), indicating involvement of β-adrenergic receptors (Fig. 6c,d)[34]. Furthermore, the current response was largely eliminated by bath application of 1.5 – 3 mM Cs^+ (Fig. 6e,f; n = 6, $P = 5.4x10^{-4}$), a blocker of cAMP-sensitive hyperpolarization-activated cation-channels[35]. Both atenolol and Cs^+ produced outward currents, indicating a standing receptor and current activation.

To estimate the time course of action of NE on spindle-related cellular activity, we combined optogenetic stimulation of LC fibers with negative current injections to generate repetitive low-threshold

burst discharges[35], known to occur during sleep spindles (Fig. 6g)[6]. This resulted in a persistent afterdepolarization that was larger and longer than the one generated by cellular bursting alone (Fig. 6h; n = 7, $P = 0.043$). The coincidence of sleep spindle activity with NE release thus generates a prolonged period of cellular depolarization, known to be sufficient to render thalamocortical cells refractory to synaptically-driven burst discharge, which is necessary to engage in a next sleep spindle[35].

Light-induced depolarizations were also observed in thalamic reticular cells recorded in the somatosensory sector of TRN (Fig. 6i,j). Corresponding currents were largely blocked by the α1-adrenergic antagonist prazosin (5 µM in bath) (Fig. 6k,l; n = 3; $P = 0.014$)[34]. However, < 15% of TRN cells showed a detectable current response (Fig. 6m), suggesting a functional heterogeneity of these cells with respect to noradrenergic modulation[36]. Thalamic reticular cells thus also respond with slowly decaying membrane depolarizations when exposed to NE release from LC fibers.

The locus coeruleus coordinates heart rate variability with sigma power on the infraslow time scale through parasympathetic signaling

As NREMS fluctuates between continuity and fragility, sigma power is anticorrelated with the HR on an infraslow time scale[4]. Is the LC involved in this coordination? Through conjointly monitoring HR and sigma power in freely sleeping C57BL/6J mice (Fig. 7a,b), we found that HR variations were suppressed by the peripheral parasympathetic antagonist methylatropine (10 mg kg^{-1}) (Fig. 7c,d; n = 7, $P = 0.035$) but not by the peripheral sympathetic antagonist atenolol (1 mg kg^{-1}) (Fig. 7e,f; n = 12, $P = 0.74$) (see Methods).

LC activity has been implied in parasympathetically driven HR variability in humans[37] and, in rodents, augments inhibitory input to preganglionic cardiac vagal neurons[38]. Therefore, we next tested whether optogenetic manipulation of LC affected variations in HR. Indeed, continuous LC stimulation during NREMS disrupted the infraslow HR variations (Fig. 7g) and decreased its anticorrelation with sigma power (Fig. 7h; n = 10, $P = 4.1 \times 10^{-3}$). To directly evaluate the capability of LC in entraining HR variations as we observed for sigma power (see Fig. 4e), we stimulated LC specifically during fragility periods. This visibly augmented HR variations and generated anticorrelations with side-peaks showing an infraslow periodicity (Fig. 7i,j; n = 8). These data show that the LC is a source of HR variability during

NREMS on an infraslow timescale. Moreover, LC is capable of coordinating sigma power and HR in a manner that supports a critical role in the generation of NREMS continuity and fragility substates.

Discussion

Noradrenergic cell groups in the rostral hindbrain are conserved across mammals, reptiles, amphibians, birds and fish[39], and they are central for wakefulness and vigilance towards the sensory world[17]. Here, we establish an analogous function for the mammalian LC during NREMS. Through imposing fluctuations in brain and body correlates of sensory arousability, the LC drives NREMS between two opposite states of continuity and fragility. Mechanistically, these are distinct by infraslow membrane fluctuations ot thalamic networks and by different HR, caused by NE-induced activation of α1- and β-adrenergic receptors and by regulation of autonomic parasympathetic output, respectively.

The infraslow time scale has not only been found in mammalian NREMS[8], but it also appears as a time scale over which reptile sleep switches between two electrophysiologically distinct sleep states[40]. This raises the possibility that infraslow time intervals are a phylogenetically preserved temporal unit to maintain vigilance that arises from fluctuating noradrenergic input during NREMS. This possibility could spur future comparative studies on the phylogeny of sleep states and how these relate to species-specific noradrenergic activity during sleep[2]. Furthermore, the human noradrenergic system remains active during NREMS[22], during which it is critical for memory consolidation[41], expression of plasticity-related genes[42] and perhaps for dreams[43]. As sleep spindles serve as EEG hallmarks to distinguish light and deep sleep states in human[6], monitoring the LC in human sleep could also shed light on these and other[9,44] unique aspects of primate sleep. Finally, there is strong evidence that LC and sleep disruptions could be linked in post-traumatic stress disorders[45], in neurodegenerative diseases such as Alzheimer's and Parkinson's disease[44,46] and in insomnia[47]. Our findings highlight a need to further develop tools to monitor LC activity in human sleep as a possible neural target for the origin of these sleep disruptions. Furthermore, we suggest that looking at the detailed temporal organization of sleep spindle occurrence[48] could help to gain insight into noradrenergic activity in human NREMS.

Implications of infraslow LC activity variations for NREMS heterogeneity and targetted memory reactivation

We find that the major wake-promoting noradrenergic nucleus of the mammalian brain is functionally active during NREMS, elevating NE levels in a pulsatile manner within thalamus. Similar patterns of free NE were also found in prefrontal cortex[20], suggesting that there is a fluctuating neuromodulatory tone of NE throughout the forebrain during NREMS. We directly show that these pulses affect primary thalamic sensory neuron excitability, underscoring previous propositions of NREMS as a heterogeneous state with distinct levels of sensory arousability[4,5]. Future research will examine whether the brain states accompanied by variable LC activity differ with respect to other neuromodulators and electrical activity patterns, as proposed for hippocampal ripples[4] or cortical slow waves[22,28,43]. Of particular interest will also be to determine whether variations in functional connectivity during NREMS[49], area-specific spectral properties[25] and cortical dendritic Ca^{2+} activity[50], other polysomnographic measures of unstable sleep[9] or other forms of behavioral output[51] relate to LC. Intriguingly, a recent study pointed out that the optimal timing of targetted memory reactivation via auditory stimuli depends on sleep spindle variations that involve infraslow timing[48]. This reinforces the notion that NREMS is segregated into functionally distinct states that also concern the sleeping brain's capability of neuronal ensemble reactivation and the replay of memory traces, which are prerequisites for memory consolidation[7].

LC-dependent control of sensory arousability during NREMS

LC activity likely controls sensory arousability through several mechanisms. First, LC responds to sensory stimuli[14], therefore, if LC neurons depolarize and discharge more action potentials, sensory throughput will be enhanced[23]. Second, LC-mediated sleep spindle suppression removes inhibitory constraints on the successful propagation of sensory inputs across the thalamocortical axis[6]. Third, sensory-evoked discharge of single or multiple thalamic and cortical units is strengthened by LC stimulation, with thalamic neurons increasing sensory responsiveness more robustly[52]. The density of LC fiber varicosities is higher in rat somatosensory thalamic compared to cortical areas[31]. In both rodents and humans, noradrenergic signaling strengthens precisely those resting state networks that optimize vigilance and perception in response to pending important input[24,53]. These findings offer several entry

points to further examine how noradrenergic modulation of thalamic circuits facilitates the processing of sensory stimuli during states of NREMS.

The role of LC for sleep spindles

Evidence that LC activity suppresses spindle activity is available for electrographically detected sleep spindles measured in hippocampus[19] and for spindles in bipolar EEG derivations[20]. Furthermore, NE levels in prefrontal cortex are low when the EEG shows spindles[20]. We demonstrate a direct mechanistic opposition between NE levels and the circuits in which sleep spindles originate. First, we rapidly and reversibly suppress local sleep spindles[25] via optogenetic LC activation and second, we find that free NE levels run opposite to locally generated sleep spindles. Third, we demonstrate that LC fiber activation promotes thalamic circuit refractoriness. The suppressive action of noradrenergic activity on sleep spindles has led to the proposition that LC activity will acutely terminate individual sleep spindle events[11,19]. However, we could not observe strong changes in sleep spindle properties in favor of this suggestion, when we pharmacologically antagonized noradrenergic signaling specifically in thalamus, although we previously identified our detection algorithm to sensitively detect regionally specific or genetically induced variations in sleep spindle properties[25]. Furthermore, we find that synaptic events caused by NE release rise slowly over seconds and are thus unlikely to shortcut individual spindle-events. Noradrenergic signaling seems instead tailored to generate prolonged relatively spindle-free periods as thalamic cells are brought into a depolarized state[35].

The cellular and ionic mechanisms underlying infraslow dynamics of sleep spindle clustering

The precise cellular mechanisms that underlie the particularly slow timing of the fluctuations in sigma power and spindle density have remained open[10]. We managed to dissect the temporal relationships between free NE levels and their ionic effects on thalamic spindle-generating circuits. The fiber photometric in combination with the cellular recording suggest that the ionic consequences of NE outlast the availability of free NE and are of primary interest as temporal determinants of the infraslow time scale. NE induces a slowly decaying membrane depolarization through activation of both α1- or β-receptors in thalamocortical and thalamic reticular neurons, which retards the re-engagement of these

cells in sleep spindle generation long after free NE levels have returned to baseline. In further support of this interpretation, we could entrain the infraslow fluctuations when we reinforced or attenuated LC activity at appropriate moments. The reinforcement of LC activity most likely triggered membrane depolarizations more consequentially across large cell populations, whereas the attenuation removed spurious LC activity, overall promoting a more synchronous entry and exit of thalamic circuits within the infraslow cycles. We remark that such a scenario does not preclude that other mechanisms causing individual spindles to terminate take place (reviewed in ref. [6]). Moreover, we currently cannot exclude that there are feedback mechanisms on the LC that modify, and perhaps accelerate, its endogenous infraslow activity.

To the best of our knowledge, the slow LC-triggered membrane depolarizations described here are the sole exclusively noradrenergically mediated postsynaptic effects described so far. LC fibers release glutamate to generate fast glutamatergic currents in parabrachial nucleus[54], with the release of NE remaining minor unless light pulses were applied repetitively at higher frequencies. We found instead that thalamic LC-fiber-elicited responses were relatively uniform in amplitude and time course over the 1 – 10 Hz frequency range. This could ensure a homogeneity of action on thalamic membrane potentials, resulting in a global depolarization across many neurons. Ultrastructural studies indeed suggest that noradrenergic terminals in the rodent ventrobasal complex do not form well-defined synaptic contacts[55], suggesting that released NE may diffuse from the site of release into the extracellular medium. Supporting this, we find that noradrenergic receptors activated by optogenetic LC fiber stimulation are the same as the ones targeted by bath-applied NE[34]. There also was a measurable noradrenergic antagonist-sensitive holding current component in our slices, consistent with an ambient NE level generating a tonic noradrenergic signal.

The LC as a source of heart rate variability

Initial studies on the continuity-fragility organization of NREMS pointed out that an infraslow periodicity was also present in the HR[4] and in pupil diameter[5]. The fragility period, during which spindles are infrequent and arousals more likely, was accompanied by a higher HR and a larger pupil diameter. Using peripherally acting drugs, we identified the parasympathetic system as key for the infraslow variations in HR, as also observed for pupil diameter variations[5]. The LC increases HR through multiple

pathways[15], amongst which one involves an inhibition of the parasympathetic preganglionic vagal nuclei[38] that is thought to underlie HR variability in humans[37]. Our study is the first to directly probe the consequences of specific optogenetic LC stimulation on HR, which needs to be further explored regarding frequency dependence, mechanisms and variation with vigilance state. Continuous 1 Hz-stimulation during NREMS abolished infraslow HR variations, thus demonstrating that LC acts to coordinate the infraslow activity patterns in brain and heart. Intriguingly, when we stimulated LC during fragility periods known to entrain sigma power fluctuations, we also increased the fluctuations of the HR and strengthened anticorrelations on the infraslow time scale. We thus establish the LC as a coordinator of brain and bodily fluctuations during NREMS, which likely involve parasympathetic signaling. This suggests that the LC neurons projecting to thalamus coordinate their activity with the ones projecting to the cardiac premotor vagal neurons, pointing to precise intra-LC mechanisms that subserve this coordination process. Furthermore, the direct demonstration of LC's role in HR variability could renew interest in the relation between HR variability and sleep disorders[56]. Finally, the neural systems underlying this coordination could reach beyond LC, as it is now clear that infraslow neuronal activities are present also in dorsomedial medulla during NREMS[57].

We find that mammalian sleep harnesses on wake promotion to enable sensory vigilance. This insight requires a renewal of current models of sleep-wake control in which reciprocal and exclusive antagonism is so far prevalent[58]. We are now able to concretize questions into the origins of a large variety of primary and secondary sleep disorders, in which hyperarousals, autonomic arousals and movement-related arousals prominently feature[9,44,47,51].

References

1 Van Someren, E. J. *et al.* Disrupted sleep: from molecules to cognition. *J Neurosci* **35**, 13889-13895, doi:10.1523/JNEUROSCI.2592-15.2015 (2015).

2 Mascetti, G. G. Adaptation and survival: hypotheses about the neural mechanisms of unihemispheric sleep. *Laterality*, 1-23, doi:10.1080/1357650X.2020.1828446 (2020).

3 Andrillon, T. & Kouider, S. The vigilant sleeper: neural mechanisms of sensory (de)coupling during sleep. *Curr Opin Physiol* **15**, 47-59, doi:10.1016/j.cophys.2019.12.002 (2020).

4 Lecci, S. *et al.* Coordinated infra-slow neural and cardiac oscillations mark fragility and offline periods in mammalian sleep. *Sci. Adv.* **3**, e1602026, doi:10.1126/sciadv.1602026 (2017).

5 Yüzgeç, O., Prsa, M., Zimmermann, R. & Huber, D. Pupil size coupling to cortical states protects the stability of deep sleep via parasympathetic modulation. *Curr Biol* **28**, 392-400 e393, doi:10.1016/j.cub.2017.12.049 (2018).

6 Fernandez, L. M. J. & Lüthi, A. Sleep Spindles: Mechanisms and Functions. *Physiol Rev* **100**, 805-868, doi:10.1152/physrev.00042.2018 (2020).

7 Klinzing, J. G., Niethard, N. & Born, J. Mechanisms of systems memory consolidation during sleep. *Nat Neurosci* **22**, 1598-1610, doi:10.1038/s41593-019-0467-3 (2019).

8 Watson, B. O. Cognitive and physiologic impacts of the infraslow oscillation. *Front Syst Neurosci* **12**, 44, doi:10.3389/fnsys.2018.00044 (2018).

9 Parrino, L., Halasz, P., Tassinari, C. A. & Terzano, M. G. CAP, epilepsy and motor events during sleep: the unifying role of arousal. *Sleep Med Rev* **10**, 267-285, doi:10.1016/j.smrv.2005.12.004 (2006).

10 Hughes, S. W., Lörincz, M. L., Parri, H. R. & Crunelli, V. Infraslow (<0.1 Hz) oscillations in thalamic relay nuclei: basic mechanisms and significance to health and disease states. *Prog Brain Res* **193**, 145-162, doi:10.1016/B978-0-444-53839-0.00010-7 (2011).

11 Aston-Jones, G. & Bloom, F. E. Activity of norepinephrine-containing locus coeruleus neurons in behaving rats anticipates fluctuations in the sleep-waking cycle. *J Neurosci* **1**, 876-886, doi: 10.1523/JNEUROSCI.01-08-00876.1981 (1981).

12 el Mansari, M., Sakai, K. & Jouvet, M. Unitary characteristics of presumptive cholinergic tegmental neurons during the sleep-waking cycle in freely moving cats. *Exp Brain Res* **76**, 519-529, doi:10.1007/BF00248908. (1989).

13 Kayama, Y., Ohta, M. & Jodo, E. Firing of 'possibly' cholinergic neurons in the rat laterodorsal tegmental nucleus during sleep and wakefulness. *Brain Res* **569**, 210-220, doi:0006-8993(92)90632-J [pii] (1992).

14 Takahashi, K., Kayama, Y., Lin, J. S. & Sakai, K. Locus coeruleus neuronal activity during the sleep-waking cycle in mice. *Neuroscience* **169**, 1115-1126, doi:10.1016/j.neuroscience.2010.06.009 (2010).

15 Samuels, E. R. & Szabadi, E. Functional neuroanatomy of the noradrenergic locus coeruleus: its roles in the regulation of arousal and autonomic function part II: physiological and pharmacological manipulations and pathological alterations of locus coeruleus activity in humans. *Curr Neuropharmacol* **6**, 254-285, doi:10.2174/157015908785777193 (2008).

16 Poe, G. R. *et al.* Locus coeruleus: a new look at the blue spot. *Nat Rev Neurosci* **21**, 644-659, doi:10.1038/s41583-020-0360-9 (2020).

17 Sara, S. J. & Bouret, S. Orienting and reorienting: the locus coeruleus mediates cognition through arousal. *Neuron* **76**, 130-141, doi:10.1016/j.neuron.2012.09.011 (2012).

18 Murphy, P. R., Robertson, I. H., Balsters, J. H. & O'Connell, R. G. Pupillometry and P3 index the locus coeruleus-noradrenergic arousal function in humans. *Psychophysiology* **48**, 1532-1543, doi:10.1111/j.1469-8986.2011.01226.x (2011).

19 Swift, K. M. *et al.* Abnormal locus coeruleus sleep activity alters sleep signatures of memory consolidation and impairs place cell stability and spatial memory. *Curr Biol* **28**, 3599-3609 e3594, doi:10.1016/j.cub.2018.09.054 (2018).

20 Kjaerby, C. *et al.* Dynamic fluctuations of the locus coeruleus-norepinephrine system underlie sleep state transitions. *Biorxiv*, doi:10.1101/2020.09.01.274977. (2020).

21 Eschenko, O. & Sara, S. J. Learning-dependent, transient increase of activity in noradrenergic neurons of locus coeruleus during slow wave sleep in the rat: brain stem-cortex interplay for memory consolidation? *Cereb Cortex* **18**, 2596-2603, doi:10.1093/cercor/bhn020 (2008).

22 Dang-Vu, T. T. *et al.* Spontaneous neural activity during human slow wave sleep. *Proc Natl Acad Sci U S A* **105**, 15160-15165, doi:10.1073/pnas.0801819105 (2008).

23 Hayat, H. *et al.* Locus coeruleus norepinephrine activity mediates sensory-evoked awakenings from sleep. *Sci Adv* **6**, eaaz4232, doi:10.1126/sciadv.aaz4232 (2020).

24 Zerbi, V. *et al.* Rapid reconfiguration of the functional connectome after chemogenetic *locus coeruleus* activation. *Neuron* **103**, 702-718 e705, doi:10.1016/j.neuron.2019.05.034 (2019).

25 Fernandez, L. M. *et al.* Thalamic reticular control of local sleep in sensory cortex. *Elife* **7**, e39111, doi:10.7554/eLife.39111 (2018).

26 Lázár, Z. I., Dijk, D. J. & Lázár, A. S. Infraslow oscillations in human sleep spindle activity. *J Neurosci Methods* **316**, 22-34, doi:10.1016/j.jneumeth.2018.12.002 (2019).

27 Csernai, M. *et al.* Dynamics of sleep oscillations is coupled to brain temperature on multiple scales. *J Physiol* **597**, 4069-4086, doi:10.1113/JP277664 (2019).

28 Eschenko, O., Magri, C., Panzeri, S. & Sara, S. J. Noradrenergic neurons of the locus coeruleus are phase locked to cortical up-down states during sleep. *Cereb Cortex* **22**, 426-435, doi:10.1093/cercor/bhr121 (2012).

29 Carter, M. E. *et al.* Tuning arousal with optogenetic modulation of locus coeruleus neurons. *Nat Neurosci* **13**, 1526-1533, doi:10.1038/nn.2682 (2010).

30 Wyatt, R. J., Chase, T. N., Kupfer, D. J., Scott, J. & Snyder, F. Brain catecholamines and human sleep. *Nature* **233**, 63-65, doi:10.1038/233063a0 (1971).

31 Agster, K. L., Mejias-Aponte, C. A., Clark, B. D. & Waterhouse, B. D. Evidence for a regional specificity in the density and distribution of noradrenergic varicosities in rat cortex. *J Comp Neurol* **521**, 2195-2207, doi:10.1002/cne.23270 (2013).

32 Cardis, R. *et al.* Local cortical arousals and heightened (somato)sensory arousability during non-REM sleep of mice in chronic pain. *Biorxiv*, 2021.01.04.425347, doi:10.1101/2021.01.04.425347 (2021).

33 Feng, J. *et al.* A genetically encoded fluorescent sensor for rapid and specific *in vivo* detection of norepinephrine. *Neuron* **102**, 745-761 e748, doi:10.1016/j.neuron.2019.02.037 (2019).

34 Lee, K. H. & McCormick, D. A. Abolition of spindle oscillations by serotonin and norepinephrine in the ferret lateral geniculate and perigeniculate nuclei *in vitro*. *Neuron* **17**, 309-321, doi:10.1016/s0896-6273(00)80162-2 (1996).

35 Lüthi, A. & McCormick, D. A. Modulation of a pacemaker current through Ca^{2+}-induced stimulation of cAMP production. *Nat Neurosci* **2**, 634-641, doi:10.1038/10189 (1999).

36 Vantomme, G., Osorio-Forero, A., Lüthi, A. & Fernandez, L. M. J. Regulation of local sleep by the thalamic reticular nucleus. *Front Neurosci* **13**, 576, doi:10.3389/fnins.2019.00576 (2019).

37 Mather, M. *et al.* Higher locus coeruleus MRI contrast is associated with lower parasympathetic influence over heart rate variability. *Neuroimage* **150**, 329-335, doi:10.1016/j.neuroimage.2017.02.025 (2017).

38 Wang, X., Pinol, R. A., Byrne, P. & Mendelowitz, D. Optogenetic stimulation of locus ceruleus neurons augments inhibitory transmission to parasympathetic cardiac vagal neurons via activation of brainstem α1 and β1 receptors. *J Neurosci* **34**, 6182-6189, doi:10.1523/JNEUROSCI.5093-13.2014 (2014).

39 Smeets, W. J. & Gonzalez, A. Catecholamine systems in the brain of vertebrates: new perspectives through a comparative approach. *Brain Res Brain Res Rev* **33**, 308-379, doi:10.1016/s0165-0173(00)00034-5 (2000).

40 Libourel, P. A. *et al.* Partial homologies between sleep states in lizards, mammals, and birds suggest a complex evolution of sleep states in amniotes. *PLoS Biol* **16**, e2005982, doi:10.1371/journal.pbio.2005982 (2018).

41 Gais, S., Rasch, B., Dahmen, J. C., Sara, S. & Born, J. The memory function of noradrenergic activity in non-REM sleep. *J Cogn Neurosci* **23**, 2582-2592, doi:10.1162/jocn.2011.21622 (2011).

42 Cirelli, C. & Tononi, G. Differential expression of plasticity-related genes in waking and sleep and their regulation by the noradrenergic system. *J Neurosci* **20**, 9187-9194, doi:10.1523/JNEUROSCI.20-24-09187.2000. (2000).

43 Siclari, F., Bernardi, G., Cataldi, J. & Tononi, G. Dreaming in NREM sleep: a high-density EEG study of slow waves and spindles. *J Neurosci* **38**, 9175-9185, doi:10.1523/JNEUROSCI.0855-18.2018 (2018).

44 Doppler, C. E. J. *et al.* Microsleep disturbances are associated with noradrenergic dysfunction in Parkinson's disease. *Sleep*, in press, doi:10.1093/sleep/zsab040 (2021).

45 Reist, C. *et al.* Prazosin for treatment of post-traumatic stress disorder: a systematic review and meta-analysis. *CNS Spectr*, 1-7, doi:10.1017/S1092852920001121 (2020).

46 Galgani, A. *et al.* Locus coeruleus magnetic resonance imaging in neurological diseases. *Curr Neurol Neurosci Rep* **21**, 2, doi:10.1007/s11910-020-01087-7 (2020).

47 Van Someren, E. J. W. Brain mechanisms of insomnia: new perspectives on causes and consequences. *Physiol Rev*, in press, doi:10.1152/physrev.00046.2019 (2020).

48 Antony, J. W. *et al.* Sleep spindle refractoriness segregates periods of memory reactivation. *Curr Biol* **28**, 1736-1743, doi:10.1016/j.cub.2018.04.020 (2018).

49 Stevner, A. B. A. *et al.* Discovery of key whole-brain transitions and dynamics during human wakefulness and non-REM sleep. *Nat Commun* **10**, 1035, doi:10.1038/s41467-019-08934-3 (2019).

50 Seibt, J. *et al.* Cortical dendritic activity correlates with spindle-rich oscillations during sleep in rodents. *Nat Commun* **8**, 684, doi:10.1038/s41467-017-00735-w (2017).

51 Ferri, R., Koo, B. B., Picchietti, D. L. & Fulda, S. Periodic leg movements during sleep: phenotype, neurophysiology, and clinical significance. *Sleep Med* **31**, 29-38, doi:10.1016/j.sleep.2016.05.014 (2017).

52 Devilbiss, D. M. & Waterhouse, B. D. The effects of tonic locus ceruleus output on sensory-evoked responses of ventral posterior medial thalamic and barrel field cortical neurons in the awake rat. *J Neurosci* **24**, 10773-10785, doi:10.1523/JNEUROSCI.1573-04.2004 (2004).

53 Hermans, E. J. *et al.* Stress-related noradrenergic activity prompts large-scale neural network reconfiguration. *Science* **334**, 1151-1153, doi:10.1126/science.1209603 (2011).

54 Yang, B. *et al.* Locus coeruleus anchors a trisynaptic circuit controlling fear-induced suppression of feeding. *Neuron* **109**, 1-16, doi:10.1016/j.neuron.2020.12.023 (2021).

55 Nothias, F., Onteniente, B., Roudier, F. & Peschanksi, M. Immunocytochemical study of serotoninergic and noradrenergic innervation of the ventrobasal complex of the rat thalamus. *Neurosci Lett* **95**, 59-63, doi:10.1016/0304-3940(88)90632-5 (1988).

56 Silvani, A., Calandra-Buonaura, G., Benarroch, E. E., Dampney, R. A. L. & Cortelli, P. Bidirectional interactions between the baroreceptor reflex and arousal: an update. *Sleep Med* **16**, 210-216, doi: 10.1016/j.sleep.2014.10.011 (2015).

57 Stucynski, J. A., Schott, A. L., Baik, J., Chung, S. & Weber, F. Regulation of REM sleep by inhibitory neurons in the dorsomedial medulla. *Biorxiv* 2020.11.30.405530, doi:10.1101/2020.11.30.405530 (2021).

58 Saper, C. B. & Fuller, P. M. Wake-sleep circuitry: an overview. *Curr Opin Neurobiol* **44**, 186-192, doi:10.1016/j.conb.2017.03.021 (2017).

59 Vantomme, G. *et al.* A thalamic reticular circuit for head direction cell tuning and spatial navigation. *Cell Rep* **31**, 107747, doi:10.1016/j.celrep.2020.107747 (2020).

60 Smith, R. D., Grzelak, M. E. & Coffin, V. L. Methylatropine blocks the central effects of cholinergic antagonists. *Behav Pharmacol* **5**, 167-175, doi:10.1097/00008877-199404000-00008 (1994).

61 Neil-Dwyer, G., Bartlett, J., McAinsh, J. & Cruickshank, J. M. β-adrenoceptor blockers and the blood-brain barrier. *Br J Clin Pharmacol* **11**, 549-553, doi:10.1111/j.1365-2125.1981.tb01169.x (1981).

62 Berens, P. CircStat: A MATLAB toolbox for circular statistics. *J Stat Software* **31**, 1-21, doi:10.18637/jss.v031.i10 (2009).

Online Methods.

Animal husbandry and numbers used for experiments

Mice from the C57BL/6J line and from the B6.FVB(Cg)-Tg(Dbh-cre)KH212Gsat/Mmucd (MMRRC Stock#036778-UCD) line, referred to here as DBH-Cre line, were bred on a C57BL/6J background and housed in a humidity- and temperature-controlled animal house with a 12 h / 12 h light-dark cycle (lights on at 9 am). Food and water were available ad libitum throughout all the experimental procedures. For viral injections, 2- to 7-week-old mice of either sex were transferred to a P2 safety level housing room with identical conditions 1 d prior to injection. For in vivo experimentation, animals were transferred to the recording room 3 d after viral injection and left to recover for at least 1 week prior to the implantation surgery, after which they were singly housed in standard-sized cages. The grids on top of the cage were removed and replaced by 30 cm-high Plexiglass walls. Fresh food was regularly placed on the litter and the water bottle inserted through a hole in the cage wall. Objects (tissues, paper rolls, ping-pong balls) were given to play. For in vitro experimentation, animals were transferred 3 d after viral injection to a housing room with identical conditions and were used 3 – 6 weeks after injection. In total, 12 male C57BL/6J mice were used for intracranial pharmacological experiments, 19 male C57BL/6J mice for cardiac pharmacology experiments and 6 male C57BL/6J mice for the fiber photometry experiments.

From the DBH-Cre line, 21 (11 males and 10 females) heterozygous Cre +/- animals were used for optogenetic experiments, and 14 (2 males and 12 females) for in vitro experiments. All experiments were conducted in accordance with the Swiss National Institutional Guidelines on Animal Experimentation and were approved by the Swiss Cantonal Veterinary Office Committee for Animal Experimentation.

Surgical procedures for viral injections

Optogenetics in vivo and in vitro: Animals were anaesthetized with ketamine (83 mg kg^{-1})/xylazine (3.5 mg kg^{-1}), kept on a thermal blanket to maintain body temperature around 37 °C, and injected i.p. with carprofen (5 mg kg^{-1}) for analgesia. Mice were then head-fixed on a stereotactic frame equipped with a head adaptor for young animals (Stoelting 51925). The scalp was disinfected, injected with a mix of lidocaine (6 mg kg^{-1})/bupivacaine (2.5 mg kg^{-1}) for local anesthesia and opened with scissors exposing the desired region of the skull. For the injections, we used a thin glass pipette (5-000-1001-X, Drummond Scientific) pulled on a vertical puller (Narishige), initially filled with mineral oil, and backfilled with the virus-containing solution just prior to injection. Injections took place at an injection rate of 100 – 200 nl min^{-1}. For optogenetic stimulation experiments, 2 animals were injected with a ssAAV5/2-hEF1α-dlox-hChR2(H134R)_mCherry(rev)-dlox-WPRE-hGHp(A) (titer: $9.1x10^{12}$ vg / ml, 0.8 – 1 µL) virus bilaterally in a region close to the LC. The stereotaxic coordinates were (relative to Bregma, given in mm here and throughout the rest of the Online Methods): lateral (L) ±1.28; antero-posterior (AP) -5.45, depth (D) -3.65), as done previously[29]. The remaining 9 animals were injected bilaterally with the same virus (0.3 – 0.6 µL) directly into the LC (L ±1.05; AP -5.45; D -3.06). The two viral injections yielded comparable results and data were pooled. For optogenetic inhibition, all animals were injected bilaterally into the LC (0.2 – 0.35 µL) with either pAAV5-CAG-FLEX-rc[Jaws-KGC-GFP-ER2] ($7x10^{12}$ vg / ml; n = 2, Addgene), AAV8-hSyn-FLEX-Jaws-KGC-GFP-ER2 ($3.2x10^{12}$ vg / ml; n = 3, UNC Vector Core) or ssAAV-5/2-hSyn1-dlox-Jaws_KGC_EGFP_ERES(rev)-dlox-WPRE-bGHp(A)-SV40p(A) (titer: $6.4x10^{12}$ vg / ml; n = 5, VVF Zürich).

Fiber photometry: For the assessment of NE dynamics in the thalamus, an AAV virus (ssAAV9/2-hSyn1-GRAB_NE1h-WPRE-hGHp(A), titer: $7.2x10^{12}$ vg / ml, VVF Zürich) containing the plasmid encoding a NE sensor (pAAV-hSyn-GRAB_NE1h, Addgene Plasmid #123309)[33] was injected into the thalamus (500 nl; L

2.0; AP -1.6; D -3.0). After the injections, the incision was sutured, and the area disinfected. Animals were carefully monitored and returned to the home cage once awake and moving around. Recovery time after injections took place for a minimum of 1 week before the next surgeries. Paracetamol was given in the water for the 4 postoperative days at a concentration of 2 mg ml^{-1}.

Surgical procedures for sleep recordings combined with optogenetics or fiber photometry

For in vivo EEG/EMG combined with local field potential (LFP) recordings, electrode implantation was as previously described[4,25,32]. In short, animals were anesthetized with isoflurane (1.5 – 2.5 %) in a mixture of O_2 and N_2O. After analgesia (i.p. carprofen 5 mg kg^{-1}) and disinfection, animals were fixed in a Kopf stereotax and injected into the scalp with a mix of lidocaine (6 mg kg^{-1})/bupivacaine (2.5 mg kg^{-1}) and a piece of the scalp was removed after 3 – 5 min, the skull exposed and the bone scratched to improve adhesion of the head implant. Then, we drilled small craniotomies (0.3 – 0.5 mm) over left frontal and parietal bones and positioned two conventional gold-coated wire electrodes in contact with the dura mater for EEG recordings. On the contralateral (right) side, a high-impedance tungsten LFP microelectrode (10–12 MΩ, 75 µm shaft diameter, FHC) was implanted in the primary somatosensory cortex (L 3; AP -0.7; D -0.85). Additionally, as a neutral reference, a silver wire (Harvard Apparatus) was inserted into the occipital bone over the cerebellum and two gold pellets were inserted into the neck muscles for EMG recordings. All electrodes were fixed using Loctite Schnellkleber 401 glue and soldered to a multisite connector (Barrettes Connectors 1.27 mm, male connectors, Conrad).

For intracranial injection of noradrenergic antagonists, we additionally made a craniotomy over the thalamus (L 2; AP -1.60) and covered it with a silicone-based sealant (Kwik-Cast Silicone Sealant, WPI). Additionally, we glued and cemented a light-weight metal head-post (Bourgeois Mécanique SAS, Lyon, France) onto the midline skull to perform painless head-fixation during injection of noradrenergic antagonists.

For optogenetic experiments, DBH-Cre animals were implanted with custom-made optic fibers[59]. A multimode fiber (225 µm outer diameter, Thorlabs, BFL37-2000/FT200EMT) was inserted and glued (heat-curable epoxy, Precision Fiber Products, ET-353ND-16OZ) to a multimode ceramic zirconia ferrule (Precision Fiber Products, MM-FER2007C-2300). The penetrating end was cut at the desired length with

a carbide-tip fiber optic scribe (Precision Fiber Products, M1-46124). The outside end was then polished using fiber-polishing films (Thorlabs). For optogenetic stimulation of the LC cell bodies (n = 11 animals) a single 3-mm fiber stub was implanted directly over the LC (L 1.0; AP -5.4; D -2.3). Out of the 11 animals, 6 animals were also implanted with a 3 mm-optic fiber stub over the somatosensory thalamus (L 2.0; AP -1.7; D -2.5). For the 5 additional animals, we implanted a custom-made optrode in S1 built with a high-impedance fine tungsten LFP microelectrodes (10 – 12 MΩ, 75 µm shaft diameter, FHC) glued to the stub of a 2 mm-optic fiber at a distance of 800 – 1,200 µm. The optrode was then inserted into S1 (L 3.0; AP -0.7; D 0.8). For optogenetic inhibition of the LC bodies (n = 10), bilateral optic fibers were implanted at a 20° lateral angle targeting the LC (L ±1.84; AP -5.4; D -2.47). To establish the final coordinates of the optic fibers, pupil diameter changes were monitored in a subgroup of 5 animals while lowering the optic fiber and applying light stimuli (Extended Data Fig. 4; 10 – 30 pulses at 10 Hz). A custom-made software developed in Matlab was used for image acquisition (See in vivo data analysis).

For fiber photometry experiments, in addition to the recording electrodes, we implanted C57BL/6J animals (n = 6) with a premade 400 µm-thick optic fiber coupled to a cannula (MFC_400/430-0.66_3.5mm_ZF1 25(G)_FLT, Doris Lenses) over the dorsal and reticular thalamus (L 1.8; AP -1.7; D 2.5) at a rate of 1 mm min^{-1}.

Finally, a dental cement structure was built to fix the implant in place. After disinfection with iodine-based cream, animals were returned to their home cage and kept in careful monitoring. Animals were provided with paracetamol (2 mg mL^{-1}) in the drinking water for at least 4 days after the procedure.

In vivo electrophysiological recordings

Once recovered from the surgery, animals were habituated to the cabling for 5 – 7 days, followed by a baseline recording to ascertain the quality of the signals. We acquired the EEG, EMG and LFP signals at a 1 kHz sampling frequency using an Intan digital RHD2132 amplifier board and a RHD2000 USB Interface board (Intan Technologies) connected via SPI cables (RHD recording system, Intan Technologies). Homemade adapters containing an Omnetics - A79022-001 connector (Omnetics Connector Corp.) linked to a female Barrettes Connector (Conrad) were used as an intermediate between

the head implant of the animal and the headstage. We acquired the data with Matlab using the RHD2000 Matlab toolbox and a customized software in the same environment[25,32].

Experimental Procedures for intracranial local pharmacology

We gently and gradually habituated mice to being head-fixed by increasing the amount of time spent in head fixation daily from 5 min to 45 min over a period of 4 – 5 days. The rest of the time, the animals spent being tethered to the recording system in their home cage. On the first experimental day, we removed the silicone cover of the craniotomy in head-fixed conditions and positioned a glass pipette (5-000-1001-X, Drummond Scientific, pulled on a vertical Narishige PP-830 puller, tip size of 15 – 25 µm) over the craniotomy and waited for 30 min while gently touching the side of the craniotomy to simulate an injection. Then, we covered the craniotomy again with the silicone-based sealant and returned the animals to the home cage for an 8 h-baseline polysomnographic recording. The next day, we removed the silicone again and injected 150 nL of noradrenergic antagonists or ACSF at two different depths within the thalamus (D: -3.2 and -2.8 mm). For the experimental group, we infused a mixture of 0.1 mM prazosin hydrochloride (prazosin) and 5 mM (S)-(-)-atenolol (atenolol), diluted in ACSF together with a red fluorescent dye (5 mM Alexa 594) for later confirmation of the injection site. For the control group, we injected ACSF together with Alexa 594. Per animal, only one injection was done (either blockers or ACSF) and the animal sacrificed after completion of the recording.

Experimental procedures for in vivo optogenetics

All optogenetic manipulation took place during the first 20 min of each hour between ZT1 and ZT9. A custom-made close-loop detection of NREMS[32] was used for state specificity. In short, NREMS was detected whenever the delta (1 – 4 Hz) to theta (5 – 10 Hz) power ratio derived from the differential frontal-parietal EEG channels crossed a threshold for 2 out of 5 s and the EMG absolute values went below a threshold during at least 3 s. This lead to reliable stimulation during NREMS (Fig. 2), with the exception of a few brief interruptions that occurred during artefacts (e.g. muscle twitches). Optogenetic stimulation of the LC cell bodies was carried out using a PlexBright Optogenetic Stimulation System (Plexon) coupled to a PlexBright Table-top blue LED Module (Wavelength 465 nm) at 1 Hz. Stimulation of

LC terminals in the thalamus or cortex was delivered at 2 Hz (Fig. 3). Optogenetic inhibition of LC cell bodies was performed using a continuous stimulation with a PlexBright Table-top orange LED Module (Wavelength 620 nm) (Fig. 2). Optogenetic stimulation (1 Hz) or inhibition (continuous) was also carried out specifically when sigma power declined or rose, limiting it preferentially to continuity or fragility substates, respectively. This was achieved via a machine-learning-based closed-loop procedure[32] built with a multilayer perceptron model neural network of 10 neurons in the hidden layer and 3 output neurons (for continuity, fragility or none). The network was fed with the last 200 s of a 9th-order polynomial fit of the sigma activity (10 – 15 Hz) calculated for each s. The neural network was then trained, validated, and tested using the sleep scoring from 13 C57BL/6J animals (642,000 epochs) that were otherwise not included in this study. Online, the same data stretches obtained from the mouse in recording were used. For each animal, multiple recording sessions took place with a random allocation of the stimulation protocol: i.e. optogenetic stimulation during NREMS in the LC bodies, its terminals (thalamus for 6 animals or cortex 5 animals), or stimulation of the LC bodies during continuity or fragility substates (in a subgroup of 9 mice). Similarly, for optogenetic inhibition of LC bodies, random allocation of inhibition protocols took place during NREMS (10 animals), continuity or fragility substates (10 animals).

Experimental procedures for in vivo fiber photometry

After the recovery (> 7 d) and habituation to the cabling procedure (> 4 d), we performed two recordings per animal with at least one day between sessions. All recordings were limited to the first 3 – 4 h from ZT1 to minimize possible photobleaching. For fluorescent measurements, we used a pulse-width-modulated sinusoidal signal of 400 Hz using a Raspberry Pi3 (Raspberry Pi Foundation) to modulate a LEDD_2 driver (Doric Lenses Inc.) connected to a blue LED (CLED 465 nm; Doric Lenses Inc.). The power of the driver was set to 200 mA. The blue LED was coupled to a fluorescence MiniCube (iFMC4_IE(400-410)_E(E460-490)_F(500-550)_S, Doric Lenses) that redirected the light to the animal via a low autofluorescence 400-µm-thick fiberoptic patchcord (MFP_400/430/1100-0.57_1m_FMC-ZF1.25_LAF, Doric Lenses Inc.). The cord was connected to the Optic fiberoptic Cannula (MFC_400/430-0.57_3mm_ZF1.25(G)_FLT) implanted in the head of the mouse. A photodetector integrated into the

MiniCube head turned the emitted light from the fluorescent NE sensor into a current signal that was fed into an analog signal of the Intan RHD2132 amplifier board.

In vitro electrophysiological recordings

Thalamic brain slice recordings were performed as previously described in detail[25,59]. Briefly, 3 – 6 weeks after viral injection, DBH-Cre mice aged 8 – 16 weeks were subjected to isoflurane anesthesia, after which they were decapitated, brains extracted and quickly immersed in ice-cold oxygenated sucrose solution (which contained in mM): NaCl 66, KCl 2.5, NaH_2PO_4 1.25, $NaHCO_3$ 26, D-saccharose 105, D-glucose 27, L(+)-ascorbic acid 1.7, $CaCl_2$ 0.5 and $MgCl_2$ 7), using a sliding vibratome (Histocom). Brains were trimmed at the level of the brainstem, glued on the trimmed surface on an ice-cold metal blade and apposed to a supporting agar block on their ventral side. Acute 300-μm-thick coronal brain slices were prepared in the same ice-cold oxygenated sucrose solution and kept for 30 min in a recovery solution at 35 °C (in mM: NaCl 131, KCl 2.5, NaH_2PO_4 1.25, $NaHCO_3$ 26, D-glucose 20, L(+)-ascorbic acid 1.7, $CaCl_2$ 2, $MgCl_2$ 1.2, *myo*-inositol 3, pyruvate 2) before being transferred to room temperature for at least 30 min. All recordings were done at room temperature.

Recording glass pipettes were pulled from borosilicate glass (TW150F-4) (WPI) with a DMZ horizontal puller (Zeitz Instr.) to a final resistance of 2 – 4 MΩ. Pipettes were filled with a K^+-based intracellular solution that contained in mM: KGluconate 140, Hepes 10, KCl 10, EGTA 0.1, phosphocreatine 10, Mg-ATP 4, Na-GTP 0.4, pH 7.3, 290–305 mOsm. Slices were placed in the recording chamber of an upright microscope (Olympus BX50WI) and continuously superfused with oxygenated ACSF containing in mM: NaCl 131, KCl 2.5, NaH_2PO_4 1.25, $NaHCO_3$ 26, D-glucose 20, L(+)-ascorbic acid 1.7, $CaCl_2$ 2 and $MgCl_2$ 1.2. Cells were visualized with differential interference contrast optics and 10X and 40X immersion objectives, and their location within the thalamic ventroposterial medial nucleus or within the somatosensory reticular thalamus could be verified based on previous studies in the lab[25,59]. Infrared images were acquired with an iXon Camera X2481 (Andor). Prior to recording, pipette offset was zeroed, and the stability of the offset verified by monitoring pipette potential in the bath for 10 min. Drifts were < 0.5 mV / 10 min. Signals were amplified using a Multiclamp 700B amplifier, digitized via a Digidata1322A and sampled at 10 kHz with Clampex10.2 (Molecular Devices). Immediately after gaining whole-cell

access, cellular membrane potential and access resistance were measured. Cells included had a resting membrane potential < -55 mV and access resistances < 15 MΩ. The cell types were identified based on their rebound bursting properties (Extended Data Fig. 5). Whole-field blue LED (Cairn Res) stimulation (455 or 470 nm, duration: 0.1 – 1 ms, maximal light intensity 0.16 and 0.75 mW/mm^2 for the two LEDs, respectively). Per slice, only one cell was recorded and exposed to light stimulation. For characterization of LC fiber-evoked membrane depolarizations, cells were held between -65 to -70 mV and exposed to 1 Hz, 3 Hz or 10 Hz stimulation (4 pulses each). Stimulation at different frequencies were applied in random order, with each frequency used maximally twice to avoid run-down of the evoked response. When light-induced depolarizations did not return to the original membrane potential, they were not included in the analysis. For the study of LC-dependent effects on prolonged afterdepolarizations, thalamocortical cells were first injected with series of repetitive negative current injections (100 – 300 pA, 20 pulses, each 120 ms) known to evoke rebound low-threshold Ca^{2+} bursts. Such protocols have been used previously to characterize the cell-intrinsic mechanisms accompanying sleep-spindle-related arrival of barrages of inhibitory synaptic potentials[35]. Following 1 – 2 such repetitive current injections (each followed by 3 – 5 min of recovery time), the current injections were preceded by LC fiber stimulation (10 Hz, 4 pulses) by 5 s, such that the maximum of the LC-evoked membrane depolarization coincided with the end of the negative current injections. For characterization of LC fiber-evoked membrane currents, cells were held in voltage-clamp at -70 mV. Baseline light-evoked currents were evoked maximally 1 – 2 times, followed by bath application of noradrenergic antagonists ((S)-(-)-atenolol (Abcam) for thalamocortical cells or prazosin hydrochloride (Abcam) for thalamic reticular cells) for 5 – 10 min before the next optogenetic stimulation. The in vitro data were manually analyzed using Clampfit v2.2 and as illustrated in Extended Data Fig. 5).

Pharmacological manipulation of heart rate

After the recovery period of the electrode implantation (> 7 d), mice were habituated to the recording conditions for one week. Mice were injected intraperitoneally with NaCl, (S)-(-)-atenolol (1 mg kg^{-1}) (Abcam), a sympathetic antagonist or methylatropine bromide (10 mg kg^{-1}) (Sigma-Aldrich), a parasympathetic antagonist, both known to poorly permeate the blood-brain barrier[60,61]. Injections were

done at 9 am and followed by polysomnographic recording for 100 min. Two recording sessions per drug took place in an intercalated manner. Experimenters were blind to the drug injected.

Histology

After all recording sessions were completed, animals were injected intraperitoneally with a lethal dose of pentobarbital. For animals implanted with electrodes for LFP recording, the position of the electrode was marked via electro-coagulation (50 µA, 8 – 10 s) of the region. Subsequently, ~45 mL of paraformaldehyde (PFA) 4% were perfused intracardially at a rate of ~2.5 mL min^{-1}. Brains were post-fixed for at least 24 h in PFA 4% cooled to 4 °C. Brains were then sliced in 100 µm-thick sections with a vibratome (Microtome Leica VT1000 S; speed: 0.25 – 0.5 mm s^{-1} and knife sectioning frequency: 65 Hz) or a freezing microtome (Microm). Brain sections were directly mounted on slides or kept in well plates filled with 0.1 M PB for later processing. Then, we confirmed the position of LFP electrodes and optic fibers and the fluorescent expression of the injected viruses or local pharmacology injections with a Nikon SMZ25 Stereomicroscope equipped with a Nikon DS-Ri2 16 Mpx color camera. When needed, higher magnification images were acquired using an Axiovision Imager Z1 (Zeiss) microscope equipped with an AxioCam MRc5 camera (objectives used EC-Plan Neofluar 2.5x/0.075 ∞/0.17, 5x/0.16 ∞/0.17, 10x/0.3 ∞/- or 20x/0.5 ∞/0.17).

In vivo data analysis

Scoring of vigilance states: We detected sleep and wake episodes following previous standard procedures in a manner blinded to the treatment[25,32]. For this purpose, we used a custom-made software developed in Matlab (MathWorks) that allows semiautomatic scoring of sleep stages. Shortly, we defined three distinct stages as follows: wakefulness, periods containing large muscle tonus or phasic activity in the EMG signal, together with low-voltage EEG exhibiting fast oscillatory components. NREMS was defined as periods containing low EMG activity together with high amplitude EEG activity showing slow oscillatory components such as slow oscillations (< 1.5 Hz), delta (1.5 – 4 Hz) or sleep spindles (10 – 15 Hz). REM sleep episodes were defined as periods with low EMG activity with prominent Theta (5 – 10 Hz) activity in the EEG. Microarousals were defined as short (< 12 s) periods of wakefulness contained

between the epochs of the same sleep stage. For the intracranial pharmacology experiments, analysis was done for the first 2 h of recording and comparisons were made in a paired manner between the baseline and drug conditions. For all optogenetic experiments, scored data for the first 20 min of each hour (during which light stimulation was done) were compared with the same periods in sham conditions (*ceteris paribus* with the LED turned off). For the fiber photometry experiments, analysis included the complete 3 – 4 h of recordings. For the pharmacological manipulation of the HR, analysis took place for the first 100 min after the i.p. injections.

Analysis of sigma and delta dynamics: Dynamics of sigma (10 – 15 Hz) and delta (1.5 – 4 Hz) activities were quantified from the S1 LFP signal using a wavelet transform with a Mother Gabor-Morlet wavelet with 4 cycles of standard deviation for the Gaussian envelope (see Fig. 1a,c). The frequency dimensions were then collapsed to the two frequency bands of interest, the 10 – 15 Hz sigma band and the 1.5 – 4 Hz delta band. The mean signals were then resampled at 10 Hz and filtered using a 100^{th} order filter with a 0.025 Hz cutoff frequency for further analysis. For NREMS bouts of ≥ 96 s, a Fast Fourier transform was calculated (Fig. 1b) to measure the strength of the 0.02 Hz oscillatory patterns defined here as the area underneath the Fourier transform from 0.01 – 0.04 Hz, subtracting the mean activity between 0.08 to 0.12 Hz (as depicted in Fig. 1b).

Sleep spindle detection, phase coupling analysis and feature extraction: Sleep spindles were detected from the S1 LFP signal for all the experiments. Spindle detection was done using a previously described algorithm[25] that is illustrated in Extended Data Fig. 1. Briefly, we filtered (FIR filter of order 2000) the raw S1 LFP signal in the sigma band (9 – 16 Hz). Then, we squared the signal and applied a threshold of 1.5 the standard deviation above the mean values in NREMS. We then detected all the peaks crossing this threshold and marked as a putative spindle all events containing at least 3 cycles. The starting and ending point of the events were extended to the closest cycle at 0 crossing before and after the threshold, respectively. Events separated by < 50 ms were merged as a single event. For display purposes, we positioned a black dot for each individual spindle event at the center of the spindle in time and a random jittered vertical position.

After spindle detection, we extracted the following features: *Amplitude,* the maximum value of the absolute filtered signal within the event. *Frequency,* mean intra-peak frequency within the detected

spindle event. *Number of cycles* in the spindle. *Duration,* timespan between the beginning and end of the event.

For the analysis of the phase coupling of the spindle events to the sigma activity we first centered the sigma activity at zero by subtracting the mean of the sigma activity in NREMS. Then we constructed a distribution using the phase of the sigma dynamics (calculated as described in *Analysis of sigma and delta dynamics*) at the center of each spindle event (half point between the beginning and the end of the spindle). By using the CircStat toolbox for Matlab (MathWorks)[62], we then confirmed the non-uniformity of the distribution by using the Rayleigh test.

Detection of infraslow cycles: We detected individual cycles of sigma within NREMS using a custom-made Matlab routine. We used the sigma dynamics as described in "*Analysis of sigma and delta dynamics"* and eliminated the regions containing artifacts. Then, we identified the peaks and troughs in the signal with a minimum distance of 25 and 20 s, respectively. Finally, we arranged the positions of successive troughs and kept the starting and ending point for each individual cycle. Next, the marked locations were used to normalize the time in 1000 points for each individual cycle and to interpolate the sigma activity to generate a mean dynamics normalized in time. The same positions were used to normalize the dynamics of NE-related fluorescent signals from the fiber photometry measurements. Only those cycles that within NREMS periods were included in the mean.

Pupil diameter measurements. To standardize the correct location of the optic fibers in the LC cell bodies stimulation or inhibition, we performed pupil diameter measurements in a subset of animals. In short, we set a Basler GigE infrared camera (Basler acA800-510 um, SVGA, 1/3.6'', 510 fps, USB3 Vision) close to one eye of the animal and used a custom-made infrared LED-based lantern directed to the recorded eye to increase the contrast between the pupil and the surrounded area. We built a custom-made software in Matlab (MathWorks) for online or offline pupil detection (using the videos recorded from online trials). First, the user manually selects both the area of interest for the analysis and the initial location of the pupil. Then, for each frame (recorded at 10 fps), a binary image was created using an Otsu's method adaptive threshold with the function `imbinarize` from Matlab (MathWorks). The threshold was set manually to adapt to the conditions of the image and the angles of the infrared light source and the camera. The size of the binary

object closest to the marked pupil was then measured. The dynamics of the pupil diameter was then tracked and z-scored for comparison (See Extended Data Fig. 4).

Fiber Photometry: Changes in bioluminescence were recorded via a photodetector connected to an analog channel in the Intan RHD2000 USB Interface board (Intan Technologies) as described before. The recorded signal fluctuated between 0 – 3.3 V with peaks at 400 Hz as the sinusoidal waveform created to modulate the excitation of the biosensors. The fluorescent dynamics signal was then created using an RMS envelope of 1 s. The changes in biofluorescence $\Delta F * F^{-1}$ were computed by dividing the enveloped signal by its fitted exponential decrease calculated from the dynamics at NREMS.

Cross correlation analysis: To study the similarity of the dynamics between the sigma activity and the NE changes or changes in HR, we performed cross correlation analysis between these two pairs of signals in Matlab (MathWorks). For each long bout (≥ 96 s) of NREMS within the time of analysis (see *Scoring of vigilance states*), we z-scored each signal individually and normalized it to the length of the bout. Then, the cross-correlation was calculated using the function `xcorr` of Matlab and normalized to the length of the bout. Mean cross correlation values were computed for each animal and across animals. Mean correlation coefficient (r) was computed between -5 to 5 s lags.

Heart rate analysis: Changes in HR were computed as previously described[4]. Shortly, EMG signal was filtered using a Chebyshev type 2 high-pass filter. We then differentiated (using the function `diff` from Matlab) and squared the signal to highlight the R peaks. The resulting signal was z-scored to normalize across animals and recording sessions. Then, the R peaks were identified using the Matlab function `findpeaks` with a heuristically found threshold of 0.3 and an interpeak distance of at least 0.08 ms. Peaks with a z-score higher than 10 were considered as artifacts and eliminated. Finally, the HR signal was constructed by measuring the inter-peak time distance and divided by 60 (1 min). An interpolation of the values was performed using the function `interp1` of Matlab and resample at 10 Hz.

Statistics

For the statistical tests, we used R statistical language version 3.6.1. and Matlab (MathWorks). First, we tested for normality of the datasets using the Shapiro-Wilk normality test. For comparisons of two parametric datasets, we used a paired Student's t test and the equivalent Wilcoxon signed rank test for non-parametric

datasets. For comparisons on multiple (> 2) groups of data (as in the case of the amplitude, onset latency and recovery time in the in-vitro experiments), a one-way ANOVA or a Kruskal-Wallis test was used for parametric and non-parametric datasets, respectively. In case of no significance, no further *post-hoc* analysis was performed. In all figures, grey lines denote paired datasets from two conditions (e.g. baseline, opto). Mean values are given by large horizontal lines, error bars indicate standard errors of the mean. Non-parametric *P* values are marked with †.

Data availability. All data included in this publication will be stored on one of the servers of the University of Lausanne and will be made available once the study is published.

Code availability. Customized MATLAB scripts for data acquisition and analysis are available from the corresponding author upon reasonable request.

Acknowledgements. We thank Paul Steffan and Dr. David McCormick for providing us with the original DBH-Cre breeders. We greatly appreciate the time-efficient support provided to us from Drs. Yulong Li and Jessie Feng regarding the NE sniffers. Particular thanks go to the Animal caretaking team headed by Michelle Blom, and to Titouan Tromme who took so good care of our animal lines. Expert veterinary advice was given by Drs. Delphine Perret and Laure Sériot. We thank Christiane Devenoges for excellent support in histological analysis. We appreciate the helpful exchange regarding optogenetic LC manipulation and NE sniffer experimentation with Drs. Simone Astori, Antoine Adamantidis, Oxana Eschenko, Jessie Feng, Paul Franken, Celia Kjaerby, Maiken Nedergaard, Ernesto Ruben, Andrea Volterra. We are indebted to Francesca Siclari and Christoph Michel for insightful discussions on the human noradrenergic system. Simone Astori and Francesca Siclari provided valuable input on preliminary versions of the manuscript. All lab members provided constructive input to this study throughout the experimental period and to preliminary versions of the manuscript. This study was funded by The Swiss National Science Foundation (n° 310030-184759 to AL), Etat de Vaud and a FBM UNIL PhD Fellowship to AOF.

Author contributions. AOF set up the techniques and acquisition tools for optogenetics, fiber photometry and pupillometry and carried out all in vivo experiments. RC developed the closed loop interference tools, contributed MATLAB scripts, and provided important input to the experiments and analysis. GV carried out in vitro experiments with contributions from AOF and AL. AGG performed many

of the viral injections and helped optimize their reproducibility and GK contributed to the pharmacological studies on HR. LF was involved in methodology and data curation. AL conceived the original experimental plan and developped it further in discussion with AOF, RC and LF and wrote the paper together with AOF. All authors commented on the manuscript and the figures.

Competing interests. The authors declare no competing interests.

Figures and figure Legends

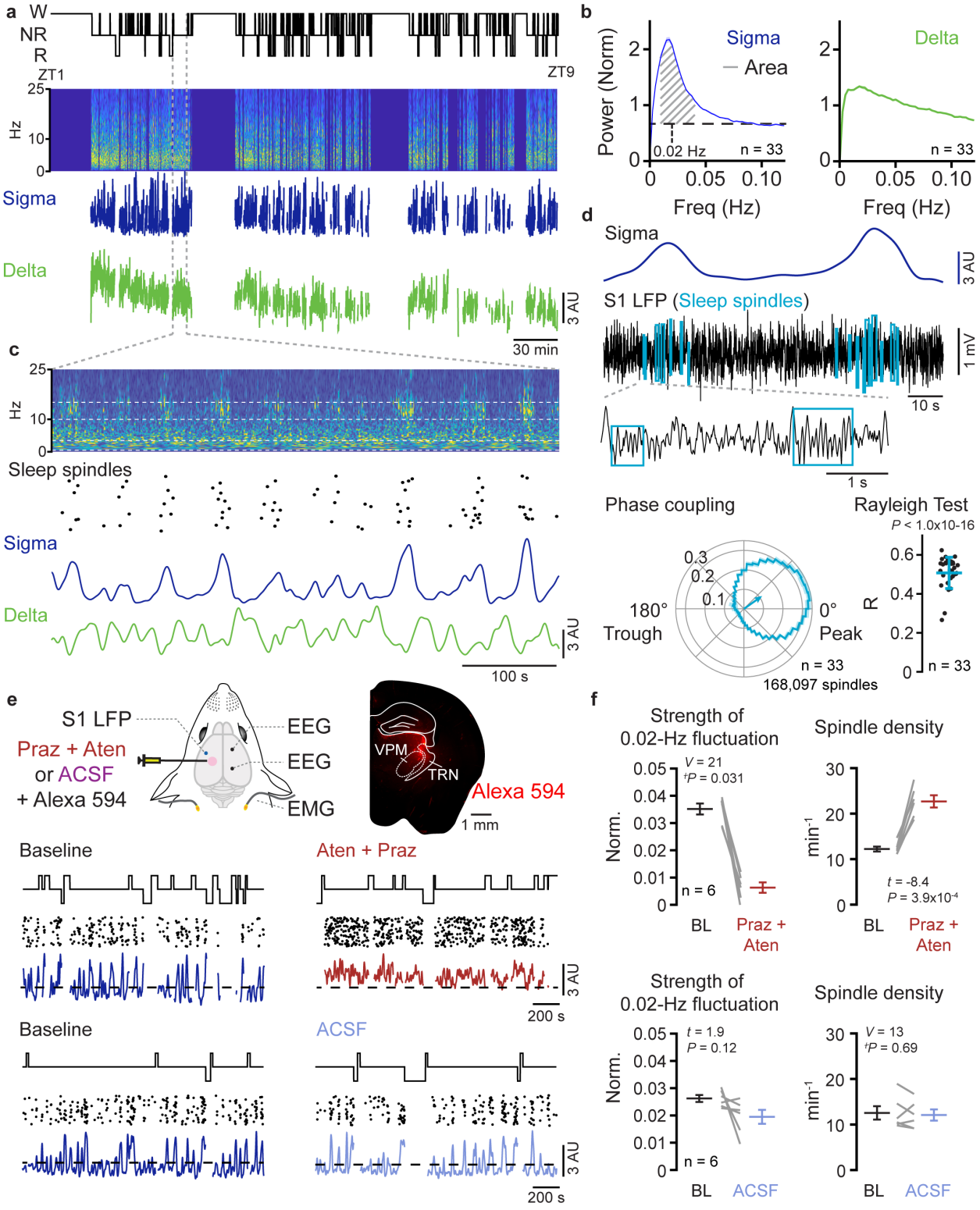

Fig. 1 | The role of noradrenergic signaling for sleep spindle clustering during mouse NREMS. **a**, Hypnogram of a C57BL7/6J mouse from ZT1-ZT9, showing wake (W), NREMS (NR) and REM sleep (R), with corresponding time-frequency distribution of S1 LFP signal below. Power in NREMS only is indicated in color code, with warm colors indicating higher power. Summed sigma (10 – 15 Hz) and delta (1.5 – 4 Hz) power dynamics were derived from the time-frequency distributions. Dashed lines, NREMS bout selected for c. **b**, Fourier transform over sigma (left) and delta (right) power dynamics for n = 33 mice. Diagonal lines, area underneath the Fourier transform used to quantify the strength of the 0.02 Hz-fluctuation in this and subsequent figures 2, 3, 4. Vertical dashed line, 0.02 Hz. Horizontal dashed line, Mean values from 0.08-0.12 Hz. **c**, Single NREMS bout indicated in a. dots, automatically detected spindle events were vertically jittered to visualize single spindles. **d**, Example S1 LFP raw trace taken from c to show detailed position of spindles (see Extended Data Fig. 1). Note how sleep spindles (in blue squares) cluster when sigma power rises (top). 'Phase coupling': sleep spindle occurrence along the 0.02 Hz-fluctuation phases shown in a circular plot; arrow, mean Rayleigh vector across animals. 'Rayleigh test': quantification of the non-uniform distribution via R values ($P < 1.0*10^{-16}$). **e**, Experimental scheme of intracranial local pharmacology in combination with EEG/EMG and S1 LFP electrodes. Prazosin hydrochloride (Praz, 0.1 mM) and (S)-(-)-Atenolol (Aten, 5 mM) or artificial cerebrospinal fluid (ACSF) were co-injected with the red dye Alexa594. Red labeling was verified post-hoc in sections from perfused brains. VPM, ventroposterial medial thalamus, TRN, thalamic reticular nucleus. Traces indicate hypnogram, sleep spindles and sigma power for two mice injected either with Aten + Praz or ACSF. Dashed horizontal line, mean sigma power in Baseline. **f**, Quantification of the strength of the 0.02 Hz-oscillation (as explained in b) and of sleep spindle densities, V, t and *P* values derived from (^{t}) Wilcoxon signed rank or paired t-tests.

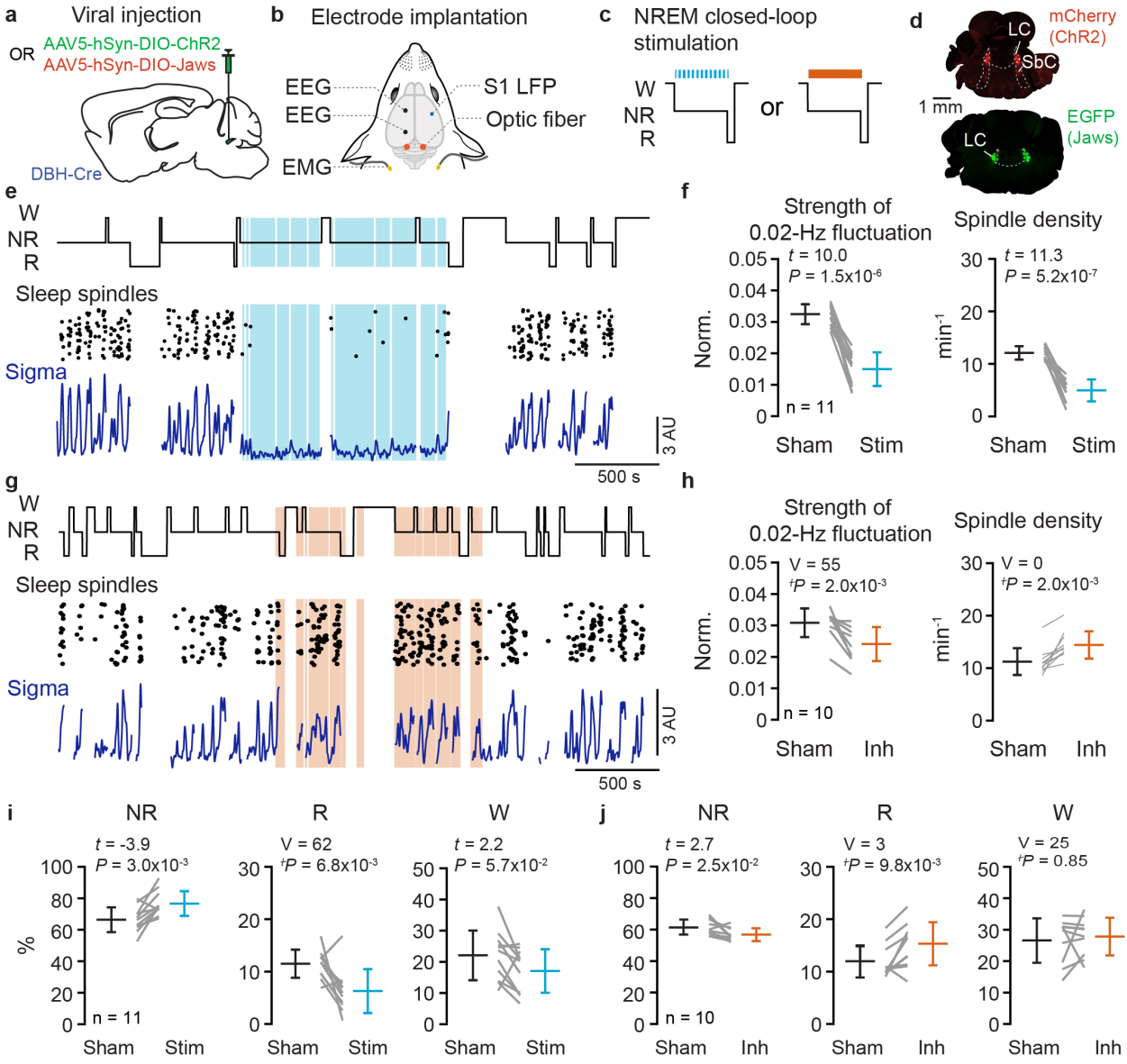

Fig. 2 | Optogenetic interrogation with the locus coeruleus during NREMS. **a**, Viral injection strategy for DBH-Cre mice. For details of the viral plasmids, see Methods. **b**, Experimental scheme for electrode implantation. **c**, Schematic indicating closed-loop stimulation (blue) or inhibition (orange) of LC during NREMS. LC optogenetic interrogation took place in the first 20 min of each hour during 8 h of the light phase (ZT1-9), with light or sham stimulation alternating over successive recording days. **d**, Fluorescent microscopy images confirming viral expression in two mice included in the dataset. **e**, Optogenetic LC stimulation, indicated by blue shading of representative data showing hypnogram, sleep spindles and sigma power derived from S1 LFP recordings. **f**, Quantification of effects on 0.02 Hz-fluctuation strength

and on spindle density. *P* values derived from paired t-tests. **g, h**, Same for optogenetic inhibition. *P* values derived from (^{t}) Wilcoxon signed rank test. **i**, Quantification of times spent in NR, R or W during LC stimulation or sham periods. **j**, Quantification of times spent in NR, R or W during LC inhibition or sham periods. V, t and *P* values derived from (^{t}) Wilcoxon signed rank or paired t-tests.

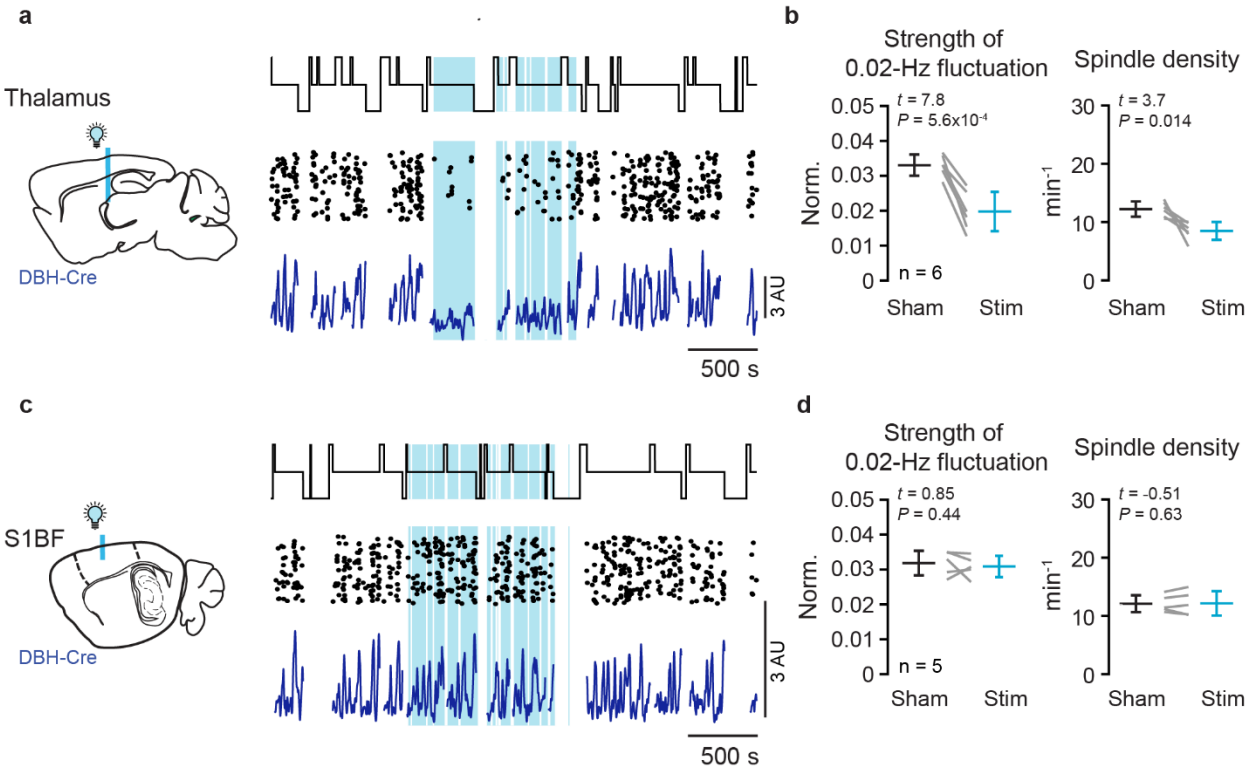

Fig. 3 | Optogenetic interrogation with locus coeruleus afferents in thalamus or cortex during NREMS. **a**, Experimental scheme indicating optic fiber positioning over thalamus. For simplicity, EEG/EMG electrode and S1 LFP electrode are not shown. Representative traces on the right, similar arrangement as in Fig. 2e. **b**, Quantification of effects on 0.02 Hz-fluctuation strength and on spindle density. **c, d**, Same layout for experiments in which the optogenetic fiber was positioned over cortex. All *P* values in the figure derived from paired t-tests.

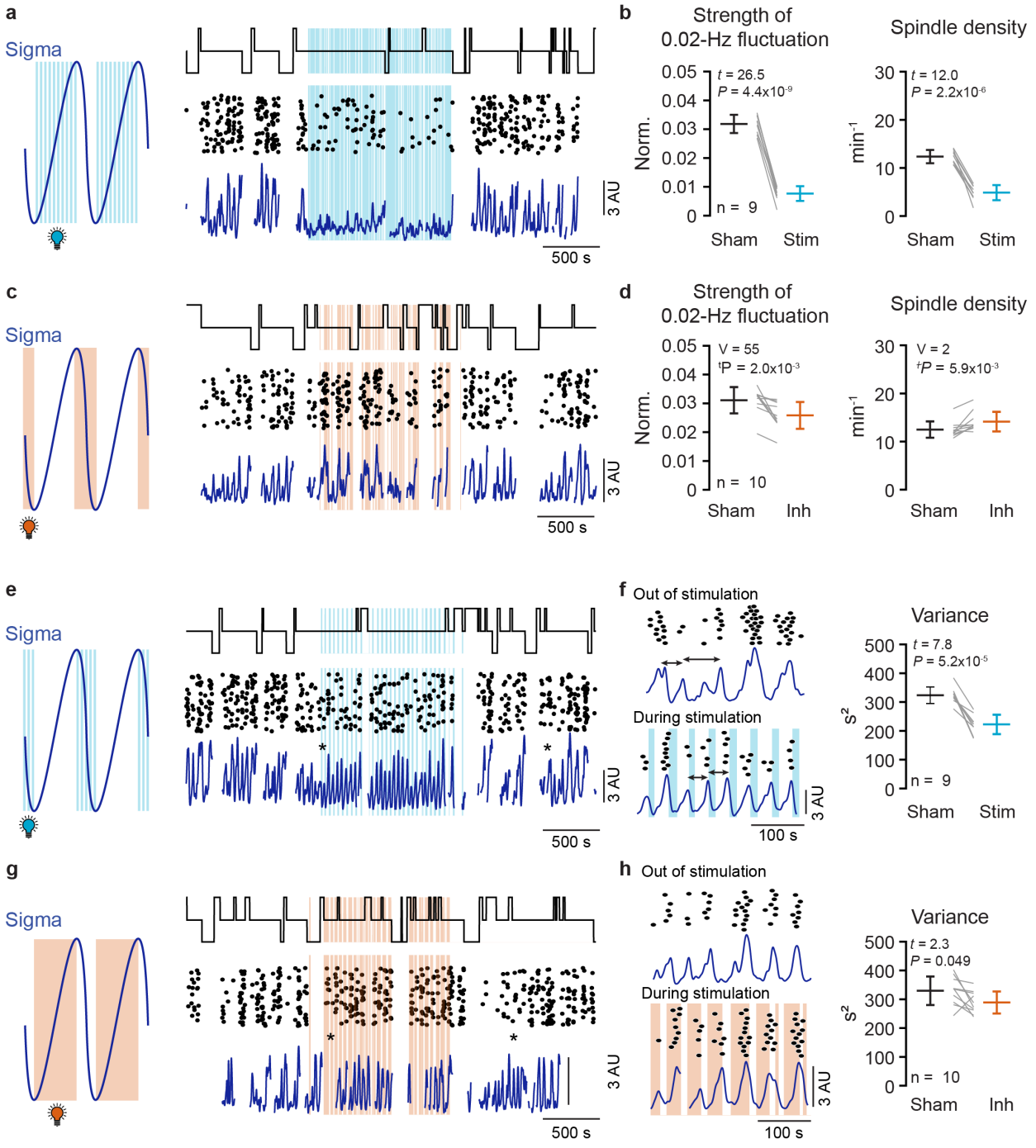

Fig. 4 | Optogenetic interrogation during continuity or fragility substates of NREMS. **a**, LC stimulation during continuity period. Blue waveform, schematic fluctuation to indicate the machine-learning-controlled timing of the light stimuli. Representative traces on the right as in Fig. 2e. **b**, Quantification of effects on 0.02 Hz-fluctuation strength and on spindle density. t and *P* values derived from paired t-tests. **c, d**, LC inhibition during fragility period. Figure panels analogous as in a, b. V, t and *P*

values values derived from (^{t}) Wilcoxon signed rank test. **e,** LC stimulation during fragility periods. Figure panels analogous as in a, c. **f**, Expanded presentation of sigma and sleep spindle traces, taken from moments marked by * in e. Double-headed arrows denote interpeak intervals of the sigma power fluctuation. The regularization of the interpeak intervals in stimulation conditions is quantified through the variance (shown on the right). Note also the tighter temporal alignment between sleep spindles and sigma power. t and *P* values derived from paired t-tests. **g, h**, LC inhibition during continuity period. Figure panels analogous as in e, f. t and *P* values derived from paired t-tests.

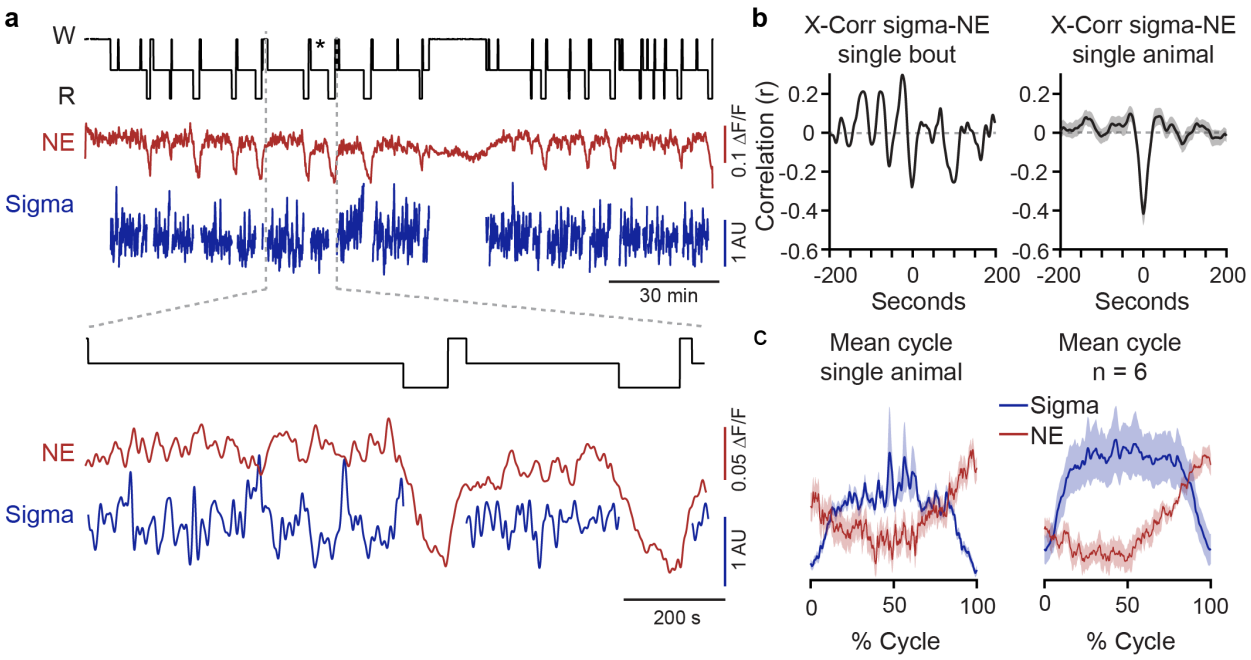

Fig. 5 | Free noradrenaline levels in thalamus anticorrelate with sleep spindles. **a**, Representative recording showing (from top to bottom) hypnogram, relative fluorescence derived from the NE biosensor $GRAB_{NE1ih}$, and sigma power dynamics. Expanded portion shown below. *, bout selected for analysis in b. **b**, Left, Cross-correlation between sigma power and the NE biosensor signal for a single NREMS bout. Right, Mean crosscorrelation across all bouts. **c**, Left, Overlay of sigma power dynamics across all infraslow cycles detected from trough to trough, with corresponding NE fiber photometry signal for one mouse. Right, Mean traces across n = 6 animals.

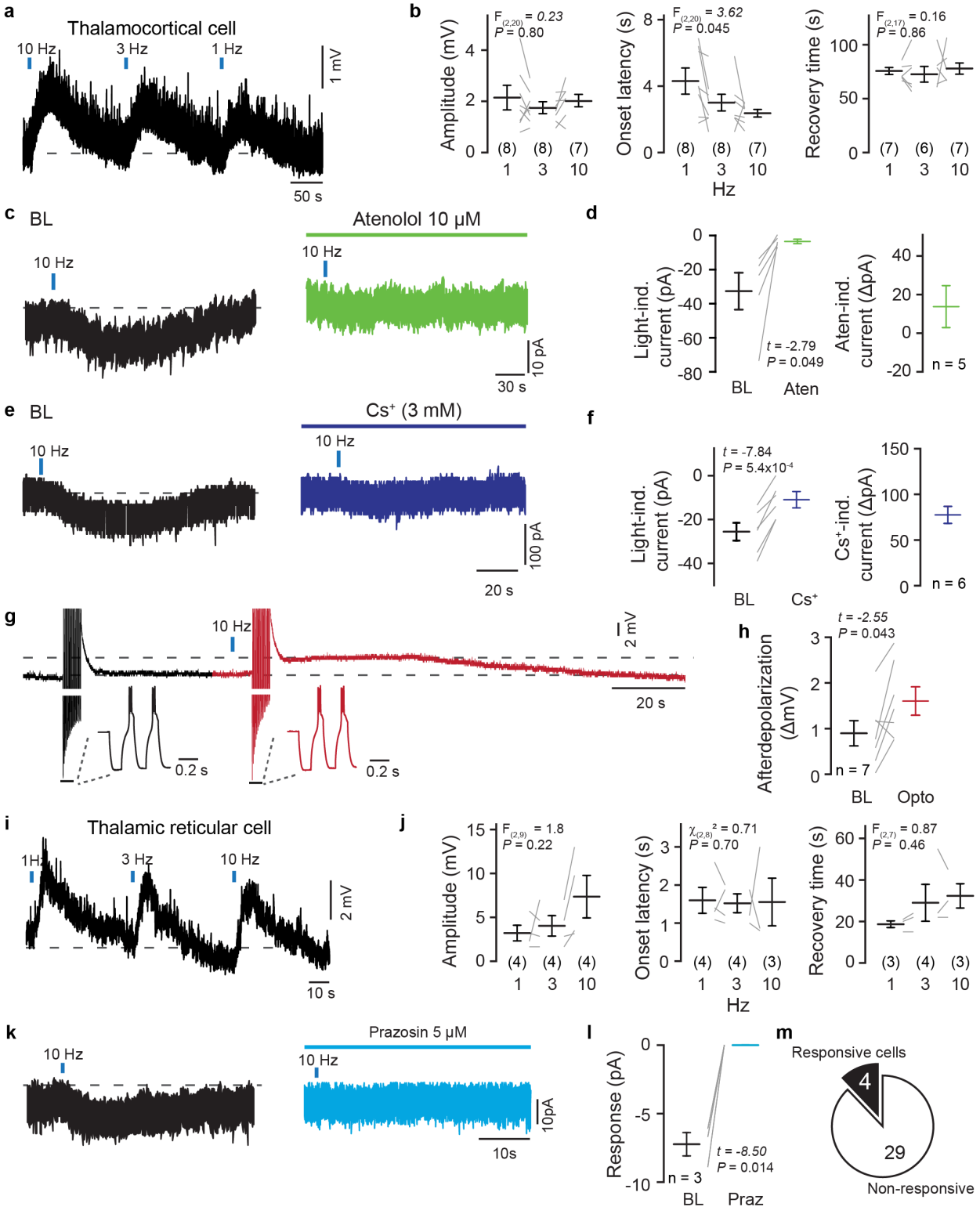

Fig. 6 | LC fiber stimulation evokes slow noradrenergic potentials in thalamic neurons. a,

Representative recording from a whole-cell-patched thalamocortical cell exposed to three successive light

stimuli at 10, 3 and 1 Hz (4 pulses, each lasting 100 μs). Dashed line, - 68 mV. **b**, Quantification of evoked response amplitudes, onset latencies and recovery times as explained in Extended Data Fig. 5. F and *P* values from One-way ANOVA followed by post-hoc *t*-tests, which yielded: 1 Hz vs 3 Hz: t = 1.6, *P* = 0.13; 1 Hz vs 10 Hz: t = 2.7, *P* = 0.024; 3 Hz vs 10 Hz: t = 1.1, *P* = 0.29) **c**, Current response in a voltage-clamped thalamocortical neuron held at -70 mV to 10 Hz-light pulses before (left) and after (right) bath application of the β-adrenergic antagonist atenolol. Dashed line, -200 pA. **d**, Left, Quantification of light-induced currents in baseline (BL) and Atenolol (Aten). Right, Aten-induced positive holding current shift. **e,f**, Same as c,d, for bath-application of Cs^+ to block the cAMP-sensitive h-channels. Dashed line, -80 pA. **g**, Example recording from a thalamocortical neuron injected with repetitive negative current pulses (-250 pA, 20 pulses, 120 ms each) to evoke low-threshold Ca^{2+} bursts. Insets show, each, two of these evoked bursts. Burst were followed by an afterdepolarization that was prolonged when light pulses (10 Hz, 4 pulses, blue bar) preceded current injections. Dashed lines, aligned to baseline membrane potential and peak of the afterdepolarization. **h**, Quantification of afterdepolarizations in baseline (BL, without light exposure) and with light exposure (Opto). **i, j**, As a,b, for a representative recording from a thalamic reticular neuron. Dashed line, -72 mV. F and χ^2 derived from ANOVA and Kruskal-Wallis test, respectively. **k,** Current response in a voltage-clamped thalamic reticular neuron held at -70 mV to 10 Hz light pulses before (left) and after (right) bath application of the α1-adrenergic antagonist prazosin. Dashed line, 10 pA. **l**, Quantification of current response amplitude in baseline (BL) and during prazosin (Praz). **m**, Number of TRN cells responding to LC optogenetic fiber stimulation. t and *P* values in d,f,h,l derived from paired t-tests.

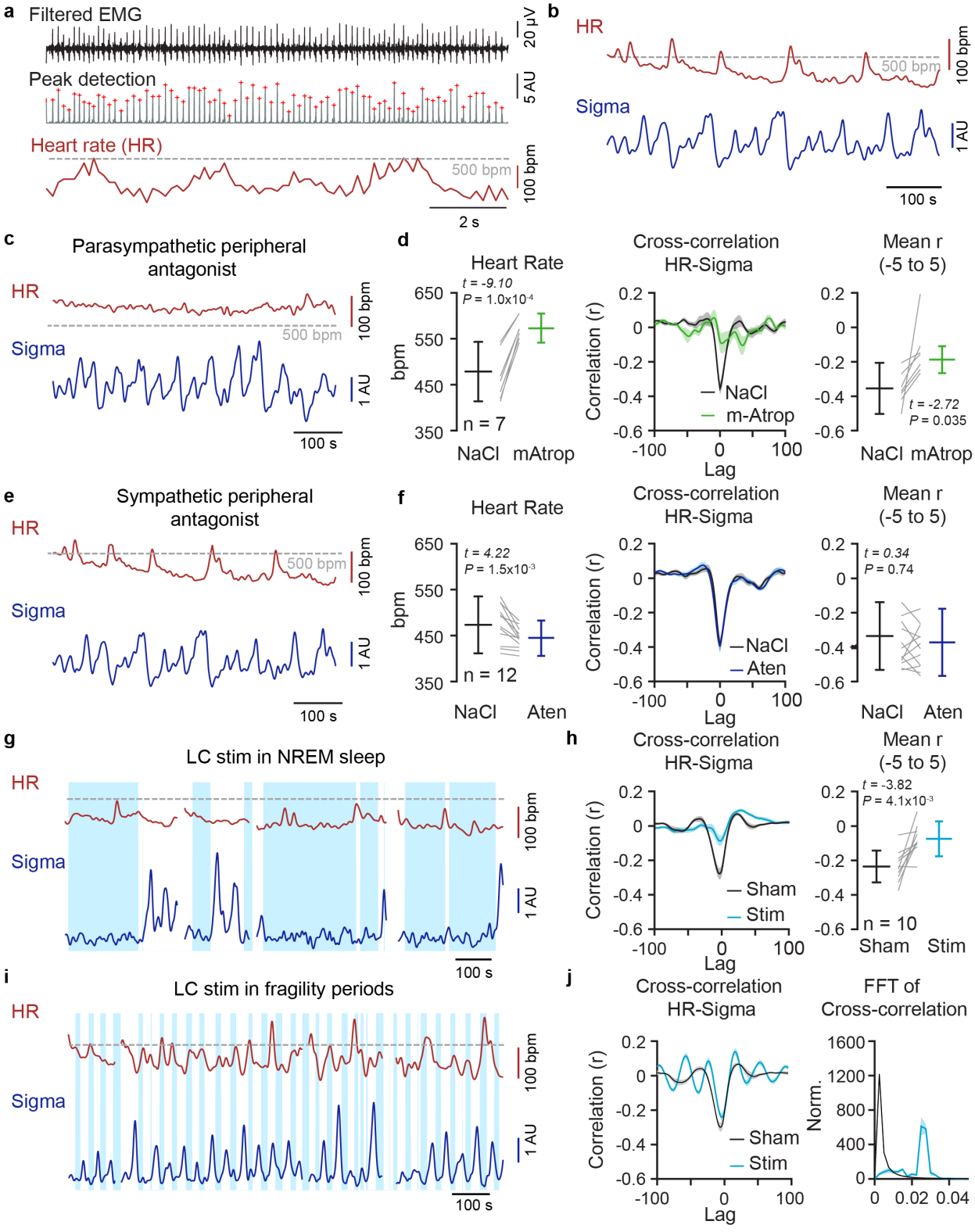

Fig. 7 | The LC as a source of HR variability during NREMS. **a**, Extraction of HR from EMG traces. Top, raw high-pass-filtered (25 Hz) EMG, used for peak detection (middle) and HR (bottom) calculation.

b, Representative NREMS traces showing sigma power dynamics and corresponding HR after an i.p. injection of NaCl. **c**, Example traces illustrating the effects of the parasympathetic antagonist methylatropine (m-Atrop, 10 mg kg^{-1}) on HR and sigma power dynamics. Dashed line, 500 bpm. **d**, Left, Quantification of mean HR following NaCl or m-Atrop injections; Middle, Corresponding Crosscorrelations, Right, Values of the crosscorrelation between -5 to +5 s. **e, f**, As c,d for injection of a sympathetic peripheral antagonist (Atenolol, 1 mg kg^{-1}). **g**, Example traces illustrating the effects of LC stimulation (stim) in NREMS on HR and sigma power dynamics. **h**, Corresponding crosscorrelations quantified as in d, f. **i**, As g, for LC stimulation restricted to machine-learning-detected fragility periods. **j**, Corresponding crosscorrelation and its Fourier transform highlight the appearance of an infraslow peak. All t and *P* values in this figure were obtained from *t*-tests.

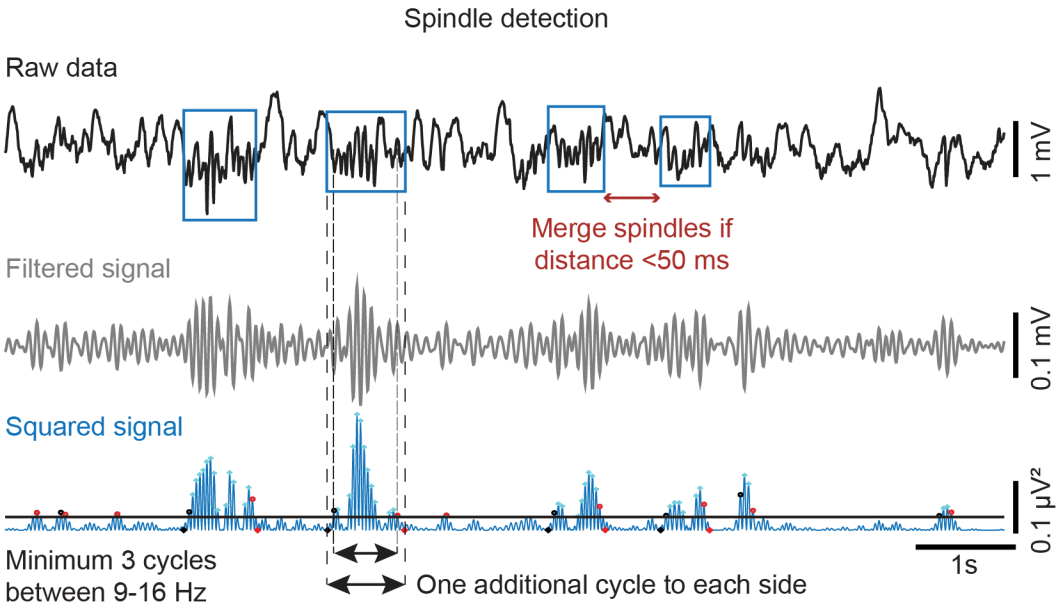

Extended Data Fig. 1 | Method of detection of individual spindles. Raw data from S1 LFP recordings (top), filtered signals (middle) and squared signals (bottom) were used to extract individual spindles according to the criteria given next to the traces. The method was identical to the one published recently[6].

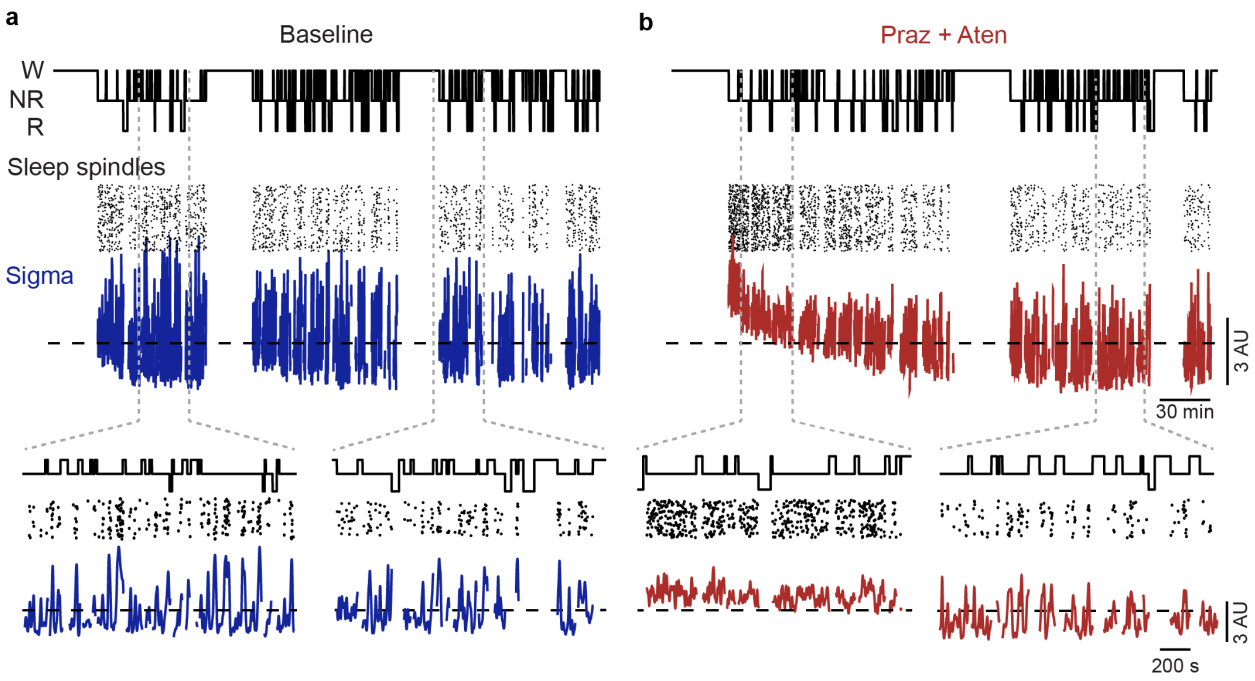

Extended Data Fig. 2 | Time course of pharmacological antagonism of noradrenergic signaling in thalamus on sigma power and sleep spindles. **a**, Animal in baseline conditions, showing, from top to bottom, hypnogram, individual sleep spindles, and sigma power dynamics, with expanded portions shown below. **b**, Same Animal, injected with Praz + Aten. Note slow recovery of the pharmacological suppression of sigma power fluctuations and sleep spindle clustering. Every animal was injected once with either antagonists or ACSF.

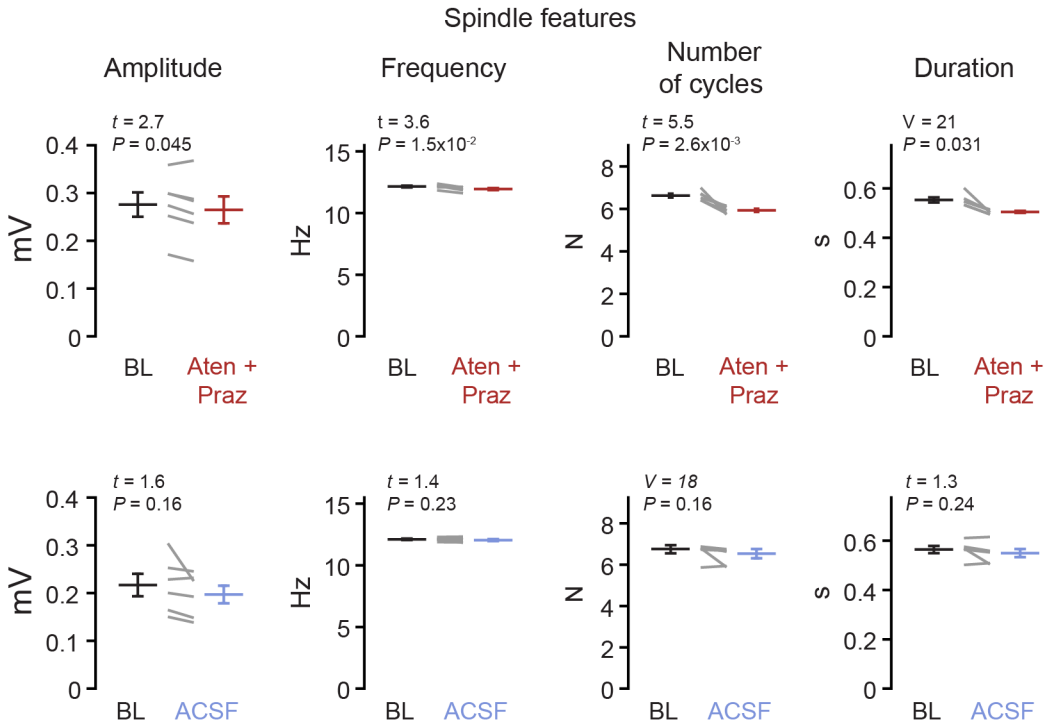

Extended Data Fig. 3 | Quantification of properties of individual sleep spindles in animals used for the pharmacology experiments. Top; Data from the 6 animals injected with antagonists, Bottom; Data from the 6 animals injected with ACSF. From left to right: Peak amplitude, Intra-spindle frequency, Number of spindle cycles, and total spindle duration, analyzed as illustrated in Extended Data Fig. 1 and according to ref. [6]. V, t and *P* in this figure were obtained from ([t]) Wilcoxon signed rank or paired *t*-tests.

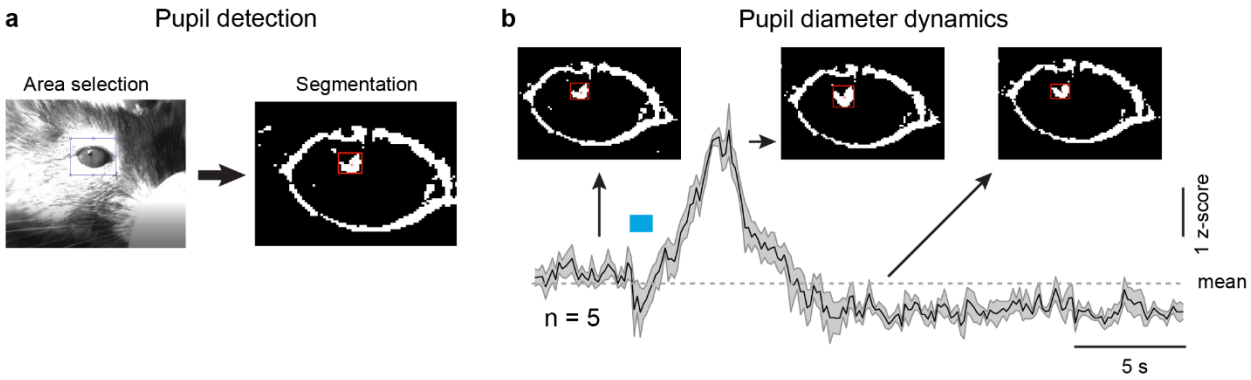

Extended Data Fig. 4 | LC stimulation-induced pupil diameter changes. **a**, Representative image taken from the mouse eye during surgical implantation of optic fiber, showing area selection (dashed square) and corresponding image segmentation with pixels selected for measurement (red square). **b**, Quantification of time course of pupil diameter changes in z-score, with representative segmented images in insets. Blue bar denotes light application. These recordings were made in a subgroup of 5 animals to optimize the position of the optic fiber.

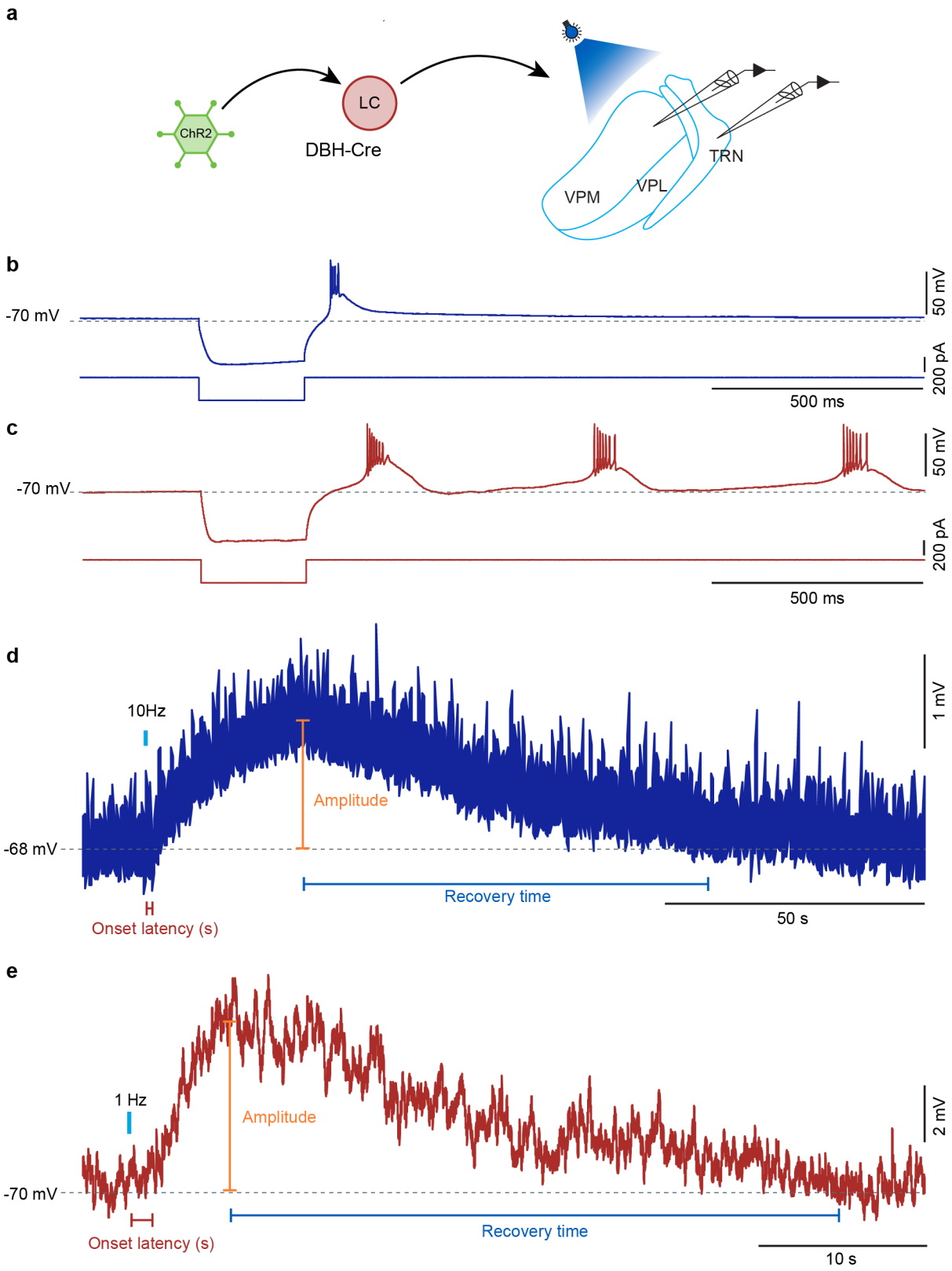

Extended Data Fig. 5 | Details for the in vitro patch-clamp recordings and analysis. **a**, Schematic showing the experimental design. VPM, ventroposterior medial nucleus, VPL, ventroposterior lateral nucleus, TRN, thalamic reticular nucleus. Recordings were performed in either VPM or TRN while light was shone to activate afferent LC fibers. **b**, Rebound bursting characteristic for a thalamocortical cell recorded in VPM and evoked through brief negative current injection. **c**, Repetitive rebound bursting characteristic for a TRN cell recorded in the somatosensory sector and evoked through brief negative current injection. **d**, Enlarged light-evoked response of a thalamocortical neuron, with indications on how quantification of onset latency, amplitude and recovery time were done. **e**, As d, for a light-evoked response in TRN. Dashed lines denote membrane potential value indicated on the left.